

**Access to and reactions of P-functional
tetrathiafulvalene derivatives**

Dissertation

zur

Erlangung des Doktorgrades (Dr. rer. nat.)

der

Mathematisch-Naturwissenschaftlichen Fakultät

der

Rheinischen Friedrich-Wilhelms-Universität Bonn

Vorgelegt von

Shahriar Kermanshahian

aus Amol, Iran

Bonn, 2023

Angefertigt mit Genehmigung der Mathematisch-Naturwissenschaftlichen Fakultät der Rheinischen Friedrich-Wilhelms-Universität Bonn

1. Gutachter: Prof. Dr. Rainer Streubel

2. Gutachter: Prof. Dr. Johannes Beck

Tag der Promotion: 13. April 2023

Erscheinungsjahr: 2023

Hiermit versichere ich, dass die vorgelegte Arbeit persönlich, selbständig und ohne Benutzung anderer als der angegebenen Hilfsmittel angefertigt wurde und alle Quellen kenntlich gemacht wurden.

To Sheida

“Capable is who is wise, Happiness from wisdom will arise”

Abol Qasem Ferdowsi Tousi

Conference contributions

1. Deutsch-Österreichischen Mitarbeiter Workshop Hauptgruppenelementchemie (MHC-10), March 15–17, 2019, Tübingen, Germany. *“Tetrathiafulvalenes fused to 1,4-dihydro-1,4-diphosphinines”* (Oral presentation).
2. 16th European Workshop on Phosphorus Chemistry (EWPC-16), April 24–26, 2019, Bristol, UK. *“Novel access to TTF-fused 1,4-dihydro-1,4-diphosphinines”* (Poster presentation).
3. KOPO 2019 – Functional π -Systems and Beyond, May 8–11, 2019, Bad Honnef, Germany. *“TTF-fused 1,4-dihydro-1,4-diphosphinines, starting anew”* (Poster presentation).
4. International Conference on Heteroatom Chemistry (ICHAC 2019), June 30–July 5, 2019, Prague, Czech Republic. *“Synthesis of 1,4-dihydro-1,4-diphosphinines fused to two TTFs”* (Poster presentation).
5. 17th European Workshop on Phosphorus Chemistry (EWPC-17), February 26–28, 2020, Rennes, France. *“New TTF-fused 1,4-dihydro-1,4-diphosphinines, synthesis and redox properties”* (Poster presentation).
6. 18th European Workshop on Phosphorus Chemistry (online) (OWPC), March 29–31, 2021. *“A P-functional TTF-fused 1,4-diphosphinine precursor”* (Poster Presentation).
7. 23rd International Conference on Phosphorus Chemistry (ICPC23), July 5–9, 2021, Częstochowa, Poland (online). *“En route to a novel TTF-fused 1,4-diphosphinine”* (Poster presentation).
8. Deutsch-Österreichischen Mitarbeiter Workshop Hauptgruppenelementchemie (MHC-11), September 3–5, 2021, Bonn, Germany. *“On combining 1,4-diphosphinine with TTF chemistry”* (Oral presentation).
9. 16th International Symposium on Inorganic Ring Systems (IRIS16), July 24–29, 2022, Graz, Austria. *“First scaffold bearing a 1,4-diphosphabarrelene and two tetrathiafulvalene motifs”* (Poster presentation).

Acknowledgments

Firstly, I would like to thank Prof. Dr. Rainer Streubel for giving me the opportunity to conduct my Ph.D. thesis in his research group. I am very grateful for his support, guidance, and academic freedom that I had working in the lab. I thank him for providing an abundance of laboratory equipment and instruments, which allowed me to expand my knowledge in various fields of research.

I would like to express my gratitude to Prof. Dr. Johannes Beck, Prof. Dr. Arne Lützen and Prof. Dr. Diana Imhof for being part of my thesis committee and spending their valuable time in the examination of my Ph.D. thesis.

I sincerely acknowledge Prof. Dr. René Boere (Department of Chemistry and Biochemistry, The University of Lethbridge, Lethbridge, Alberta, Canada), for his guidance and also fruitful discussions regarding cyclic voltammetry measurements and redox properties of my compounds.

I thank Prof. Dr. Laszlo Nyulaszi and Dr. Zsolt Kelemen (Department of Inorganic and Analytical Chemistry, Budapest university of Technology and Economy, Budapest, Hungary) and Tim Kalisch for the theoretical calculations.

Without the timely and careful service of our Analytical department, it would be impossible to carry out the work properly, and therefore, I thank Dr. Gregor Schnakenburg and Ms. Charlotte Rödde (single crystal X-ray diffraction measurements), Dr. Senada Nozinovic, Ms. Karen Procknicki, Ms. Hannelore Spitz and Ms. Ulrike Weynand (NMR spectroscopy), Dr. Marianne Engeser and her colleagues (Mass spectrometry), Dr. Sabine Rings, Ms. Charlotte Rödde and Ms. Hannelore Spitz (Elemental Analyses) and also, all members in Chemical Store, Glass Blowing section, Mechanical and Electrical workshops. In addition, I want to thank Prof. Dr. Olav Schiemann and Mr. Hamed Alaei for the EPR measurements.

I deeply thank Dr. Abhishek Koner, Dr. Nabila Rauf Naz and Dr. Philip Junker for the watchful introductory guidance into the inert atmosphere techniques and lab culture. A special thank goes for all the encouragement, scientific and moral support even outside of the university to Philipp,

Tim, Mridhul, Florian, David and Tatjana; this Ph.D. would not have been delightful without all of you.

I warmly forward my gratefulness to DAAD and the University of Bonn for the financial support during my study in Bonn.

Last but not least, I would like to thank Sheida who provided endless love and support since the first day that I met her; also my family, for their encouragement even from the other side of the world.

Contents

1	Introduction	1
1.1	Tetrathiafulvalene	1
1.1.1	Phosphanylated tetrathiafulvalenes.....	2
1.1.2	Bridged tetrathiafulvalenes	3
1.2	Phosphinines	6
1.3	Diphosphinines.....	10
1.3.1	1,4-Dihydro-1,4-diphosphinines and 1,4-diphosphinines	12
2	Aim of this Ph.D. thesis.....	21
3	Mono P-functional phosphanylated tetrathiafulvalenes.....	22
3.1	Synthesis of P-functional tetrathiafulvalenes	22
3.2	Cyclic voltammetry studies of phosphanylated tetrathiafulvalenes	25
4	Chlorophosphanyl-substituted tetrathiafulvalenes.....	29
4.1	Synthesis of chlorophosphanyl-substituted tetrathiafulvalenes in one step	29
4.1.1	Isolation of mono-bridged compounds 5a,b	30
4.1.2	Cyclic voltammetry studies of 5a,b	31
4.2	Exchanging one amino group for a chlorine atom.....	33
4.3	Cyclic voltammetry studies of chlorophosphanyl-substituted TTFs	35
4.4	Reduction of chloro(diethylamino)phosphanyl-substituted TTFs	36
4.4.1	Electrochemical reduction of 4d,f	36
4.4.2	Chemical reduction of chlorophosphanyl-substituted TTFs.....	40
4.4.3	Chloride abstraction reaction from 4d,f with GaCl ₃	41
5	Tetrathiafulvalene-fused 1,4-diphosphinine chemistry.....	49
5.1	New 1,4-dihydro-1,4-diphosphinine derivatives fused to two TTF	49
5.2	Cyclic voltammetry studies of new 1,4-dihydro-1,4-diphosphinines	54
5.3	Reactivity studies of TTF-fused 1,4-dihydro-1,4-diphosphinines	57
5.3.1	Oxidation of the <i>P</i> -centers in 1,4-bis(diethylamino)-1,4-dihydro-1,4-diphosphinines.....	58
5.3.2	Oxidation of the <i>P</i> -centers in 11d,f using elemental sulfur and selenium.....	61

5.3.3	Cyclic voltammetry studies of oxidized 1,4-dihydro-1,4-diphosphinines	65
5.4	Scrambling reaction of 11d,d' and 11f,f' with PCl ₃	70
5.5	Reducing the P–Cl substituted 1,4-dihydro-1,4-diphosphinine 15	73
5.6	Trapping of a TTF-fused 1,4-diphosphinine	76
5.6.1	Cyclic voltammetry study of 1,4-diphosphabarrelene 18	79
6	Oligomers containing TTF units linked by 1,4-dihydro-1,4-diphosphinine rings	81
6.1	Doubly-phosphanylated TTFs as precursor for oligomeric products.....	82
6.1.1	Cyclic voltammetry studies of doubly-phosphanylated tetrathiafulvalenes.....	85
6.1.2	Bis(chlorophosphanyl)tetrathiafulvalenes	87
6.1.3	Ring-closing/oligomerization reaction.....	88
6.2	Desulfurization of tricyclic 1,4-dihydro-1,4-diphosphinines annulated to two 1,3-dithiole-2-thiones.....	88
7	Summary.....	92
8	Experimental section	102
8.1	General techniques	102
8.1.1	Melting point determination	103
8.1.2	Elemental analysis.....	103
8.1.3	NMR spectroscopy	103
8.1.4	EPR spectroscopy	103
8.1.5	Mass spectrometry	104
8.1.6	Cyclic voltammetry	104
8.1.7	Single crystal X-ray diffraction studies.....	105
8.1.8	Chemicals	106
8.2	Synthesis of C-phosphanylated tetrathiafulvalenes 3a–f	108
8.2.1	4-Diethylamino(phenyl)phosphanyl-2,2'-bis(1,3-dithiolylidene) (3a)	109
8.2.2	4-Bis(diethylamino)phosphanyl-2,2'-bis(1,3-dithiolylidene) (3b).....	110
8.2.3	4-Diethylamino(phenyl)phosphanyl-4',5'-dimethyl-2,2'-bis(1,3-dithiolylid-ene) (3c)	111
8.2.4	4-Bis(diethylamino)phosphanyl-4',5'-dimethyl-2,2'-bis(1,3-dithiolylidene) (3d).	112
8.2.5	4-Diethylamino(phenyl)phosphanyl-4',5'-di- <i>n</i> -propyl-2,2'-bis(1,3-dithiolylidene) (3e)	113

8.2.6	4-Bis(diethylamino)phosphanyl-4',5'-di- <i>n</i> -propyl-2,2'-bis(1,3-dithiolylidene) (3f).....	114
8.3	Synthesis of 4-chlorophosphanyltetrathiafulvalenes 4a–h	115
8.3.1	4-Chloro(phenyl)phosphanyl-2,2'-bis(1,3-dithiolylidene) (4a).....	116
8.3.2	4-Chloro(diethylamino)phosphanyl-2,2'-bis(1,3-dithiolylidene) (4b).....	117
8.3.3	4-Chloro(phenyl)phosphanyl-4',5'-dimethyl-2,2'-bis(1,3-dithiolylidene) (4c).....	118
8.3.4	4-Chloro(diethylamino)phosphanyl-4',5'-dimethyl-2,2'-bis(1,3-dithiolyli-dene) (4d).....	119
8.3.5	4-Chloro(phenyl)phosphanyl-4',5'-di- <i>n</i> -propyl-2,2'-bis(1,3-dithiolylidene) (4e) .	120
8.3.6	4-Chloro(diethylamino)phosphanyl-4',5'-di- <i>n</i> -propyl-2,2'-bis(1,3-dithiolylidene) (4f).....	121
8.3.7	4-Dichlorophosphanyl-4',5'-dimethyl-2,2'-bis(1,3-dithiolylidene) (4g).....	122
8.3.8	4-Dichlorophosphanyl-4',5'-di- <i>n</i> -propyl-2,2'-bis(1,3-dithiolylidene) (4h).....	122
8.4	Synthesis of bis(tetrathiafulvalenyl)aminophosphanes 5a,b	123
8.4.1	Bis[2-(4,5-dimethyl-1,3-dithiol-2-ylidene)-1,3-dithiol-4-yl]diethylamino-phosphane (5a).....	124
8.4.2	Bis[2-(4,5-di- <i>n</i> -propyl-1,3-dithiol-2-ylidene)-1,3-dithiol-4-yl]diethylamino-phosphane (5b).....	125
8.5	Synthesis of Bis(tetrathiafulvalenyl)chlorophosphanes 6a,b	126
8.5.1	Bis[2-(4,5-dimethyl-1,3-dithiol-2-ylidene)-1,3-dithiol-4-yl]chlorophospha-ne (6a) ..	126
8.5.2	Bis[2-(4,5-di- <i>n</i> -propyl-1,3-dithiol-2-ylidene)-1,3-dithiol-4-yl]chlorophos-phane (6b).....	127
8.6	Chloride abstraction reaction of 4d,f	128
8.7	Anion exchange reaction of 9a,b	128
8.8	Synthesis of 1,4-bis(diethylamino)-1,4 <i>H</i> -1,4-diphosphinines 11d,d'–f,f'	129
8.8.1	2,6-Bis(4,5-dimethyl-1,3-dithiol-2-ylidene)-bis(1,3-dithiole)[2,3-d:5,6-d']-4, 8-bis(diethylamino)-4,8 <i>H</i> -4,8-diphosphinine (11d,d').....	130
8.8.2	2,6-Bis(4,5-dipropyl-1,3-dithiol-2-ylidene)-bis(1,3-dithiole)[2,3-d:5,6-d']-4, 8-diphenyl-4,8 <i>H</i> -4,8-diphosphinine (11e,e').....	131
8.8.3	2,6-Bis(4,5-dipropyl-1,3-dithiol-2-ylidene)-bis(1,3-dithiole)[2,3-d:5,6-d']-4, 8-bis(diethylamino)-4,8 <i>H</i> -4,8-diphosphinine (11f,f').....	132
8.9	Oxidation of the 1,4-bis(diethylamino)-1,4 <i>H</i> -1,4-diphosphinines with hydrogen peroxide-urea adduct 12	133

8.9.1	2,6-Bis(4,5-dimethyl-1,3-dithiol-2-ylidene)-bis(1,3-dithiole)[2,3-d:5,6-d']-4, 8-bis(diethylamino)-4,8 <i>H</i> -4,8-dioxide-4,8-diphosphinine (12a,a')	133
8.9.2	2,6-Bis(4,5-dipropyl-1,3-dithiol-2-ylidene)-bis(1,3-dithiole)[2,3-d:5,6-d']-4, 8-bis(diethylamino)-4,8 <i>H</i> -4,8-dioxide-4,8-diphosphinine (12b,b')	134
8.10	Oxidation of the 1,4-bis(diethylamino)-1,4 <i>H</i> -1,4-diphosphinines with elemental sulfur 13	135
8.10.1	2,6-Bis(4,5-dimethyl-1,3-dithiol-2-ylidene)-bis(1,3-dithiole)[2,3-d:5,6-d']-4, 8-bis(diethylamino)-4,8 <i>H</i> -4,8-diphosphinine-4,8-disulfide (13a,a')	136
8.10.2	2,6-Bis(4,5-dipropyl-1,3-dithiol-2-ylidene)-bis(1,3-dithiole)[2,3-d:5,6-d']-4, 8-bis(diethylamino)-4,8 <i>H</i> -4,8-diphosphinine-4,8-disulfide (13b,b')	137
8.11	Oxidation of the 1,4-bis(diethylamino)-1,4 <i>H</i> -1,4-diphosphinines with elemental selenium 14	138
8.11.1	2,6-Bis(4,5-dimethyl-1,3-dithiol-2-ylidene)-bis(1,3-dithiole)[2,3-d:5,6-d']-4, 8-bis(diethylamino)-4,8 <i>H</i> -4,8-diphosphinine-4,8-diselenide (14a,a')	138
8.11.2	2,6-Bis(4,5-dipropyl-1,3-dithiol-2-ylidene)-bis(1,3-dithiole)[2,3-d:5,6-d']-4, 8-bis(diethylamino)-4,8 <i>H</i> -4,8-diphosphinine-4,8-diselenide (14b,b')	139
8.12	Synthesis of 10-butyl-2,6-bis(4,5-dipropyl-1,3-dithiol-2-ylidene)-4,8-ethano[1,4]diphosphinino[2,3-d:5,6-d']bis([1,3]dithiole) 18	140
8.13	Synthesis of doubly-phosphorylated tetrathiafulvalenes 19	142
8.13.1	Bis(diethylamino(phenyl)phosphanyl)-2,2'-bis(1,3-dithiolylidene) (19a,a')	142
8.13.2	Bis(bis(diethylamino)phosphanyl)-2,2'-bis(1,3-dithiolylidene) (19b,b')	143
8.14	Synthesis of Bis(chlorophosphanyl)tetrathiafulvalenes 20	144
8.14.1	Bis(chlorophenylphosphanyl)-2,2'-bis(1,3-dithiolylidene) (20a,a').....	145
8.14.2	Bis(chloro(diethylamino)phosphanyl)-2,2'-bis(1,3-dithiolylidene) (20b,b').....	146
8.15	Synthesis of a mixture of oligomeric products containing TTF units via ring-closing reaction 21a,b	147
8.16	Synthesis of a mixture of oligomeric products containing TTF units via desulfurization 22c	147
References		149
Abbreviations		156
Appendix		159
	Cyclic voltammograms	159
	EPR spectrum	184

Frontier molecular orbitals	185
Crystal data and structure refinement for compound 3c	188
Crystal data and structure refinement for compound 3d	191
Crystal data and structure refinement for compound <i>cis</i> - 11d	194
Crystal data and structure refinement for compound <i>trans</i> - 12a	197
Crystal data and structure refinement for compound <i>cis</i> - 14b	200
Crystal data and structure refinement for pseudo- <i>E</i> - 19b	204

1 Introduction

1.1 Tetrathiafulvalene

Although the parent tetrathiafulvalene (TTF) **1a** (Figure 1.1) was reported in 1970 by Wudl¹, the chemistry of TTF derivatives is considerably older. For example, the dibenzo-fused TTF **I**² (Figure 1.1) was synthesized by Hurtley and Smiles in 1926 and dimethyl-TTF **II** and diphenyl-TTF **III** derivatives (Figure 1.1) were reported by Prinzbach *et al.* in 1965.³ However, great interest in these sulfur-containing molecules started in the early 1970s after the discovery of high electric conductivity in a chloride salt of TTF⁴ and the formation of the charge-transfer complexes with easily reducible organic compounds, e.g., tetracyanoquinodimethane (TCNQ) **IV**^{5,6} (Figure 1.1), which initiated the field of organic metals. In these organic materials (also known as "low-dimensional" or "one-dimensional metals"), electrical conductivity increases with decreasing temperature in the solid state and the molecular charge carriers stack uniformly along a given axis. The solid-state packing arrangement of all of these compounds consists of independent, uniform stacks of donors and/or acceptors. Since then, a huge number of TTF derivatives have been synthesized and TTF and its derivatives have probably become the most famous electron donor molecules with not only applications in molecular conductors⁷ but as building blocks in many areas of organic, supramolecular, and materials chemistry.⁸

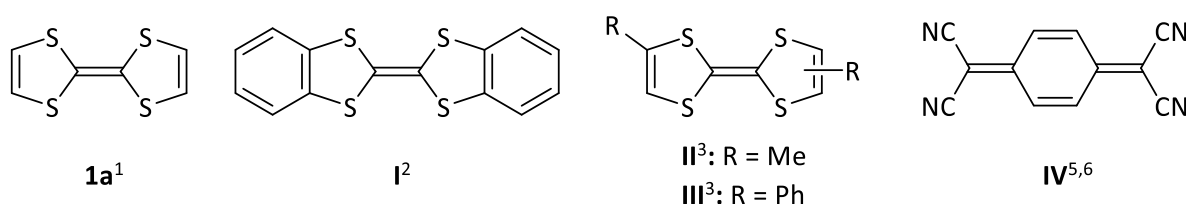
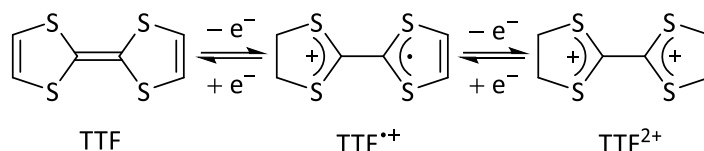


Figure 1.1. Tetrathiafulvalene (**1a**), its first known derivatives (**I-III**) and TCNQ (**IV**).^{1-3,5,6}

Tetrathiafulvalene is a non-aromatic 14π -electron molecule⁹, which could be sequentially and reversibly oxidized to form the related radical cation and dication species at relatively low oxidation potential values ($E_{1/2}^1 = +0.34$; $E_{1/2}^2 = +0.78$ V vs. Ag/Ag⁺ in acetonitrile) (Scheme 1.1). As a result of the 6π -electron heteroaromaticity of the 1,3-dithiolium cation, both the radical cation

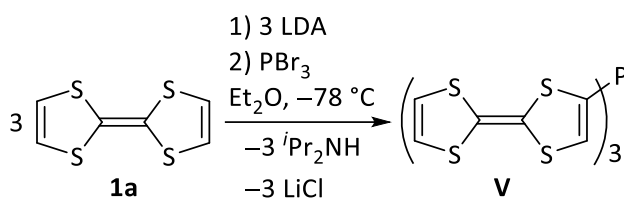
and dication species are aromatic according to the Hückel rule⁹, in contrast to the neutral TTF molecule. This difference affects the geometry of these species, where TTF^{•+} has a planar D_{2h} symmetry, but TTF²⁺ is not planar and has a D_2 symmetry, whereas neutral TTF shows a slightly boatlike structure with C_{2v} symmetry.^{10,11}



Scheme 1.1. TTF and its radical cation and dication.

1.1.1 Phosphanylated tetrathiafulvalenes

The first example of a tetrathiafulvalenylphosphane was reported in 1991 by Fourmigué *via* the monolithiation of the unsubstituted TTF followed by the reaction with PBr_3 (Scheme 1.2).¹²



Scheme 1.2. Synthesis of the first tetrathiafulvalenylphosphane.¹²

Shortly after this first report, mono- and doubly-phosphorylated TTFs **VI** and **VII** (Figure 1.2) were introduced by the same group.¹³ It is noteworthy that the *ortho*-chelating diphosphane **VII** cannot be prepared from TTF itself as the dilithiation affects the two dithiole rings. In order to prepare selectively an *ortho*-dilithiated TTF species, the unsymmetrically substituted 4,5-dimethyl-TTF **1b** has been used as starting material (Scheme 1.3).¹³

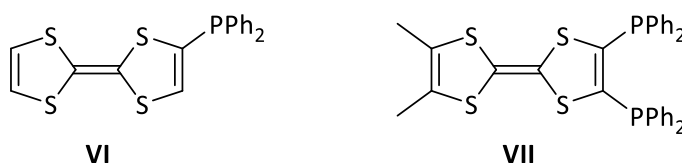
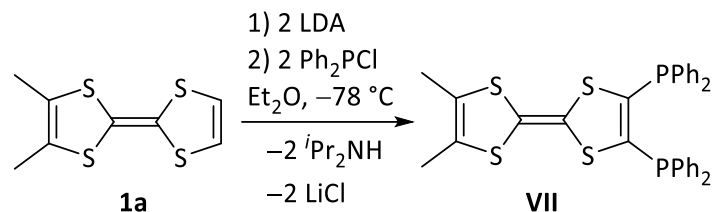


Figure 1.2. Mono- and doubly-phosphanylated TTFs.¹³



Scheme 1.3. Synthesis of *ortho*-phosphanylated TTF.¹³

Following the same chemical pathway, by varying the nature of the phosphorus halide, a variety of TTF-substituted phosphanes were prepared.^{14,15} Also depending on the amount of base used in the lithiation step, it is possible to form the mono (**VIII**, **IX**), the bis-(4,4') (*E,Z*-**XI**) and the tetrakis phosphanylated species (**X**) (Figure 1.3).¹⁶ However, in all these reported compounds further functionalizations on the phosphorus atom were prohibited due to the strong P–C bonds.

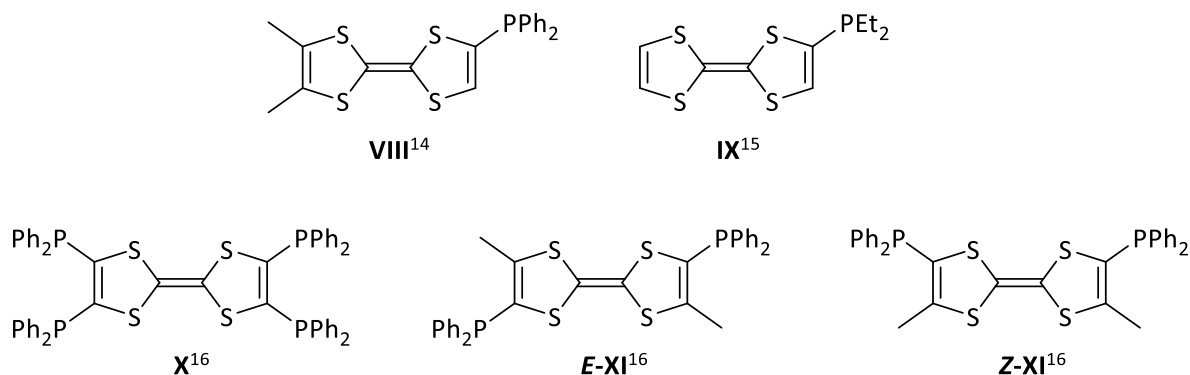


Figure 1.3. Mono, bis-(4,4') and tetrakis-phosphanylated TTFs.^{14–16}

1.1.2 Bridged tetrathiafulvalenes

To achieve the metallic behavior in molecular complexes a mixed valence state in the donor and/or acceptor species is required which can be obtained by incomplete charge transfer from donor to the acceptor in 1:1 complexes, e.g. in TTF-TCNQ or by complexes with stoichiometry other than 1:1, such as the superconducting salts of tetramethyltetraselenafulvalene (TMTSF) **XII** and bis(ethylenedithio)tetrathiafulvalene (BEDT-TTF) **XIII** (Figure 1.4) having the general formula (Donor)₂(Anion)₁.^{17–20}

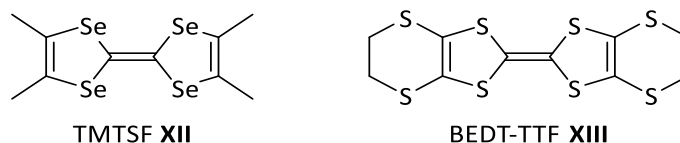
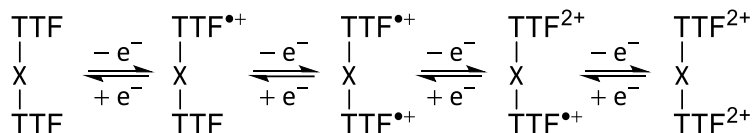


Figure 1.4. Tetramethyltetraselenafulvalene (**XII**) and bis(ethylenedithio)tetrathiafulvalene (**XIII**).

In order to control the degree of charge transfer, a balance between the ionization potential of the donor and the electron affinity of the acceptor is required and, hence, the search for new TTF derivatives has significant importance. One way of modification of TTF, is the preparation of the bridged molecules, in which the TTF units are linked by one or more spacer groups. In such electron-donor systems, depending on the nature of the linkage, electronic communication between redox-active TTF units can be promoted by through-bond or through-space interactions or shut down to achieve mixed valance states.^{21–23} These so-called “dimeric” (X-linked) TTF molecules can display multi-stage redox behavior (Scheme 1.4), which has a strong effect on the formation, structures, and physical properties of their related charge transfer complexes and ion radical salts.^{24,25}



Scheme 1.4. Multi-stage redox behavior in “dimeric” TTF compounds.²²

Despite most of the conductive materials which have crystal structures, consisting of segregated, uniformly stacked columns of planar π -donor and acceptor molecules²⁶, the bridged TTFs and related compounds, are not limited to planar structures, and can provide rather unique examples of non-planar electron donors.²⁷ Based on the number and position of the linkage of the spacer groups, these compounds can be categorized into the following four types: i) a single-linkage (**a**), ii) a double-linkage (**b**), iii) a cyclophane type double-linkage (**c**) and iv) a cyclophane type quadruple-linkage (**d**) (Figure 1.5).²² However, not only these generic types but also the nature of the spacer groups determine the orientation and degree of interaction between the TTF units and, hence, have a strong effect on the molecular structures and the physical properties of the bridged TTF molecules. Molecules of type **a** and **b** with conjugated or rigid spacer groups are

presumed to form stretched conformations while having non-conjugated or flexible spacer groups favors V-shaped or U-shaped folded conformations. On the other hand, the cyclophane-type molecules (**c** and **d**) are more likely to have double-decker structures.²²

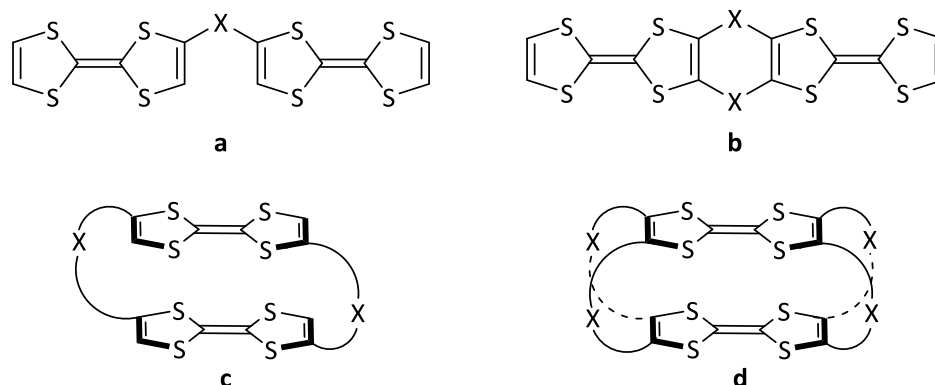
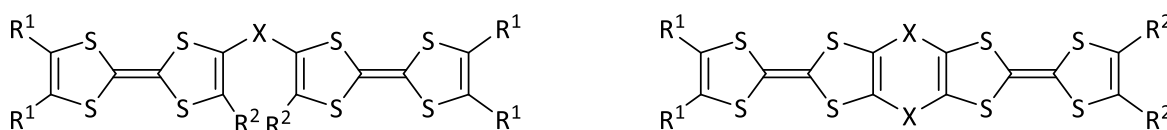


Figure 1.5. Different types of “dimeric” TTFs.²²

Different main group elements have been used to link two TTF units and form the $X(\text{TTF})_2$ type in which X stands for S²⁸, Se²⁸, Te²⁹, SiMe₂³⁰, PPh³⁰, Hg³⁰ (Figure 1.6). It was proposed that intramolecular C-X-C through-bond interactions are limited due to free rotation around the X–C_{TTF} single bonds.³¹ The molecular rigidity can be enhanced by using two atoms or units X as linkers, leading to derivatives, often formulated as X₂(TTF)₂ (Figure 1.6), in which two TTF units are fused to a 1,4-dithiine (X = S)³², 1,4-ditellurine (X = Te)^{33,34} or 1,4-dihydro-1,4-diphosphinine (X=PPh).³¹



XIV: R¹ = R² = H, X = S²⁸

XV: R¹ = R² = H, X = Se²⁸

XVI: R¹ = R² = H, X = Te²⁹

XVIIa: R¹ = R² = H, X = SiMe₂³⁰

XVIIIa: R¹ = R² = H, X = PPh³⁰

XIXa: R¹ = R² = H, X = Hg³⁰

XVIIb: R¹ = Me, R² = H, X = SiMe₂³⁰

XVIIIb: R¹ = Me, R² = H, X = PPh³⁰

XIXb: R¹ = Me, R² = H, X = Hg³⁰

XVIIc: R¹ = R² = Me, X = SiMe₂³⁰

XVIIIc: R¹ = R² = Me, X = PPh³⁰

XIXc: R¹ = R² = Me, X = Hg³⁰

XXa: R¹ = R² = H, X = S³²

XXb: R¹ = H, R² = Me, X = S³²

XXc: R¹ = H, R² = SMe, X = S³²

XXd: R¹ = Me, R² = SMe, X = S³²

XX1a: R¹ = R² = Me, X = Te³⁴

XX1b: R¹ = R² = SMe, X = Te³⁴

XXII: R¹ = R² = Me, X = PPh³¹

Figure 1.6. Examples of mono- and doubly-bridged TTFs with main group elements as linker.^{28–32,34}

1.2 Phosphinines

Phosphinines, also known as phosphabenzene, are P-analogs of benzene and pyridine, and contain a planar, six-membered, aromatic heterocyclic ring with a $\sigma^2\lambda^3$ -phosphorus atom in the ring. π -conjugation within the phosphinine ring is disturbed due to the presence of the phosphorus atom and hence the aromaticity is decreased compared to the benzene ring (almost 90%).³⁵ In addition to this slight reduction in aromaticity, the inclusion of the P-atom in the ring has further effects on molecular orbitals. As a comparison between the phosphinine and their lighter homolog, pyridine, there is a substantial difference in the nature of the lone pair. The lone pair in phosphinine resides in the less directional and more diffused HOMO-2 orbital (Figure 1.7)³⁶ and, hence, has little to no nucleophilic character. Also, LUMO in phosphinine is mostly located on the phosphorus atom and has much lower energy compared to the LUMO in pyridine. Altogether, this frontier molecular orbital situation suggests that phosphinines are much weaker σ -donor and much stronger λ -acceptor ligands compared to pyridine.

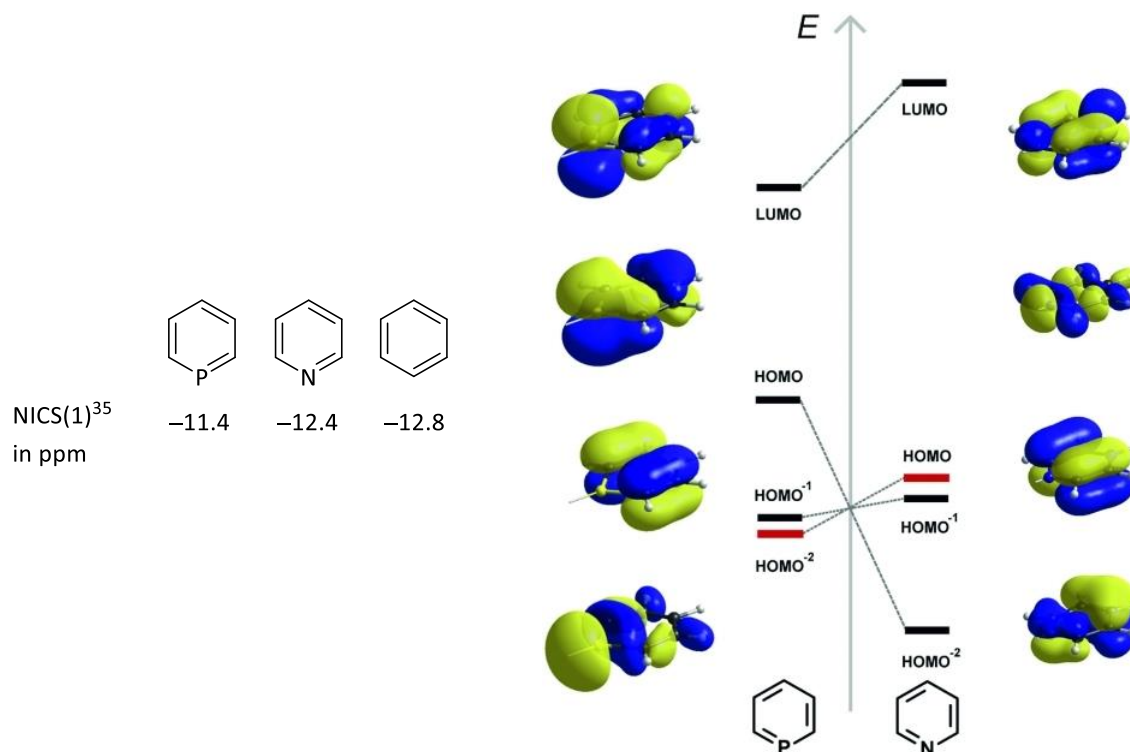
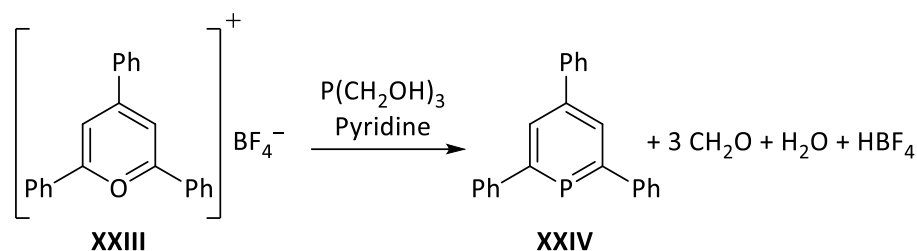


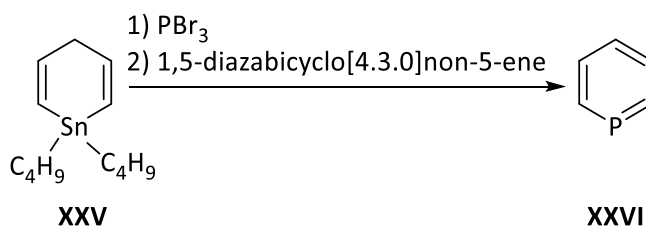
Figure 1.7. NICS(1) values of benzene and its hetero-analogs³⁵ as well as frontier molecular orbital energies of phosphinine and pyridine, molecular orbitals representing the lone pairs are shown in red (taken from the literature, contribution of C. Müller).³⁶

The first example of phosphinine was reported by Märkl in 1966 and has opened a new area in the chemistry of low-coordinate phosphorus. 2,4,6-Triphenylphosphinine **XXIV** was synthesized by the thermal reaction between $P(\text{CH}_2\text{OH})_3$ as a formal PH_3 source and pyrylium salt **XXIII** in pyridine (Scheme 1.5)^{37,38} and remained the most easily accessible derivative for a long time.



Scheme 1.5. Synthesis of 2,4,6-triphenylphosphinine (**XXIV**).³⁸

The most important addition to this field of research was the synthesis of the parent phosphinine **XXVI** by Ashe in 1971 by the reaction of the 1,4-dihydro-1,1-di-*n*-butylstannabenzene (**XXV**) with phosphorus tribromide, followed by the addition of 1,5-diazabicyclo[4.3.0]non-5-ene which led to the dehydrohalogenation of the formed 1-bromo-phosphacyclohexadiene (Scheme 1.6).³⁹ The final product **XXVI** was found to be a colorless, volatile liquid while **XXIV** was isolated as a crystalline solid.



Scheme 1.6. Synthesis of the parent phosphinine.³⁹

Following these publications, several new synthetic routes to λ^3 -phosphinines were reported and some of the examples are shown in Figure 1.8. Compound **XXVII** was synthesized by a [4+2]-cycloaddition reaction between 1,3-cyclopentadiene and $^t\text{BuCP}$.^{40,41} Thermal elimination of a small molecule leading to aromatization can also be used to form phosphinines, e.g., compound **XXVIII** was obtained upon heating 1-benzyl-1,2-dihydro-phosphanaphthalene at 260-300°C and elimination of a molecule of toluene.⁴² To synthesize compound **XXIX** ethyldiazoacetate was reacted with a phosphole sulfide. During the course of the reaction, a bicyclic derivative was

initially generated due to the addition of a carbene at the C^2-C^3 bond of the phosphole which, under thermal conditions, subsequently rearranges to the final product.⁴³ A [4+2]-cycloaddition reaction between an 1,3-azaphosphinine and an alkyne, followed by elimination of a nitrile unit was employed to synthesize compound **XXX**.⁴⁴ As the last example, compound **XXXI** was achieved by ring expansion of zirconacyclopentadienes by insertion of chloro(trimethylsilyl)methyl lithium, followed by the reaction with phosphorus trichloride.⁴⁵ There are several more synthetic routes available to phosphinines as their chemistry has seen an enormous development since the first report by Märkl, and is still developing.

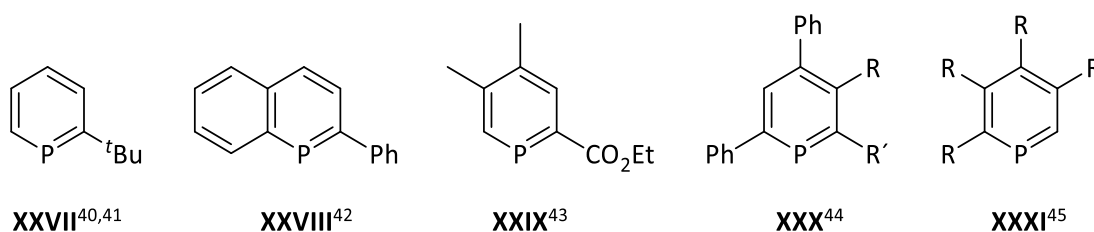
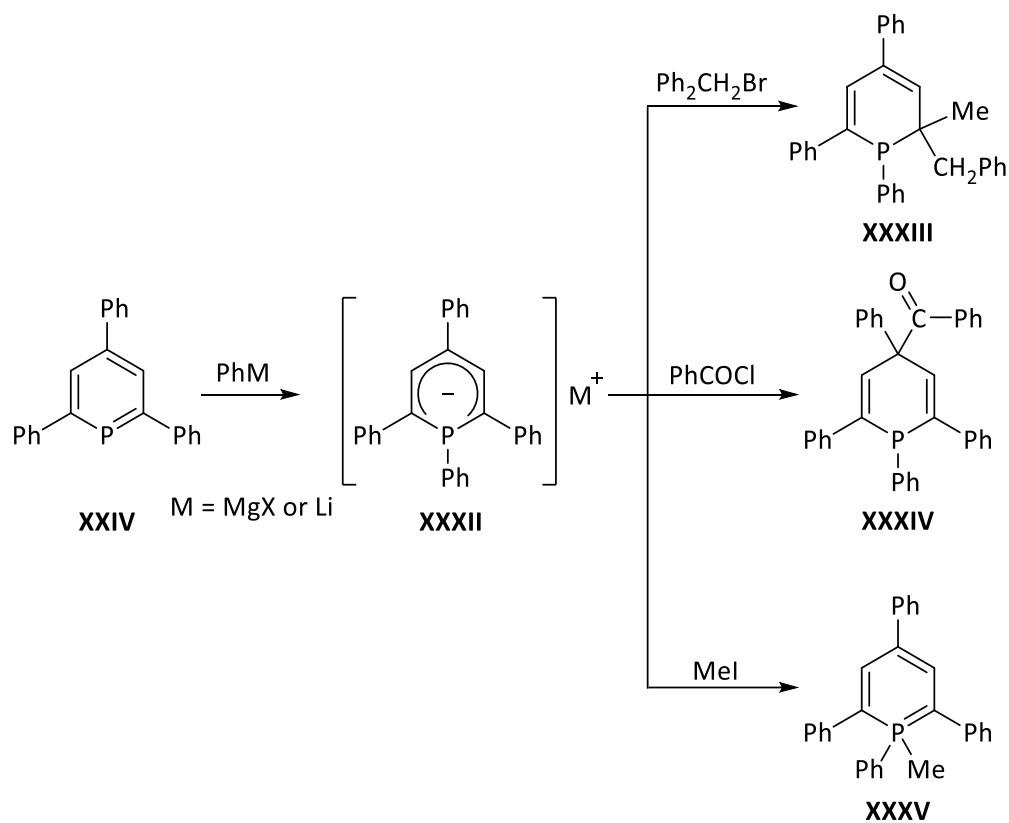


Figure 1.8. Selected examples of phosphinines to illustrate motifs accessible via different synthetic routes.⁴⁰⁻⁴⁵

Due to the π -ligand accepting properties, and the presence of an electrophilic phosphorus center, phosphinines readily undergo nucleophilic substitution reaction using Grignard or organolithium reagents resulting in λ^4 -phosphinines **XXXII** which, depending on the nature of the electrophile used in the next step can give access to regiochemically different substitution products, i.e., 1,1- or 1,2- or 1,4-regioisomers (Scheme 1.7).⁴⁶⁻⁵²

$\sigma^2\lambda^3$ -Phosphinines can be easily transformed into the related λ^5 derivatives via anionic, cationic and radical intermediates and, hence, the chemistry of λ^5 -phosphinines has expanded rapidly.⁵³ $\sigma^2\lambda^3$ -Phosphinines have low basicity and, hence, only by treating with very strong and non-oxidizing acids having weakly coordinating anions, a protonation reaction can be achieved to form **XXXVI**⁵⁴ (Figure 1.9). By using oxidation reagents such as H_2O_2 , $Hg(OAc)_2$, diols and amines a large number of oxidized $\sigma^4\lambda^5$ -phosphinine derivatives e.g., **XXXVII** and **XXXVIII** has been reported.^{55,56} In addition, heating the toluene solutions of phosphinines in presence of elemental sulfur can lead to the oxidized compounds **XXXIX**.^{57,58} Phosphinium cations **XL** can be formed by a reaction between λ^4 -phosphinines and hexachloroethane followed by chloride abstraction

with GaCl_3 .⁵⁹ Phosphinines can also be used to synthesize the related phosphabarrelenes **XLI** via [4+2]-cycloadditions with activated alkynes.⁶⁰



Scheme 1.7. Sequential reactions of phosphinine **XXIV** with nucleophiles and electrophiles.^{46–51}

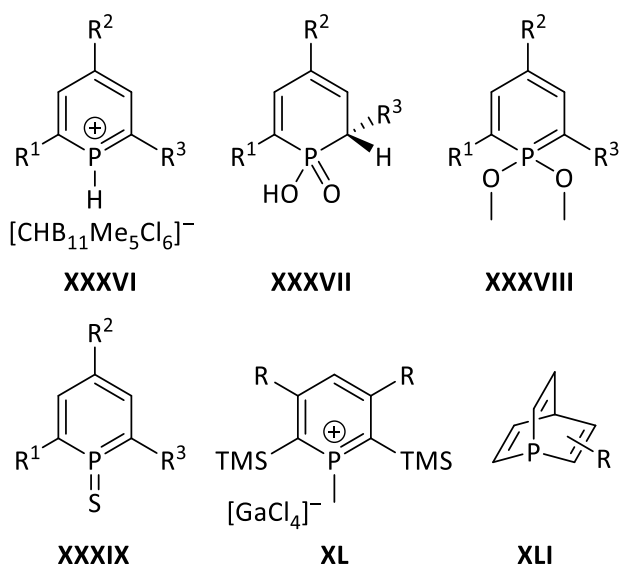


Figure 1.9. Examples of higher coordinated compounds accessed from $\sigma^2\lambda^3$ -phosphinines.^{54–60}

1.3 Diphosphinines

In contrast to phosphinines, the chemistry of diphosphinines was largely underdeveloped (till recent reports from Streubel's group) mainly due to their high reactivity and instability. Three different regioisomers for diphosphinines can be expected, i.e., 1,2-diphosphinine, 1,3-diphosphinine and 1,4-diphosphinine (Figure 1.10).

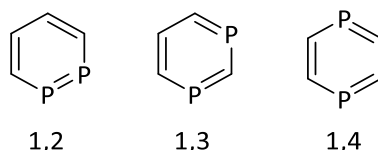
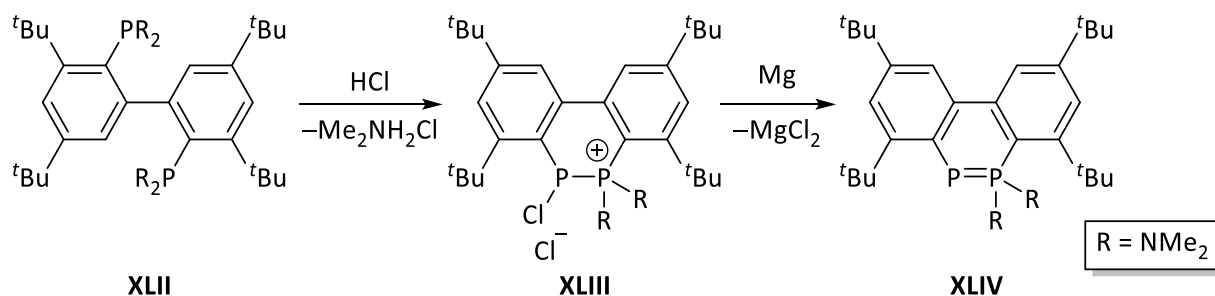


Figure 1.10. Different regioisomers of $\sigma^3\lambda^3$ -diphosphinines.

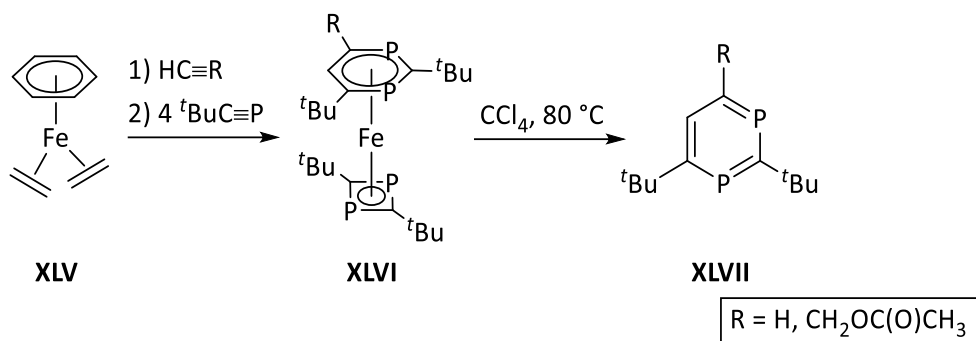
In the case of 1,2-diphosphinines, Bickelhaupt and co-workers reported the synthesis of λ^5, λ^3 -diphosphaphenanthrene. The reaction of compound **XLII** with hydrogen chloride led to the formation of a cyclic intermediate **XLIII** instead of the originally targeted bis-dichlorophosphane derivative. This cyclic intermediate was subsequently reduced with Mg to form the related $1\lambda^5, 2\lambda^3$ -diphosphinine **XLIV** (Scheme 1.8). Formation of the compound **XLIV** was postulated on the basis of ^{31}P NMR spectroscopic data, but it could not be isolated in pure form. Two doublets at 94.5 and -129 ppm with a large $^1J_{\text{P,P}}$ coupling constant of 469 Hz in the ^{31}P NMR spectrum, evidenced the presence of the proposed $1\lambda^5, 2\lambda^3$ -diphosphinine in solution.⁶¹



Scheme 1.8. Synthesis of the 1,2-diphosphinine **XLIV**.⁶¹

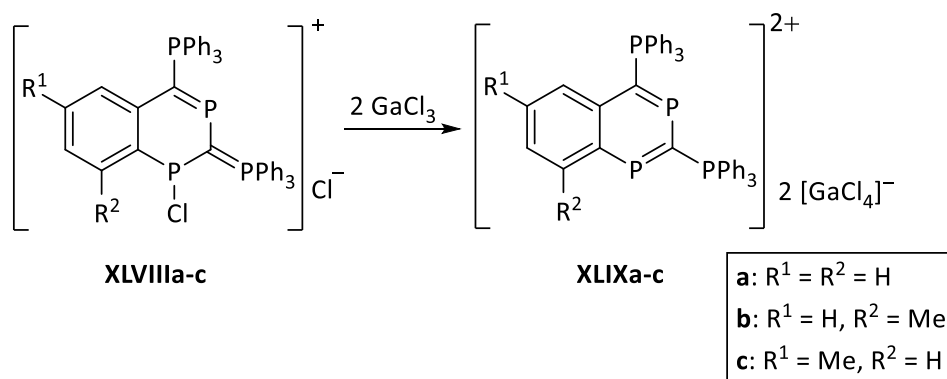
The chemistry of 1,3-diphosphinines is comparatively more developed. The first example of a stable $1\lambda^3, 3\lambda^3$ -diphosphinine **XLVII** was reported by Zenneck and co-workers via regioselective [2+2+2]-cycloaddition of two molecules of *tert*-butyl-phosphaethyne with a terminal alkyne in

the coordination sphere of an iron(0) complex followed by oxidation with CCl_4 at elevated temperature which led to the formation of the free 1,3-diphosphinine **XLVII** (Scheme 1.9).⁶²



Scheme 1.9. Synthesis of the first 1,3-diphosphinine **XLVII**.⁶²

As another example of a $1\lambda^3,3\lambda^3$ -diphosphinine, Jochem and Schmidpeter in 1996 reported the synthesis of bis-phosphonium substituted 1,3-diphosphinines **XLIX** via dechlorination of the corresponding 1,3-diphosphatetraline derivative **XLVIII**, using GaCl_3 (Scheme 1.10).⁶³



Scheme 1.10. Synthesis of bis-phosphonium substituted 1,3-diphosphinine **XLIX**.⁶³

$1\lambda^5,3\lambda^5$ -diphosphinines also have been studied, even in more detail compared to $1\lambda^3,3\lambda^3$ -diphosphinines and a wide range of these compounds are known in the literature, e.g., compound **L** (Figure 1.11) was reported by Fluck and co-workers as the product of a Diels-Alder reaction between their originally targeted 1,1,3,3,-tetrakis(dimethylamino)- $1\lambda^5,3\lambda^5$ -diphosphete and an alkyne.⁶⁴ The most stable derivative of $1\lambda^5,3\lambda^5$ -diphosphinines **LI** was synthesized by Märkl in 1963 via stepwise deprotonation of 1,1,3,3,-tetraphenyl-1,3-diphosphoniocyclohex-4-ene.⁶⁵

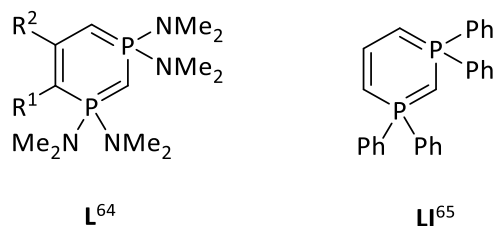
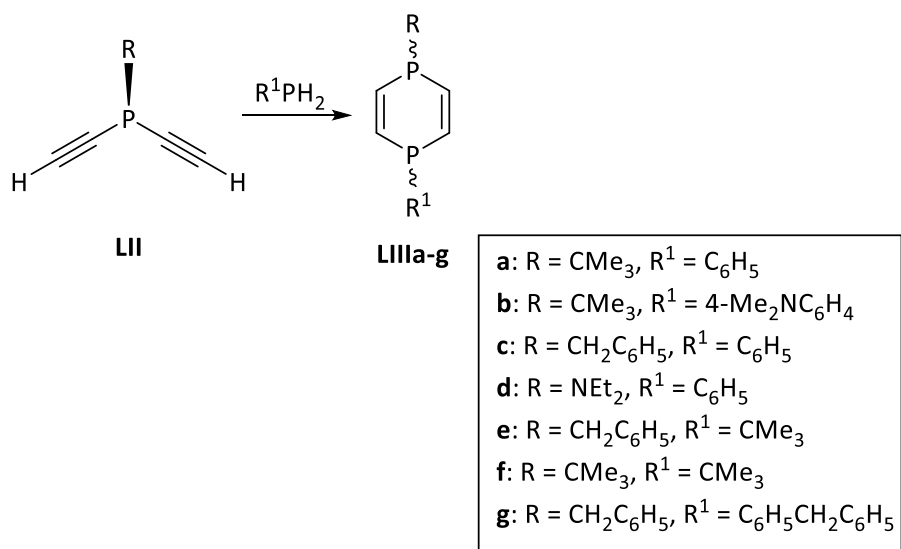


Figure 1.11. Examples of reported $1\lambda^5,3\lambda^5$ -diphosphinines.^{64,65}

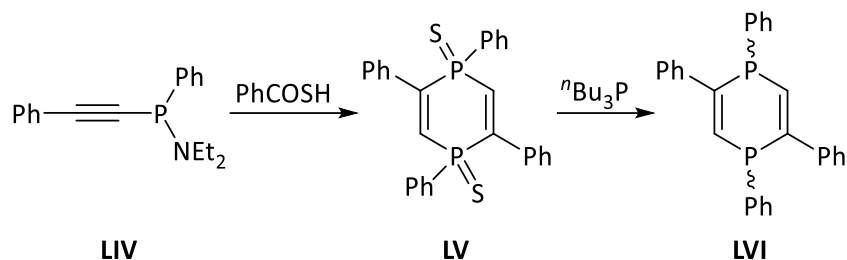
1.3.1 1,4-Dihydro-1,4-diphosphinines and 1,4-diphosphinines

Only a few examples of monocyclic 1,4-dihydro-1,4-diphosphinines have been reported in the literature⁶⁶, e.g., compound **LIII** was synthesized by Märkl *et al.* via the double hydrophosphinations of alkyldiethynylphosphane with alkylphosphanes (Scheme 1.11). The final product was obtained as a mixture of *cis* and *trans* isomers (55:45 ratio).⁶⁷



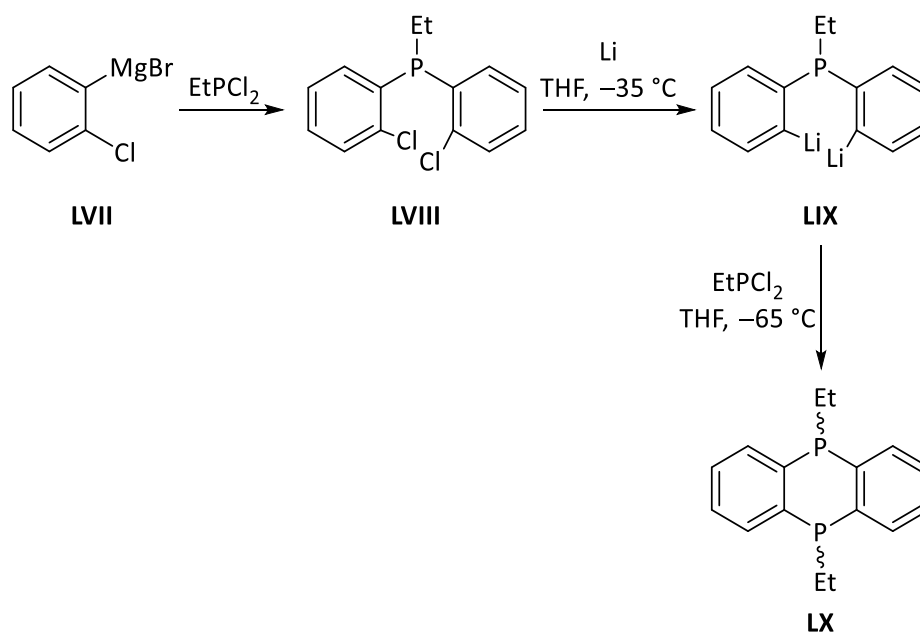
Scheme 1.11. Synthesis of monocyclic 1,4-dihydro-1,4-diphosphinines **LIIIIa-g** reported by Märkl *et al.*⁶⁷

As another example, the synthesis of compound **LVI** was achieved by the reaction of thio- or dithiocarbonic acids with ethynylaminophosphanes followed by desulfurization of the formed 1,4-dihydro- $1\lambda^5,4\lambda^5$ -diphosphinine-1,4-disulfides **LV** using tri-*n*-butylphosphane (Scheme 1.12).⁶⁸



Scheme 1.12. Synthesis of monocyclic 1,4-dihydro-1,4-diphosphinines **LVI**.⁶⁸

The first benzo-fused tricyclic 1,4-dihydro-1,4-diphosphinine was reported by Davis and Mann in 1964 via a stepwise ring-closing reaction with dichloro(organyl)phosphane. The bridging phosphinine intermediate **LVIII** was obtained by the reaction of dichloro(ethyl)phosphane with the Grignard reagent. This compound was further reacted with Li and subsequently EtPCl₂ to form the related 1,4-diethyl-1,4-diphosphinine **LX** (Scheme 1.13).⁶⁹ The structure and characterization of this compound were later reported by Akutsu.⁷⁰ Cullen *et al.* reported the synthesis of the similar fluorinated analog **LXI** (Figure 1.12) by reacting 1,2-diiodotetrafluorobenzene with MeLi, followed by the addition of PhPCl₂.⁷¹ Reaction of 4,5-dibromo-*o*-xylene with ⁿBuLi and PhPCl₂ yielded compound **LXII** (Figure 1.12).⁷²



Scheme 1.13. Synthesis of the first benzo-fused tricyclic 1,4-dihydro-1,4-diphosphinine.⁶⁹

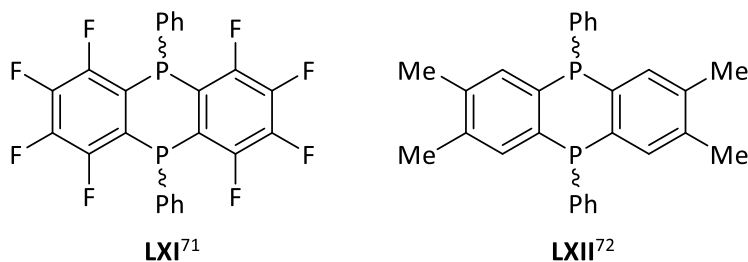


Figure 1.12. Examples of benzo-fused tricyclic 1,4-dihydro-1,4-diphosphinine.^{71,72}

Heterocycle-fused 1,4-dihydro-1,4-diphosphinines have been commonly synthesized via backbone lithiation of the corresponding heterocycles and subsequent reaction with dichloro(organyl)phosphanes, e.g., repeated lithiation followed by the addition of PhPCl_2 was employed by Ren *et al.* to achieve ladder-type π -conjugated 1,4-dihydro-1,4-diphosphinine **LXIII** (Figure 1.13).⁷³ Compound **LXIV** was also synthesized using a similar protocol.⁷⁴ Fenske and co-workers reported the synthesis of heterocycle-fused 1,4-diphosphinine **LXV** ($X = \text{O}, \text{S}$) using a different synthetic approach. Elimination of chlorotrimethylsilane in the reaction of dichloromaleic anhydride or thioanhydride with bis(trimethylsilyl)phenylphosphane led to the formation of **LXV**.⁷⁵ The first N-containing 1,4-dihydro-1,4-diphosphinines **LXVI** was reported by Ivonin and co-workers by reacting 2,5-dimethyl-*N*-aryl-pyrroles with PBr_3 in pyridine.⁷⁶ Reaction of 4-phosphanylated imidazoles with PCl_3 resulted in the formation of 1,4-dichloro-1,4-diphosphinine which was subsequently converted into compound **LXVII** by the addition of dimethylamine.⁷⁷ In 2004, Fourmigué and Avarvari reported the synthesis of 1,4-dihydro-1,4-diphosphinine fused to two TTF units **LXVIII** in a one-pot procedure by bis-lithiation of *ortho*-dimethyltetraathiafulvalene with LDA, followed by trapping the resulting dianion with one equivalent of phenyldichlorophosphane. This TTF “dimer” was obtained as a *cis/trans* mixture in which the *cis* isomer is largely predominant.³¹

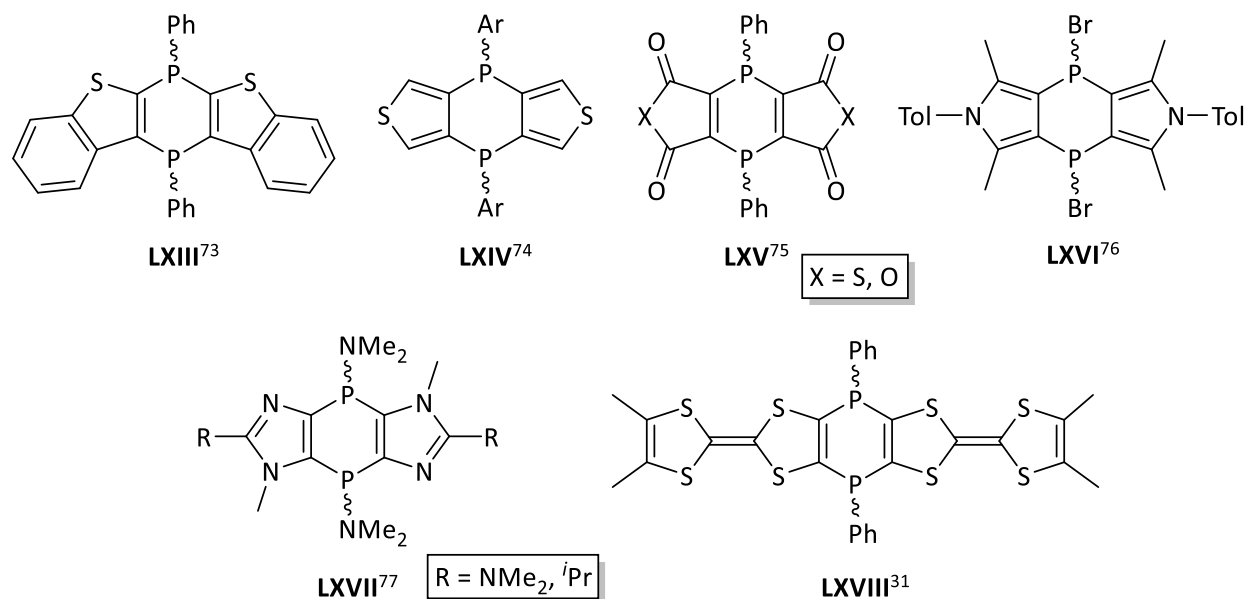
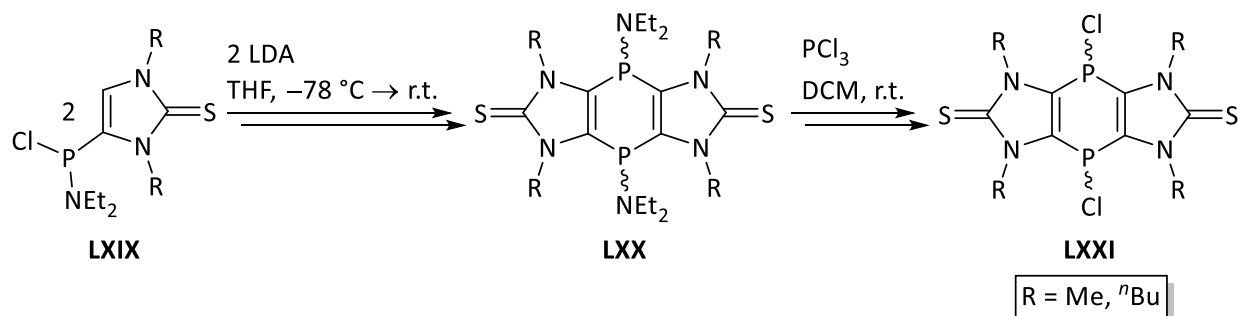


Figure 1.13. Examples of heterocycle-fused 1,4-dihydro-1,4-diphosphinines.^{31,73–77}

In recent years, a series of stepwise lithiation and phosphanylation of five-membered ring systems have been described by the Streubel group. Based on this background knowledge, Koner *et al.* reported the synthesis and reactivity of the first example of tricyclic 1,4-dihydro-1,4-diphosphinine fused to imidazole-2-thione **LXX**. The backbone C⁵–H of amino(chloro)phosphanyl imidazole-2-thione **LXIX** was deprotonated using lithium diisopropylamide (LDA) as the base and the subsequent intermolecular nucleophilic substitution reaction yielded **LXX** as a mixture of *cis/trans* stereoisomers. Compound **LXX** was further reacted with PCl₃ in dichloromethane to obtain the tricyclic P-Cl substituted derivative **LXXI** (Scheme 1.14).⁷⁸ Soon after, the heterocycle-fused 1,4-dihydro-1,4-diphosphinine chemistry was expanded to the thiazol-2-thiones⁷⁹, 1,3-dithiol-2-thione⁸⁰ and imidazole-2-selones⁸¹ motifs resulting in compounds **LXXII–LXXIV** (Figure 1.14).



Scheme 1.14. Synthesis of the first tricyclic 1,4-dihydro-1,4-diphosphinine fused to imidazole-2-thione **LXX**.⁷⁸

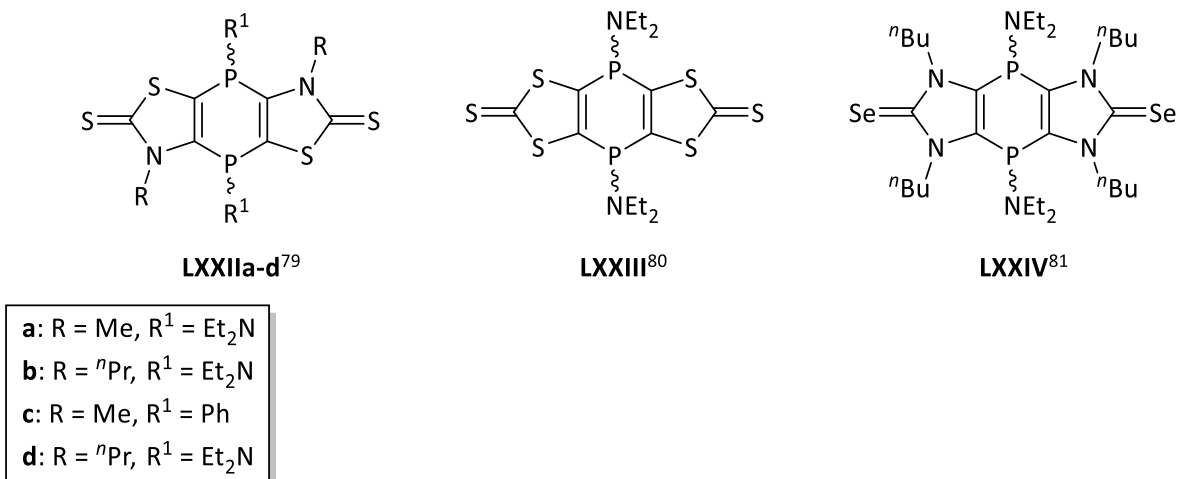
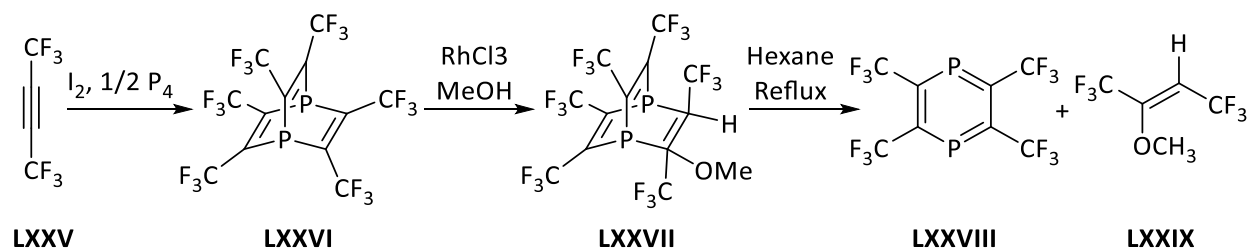
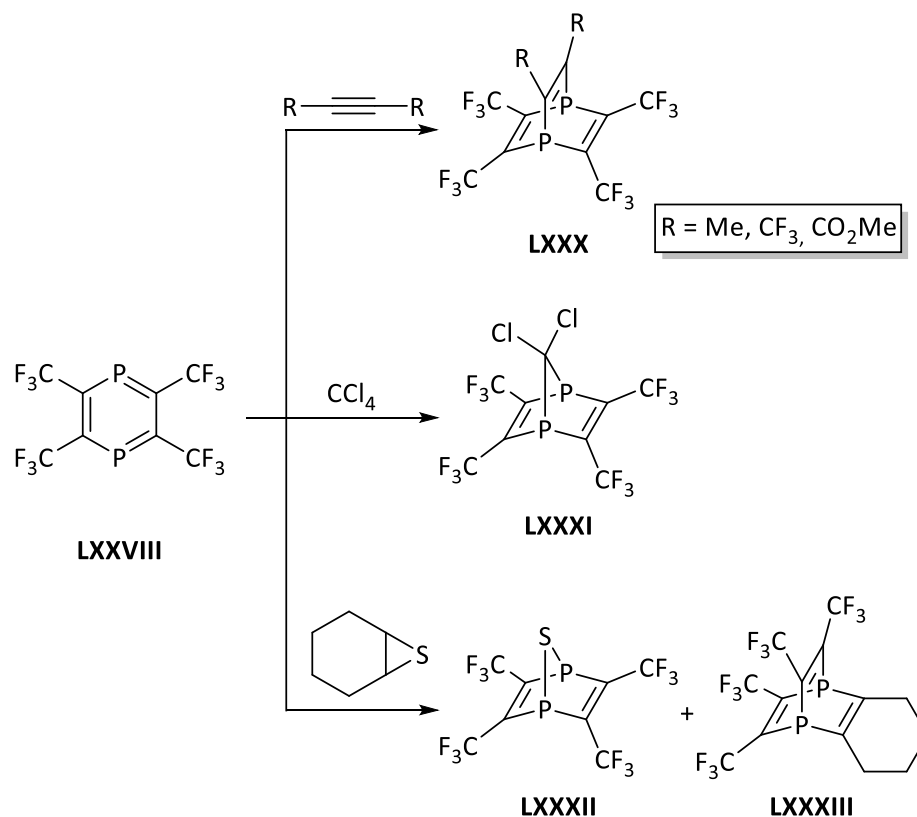


Figure 1.14. Reported 1,4-dihydro-1,4-diphosphinines by the Streubel group.^{79–81}

The first thermally stable $1\lambda^3,4\lambda^3$ -diphosphinine **LXXVIII** was reported by Kobayashi and co-workers. **LXXVIII** was obtained via a stepwise synthetic protocol in which rhodium trichloride catalyzes the addition of methanol to hexakis(trifluoromethyl)-1,4-diphosphabarrelene to form compound **LXXVII**. After refluxing in n-hexane, **LXXVII** eliminates the alkene fragment **LXXIX** and produces **LXXVIII** (Scheme 1.15).⁸² Due to its extreme air and moisture sensitivity, compound **LXXVIII** could only be obtained as an n-hexane solution, hence its chemistry remained largely unexplored and only a few reactions were reported, resulting in formal [4+1]- and [4+2]-cycloaddition reaction products (Scheme 1.16).^{83,84}

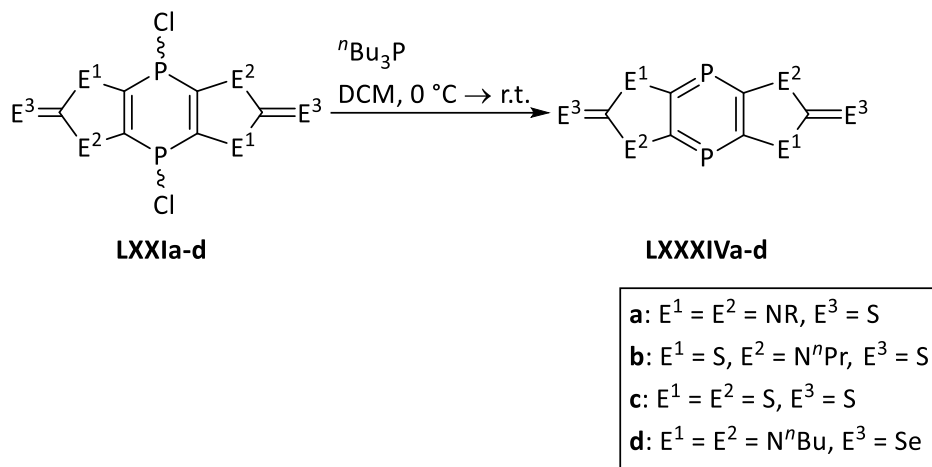


Scheme 1.15. Synthesis of the first 1,4-diphosphinine.⁸²

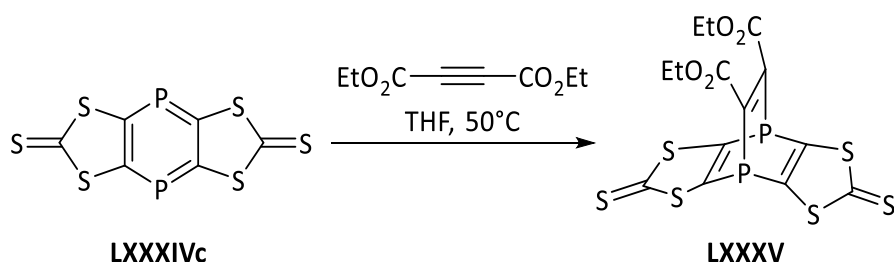


Scheme 1.16. Reactions of 1,4-diphosphinine **LXXVIII**.^{83,84}

The easy access to imidazole-2-thione-based tricyclic 1,4-dichloro-1,4-diphosphinines **LXXI** by Streubel and co-workers has revived this research area. Stable tricyclic $\sigma^2\lambda^3$ -diphosphinines were reported via selective reduction of the related tricyclic P-Cl-substituted derivatives (Scheme 1.17).^{78,80,81,85} In the case of the 1,3-dithiole-2-thione-based 1,4-diphosphinine, due to the insolubility of the related P-Cl precursor and also the desired product, **LXXXIVc** could not be isolated. To probe the assumption that the raw product mixture contained the tricyclic 1,4-diphosphinine, it was reacted with diethylacetylene dicarboxylate (DEAD) in THF at elevated temperature (Scheme 1.18). [4+2]-Cycloaddition product was isolated and characterized as an indirect proof of the formation of the desired 1,4-diphosphinine.⁸⁰



Scheme 1.17. Synthesis of stable tricyclic $\sigma^2\lambda^3$ -diphosphinines **LXXXIV** by the Streubel group.^{78,80,81,85}



Scheme 1.18. [4+2]-Cycloaddition reaction of **LXXXIVc** to form the related diphosphabarrelene **LXXXV**.⁸⁰

The reactivity of 1,4-diphosphinines can be predicted, to some extent, by their HOMO/LUMO symmetries and energies, as well as the degree of aromaticity compared to benzene. For **Me-LXXXIVa**, **Me-LXXXIVb** and **LXXXIVc**, calculations by Kalisch show similar π -symmetric geometries for both the HOMOs and LUMOs (Figure 1.15).⁶⁶ The HOMOs exhibit no contribution to the phosphorus atoms and consist of the antibonding combination of the HOMOs of the respective five-membered rings.⁷⁸ On the other hand, the good acceptor abilities of these compounds can be explained by their low energy LUMOs with π^* -symmetry of the LUMO of parent 1,4-diphosphinine^{66,78} and large contribution at phosphorus atoms. Also, the HOMO/LUMO gaps for the tricyclic 1,4-diphosphinines increase with a higher amount of sulfur in the related five-membered rings (Table 1.1).⁶⁶ NICS(0) and NICS(1) calculations show a decrease in aromaticity from benzene to phosphinine and 1,4-diphosphinine and also the same trend of decreasing aromaticity for **Me-LXXXIVa**, **Me-LXXXIVb** and **LXXXIVc** with the increase of the sulfur contents

(Table 1.1).⁸⁰ For all three tricyclic compounds, the central six-membered rings have higher aromaticity compared to the five-membered rings based on the calculated NICS values.

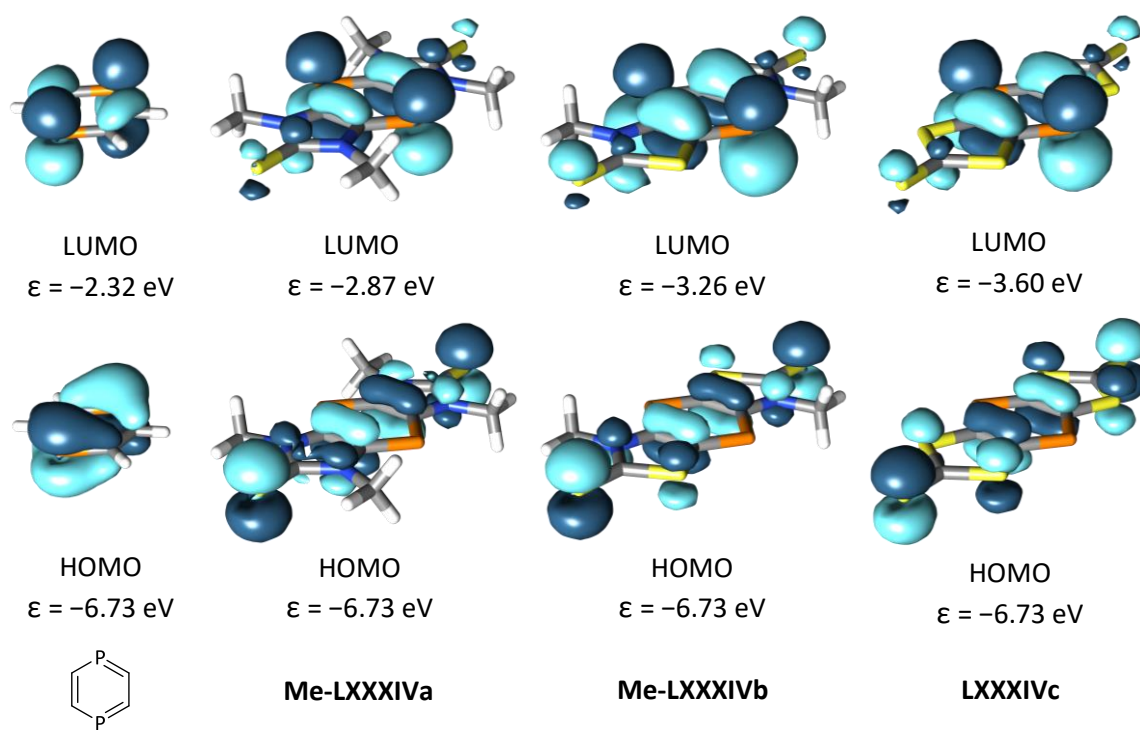
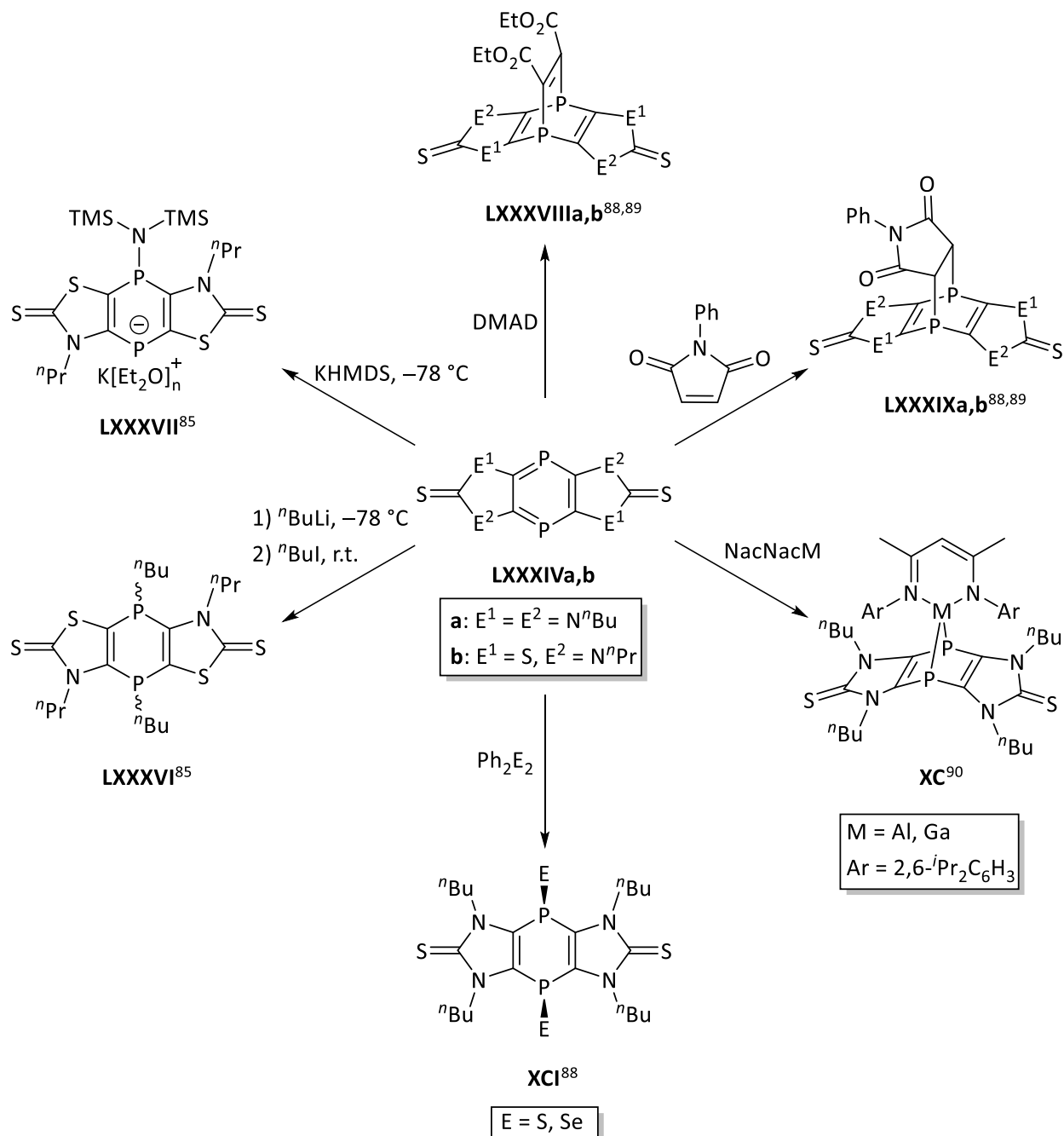


Figure 1.15. HOMO and LUMO Kohn–Sham molecular orbitals (TPSS-D3BJ/def2-TZVP//PW6B95-D3BJ/def2-QZVP) of 1,4-diphosphinines.⁶⁶

Table 1.1. Computed HOMO/LUMO gaps (eV), NICS(0) and NICS(1) values (ppm) for benzene⁸⁶, phosphinine, 1,4-diphosphinine⁸⁵, Me-LXXXIVa, Me-LXXXIVb and LXXXIVc.⁸⁷

Compound	HOMO/LUMO gap	Central ring		Outer ring	
		NICS(0)	NICS(1)	NICS(0)	NICS(1)
C_6H_6	–	–	–12.8	–	–
C_5H_5P	–	–	–11.4	–	–
$C_4H_4P_2$	–	–7.9	–10.4	–	–
Me-LXXXIVa	2.73	–6.9	–8.5	–6.8	–6.1
Me-LXXXIVb	2.86	–5.8	–7.6	–5.3	–4.4
LXXXIVc	3.01	–4.8	–6.6	–2.9	–2.8

The chemistry of **LXXXIVa,b** was further investigated in terms of reactivity studies, e.g., sequential reactions with nucleophiles and electrophiles, [4+2]- and [4+1]-cycloaddition reactions (Scheme 1.19).^{85,88–90}



Scheme 1.19. Reactivity studies of tricyclic 1,4-diphosphinines **LXXXIVa,b**.^{85,88–90}

2 Aim of this Ph.D. thesis

Based on this background, the aim of this thesis was to explore and exploit 1,4-diphosphinine chemistry by establishing it as a linker between two TTF units, thus enabling new P-functional redox systems.

The main goals of this Ph.D. thesis are:

- I. Synthesis and reactivity study of new phosphanylated TTFs, as well as the study of their redox properties.
- II. Synthesis and reactivity study of new 1,4-dihydro-1,4-diphosphinines and 1,4-diphosphinines fusing two TTF units; study of their redox properties and electronic communication between two TTF groups having an aromatic or non-aromatic middle ring as the linker.
- III. Transformation of 1,4-diphosphinines (from II) into novel 1,4-diphosphabarrelenes.

3 Mono P-functional phosphanylated tetrathiafulvalenes

3.1 Synthesis of P-functional tetrathiafulvalenes

In order to obtain phosphanylated tetrathiafulvalenes as precursors for low-coordinate phosphorus chemistry containing 1,4-dihydro-1,4-diphosphinine, the synthesis of unsubstituted and *ortho*-substituted TTFs was required. Tetrathiafulvalene (2,2'-bi(1,3-dithiolylidene)) **1a** (Figure 3.1) was synthesized following the literature-known protocols.⁹¹⁻⁹³ The synthesis of unsymmetrically substituted TTFs **1b,c** (Figure 3.1) was achieved by condensation between an iminium ion and a phosphonate ester, forming the central fulvalene bond in the final step.⁹⁴⁻⁹⁶

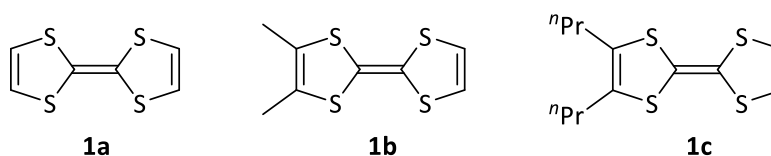
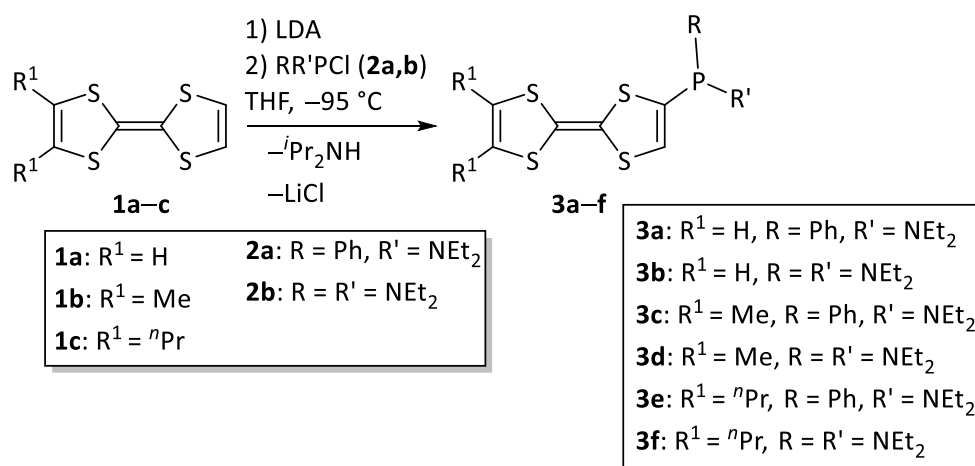


Figure 3.1. Tetrathiafulvalenes used as starting material according to known protocols.⁹¹⁻⁹⁶

To accomplish the synthesis of phosphanylated tetrathiafulvalenes, the synthetic protocol already established by Sauerbrey and Majhi⁹⁷ was employed, but with required modifications such as reaction time, temperature regime and the base (Scheme 3.1).



Scheme 3.1. Synthesis of phosphanylated TTFs **3a-f**.

Due to the possibility of a lithiation on both sides of the TTF molecule **1a**, LDA (instead of $n\text{BuLi}$) was used, to eliminate the chance of having an excess of base and ease the exact and quantitative addition. Also, to examine the stability of the lithiated species, *ortho*-dimethyl TTF **1b** was reacted with 1 eq. of LDA, and then the solution was subjected to a Variable Temperature NMR (VT NMR) spectroscopic study (Figure 3.2). It revealed that the lithiated TTF is not stable above $-70\text{ }^\circ\text{C}$ and the related resonance for $\text{C}^5\text{-H}$ in the ^1H NMR spectrum (at 5.4 ppm) decreased above this temperature and completely vanished at $-20\text{ }^\circ\text{C}$. Hence, in the lithiation step, the temperature was always kept between $-95\text{ }^\circ\text{C}$ and $-75\text{ }^\circ\text{C}$.

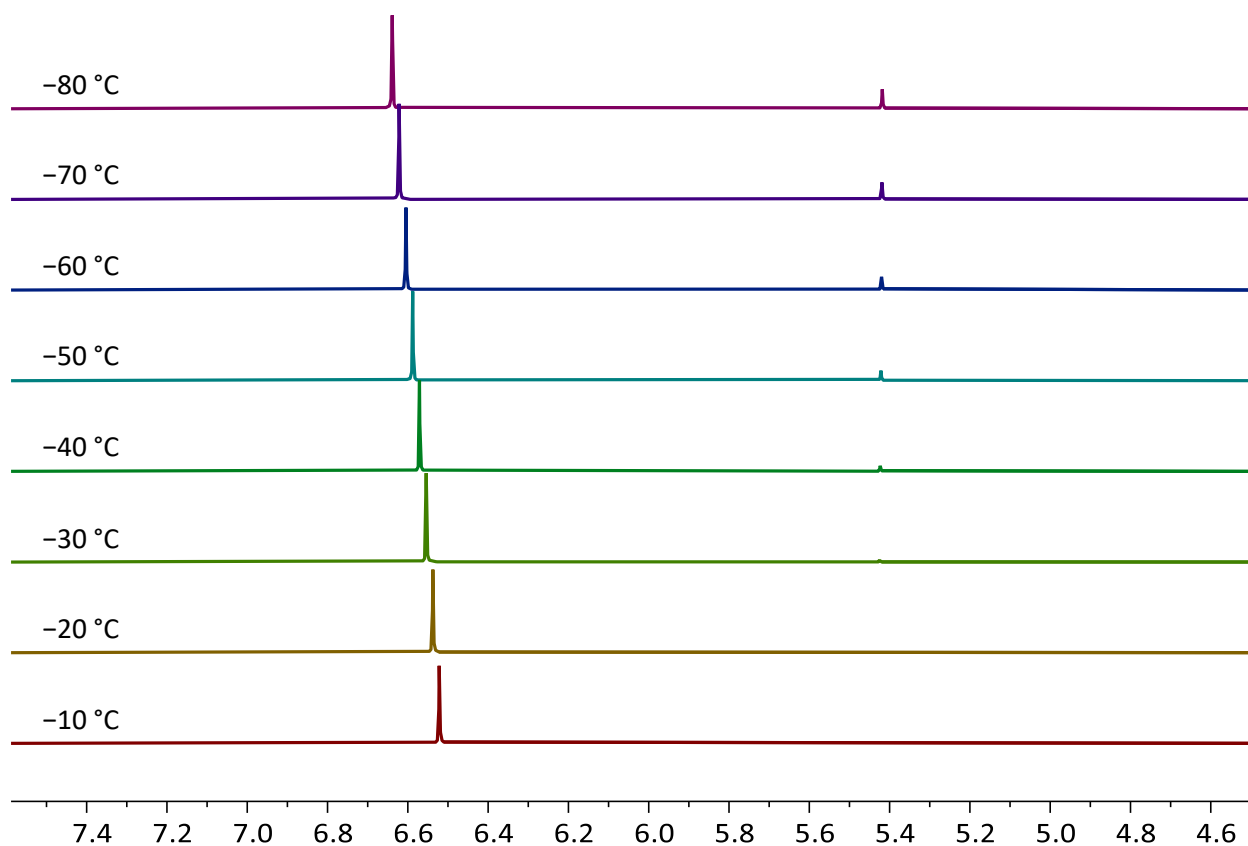


Figure 3.2. VT-NMR study of lithiated *ortho*-dimethyl TTF in THF-d_8 (resonance at 6.6 ppm is corresponding to $\text{C}^{4,5}\text{-H}$ in *ortho*-dimethyl TTF **1b**).

However, for **1a** completely selective lithiation and phosphanylation were not obtained even after trying various reaction conditions (different stirring times and temperature regimes). The best outcome was achieved by treating the THF solution of TTF **1a** with one equivalent of LDA at $-95\text{ }^\circ\text{C}$, stirring for three hours (between $-95\text{ }^\circ\text{C}$ and $-75\text{ }^\circ\text{C}$), followed by the addition of

chloro(diorganyl)phosphanes **2a,b** (Scheme 3.1). But in the case of **1b,c**, the desired products were formed selectively. The progress of each reaction was monitored by $^{31}\text{P}\{^1\text{H}\}$ NMR spectroscopy which showed new resonance signals (Table 3.1), while the starting phosphane signal had disappeared. These chemical shifts are comparable with the previously reported P-functional imidazole-2-thiones^{98,99}, thiazole-2-thiones¹⁰⁰, 1,3-dithiole-2-thiones⁸⁰ and imidazole-2-selones.¹⁰¹ After the removal of all volatiles in *vacuo* (8×10^{-3} mbar) and the LiCl salt via filtration, compounds **3c–f** were isolated in moderate to good yields (Table 3.1). These compounds were fully characterized by various analytical techniques including multinuclear NMR spectroscopy, mass spectrometry (MS) and elemental analysis (EA).

In case of **3a,b**, residues were subjected to room or low-temperature column chromatography to remove side-products (unreacted TTF and doubly-phosphanylated TTF). Also, the unreacted TTF was partially removed via sublimation out of the raw product using an ultrahigh vacuum pump (1×10^{-5} mbar). These purification attempts were met with limited success and pure compounds couldn't be obtained. However, ^1H , $^{13}\text{C}\{^1\text{H}\}$ and ^{31}P NMR spectroscopic and mass spectrometric data confirmed the formation of the desired products. Selected NMR data and (non-isolated) yields for compounds **3a–f** are given in Table 3.1.

Table 3.1. Selected NMR data (in CDCl_3) and yields (* via NMR integration) for compounds **3a–f**.

Compound	$\delta \text{ }^{31}\text{P}\{^1\text{H}\}/\text{ppm}$	$\delta \text{ }^1\text{H}/\text{ppm}$ ($\text{C}^5\text{--H}$)	$\delta \text{ }^{13}\text{C}\{^1\text{H}\}/\text{ppm}$ (C^4)	Yield%
3a	52.9	6.63 (<i>d</i> , $^3J_{\text{P,H}} = 9$ Hz)	138.6 (<i>d</i> , $^1J_{\text{P,C}} = 48.2$ Hz)	82*
3b	84.4	6.10 (<i>d</i> , $^3J_{\text{P,H}} = 1.7$ Hz)	140.3 (<i>d</i> , $^1J_{\text{P,C}} = 18.3$ Hz)	78*
3c	52.9	6.61 (<i>d</i> , $^3J_{\text{P,H}} = 8.9$ Hz)	138.4 (<i>d</i> , $^1J_{\text{P,C}} = 39.1$ Hz)	80
3d	84.7	6.09 (<i>d</i> , $^3J_{\text{P,H}} = 1.7$ Hz)	140.4 (<i>d</i> , $^1J_{\text{P,C}} = 18.4$ Hz)	50
3e	52.9	6.60 (<i>d</i> , $^3J_{\text{P,H}} = 9$ Hz)	138.4 (<i>d</i> , $^1J_{\text{P,C}} = 40.7$ Hz)	88
3f	84.7	6.09 (<i>d</i> , $^3J_{\text{P,H}} = 1.8$ Hz)	140.4 (<i>d</i> , $^1J_{\text{P,C}} = 18.1$ Hz)	70

Single crystals of **3c** and **3d**, suitable for X-ray diffraction measurements, were grown from their saturated diethylether solutions (Figure 3.3). Selected bond lengths and angles are given in Table 3.2.

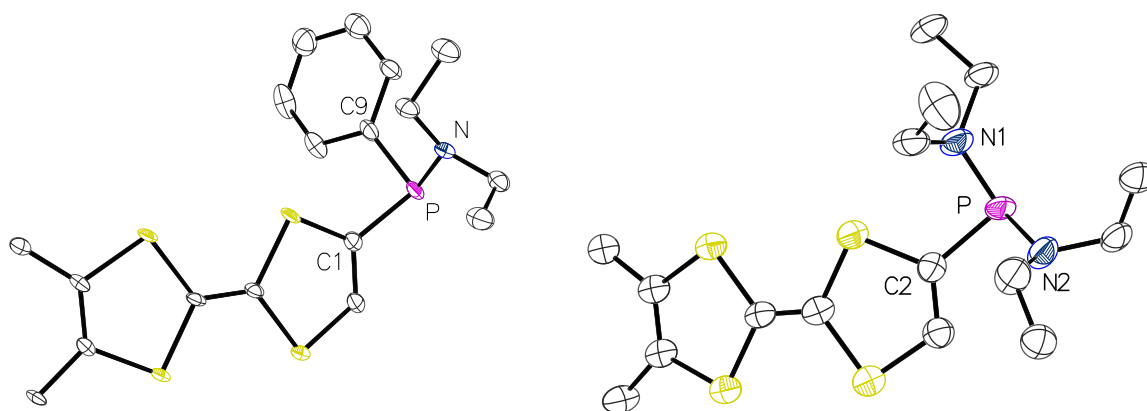


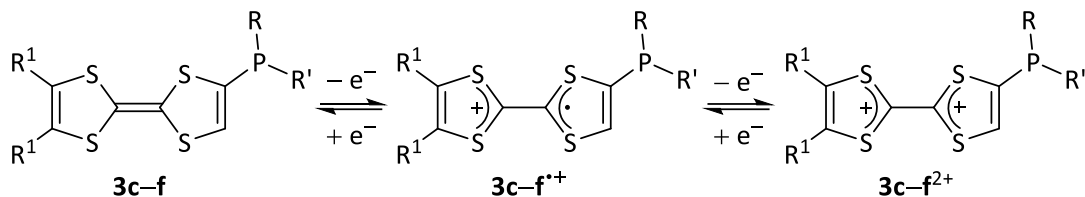
Figure 3.3. ORTEP drawings of the molecular structure of **3c** (left) and **3d** (right) in the solid state (ellipsoids are set at 50% probability level and hydrogen atoms are omitted for clarity).

Table 3.2. Selected bond lengths and angles for **3c** and **3d**.

Compound	P–C/Å	P–N/Å	$\Sigma(\angle P)/^\circ$	$\Sigma(\angle N)/^\circ$
3c	P–C1: 1.833(4)	P–N: 1.695(4)	308.73	353.3
	P–C9: 1.832(5)			
3d	P–C2: 1.828(17)	P–N1: 1.671(13)	312.4	$\Sigma(\angle N1)$: 357.4
		P–N2: 1.675(13)		$\Sigma(\angle N2)$: 352.2

3.2 Cyclic voltammetry studies of phosphanylated tetrathiafulvalenes

The electrochemical properties of **3c–f** were investigated by means of cyclic voltammetry using dichloromethane as solvent. For all of these compounds, two distinct redox waves were observed in the oxidation region (Figure 3.4, A5 and A8) which are corresponding to the sequential one-electron step processes, forming the related TTF radical cation and then dication (Scheme 3.2).¹⁰²



Scheme 3.2. Redox processes of **3c-f**.

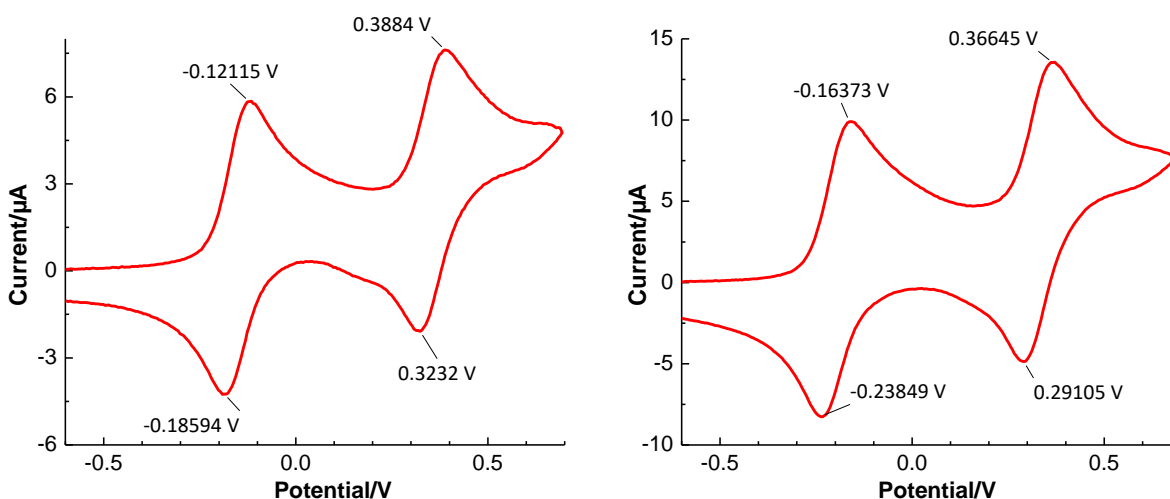


Figure 3.4. Cyclic voltammograms of **3c** (left) and **3d** (right) Vs. $\text{Fc}^{0/+}$ (0.4 M $n\text{Bu}_4\text{PF}_6$ in DCM, 100 mVs^{-1}).

A measure of the reversibility of the electrochemical processes is given by the difference between the anodic and cathodic peak potentials ΔE_p . For an electrochemically reversible redox process, a theoretical ΔE_p of $59 \text{ mV}/n$ (n is the number of transferred electrons) at room temperature is expected according to the Nernst equation. For a real measurement, however, the ΔE_p value of a reversible process is generally larger due to uncompensated solution resistance and non-linear diffusion.¹⁰³ $E_{1/2}$, ΔE_p and I_p values for the first and second redox waves, are given in Table 3.3. Based on the obtained data, these processes could be considered quasi-reversible.

In order to get a deeper insight into the electrochemical behavior of these compounds and study the effect of the substituents on redox potentials, DFT calculations were performed by Nyulaszi and co-workers. Investigating the Kohn-Sham molecular orbitals of **3a-d** at B3LYP/6-311+G**//M06-2X/6-311+G** level of theory revealed that, as expected, HOMO is mainly located on the TTF unit and also changing the substituent from phenyl to diethylamino group, has a minor effect on the energy level of the frontier orbitals (see Figures A52-A55 in the appendix). This aspect is reflected in the results of CV measurements, where the related

potentials for the first and second oxidation processes are reduced by only 0.05 and 0.03 V, from **3c,e** to **3d,f**, while changing the substituent on TTF unit has almost no effect on the redox potentials.

Additionally, CVs were recorded at various scan rates (50, 100, 200, 400 and 800 mVs⁻¹) (see the appendix). The plot of the anodic peak current versus the square root of the scan rates is depicted for both redox waves in Figure 3.5. The peak current linearly increased with respect to the square root of the scan rate based on the Randles–Ševčík equation (Equation 3.1), indicating the redox processes are diffusion controlled as another proof of electrochemical reversibility.

$$I_p = 0.4463 \cdot A \cdot C \sqrt{\frac{n^3 F^3 D \nu}{RT}} \quad (\text{Equation 3.1})$$

Where I_p is the peak current, A is the surface of the electrode, C is the concentration of the analyte, n is the number of transferred electrons in the redox process, F is Faraday coefficient, D is the diffusion coefficient, ν is the scan rate, R is the ideal rate constant and T is temperature.

Table 3.3. Half-wave potentials (Vs. Fc^{0/+}), ΔE_p , cathodic and anodic currents for **3c–f** (0.4 M ⁿBu₄PF₆ in DCM, 100 mVs⁻¹).

Compound	$E_{1/2}^1/V$	$\Delta E_p/mV$	$I_p^a/\mu A$	$I_p^c/\mu A$	$E_{1/2}^2/V$	$\Delta E_p/mV$	$I_p^a/\mu A$	$I_p^c/\mu A$
3c	-0.15	64.7	5.4	4.4	0.36	69.4	4.7	4.4
3d	-0.20	78.3	9.5	7.8	0.33	77.1	8.3	7.6
3e	-0.16	70.1	9.7	7.4	0.35	90.4	7.4	7.1
3f	-0.21	73.7	9.9	8.2	0.32	84.3	8.5	8.3

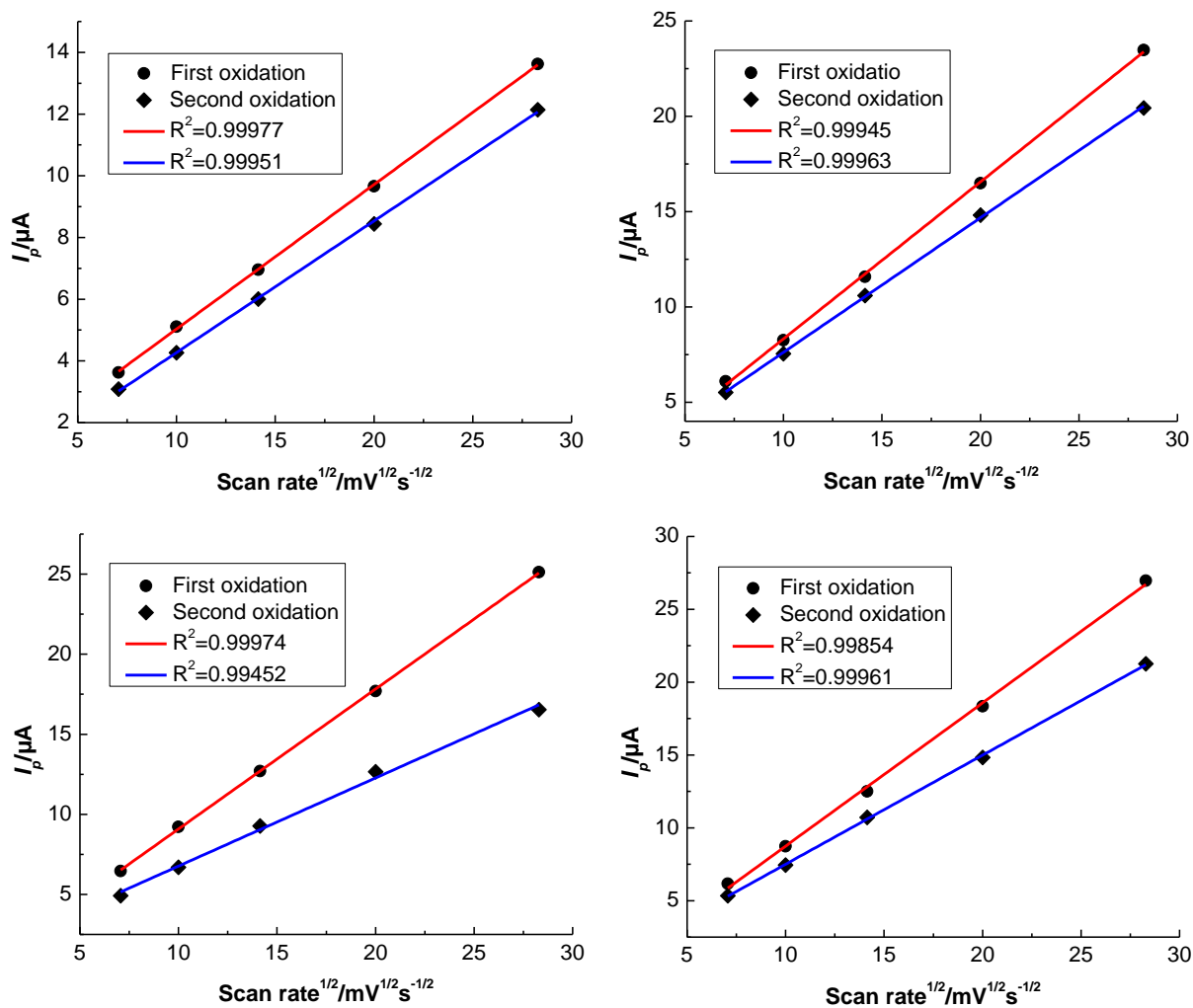
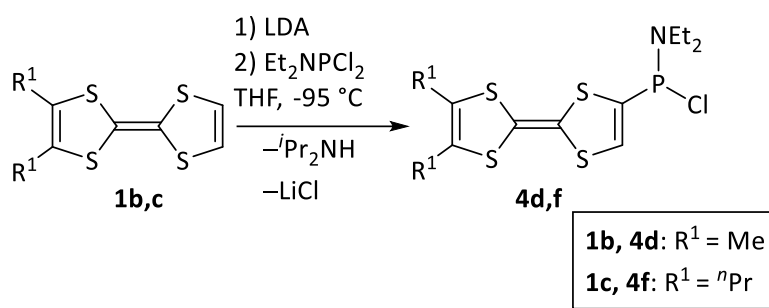


Figure 3.5. Dependency of the anodic peak currents on the scan rate for **3c** (top left), **3d** (top right), **3e** (bottom left) and **3f** (bottom right).

4 Chlorophosphanyl-substituted tetrathiafulvalenes

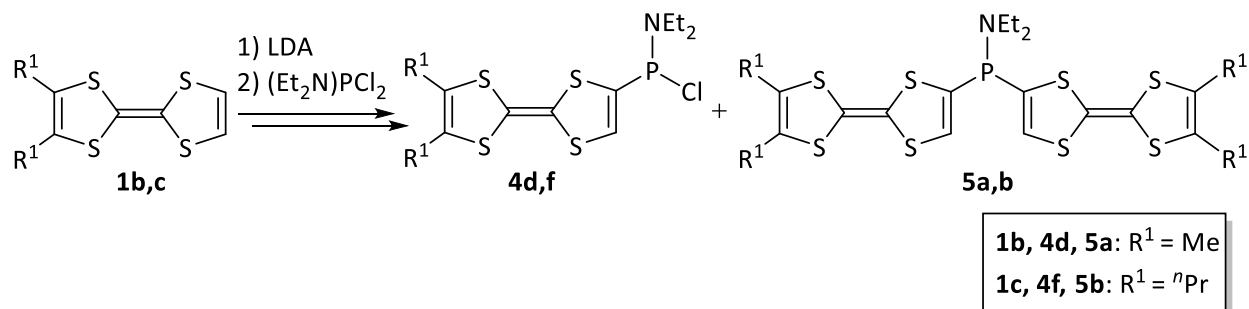
4.1 Synthesis of chlorophosphanyl-substituted tetrathiafulvalenes in one step

Aiming to employ the chlorophosphanyl-substituted TTFs in low-coordinate phosphorus chemistry, and targeting 1,4-dihydro-1,4-diphosphinines, the synthesis of such derivatives was required. To examine the possibility of the synthesis of the desired chloro(diethylamino)phosphanyl-substituted tetrathiafulvalenes in one step, *ortho*-substituted TTFs **1b,c** were lithiated by using LDA at $-95\text{ }^{\circ}\text{C}$ and subsequently reacted with one equivalent of Et_2NPCI_2 (Scheme 4.1).



Scheme 4.1. Proposed reaction pathway to synthesize chlorophosphanylated TTFs in one step.

$^{31}\text{P}\{^1\text{H}\}$ NMR spectroscopic monitoring revealed that in this reaction, in addition to the desired product (at 118 ppm), another major resonance appeared at around 42 ppm (with the ratio of 71:29 and 88:12 for the reactions using **1b** and **1c**, respectively) (Figure 4.1) which could be assigned to the related $P\text{-NEt}_2$ bridged compounds having two TTF units (Scheme 4.2).



Scheme 4.2. Proposed products for the reaction of **1b,c** with LDA and 1 eq. dichloro(diethylamino)phosphine.

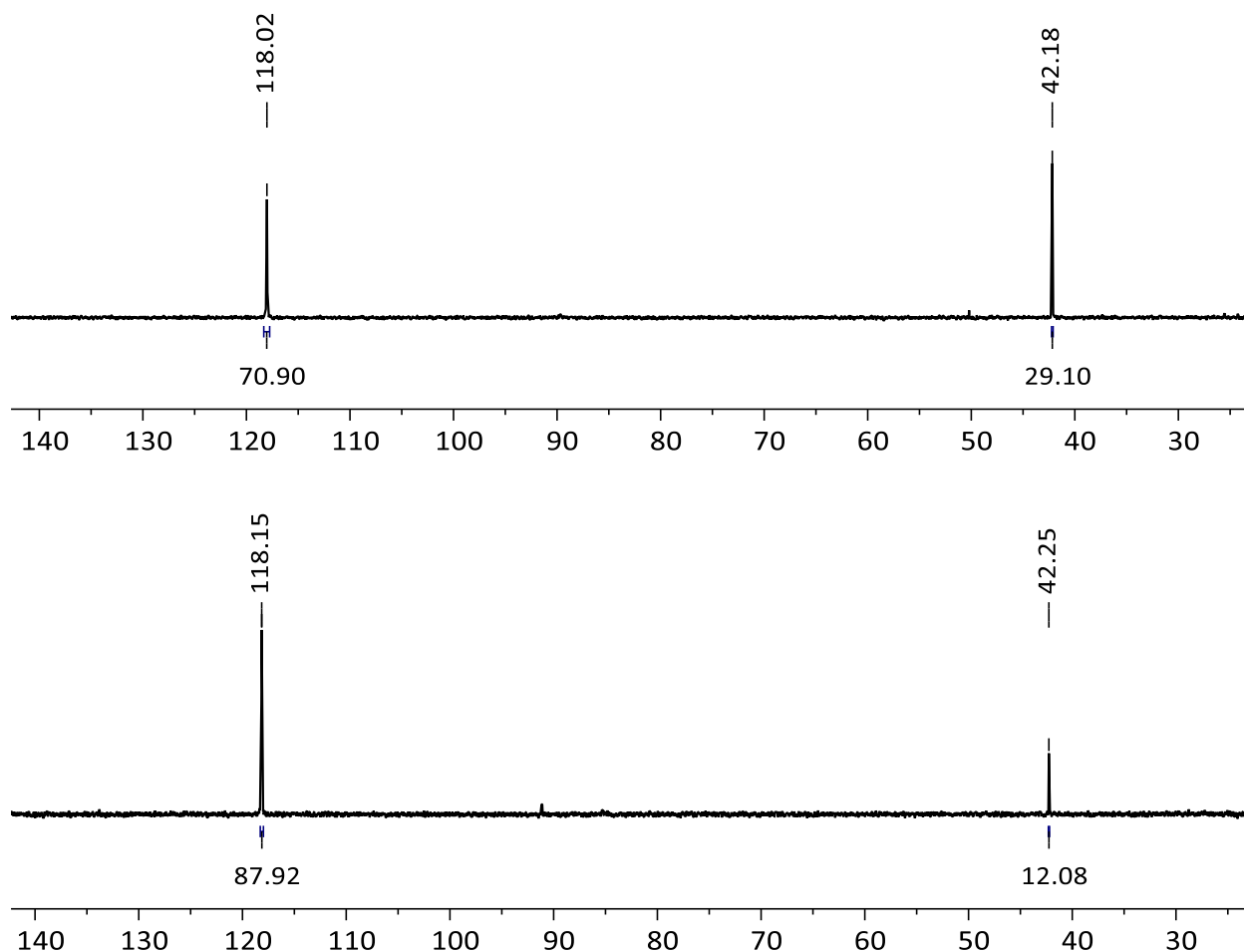
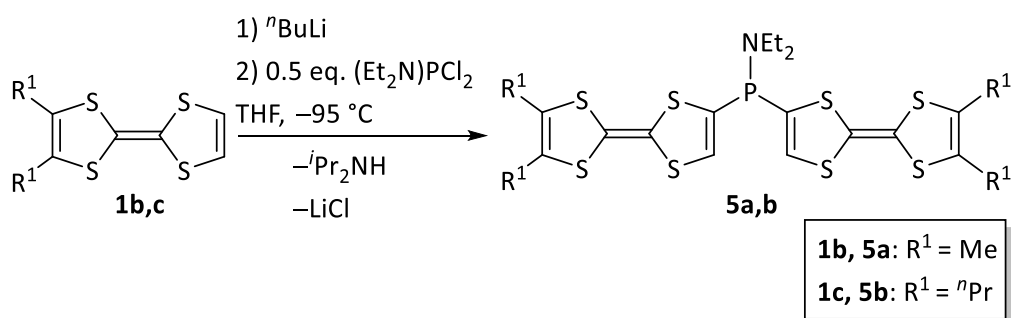


Figure 4.1. $^{31}\text{P}\{^1\text{H}\}$ NMR spectrum for the reaction of **1b** (top) and **1c** (bottom) with LDA and 1 eq. dichlorophosphane (reaction mixture).

4.1.1 Isolation of mono-bridged compounds **5a,b**

p-Block element-bridged TTF compounds can exhibit interesting electrochemical properties due to the possible electronic communication between the TTF units. Depending on the nature of the linkage, this communication can be promoted by through-bond or through-space interactions or shut down to achieve a mixed valance state.^{21–23} Different main group elements have been used to link two TTF units and form the $\text{X}(\text{TTF})_2$ type compounds, in which X stands for S, Se²⁸, Te²⁹, SiMe₂, Hg and PPh.³⁰ Since having a different bridging unit, can influence the degree of interaction between the TTF moieties and also affect the solubility of the “dimeric” compounds, isolation of these new bridged products was aimed.

In order to have the desired compound as the major product in the reaction, the protocol has been modified and only a half equivalent of Et_2NPCI_2 was used after the lithiation step (Scheme 4.3). $^{31}\text{P}\{^1\text{H}\}$ NMR spectroscopic monitoring showed the selective formation of **5a,b** and the products could be obtained in good yields after the removal of all volatiles in *vacuo* (8×10^{-3} mbar) and the LiCl salt via filtration. These compounds were characterized by multinuclear NMR spectroscopy and MS spectrometry. Selected NMR data and non-isolated yields are given in Table 4.1.



Scheme 4.3. Selective synthesis of mono-bridged compounds **5a,b**.

Table 4.1. Selected NMR data (in CDCl_3) and yields (via NMR integration) for **5a,b**.

Compound	$\delta \text{}^{31}\text{P}\{^1\text{H}\}/\text{ppm}$	$\delta \text{}^1\text{H}/\text{ppm}$ ($\text{C}^5\text{-H}$)	$\delta \text{}^{13}\text{C}\{^1\text{H}\}/\text{ppm}$ (C^4)	Yield%
5a	42	6.52 ($d, \text{}^3J_{\text{P,H}} = 7 \text{ Hz}$)	136.2 ($d, \text{}^1J_{\text{P,C}} = 40.6 \text{ Hz}$)	92
5b	42.1	6.52 ($d, \text{}^3J_{\text{P,H}} = 7 \text{ Hz}$)	136.3 ($d, \text{}^1J_{\text{P,C}} = 40.6 \text{ Hz}$)	92

4.1.2 Cyclic voltammetry studies of **5a,b**

For compounds with multi-stage redox properties, the nature of the cyclic voltammogram depends on $\Delta E_{1/2}$ ($E_{1/2}^2 - E_{1/2}^1$), the reversibility and the number of transferred electrons in each step.¹⁰⁴ Calculated cyclic voltammograms for different values of $\Delta E_{1/2}$ in a system with two one-electron steps were reported by Polcyn and Shain.¹⁰⁵ These calculations show when $\Delta E_{1/2} \geq 180$ mV, two well-separated waves are observed, while for $\Delta E_{1/2}$ between 0 and 100 mV, the individual waves are merged into a broad one. For $\Delta E_{1/2} = 0$, a single peak with a current between those of single-step one and two electrons transfer was found with $E_p^a - E_p^c = 21 \text{ mV}$.¹⁰⁵ Considering this background, the redox behavior of compounds with two TTFs in their structure,

depending on the degree of communication between two redox-active units can be divided into three main categories. i) If two TTF units have no interaction, i.e. oxidation of one TTF molecule does not affect the oxidation potential of the other TTF unit, the cyclic voltammogram shows only two redox waves, each representing a two-electron transfer process³³; ii) For compounds with strong communication between TTF units, four separate one-electron transfer processes are expected^{21,106}; iii) In weakly interacting systems, the separation between oxidation potentials are smaller and hence broad waves, sometimes with no clear separation, in cyclic voltammograms are expected. In these cases, it is also possible that the third and fourth oxidations occur in a single potential together with an enlarged current and narrow peak.^{30–32}

To investigate the electrochemical properties of **5a,b** cyclic voltammetry studies were performed in dichloromethane. For **5a** Three distinct oxidation processes were observed, while four waves were detected for **5b** (Figure 4.2). These processes could be attributed to the sequential formation of the related radical cation and then dication followed by further oxidation to the tri- and tetracationic species. Due to the lower solubility of the oxidized species for **5a** and adsorption/precipitation phenomena at the surface of the electrode, the last two oxidations were recorded as a broad wave along with a two-electron reduction at a single potential (note the increase in the related cathodic current in Table 4.2), while sequential oxidation to the tri- and tetracations was observed for **5b** (Figure 4.2).

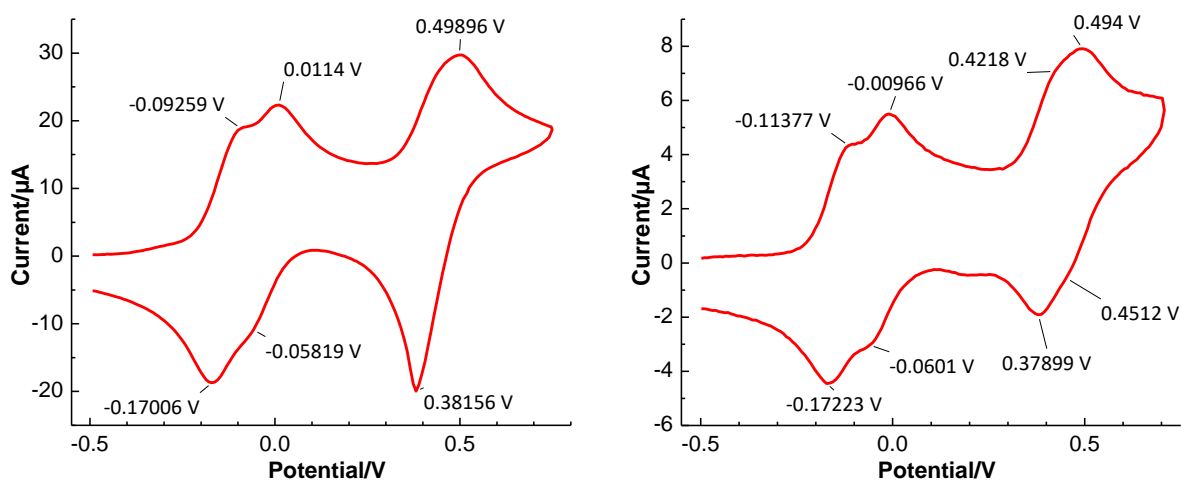


Figure 4.2. Cyclic voltammograms of **5a** (left) and **5b** (right) Vs. $\text{Fc}^{0/+}$ (0.4 M $n\text{Bu}_4\text{PF}_6$ in DCM, 200 mVs^{-1}).

The separation between the two first redox potentials, also third and fourth in the case of **5b** (Table 4.2) are of particular interest. These values are in good agreement with the previously reported compounds, having a main group element as the bridge between two TTF moieties^{28–30}, but smaller than the cases where the two redox-active units are connected via an aromatic linker.¹⁰⁶ $E_{1/2}$, ΔE_p and I_p values, obtained from voltammograms are given in Table 4.2., which are indicating the quasi-reversibility of the first two oxidation processes. However, due to the adsorption/precipitation of the analyte at the surface of the electrode for **5a** and the proximity of the third and fourth oxidation potentials for **5b**, the ΔE_p values for these processes deviated from the Nernst equation.

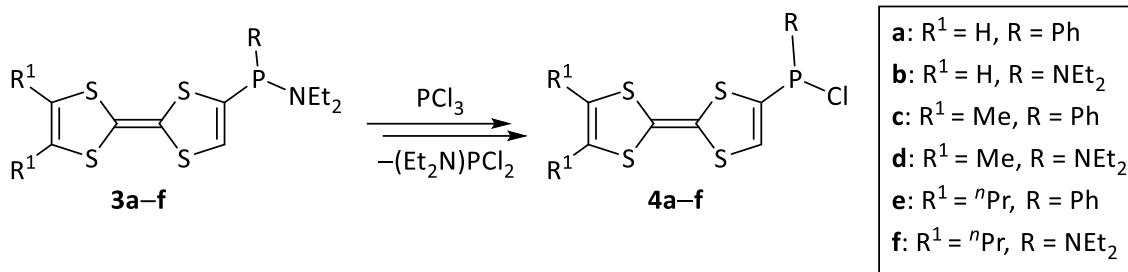
Table 4.2. Half wave potentials (Vs. $\text{Fc}^{0/+}$), $\Delta E_{1/2}$, cathodic and anodic currents for **5a,b** (0.4 M $n\text{Bu}_4\text{PF}_6$ in DCM, 200 mVs^{-1}).

Compound	$E_{1/2}^1/\text{V}$ ($\Delta E_p/\text{mV}$)	$E_{1/2}^{1'}/\text{V}$ ($\Delta E_p/\text{mV}$)	$\Delta E_{1/2}^{1,1'}$	$E_{1/2}^2/\text{V}$ ($\Delta E_p/\text{mV}$)	$E_{1/2}^{2'}/\text{V}$ ($\Delta E_p/\text{mV}$)	$\Delta E_{1/2}^{2,2'}$
	$[I_p^a: I_p^c/\mu\text{A}]$	$[I_p^a: I_p^c/\mu\text{A}]$	/mV	$[I_p^a: I_p^c/\mu\text{A}]$	$[I_p^a: I_p^c/\mu\text{A}]$	/mV
5a	-0.13 (77.5) [15.9:17.1]	-0.03 (69.6) [15:12.4]	110	0.44 (117.4) [16.1:28.6]	–	–
5b	-0.14 (66.8) [4.0:3.7]	-0.04 (54.5) [3.2:2.8]	100	0.40 (42.8) [3.6:3.1]	0.47 (42.8) [3.0:2.0]	70

4.2 Exchanging one amino group for a chlorine atom

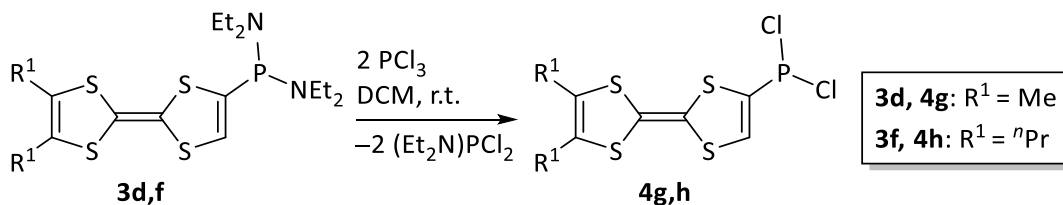
To achieve the selective formation of the chlorophosphanyl-substituted tetrathiafulvalenes, compounds **3a–f** were subjected to a scrambling reaction (σ bond metathesis) using PCl_3 (Scheme 4.4). In the case of **3a**, **3c** and **3e** reactions were performed in dichloromethane at room temperature and $^{31}\text{P}\{^1\text{H}\}$ NMR spectroscopic monitoring showed the selective formation of the desired products by the appearance of a new resonance signal at around 64 ppm while the precursor signal had vanished. But for **3b**, **3d** and **3f** the same reaction condition was resulting in the formation of a mixture of chloro(diethylamino) and dichlorophosphanylated TTFs (with $^{31}\text{P}\{^1\text{H}\}$ NMR chemical shifts at 118 and 135 ppm respectively). The possibility of exchanging both diethylamino groups for two chlorine atoms was avoided by performing reactions in diethylether at low temperature and after trying different reaction conditions, $^{31}\text{P}\{^1\text{H}\}$ NMR monitoring

revealed that reactions were completed after 1 hour at $-90\text{ }^{\circ}\text{C}$ and amino(chloro)phosphanyl-substituted TTFs **5b,d,f** were formed selectively.



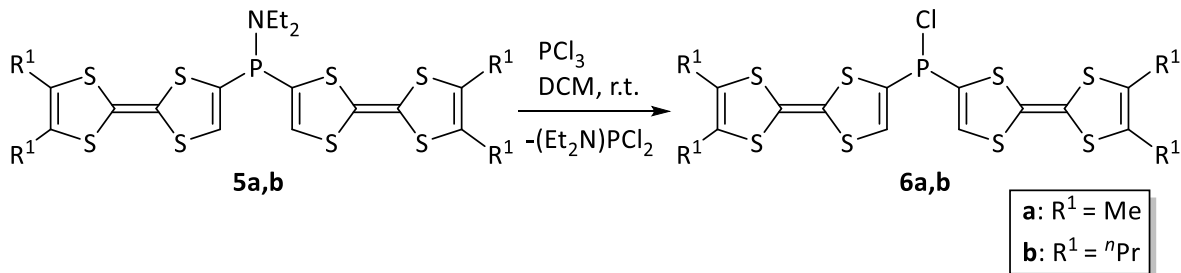
Scheme 4.4. The scrambling reaction of **3a–f** with PCl_3 .

Selective formation of dichlorophosphanylated TTFs was examined by the reaction of **3d** and **3f** with two equivalents of PCl_3 in dichloromethane at room temperature (Scheme 4.5). Exchanging both amino groups for chlorine atoms was achieved after 3 hours based on the $^{31}\text{P}\{^1\text{H}\}$ NMR spectroscopic monitoring.



Scheme 4.5. Selective formation of dichlorophosphanylated TTFs **4g,h**.

In addition, compounds **5a,b** were also subjected to scrambling reactions. For these compounds, the same reaction condition as for **3a,c,e** was applied (Scheme 4.6), and the desired products were formed selectively after 3 hours.



Scheme 4.6. The scrambling reaction of **5a,b** with PCl_3 .

After removal of all volatiles in *vacuo* (8×10^{-3} mbar), products were extracted from the crude, using diethylether (**4a–h** and **6b**) or toluene (**6a**), and could be obtained in moderate to excellent yields (Table 4.3). These compounds were characterized by various analytical techniques including multinuclear NMR spectroscopy and MS spectrometry.

Table 4.3. Selected NMR data (in CDCl₃) and yields (* via NMR integration only) for compounds **4a–f** and **6a,b**.

Compound	δ ³¹ P{ ¹ H}/ppm	δ ¹ H/ppm (C ⁵ –H)	δ ¹³ C{ ¹ H}/ppm (C ⁴)	Yield%
4a	63.9	6.96 (<i>d</i> , ³ <i>J</i> _{P,H} = 10.8 Hz)	136.7 (<i>d</i> , ¹ <i>J</i> _{P,C} = 61.2 Hz)	85*
4b	117.9	6.73 (<i>d</i> , ³ <i>J</i> _{P,H} = 2.6 Hz)	136.9 (<i>d</i> , ¹ <i>J</i> _{P,C} = 50.9 Hz)	95*
4c	64	6.95 (<i>d</i> , ³ <i>J</i> _{P,H} = 10.7 Hz)	136.6 (<i>d</i> , ¹ <i>J</i> _{P,C} = 60.6 Hz)	90
4d	118.2	6.72 (<i>d</i> , ³ <i>J</i> _{P,H} = 2.7 Hz)	136.8 (<i>d</i> , ¹ <i>J</i> _{P,C} = 51. Hz)	95
4e	64.1	6.95 (<i>d</i> , ³ <i>J</i> _{P,H} = 10.7 Hz)	136.6 (<i>d</i> , ¹ <i>J</i> _{P,C} = 60.4 Hz)	98
4f	118.4	6.72 (<i>d</i> , ³ <i>J</i> _{P,H} = 2.6 Hz)	136.8 (<i>d</i> , ¹ <i>J</i> _{P,C} = 50.8 Hz)	100
4g	134.2	7.12 (<i>d</i> , ³ <i>J</i> _{P,H} = 12.8 Hz)	138.7 (<i>d</i> , ¹ <i>J</i> _{P,C} = 77.2 Hz)	98
4h	134.3	7.12 (<i>d</i> , ³ <i>J</i> _{P,H} = 12.9 Hz)	138.7 (<i>d</i> , ¹ <i>J</i> _{P,C} = 77.1 Hz)	92
6a	48.6	6.92 (<i>d</i> , ³ <i>J</i> _{P,H} = 11.2 Hz)	133.6 (<i>d</i> , ¹ <i>J</i> _{P,C} = 54.6 Hz)	71
6b	48.8	6.92 (<i>d</i> , ³ <i>J</i> _{P,H} = 11.2 Hz)	133.6 (<i>d</i> , ¹ <i>J</i> _{P,C} = 54.7 Hz)	80*

4.3 Cyclic voltammetry studies of chlorophosphanyl-substituted TTFs

The electrochemical properties of **4c–f** were investigated by employing cyclic voltammetry, and dichloromethane was used as solvent. Same as for **3c–f**, these compounds exhibited two distinct redox processes in the oxidation region (Figure 4.3, A15 and A17), which could be attributed to the stepwise formation of the related radical cation and dication. To evaluate the reversibility of these processes, $E_{1/2}$, ΔE_p and I_p values are extracted from cyclic voltammograms and given in Table 4.4. Based on the obtained data, these processes could be considered quasi-reversible. It is also noteworthy that the exchange of one amino group with a chlorine atom, increases the

oxidation potentials by around 0.1 V, while the related potentials are reduced by 0.04 and 0.07 V, from **4c** to **4d** and **4e** to **4f**, respectively.

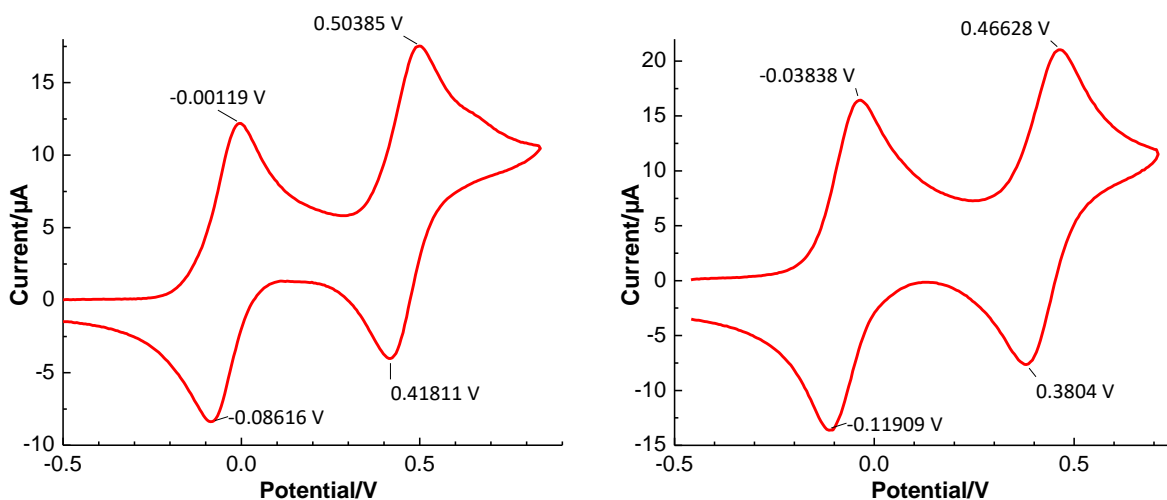


Figure 4.3. Cyclic voltammograms of **4c** (left) and **4d** (right) Vs. $\text{Fc}^{0/+}$ (0.4 M $t\text{Bu}_4\text{PF}_6$ in DCM, 200 mVs^{-1}).

Table 4.4. Half wave potentials (Vs. $\text{Fc}^{0/+}$), ΔE_p , cathodic and anodic currents for oxidation processes of **4c–f** (0.4 M $t\text{Bu}_4\text{PF}_6$ in DCM, 200 mVs^{-1}).

Compound	$E_{1/2}^1/\text{V}$	$\Delta E_p/\text{mV}$	$I_p^a/\mu\text{A}$	$I_p^c/\mu\text{A}$	$E_{1/2}^2/\text{V}$	$\Delta E_p/\text{mV}$	$I_p^a/\mu\text{A}$	$I_p^c/\mu\text{A}$
4c	-0.04	80.2	12.0	9.7	0.46	80.5	11.5	10.2
4d	-0.08	80.2	15.5	13.0	0.42	81	13.5	12.6
4e	-0.03	65.2	11.4	9.7	0.47	85.8	12.2	9.5
4f	-0.10	75.1	15.5	13.4	0.40	95.6	12.6	12.6

4.4 Reduction of chloro(diethylamino)phosphanyl-substituted TTFs

4.4.1 Electrochemical reduction of **4d,f**

For compounds **4d,e,f**, in addition to the two oxidation processes, irreversible reductions were observed in the CV experiments (Figure 4.4) which could be interpreted as one-electron reduction followed by the cleavage of the P–Cl bond. Reduction potentials and related peak currents are given in Table 4.5. Also during the course of the CV measurements for **5d** and **5f**, the

shape of the previously described redox waves changed (Figure 4.5). This is likely due to the presence of new species, generated upon the reduction of the original compounds.

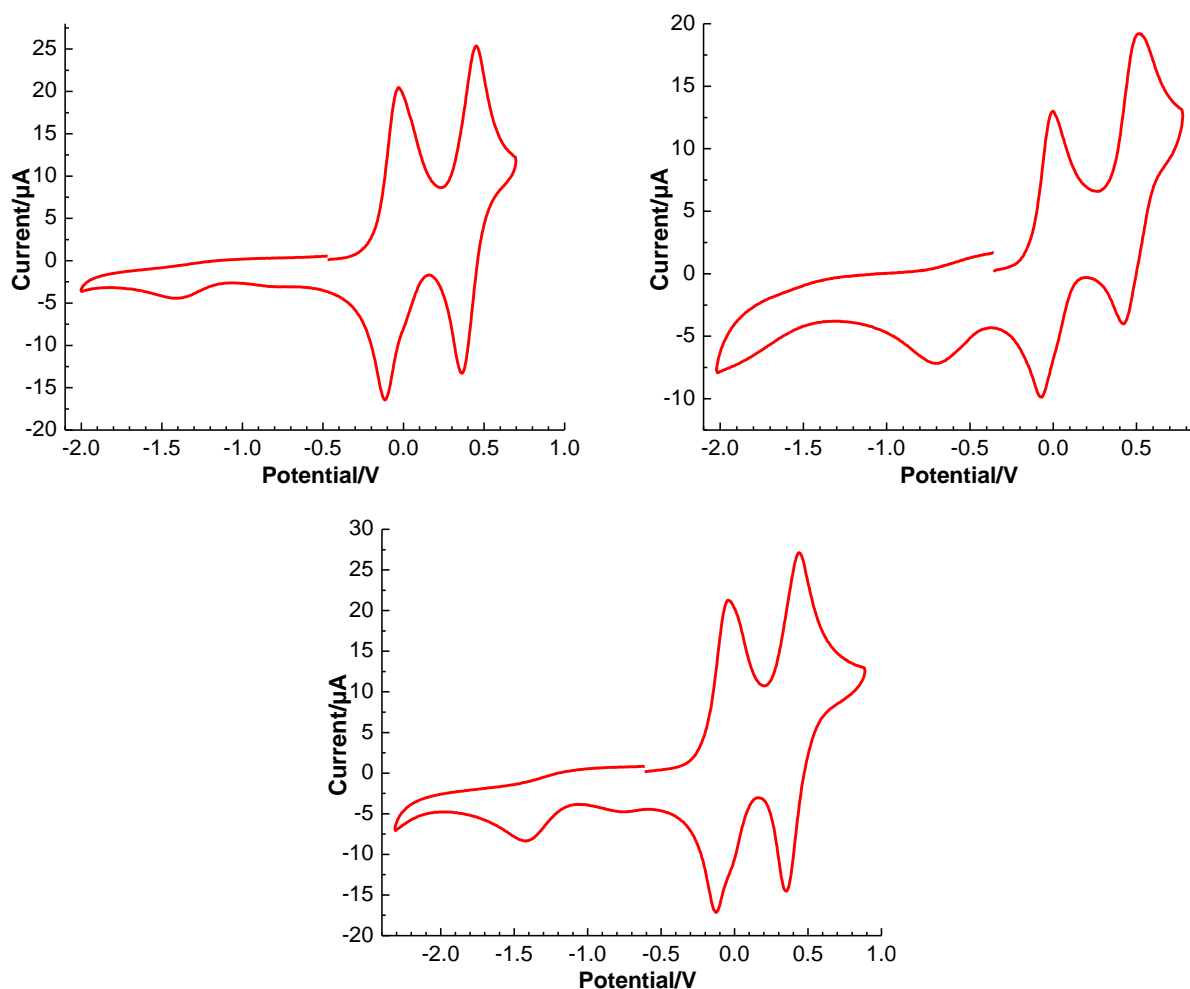


Figure 4.4. Cyclic voltammograms (wide range) of **4d** (top left), **4e** (top right) and **4f** (bottom) Vs. $\text{Fc}^{0/+}$ (0.4 M $n\text{Bu}_4\text{PF}_6$ in DCM, 200 mVs^{-1}).

Table 4.5. Reduction potentials (Vs. $\text{Fc}^{0/+}$) and related peak currents for **4d–f** (0.4 M $n\text{Bu}_4\text{PF}_6$ in DCM, 200 mVs^{-1}).

Compound	E_p^{c1}/V	$I_p^{c1}/\mu\text{A}$	E_p^{c2}/V	$I_p^{c2}/\mu\text{A}$
4d	-1.40	1.8	–	–
4e	-0.71	2.8	–	–
4f	-0.75	1.1	-1.42	4.1

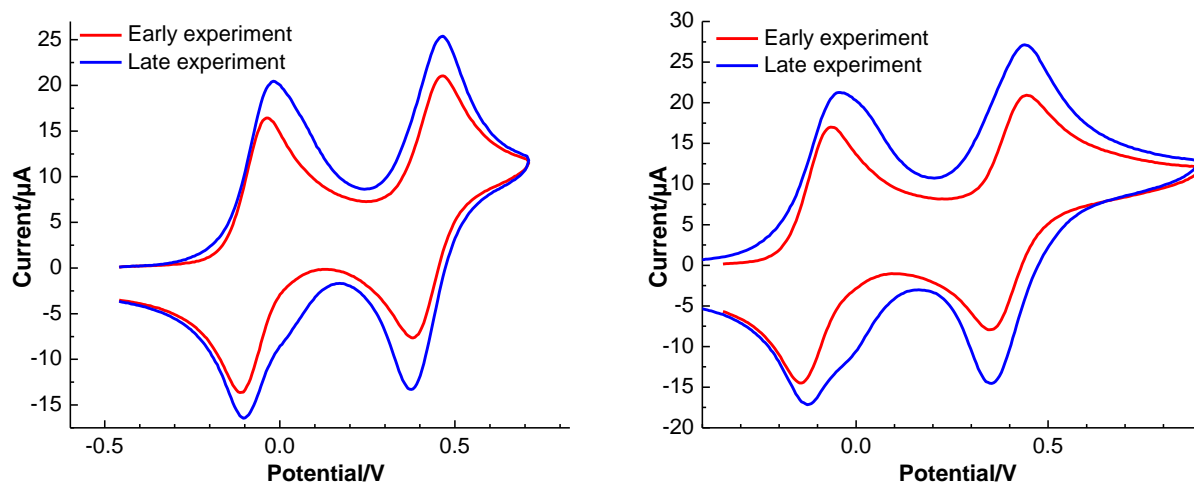


Figure 4.5. Change in the shape of cyclic voltammograms during measurement for **4d** (left) and **4f** (right) (Vs. $\text{Fc}^{0/+}$, 0.4 M $n\text{Bu}_4\text{PF}_6$ in DCM, 200 mVs^{-1}) (Early experiment: measurement after having the compound in DCM solution for few minutes; late experiment: measurement after having the compound for around half an hour in DCM solution during the course of CV studies).

To have a closer look into these reduction processes, cyclic voltammetry studies were conducted for compound **4d** in acetonitrile and THF to enable the possibility of scanning lower potentials. In both solvents, two irreversible reduction waves were observed (Figure 4.6), but in the case of acetonitrile, these processes occurred at higher potentials, indicating the relatively easier reduction of **4d** (Table 4.6).

Table 4.6. Reduction potentials (Vs. $\text{Fc}^{0/+}$) and related peak currents for **4d** in MeCN (0.1 M $n\text{Bu}_4\text{PF}_6$) and THF (0.2 M $n\text{Bu}_4\text{PF}_6$) at 200 mVs^{-1} .

Solvent	E_p^{c1}/V	$I_p^{c1}/\mu\text{A}$	E_p^{c2}/V	$I_p^{c2}/\mu\text{A}$
MeCN	-1.04	1.1	-1.41	2.6
THF	-1.51	1.2	-2.33	1.0

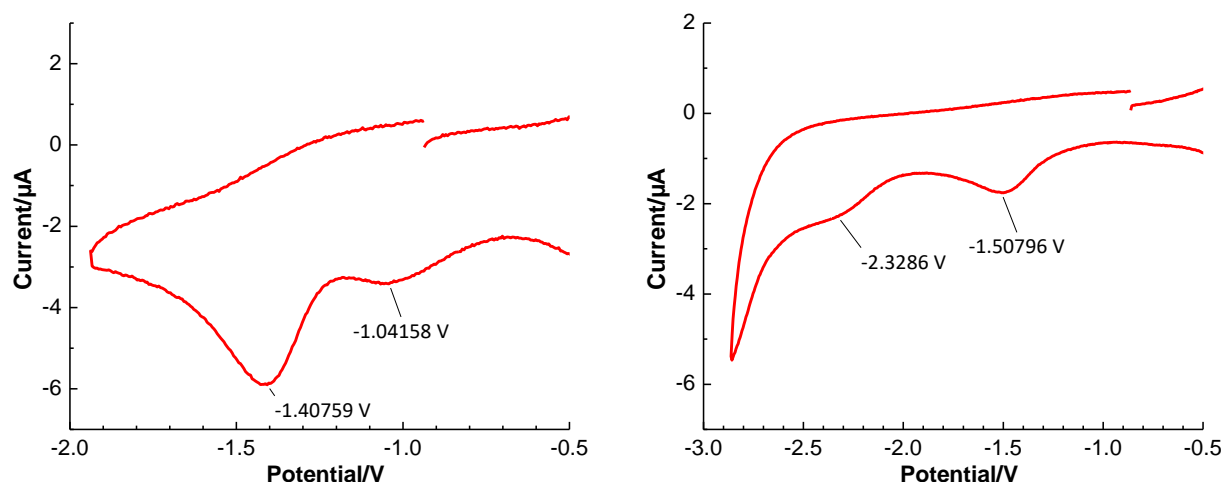


Figure 4.6. Cyclic voltammograms (reduction region) of **4d** in MeCN (left) and THF (right) Vs. $Fc^{0/+}$ (200 mVs^{-1}).

In addition, CV experiments were recorded at various scan rates (50, 100, 200, 400 and 800 mVs^{-1}) (see the appendix) and the plots of the anodic peak currents versus the square root of the scan rates were depicted (Figure 4.7). The peak current linearly increased with respect to the square root of the scan rate based on the Randles–Ševčík equation (Equation 3.1), indicating the reduction processes are diffusion controlled.

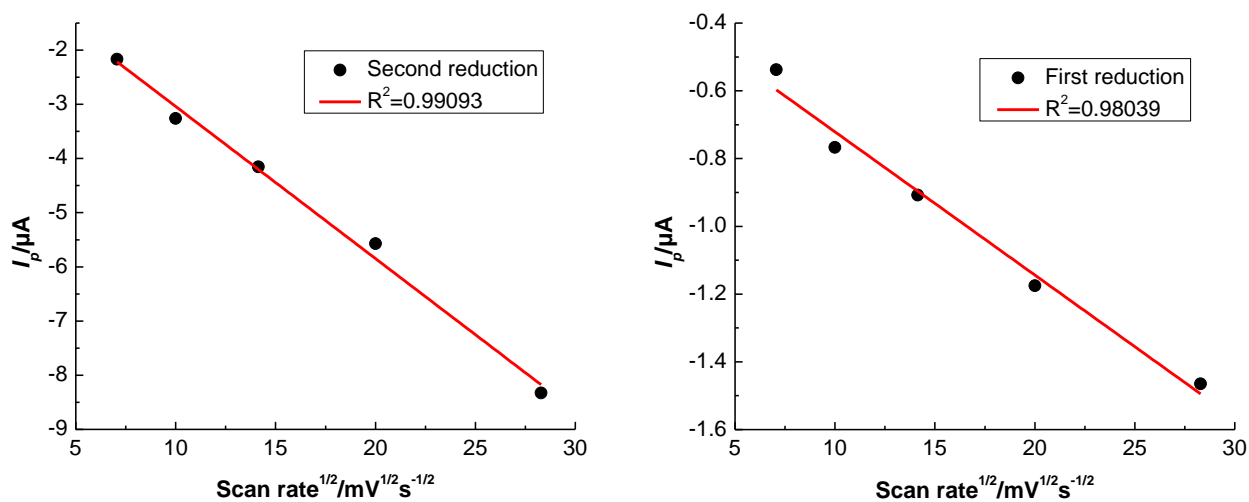
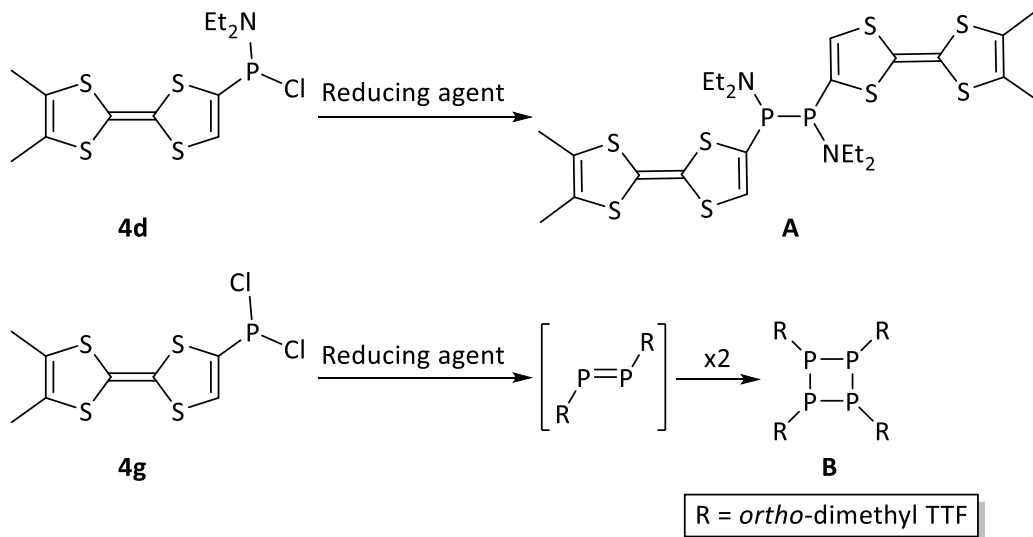


Figure 4.7. Dependency of the cathodic peak currents on the scan rate for reduction of **4d** in MeCN (left) and THF (right).

4.4.2 Chemical reduction of chlorophosphanyl-substituted TTFs

Chlorophosphanyl-substituted TTFs are of interest as they could serve as precursors for the synthesis of the related diphosphane or cyclophosphane having two or four TTF units linked by phosphorus atoms; such electron-donor systems, depending on the degree of electronic communication between redox-active TTF units could display unique multi-stage redox behavior. By comparing the results of the cyclic voltammetry studies with the reported potentials for reducing agents by Connelly and Geiger¹⁰⁷, it could be concluded that to perform the chemical reduction of the P–Cl bond in **4d** using THF as solvent, a strong reagent will be required; but if DCM or acetonitrile would be used as solvent, this goal could be accomplished by using a weaker reducing agent.¹⁰⁷ Different reagents and reaction conditions (Table 4.7) were applied to achieve the P–Cl bond cleavage in **4d,g** and the formation of the targeted diphosphane (**A**) or cyclotetraphosphane (**B**) as final products (Scheme 4.7) but these attempts were not successful and either no reaction was observed via ³¹P NMR spectroscopic monitoring or it showed no resonances which could be safely attributed to the desired products (Table 4.7).



Scheme 4.7. Planned reductions of **4d,g** to access diphosphanes **A** and cyclotetraphosphanes **B**.

Table 4.7. Reducing agents and reaction conditions used for reducing P–Cl bond in **4d,g** (*: 1,4-Dihydro-1,4-bis(trimethylsilyl)pyrazine, **: Tetrakis(dimethylamino)ethylene).

Compound	Reducing agent (eq.)	Solvent (T)	$^{31}\text{P}\{^1\text{H}\}$ NMR resonances/ppm (intensity/%)
4d	BTP* (0.5)	THF (r.t)	-12.4 (3), -2.1 (8), 77.1 (19), 77.4 (11), 77.5 (28), 118.0 (s.m., 28), 133.1 (3).
4d	BTP* (1)	THF (r.t)	-12.4 (3), 77.1 (67), 77.5 (15), 85.3 (15).
4d	Mg (2)	Et ₂ O (r.t)	18.6 (3), 117.1 (s.m., 93), 135.2 (4).
4d	TDAE** (1)	DCM (-80 °C)	-4.3 (14), 2.6 (6), 7.9 (22), 10.5 (5), 84.6 (17), 87.3 (30), 89.3 (6).
4d	CoCp* ₂ (1)	DCM (-80 °C)	8.4 (3), 119.1 (s.m., 97)
4g	BTP (2)	DCM (r.t)	-56.4 (3), -13.4 (2), 52.1 (7), 58.8 (12), 62.2 (49), 63.1 (18), 76.5 (5), 81.6 (4).
4g	Mg (4)	Et ₂ O (r.t)	135.2 (s.m.)
4g	KC ₈ (2)	Et ₂ O (r.t)	135.2 (s.m.)
4g	Mg (4)	THF (50 °C)	No resonance
4g	KC ₈ (2)	THF (50 °C)	No resonance

4.4.3 Chloride abstraction reaction from **4d,f** with GaCl₃

In general, P-chloro compounds can be used as precursors for the synthesis of a great variety of phosphonium compounds such as **XCII–XCVII** (Figure 4.8).^{108–116} One of the most widely used methods to synthesize such dicoordinate phosphorus cation-containing compounds is the phosphorus-halogen bond heterolysis using AlCl₃, GaCl₃ or in some cases FeCl₃ and PCl₅ as chloride abstracting reagents. The low coordinating ability and high dielectric constant of dichloromethane make it the suitable solvent for these reactions, which are usually performed at low temperatures (-78 °C).¹¹³ With this background, the reactions of **4d,f** with GaCl₃ were performed to achieve the related phosphonium compounds (Scheme 4.8).

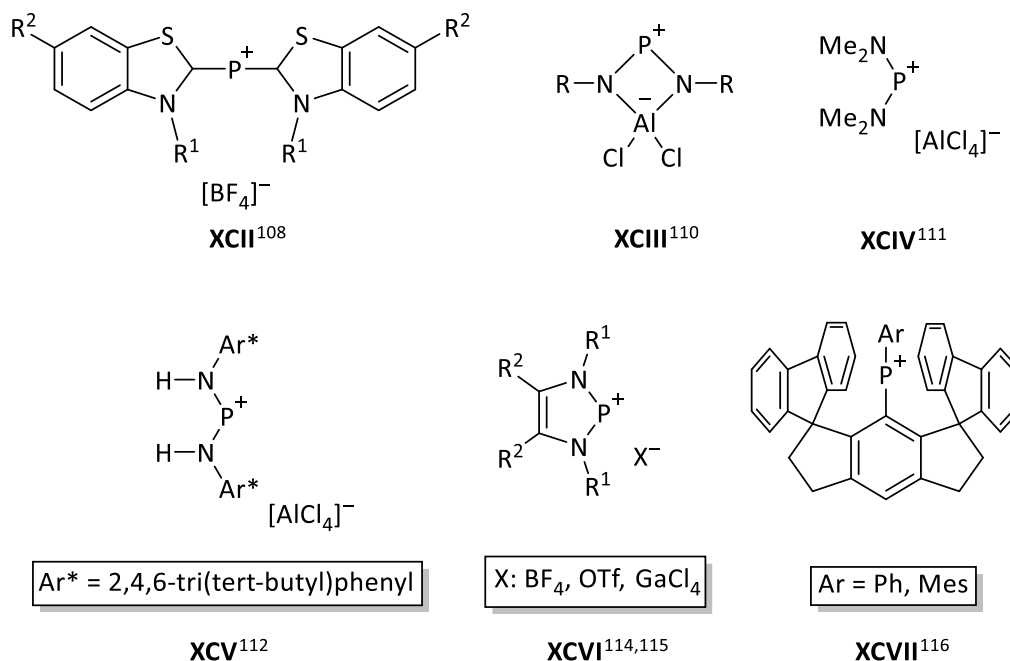
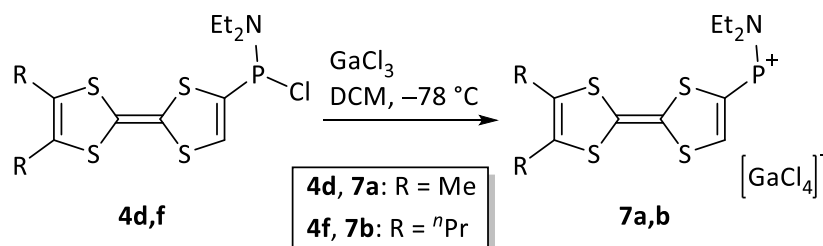


Figure 4.8. Examples of known phosphonium compounds.^{108,110–112,114–116}



Scheme 4.8. Planned synthesis of phosphonium compounds **7a,b**.

Upon the addition of the dichloromethane solution of GaCl_3 to **4d,f** at -78°C , a fast color change from orange to dark red and then dark green was observed. ^{31}P NMR reaction monitoring of the reaction mixtures revealed the disappearance of the resonance related to the starting material, but even though no precipitate was formed, the ^{31}P NMR spectra showed no signals. This observation could be attributed to the formation of paramagnetic compounds which were stable both at low and at room temperature. To probe this assumption, an experiment using *Electron Paramagnetic Resonance* (EPR) spectroscopy was performed at 58 K and revealed a singlet resonance signal for both reaction mixtures with g values equal to 2.008 and 2.007 for the reactions of **4d** and **4f** with GaCl_3 , respectively (Figure 4.9 and A51). To enable the EPR measurement at higher temperatures reaction of **4f** with GaCl_3 was performed in toluene and

the reaction mixture showed a signal with less intensity compared to the DCM solution (most probably due to the low(er) solubility of the product), at 60 K, but increasing the temperature resulted in a much sharper signal at 290 K (Figure 4.9). The EPR spectroscopic results, together with no resonance signal in ^{31}P NMR spectra can be attributed to the formation of radical compounds.

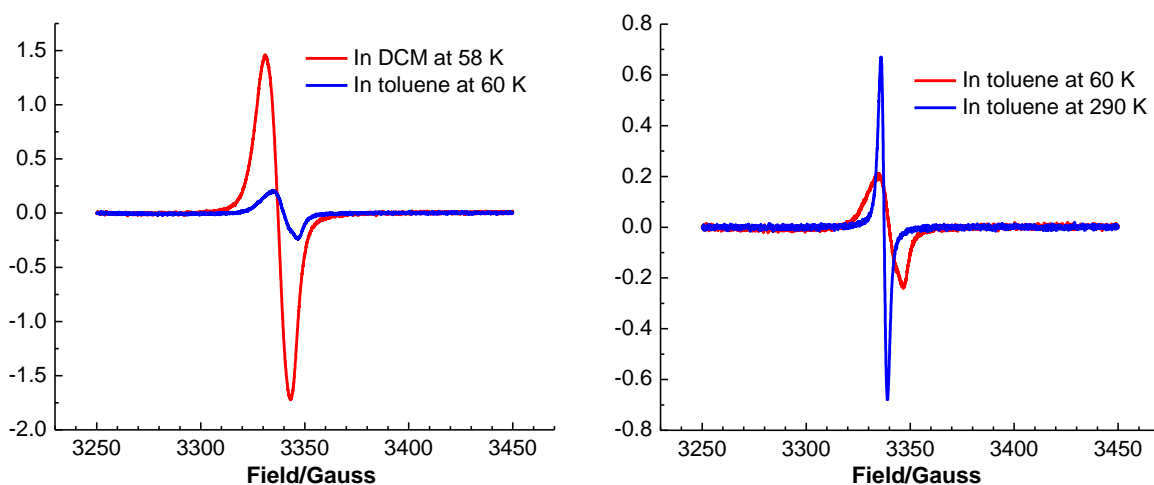


Figure 4.9. CW EPR spectra from the reaction mixtures of **4f** with GaCl_3 .

Early studies on the characterization of radical-containing phosphorus species have used (proposed) phosphorus-centered radical mechanisms.^{117,118} But the first spectroscopic evidence for a phosphorus-containing compound with an unpaired electron was achieved in 1969 from the reaction of a trialkylphosphane with *tert*-butoxyl radical.¹¹⁹ Since then, several persistent or stable phosphorus-centered radicals have been described by employing one or both of the following general stabilizing approaches: i) providing kinetic and thermodynamic stabilization by increasing steric bulk surrounding the radical center to avoid unwanted reactivity or dimerization^{120,121}; and ii) distributing the radical character through a conjugated system to provide electronic stabilization of the singly occupied molecular orbital (SOMO).^{122,123} Phosphorus-centered radicals can be divided into different subclasses including phosphanyl ($\text{R}_2\text{P}^\bullet$)^{120–130}, phosphonyl ($\text{R}_2\text{OP}^\bullet$)¹³¹, phosphoniumyl¹³² ($\text{R}_3\text{P}^{*\bullet}$) and phosphoranyl radicals ($\text{R}_4\text{P}^\bullet$).¹³²

Phosphanyl radicals can be synthesized by different routes, e.g., the first persistent phosphanyl radicals **XCVIII** (Figure 4.10) were reported by Lappert in 1976 via the reduction of

chlorophosphane precursors.¹²⁰ The same synthetic strategy was employed by the groups of Cummins¹²³, Bertrand¹²² and Ishida and Iwamoto¹²¹ to obtain the isolable crystalline radicals **XCIX–CI** (Figure 4.10). Also, the phosphanyl radical cation with a positive charge residing on the iminium unit **CII** was synthesized using the same approach with a complementary oxidation step.¹²⁴

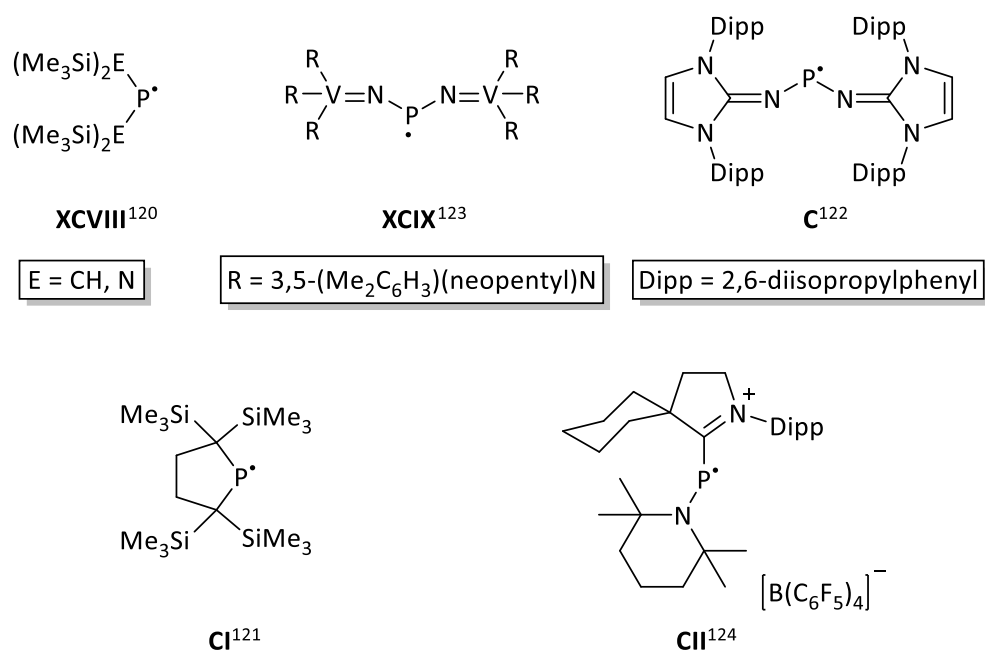
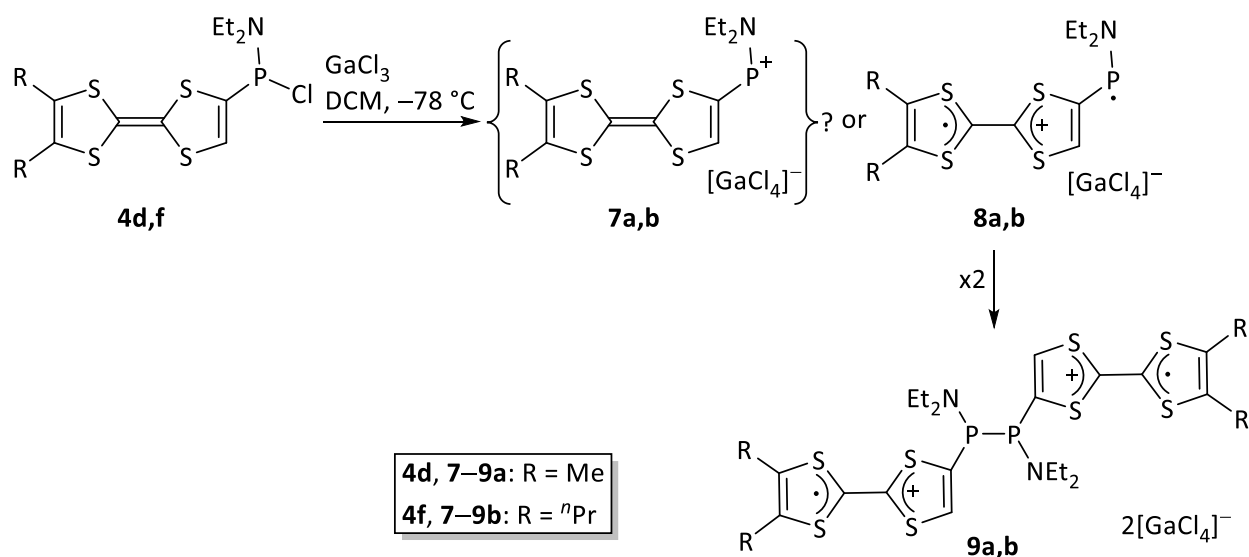


Figure 4.10. Molecular structures of persistent and/or isolable phosphanyl radicals.^{120–124}

As it was mentioned earlier, in the reaction of **4d,f** with GaCl₃, a heterolytic P–Cl bond cleavage was expected to form the related phosphonium compounds (Scheme 4.9). However, the reaction had a surprising outcome, i.e., the color change from yellow to green, not typical for phosphonium compounds, the ³¹P NMR spectra having no signal, and the EPR spectra revealing an open-shell species. One possible interpretation could be that after the formation of **7a,b** an intramolecular one-electron transfer from the readily oxidizable tetrathiafulvalene moiety to the cationic phosphorus center led to the formation of the related biradical cationic species **8a,b** (Scheme 4.9), which can further undergo dimerization to form the related P–P dimer **9a,b** (Scheme 4.9), as highly unexpected products. This can also explain the absence of hyperfine interaction between the unpaired electron and phosphorus nuclei in EPR spectra in two different

solvents and temperature. Several attempts were made to characterize **9a,b** using X-ray diffraction measurements, but no suitable single crystals were obtained.



Scheme 4.9. Proposed mechanism to form **9a,b**.

Our hypothesis was further investigated theoretically by DFT calculation (Kalisch, level of theory: TPSS-D3BJ(CPCM_{THF})/def2-TZVP // PW6B95-D3BJ(CPCM_{THF})/def2-QZVP). The result was a small energy difference (7.4 kcal/mol) between the singlet (phosphenium cation) to the triplet (monomeric biradical cation) states, while the dimer is revealed to be more stable compared to the related monomer by 37.7 kcal/mol (Figure 4.11). These calculations also showed a high spin density contribution on the phosphorus atom (53%) for the monomeric biradical cation (Table 4.8) and almost no spin population on the phosphorus centers for the dimer (Figure 4.12). The latter is in good agreement with the results of EPR spectroscopy, showing no hyperfine coupling between the unpaired electron and phosphorus nuclei.

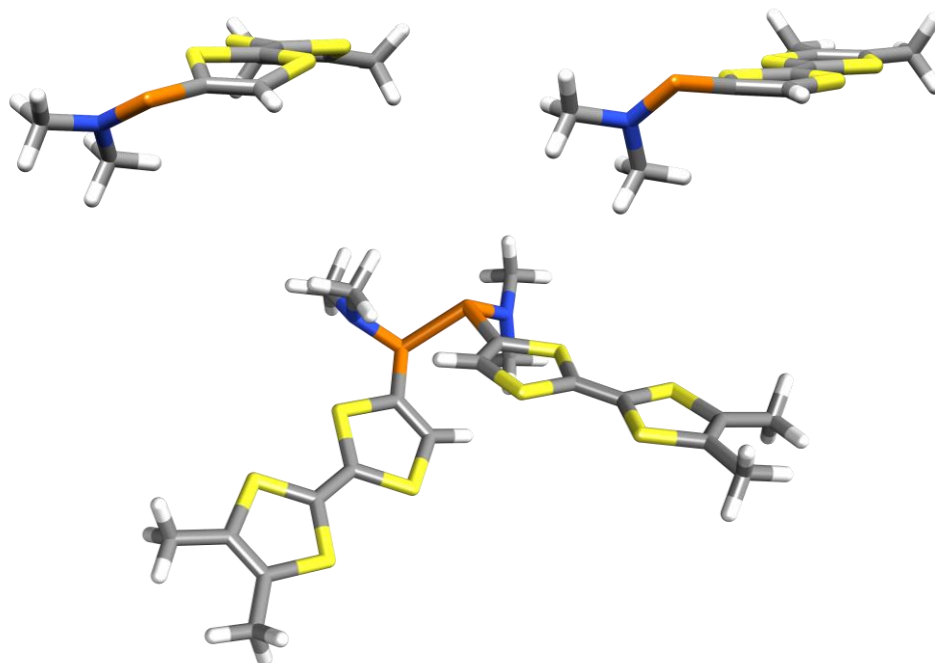


Figure 4.11. Calculated geometries of TTF-PNMe₂ phosphonium cation (top left), monomeric biradical cation (top right) and the related dimer (bottom) (level of theory: TPSS-D3BJ(CPCM_{THF})/def2-TZVP // PW6B95-D3BJ(CPCM_{THF})/def2-QZVP).

Table 4.8. Calculated Löwdin spin populations of TTF-PNMe₂ biradical cation and the related dimer (level of theory: TPSS-D3BJ(CPCM_{THF})/def2-TZVP // PW6B95-D3BJ(CPCM_{THF})/def2-QZVP).

Atom	TTF-PNMe ₂ biradical cation	Dimer	Atom	TTF-PNMe ₂ biradical cation	Dimer
P1	0.53	0.01	P2	—	0.01
N1	0.20	0.00	N2	—	0.00
C1	0.11	0.00	C4	—	0.00
S1	0.17	0.14	S5	—	0.14
S2	0.17	0.15	S6	—	0.15
S3	0.15	0.15	S7	—	0.15
S4	0.15	0.15	S8	—	0.15
C2	0.13	0.10	C5	—	0.10
C3	0.11	0.12	C6	—	0.12

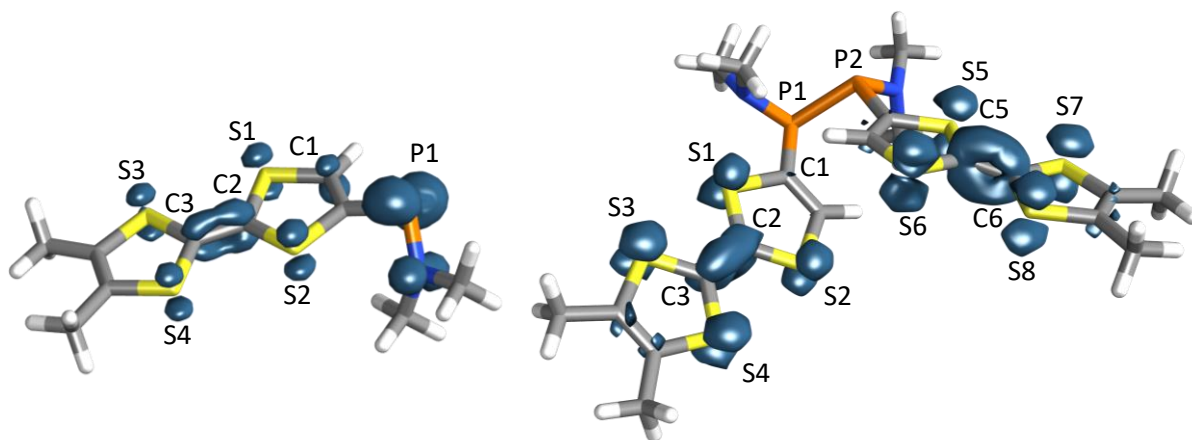
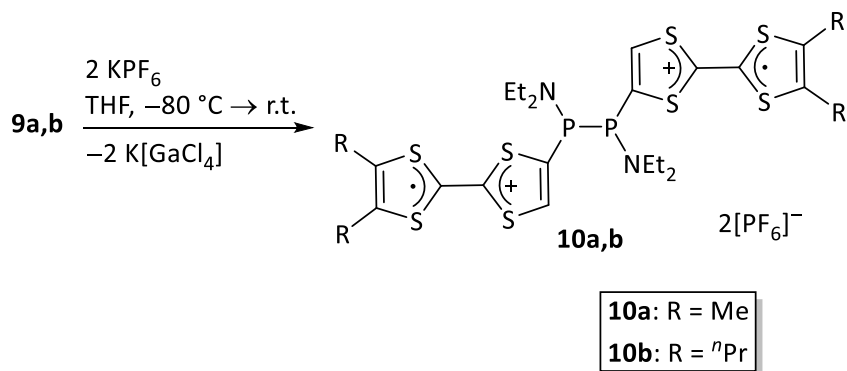


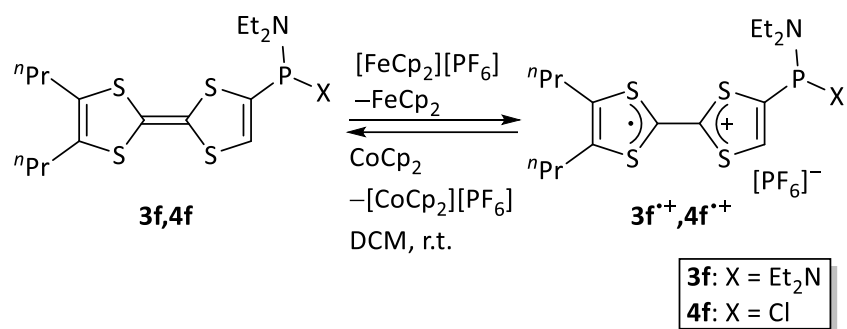
Figure 4.12. Spin density distributions of TTF-PNMe₂ radical (top left), TTF radical cation (top right) and TTF-PNMe₂ biradical cation (bottom) (level of theory: TPSS-D3BJ(CPCM_{THF})/def2-TZVP // PW6B95-D3BJ(CPCM_{THF})/def2-QZVP).

To gain further insight into this result, first anion exchange was tried using potassium hexafluorophosphate (Scheme 4.10). But no clear-cut result was obtained beyond the color change from green (= primary product solution) to orange, finally. But again, no product signal had appeared in the ³¹P NMR spectra of the reaction mixtures; also the signal resonance related to hexafluorophosphate anion could not be observed. After evaporation of the solvent in *vacuo* (8×10⁻³ mbar) the residue was dissolved in diethylether resulting in an orange solution and colorless precipitate. The solution was filtered to remove the (possibly) formed potassium tetrachlorogallate and **10a,b** were obtained after the removal of solvent in *vacuo* (8×10⁻³ mbar). Next, the reduction of *in situ* formed **9a,b** and also **10a,b** using one and two equivalents of decamethylcobaltocene (for **9a,b**) and KC₈ (for **10a,b**) were performed; but in all cases ³¹P NMR spectra of the reaction mixtures showed no resonance.



Scheme 4.10. Attempted anion exchange reaction of **9a,b** using KPF₆.

To examine the effect of the formation of TTF radical cationic substituents on the ^{31}P NMR resonances and achieve reversible chemical oxidation and reduction of **3f** and **4f**, these compounds were treated with one equivalent of ferrocenium hexafluorophosphate (Scheme 4.11). This resulted in dark green reaction mixtures and the disappearance of the resonances of the starting material (**3f**, **4f**) and hexafluorophosphate anion in the ^{31}P NMR spectrum. This observation is in good agreement with the results of the reaction of **4d,f** with GaCl_3 and anion exchange reaction of **9a,b** using KPF_6 . The resulting radical cations, were then reduced via reaction with cobaltocene to re-form compounds **3f** and **4f** (Scheme 4.11), and the formation of the latter was proven by the reappearance of their ^{31}P NMR resonances.



Scheme 4.11. Reversible oxidation and reduction of **3f** and **4f**.

5 Tetrathiafulvalene-fused 1,4-diphosphinine chemistry

5.1 New 1,4-dihydro-1,4-diphosphinine derivatives fused to two TTF

In 1964, Mann and co-workers reported the first example of a six-membered heterocyclic compound, having two $\sigma^3\lambda^3$ -phosphorus centers, known as 1,4-dihydro-1,4-diphosphinine **LX** (Figure 5.1) by a stepwise ring closure using dichloro(organyl)phosphanes.⁶⁹ The reported synthetic protocol was later improved by Uchida and co-workers and the structural and electron donor properties of **LX** were investigated.⁷⁰ The synthesis of the mono-heterocyclic compound **LIII** (Figure 5.1) with different substituents at the P-center was reported by Märkl via the reaction of diethynylphosphanes with primary phosphane.⁶⁷ Later on, different structural motifs were used instead of benzene rings resulting in compounds shown in Figure 5.1.^{31,74,75,77}

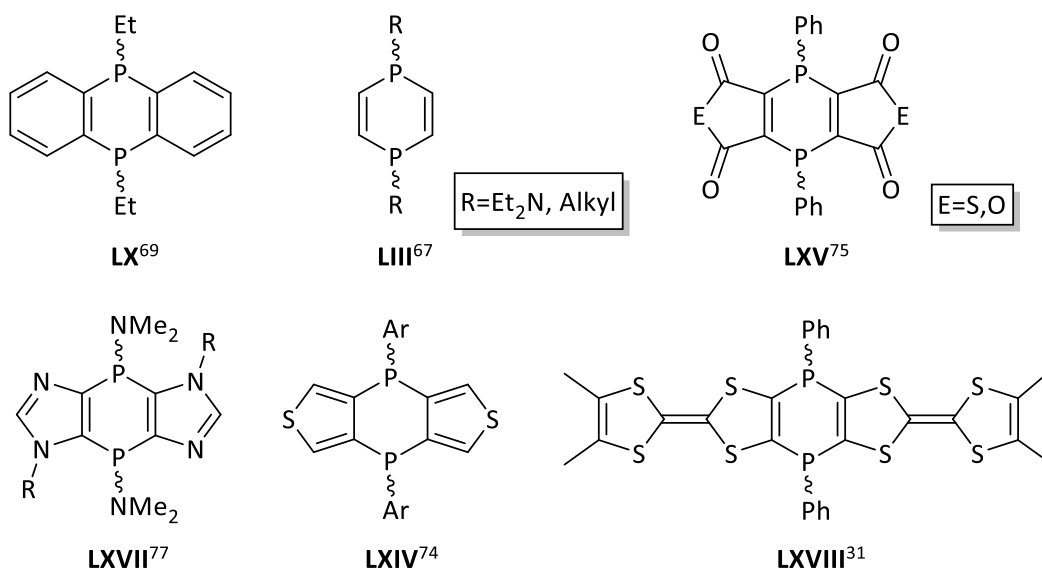


Figure 5.1. Literature known examples of 1,4-dihydro-1,4-diphosphinines.^{31,67,69,74,75,77}

In recent years, tricyclic compounds having a 1,4-dihydro-1,4-diphosphinine motif as the central ring with different fused heterocycles such as imidazole-2-thione **LXX**^{98,133}, thiazole-2-thione **LXXII**⁸⁵, imidazole-2-selone **LXXIII**⁸¹ and dithiole-2-thione **LXXIV**⁸⁰ (Figure 5.2) were introduced by the Streubel group. These compounds were synthesized via backbone deprotonation of the C⁴-

chloro(organyl)phosphanylated starting materials followed by an in situ cyclization and lithium chloride elimination.

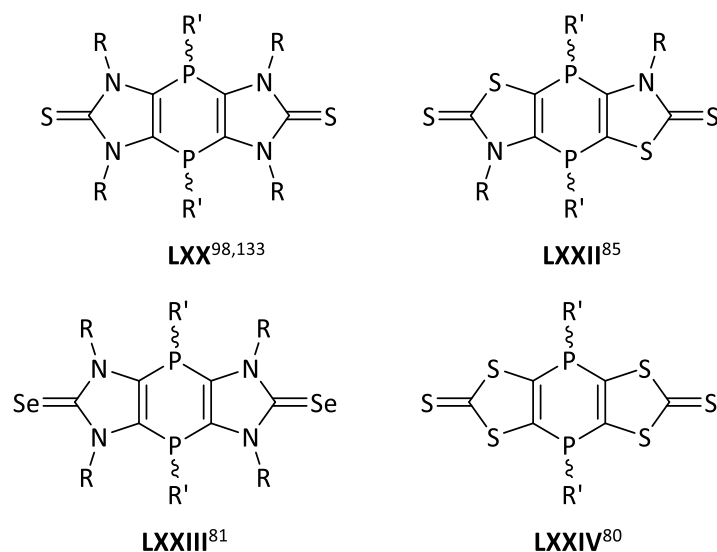
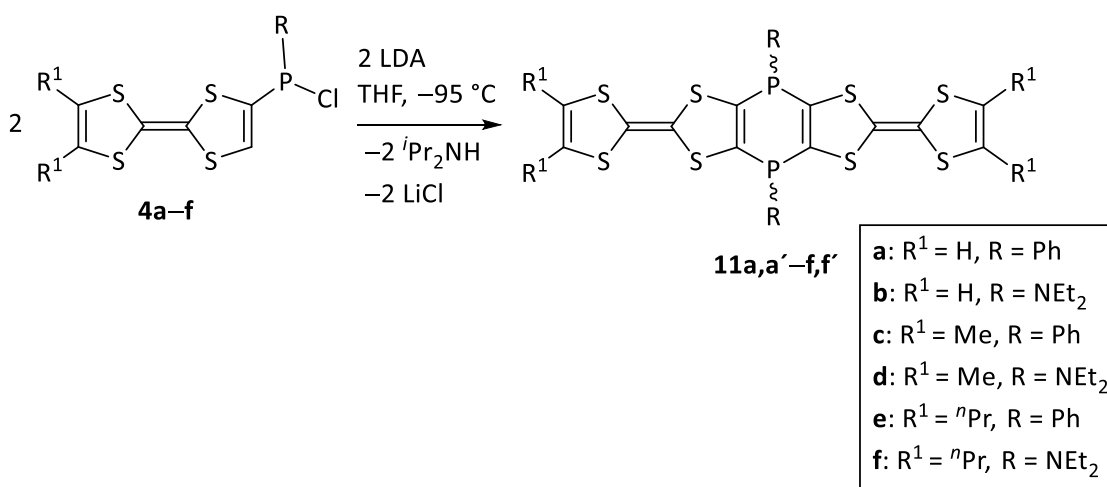


Figure 5.2. 1,4-Dihydro-1,4-diphosphinines reported by Streubel and co-workers.^{80,81,85,98,133}

To perform the ring-closing reaction it was decided to follow the synthetic methodology reported previously. Therefore, **4a–f** were treated with LDA at low temperature to achieve deprotonation of C⁵ atom in chloro(organyl)phosphanyl-substituted TTFs followed by intermolecular nucleophilic substitution which resulted in the formation of the expected 1,4-dihydro-1,4-diphosphinines **11** (Scheme 5.1).



Scheme 5.1. Synthesis of *cis/trans* mixtures of 1,4-dihydro-1,4-diphosphinines **11** fused to two TTF units.

Reaction of **4c** with LDA, led to the formation of two isomers having ^{31}P NMR resonances at -26.1 and -22.1 ppm (ratio 1:0.7) being in good agreement with the reported values by Avarvari³¹ for **LXVIII**. However, the *cis/trans* ratio is significantly different compared to the reported *cis/trans* ratio of 15:1 for **LXVIII**. In the cases of **4d,e,f**, $^{31}\text{P}\{^1\text{H}\}$ NMR spectra showed a clean conversion into the corresponding isomeric mixtures of desired products with resonances of **11d,d'** (29.3 and 32.1, ratio 1:0.9), **11e,e'** (-26.2 and -21.9 , ratio 0.7:1) and **11f,f'** (29.7 and 32.5, ratio 1:0.9) which are comparable with the previously reported chemical shifts from Avarvari³¹ and for the 1,3-dithiole-2-thione derived tricyclic compound **LXXIV**⁸⁰. **11d,d'-f,f'** could be isolated in moderate to excellent yields after the removal of volatiles in *vacuo* (8×10^{-3} mbar) and the LiCl salt via filtration. These compounds were characterized by various analytical techniques such as multinuclear NMR, MS and elemental analysis. Also, for **11d**, single crystals of the *cis* isomer could be obtained from the saturated solution of the isomeric mixture in diethylether. It is crystallized in a monoclinic lattice with space group $P2_1/n$ (Figure 5.3); selected structural parameters are given in Table 5.1. The bond lengths are in the typical range of P–C and P–N single bonds but the planar environment at the nitrogen centers is noteworthy. Of particular note is the boat-type conformation of the central 1,4-dihydro-1,4-diphosphinine ring with small folding along the P1–P2 hinge by $11.5(5)^\circ$ (Figure 5.3), which is much weaker than the reported values for the 1,4-ditellurine (67.8°)³³ and 1,4-diphenyl-1,4-diphosphinine (30.4°)³¹ derivatives.

In the cases of **4a,b**, due to the accessibility of protons at the opposing ring in the TTF unit, reactions with LDA were not selective and the desired 1,4-dihydro-1,4-diphosphinines were obtained just as a minor product (**4a**) or was not formed at all (**4b**) (Figure 5.4). The major product which was formed in these reactions was the related mono-bridged compounds ((TTF)₂PR) ($\delta = -22.6$ and 42.1 ppm) (Scheme 5.2). The formation of a precipitate that was not soluble in common solvents could be an indication of oligomeric side-products. Different bases and reaction conditions were examined in the case of **4b** to form the desired product. The best outcome was achieved by using KHMDS as base with almost 30% conversion to the 1,4-dihydro-1,4-diphosphinine **11b** (Figure 5.5).

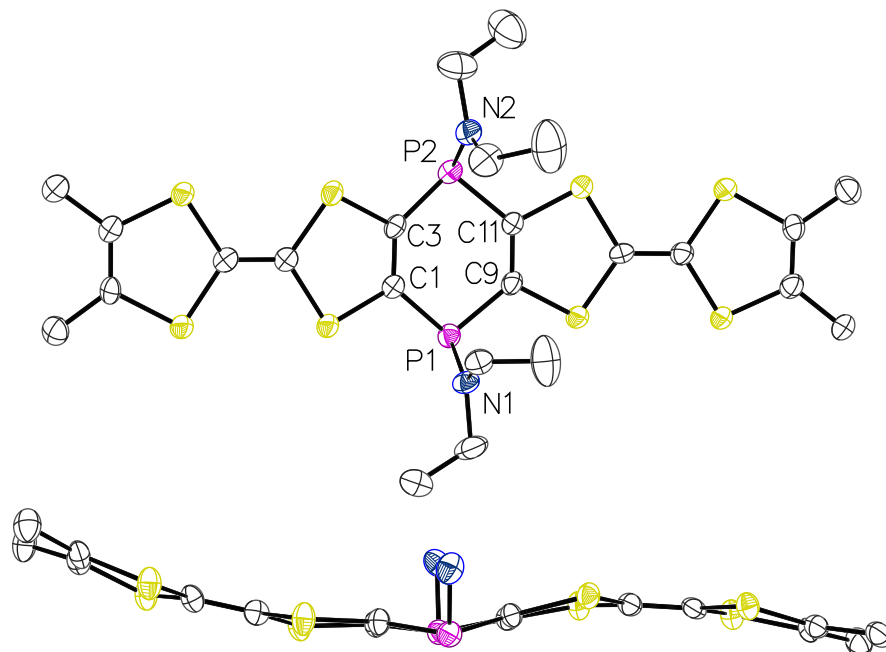


Figure 5.3. Top: ORTEP drawing of the molecular structure of *cis-11d* in the solid state (ellipsoids are set at 50% probability level and hydrogen atoms are omitted for clarity); bottom: Side view of the ORTEP drawing of the molecular structure of *cis-11d* in the solid state (ellipsoids are set at 50% probability level, hydrogen atoms and ethyl groups are omitted for clarity).

Table 5.1. Selected bond lengths and angles for *cis-11d*.

Bond lengths/Å		Bond angles/°	
P1–C1	1.821(5)	N1–P1–C1	100.3(2)
P1–C9	1.827(5)	N1–P1–C9	104.0(2)
P1–N1	1.684(5)	C1–P1–C9	98.5(2)
P2–C3	1.819(5)	N2–P2–C3	103.2(2)
P2–C11	1.816(5)	N2–P2–C11	104.2(2)
P2–N2	1.657(5)	C3–P2–C11	97.7(2)
C1–C3	1.342(7)	$\Sigma(\angle N1)$	359.9
C9–C11	1.343(7)	$\Sigma(\angle N2)$	359

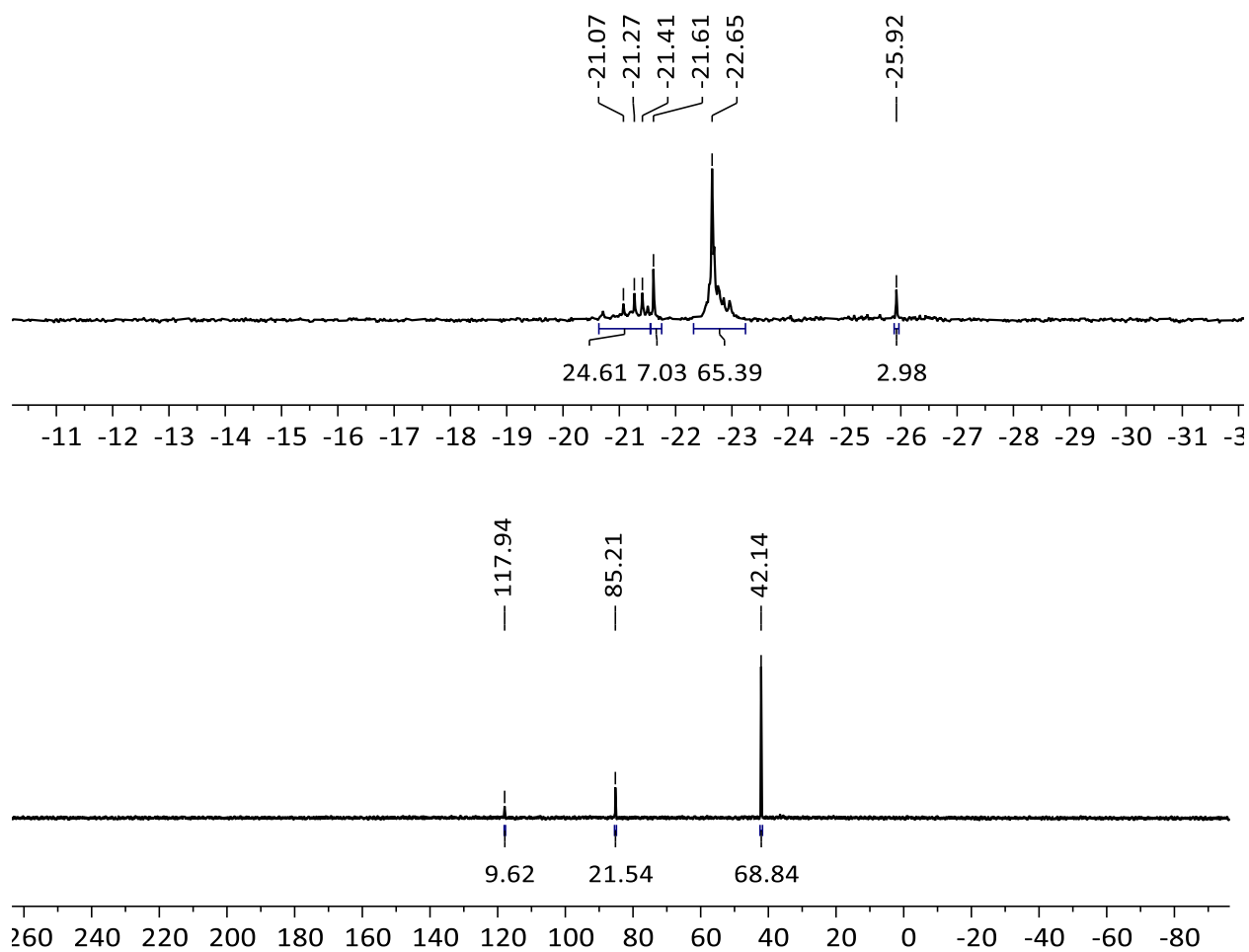
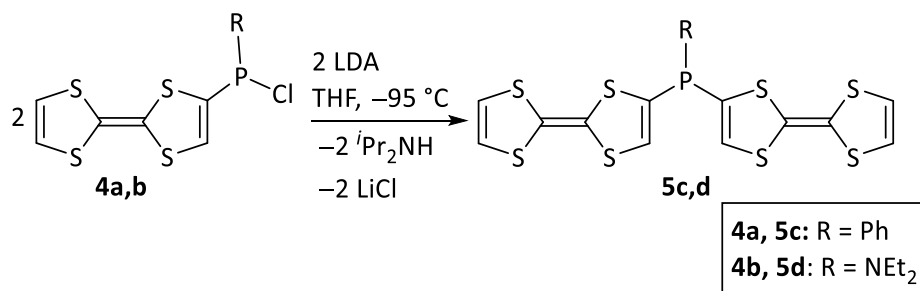


Figure 5.4. $^{31}\text{P}\{^1\text{H}\}$ NMR spectrum for the reaction of **4a** (top) and **4b** (bottom) with LDA (reaction mixture).



Scheme 5.2. Reaction of **4a,b** with LDA.

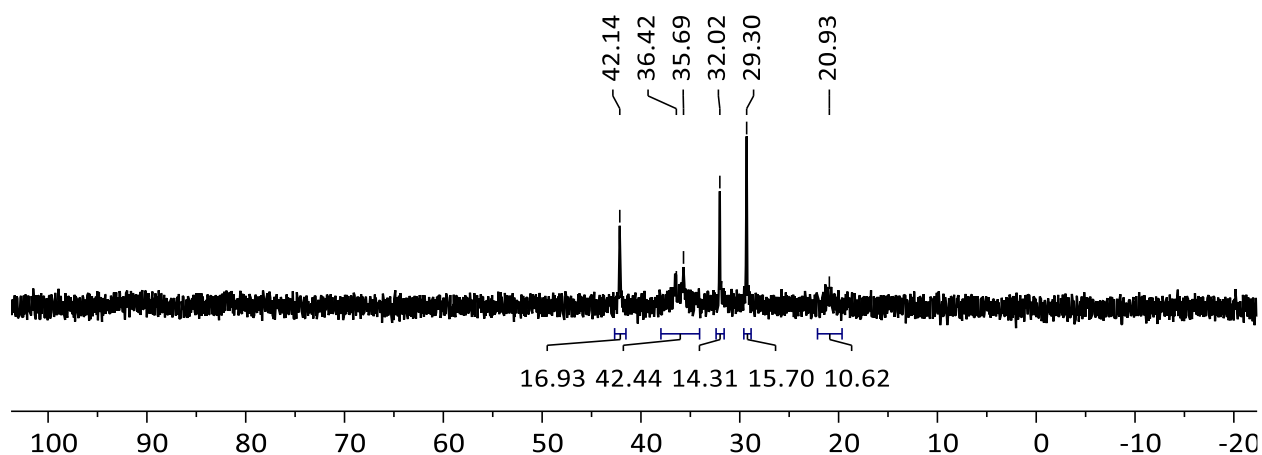


Figure 5.5. $^{31}\text{P}\{^1\text{H}\}$ NMR spectrum for the reaction of **4b** with KHMDS (reaction mixture).

5.2 Cyclic voltammetry studies of new 1,4-dihydro-1,4-diphosphinines

As was mentioned in the introduction, one way of modifying the redox properties of TTF is the preparation of the bridged and/or fused molecules, in which the TTF units are linked by one or more spacer groups. These so-called “dimeric” TTF molecules can display multi-stage redox behavior. To investigate the electrochemical properties of new TTF fused compounds, cyclic voltammetry studies were performed in dichloromethane. For these compounds, four sequential, one-electron transfer processes yielding a tetracation species were expected and cyclic voltammograms showed these processes (Figure 5.6). However, the separation between the third and fourth waves is not as distinct as the first and second redox processes, which is mainly due to the higher potential (closer to the solvent limit) and/or less solubility of the oxidized species; a lower concentration of the analyte (less than 1 mM) can make this separation more pronounced but at the other hand reduces the overall quality of the CV study, i.e. less current to capacitance ratio. To evaluate the reversibility of these processes, $E_{1/2}$, ΔE_p and I_p values were extracted from the cyclic voltammograms and given in Table 5.2. Based on the obtained data, these processes could be considered quasi-reversible. Another important aspect of the electrochemical properties of these compounds is the separation between the first and second, and also third and fourth redox potentials, which is a measure of the degree of communication between two TTF units. These differences for **11d,d'-f,f'** (Table 5.2) are in good agreement with the previously reported compound, having a non-aromatic 1,4-dihydro-1,4-

diphosphinine ring with PPh groups as the bridge between two TTF moieties (120 mV)³¹, but smaller than the cases where the two redox-active units are connected via an aromatic linker (160–260 mV).¹⁰⁶

Additionally, CVs were recorded at various scan rates (50, 100, 200, 400 and 800 mVs⁻¹) (see the appendix) and the plots of the anodic peak current versus the square root of the scan rates were depicted for the first and second redox waves (Figure 5.7). The diffusion-controlled origin of these redox processes was indicated by the linear increase of the peak current with respect to the square root of the scan rate, based on the Randles–Ševčík equation (Equation 3.1), as another proof of electrochemical reversibility.

Table 5.2. Half wave potentials (Vs. Fc^{0/+}), $\Delta E_{1/2}$, cathodic and anodic currents for **11d,d'**–**f,f'** (0.4 M ⁿBu₄PF₆ in DCM, 100 mVs⁻¹).

Compound	$E_{1/2}^1/V$ ($\Delta E_p/mV$)	$E_{1/2}^{1'}/V$ ($\Delta E_p/mV$)	$\Delta E_{1/2}^{1,1'}$	$E_{1/2}^2/V$ ($\Delta E_p/mV$)	$E_{1/2}^{2'}/V$ ($\Delta E_p/mV$)	$\Delta E_{1/2}^{2,2'}$
	$[I_p^a: I_p^c/\mu A]$	$[I_p^a: I_p^c/\mu A]$	/mV	$[I_p^a: I_p^c/\mu A]$	$[I_p^a: I_p^c/\mu A]$	/mV
11d,d'	-0.10 (65.4) [7.7:6.5]	0.02 (59.9) [6.8:6.2]	120	0.43 (64.6) [6.4:6.9]	0.53 (55.6) [5.9:6.6]	100
11e,e'	-0.06 (60.0) [8.4:7.9]	0.05 (69.9) [6.7:6.1]	110	0.44 (74.9) [7.2:7.5]	0.55 (60.1) [6.2:6.3]	110
11f,f'	-0.10 (72.2) [11.6:11.5]	0.02 (72.2) [11.1:10.7]	120	0.44 (71.9) [9.4:10.3]	0.55 (56.4) [8.7:9.3]	110

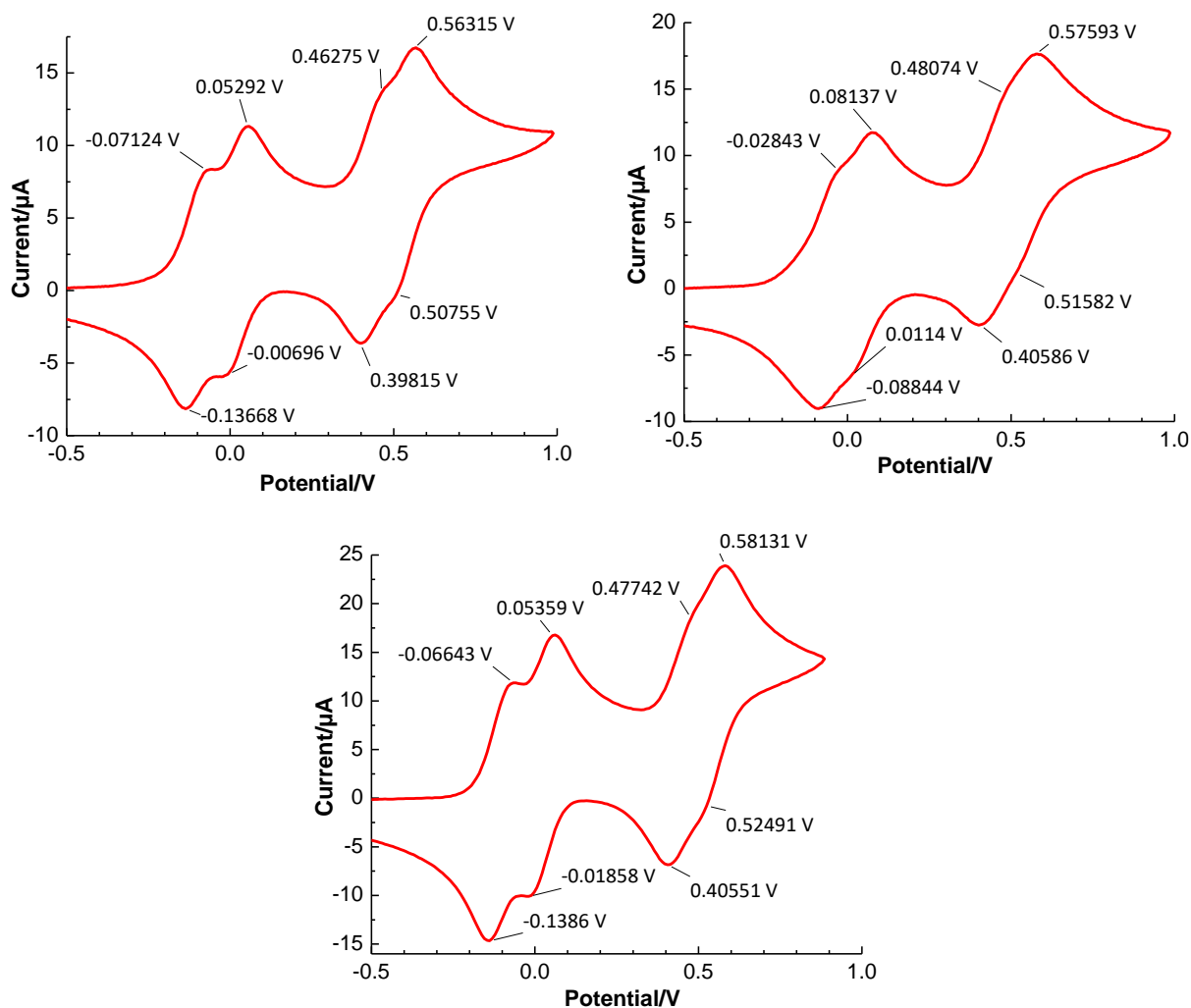


Figure 5.6. Cyclic voltammograms of **11d,d'** (top left), **11e,e'** (top right) and **11f,f'** (bottom) Vs. $\text{Fc}^{0/+}$ (0.4 M $n\text{Bu}_4\text{PF}_6$ in DCM, 100 mVs^{-1}).

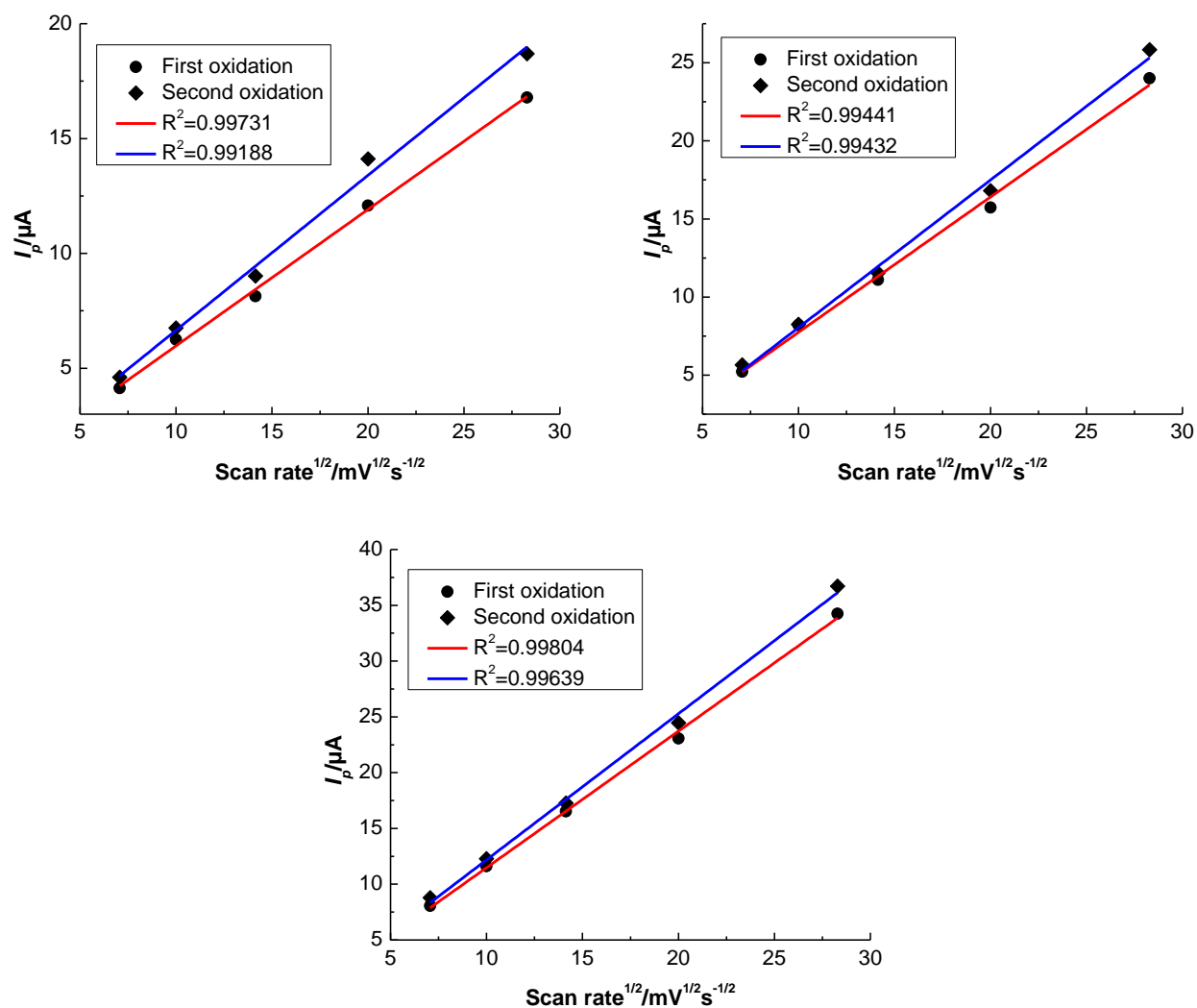


Figure 5.7. Dependency of the anodic peak currents (first and second redox processes) on the scan rate for **11d,d'** (top left), **11e,e'** (top right) and **11f,f'** (bottom).

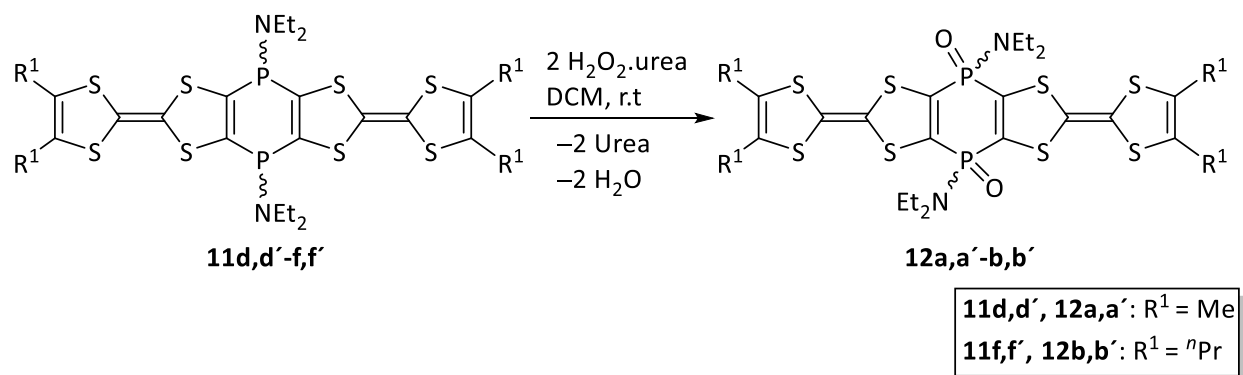
5.3 Reactivity studies of TTF-fused 1,4-dihydro-1,4-diphosphinines

The only previous example of tetrathiafulvalene-based 1,4-dihydro-1,4-diphosphinine, reported by Avarvari³¹, was bearing phenyl substitution at phosphorus centers, thus clearly was restricted from further “simple” functionalization and only its reaction with elemental sulfur and coordination chemistry of the P-centers towards $\text{Mo}(\text{THF})(\text{CO})_5$ and $\text{W}(\text{THF})(\text{CO})_5$ metal complexes were described.¹³⁴ Therefore, the reactivity of the new 1,4-bis(diethylamino)-1,4-dihydro-1,4-diphosphinines **11d,d'-f,f'** was explored. Inspired by the electrochemical oxidation of these compounds through cyclic voltammetry, the reactivity studies focused on attempts at chemical oxidation of the P-centers with chalcogens; and, later on, the exchange of the amino

group for chloride (scrambling reaction), as a crucial step towards the synthesis of the related 1,4-diphosphinines, was examined.

5.3.1 Oxidation of the *P*-centers in 1,4-bis(diethylamino)-1,4-dihydro-1,4-diphosphinines

In order to study the oxidation of the *P*-centers of 1,4-bis(diethylamino)-1,4-dihydro-1,4-diphosphinines, dichloromethane solutions of isomeric mixtures of **11d,d'** and **11f,f'** (*cis/trans* ratio: 0.32:1 and 1:0.89, respectively) were treated with a slight excess of H₂O₂-urea adduct at room temperature. A slow but clean reaction resulted in the formation of a mixture of *cis/trans* of the P(V/V) 1,4-dihydro-1,4-diphosphinines **12a,a'-b,b'** (Scheme 5.3), while the complete consumption of the starting material was observed after 24 hours via ³¹P{¹H} NMR reaction monitoring.



Scheme 5.3. Oxidation reaction of **11d,d'** and **11f,f'** with H₂O₂-urea adduct.

³¹P{¹H} NMR spectroscopy displayed two signals at -2.1, -0.8 for **12a,a'** (with the ratio of 1:0.3) and -2.1, -0.7 for **12b,b'** (with the ratio of 1:0.7) assigned to the *cis/trans* isomers. These chemical shifts, which are notably high-field shifted in comparison to the starting materials (Figure 5.8), are in good agreement with the similar compounds previously described by the Streubel group.¹³³ After filtration of the unreacted urea and removal of the volatiles in *vacuo* (8x10⁻³ mbar), **12a,a'** and **12b,b'** were obtained in good yields (Table 5.3). These compounds were further characterized by various analytical techniques such as multinuclear NMR, MS and elemental analysis.

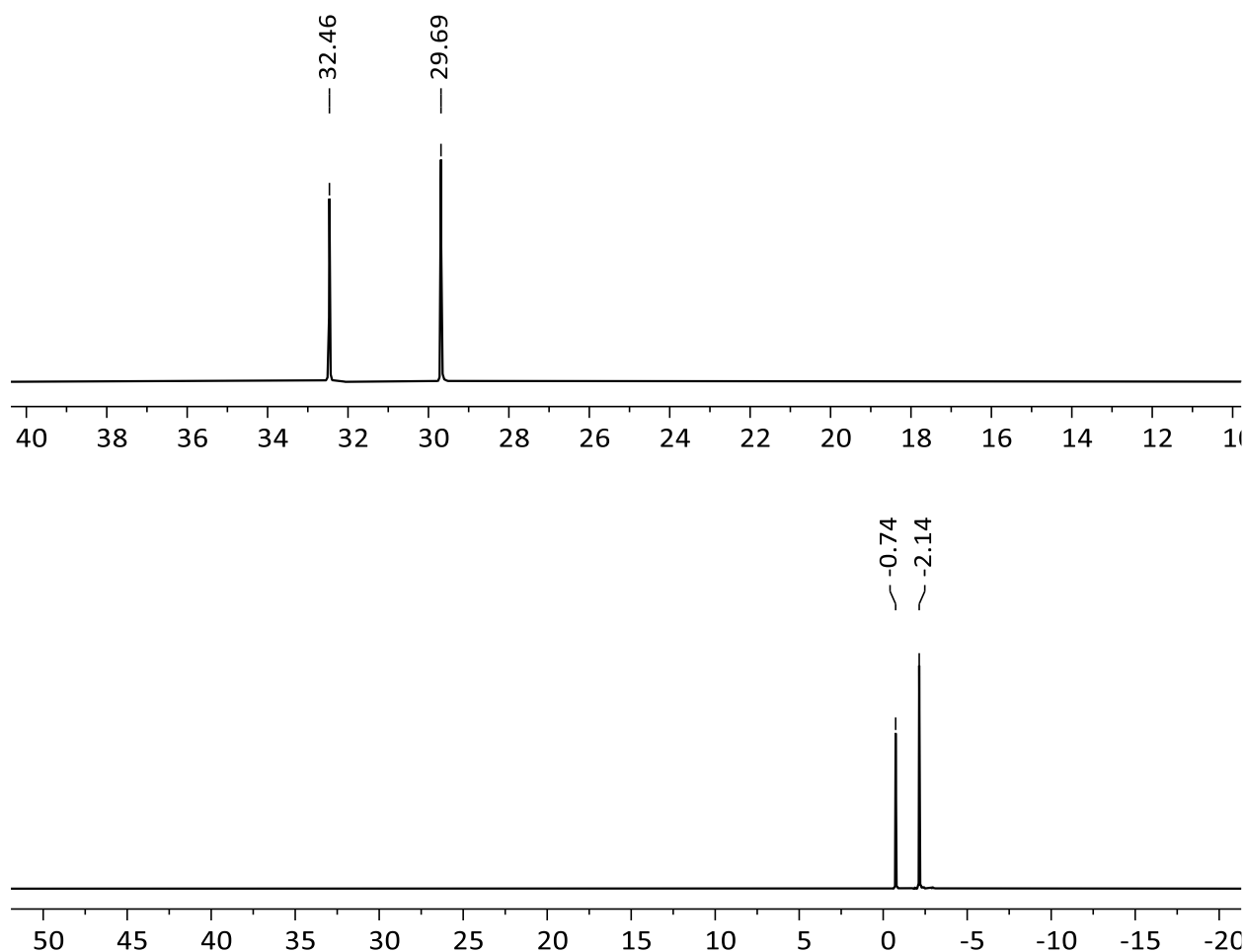


Figure 5.8. Comparison of $^{31}\text{P}\{^1\text{H}\}$ NMR spectra of compounds **11f,f'** (top) and **12b,b'** (bottom).

Table 5.3. $^{31}\text{P}\{^1\text{H}\}$ NMR data (in CDCl_3), isomeric ratio (isolated) and yields for compounds **12a,a'-b,b'**.

Compound	$\delta^{31}\text{P}\{^1\text{H}\}/\text{ppm}$	Isomeric ratio	Yield%
12a,a'	-2.1, -0.8	1:0.3	74
12b,b'	-2.1, -0.7	1:0.7	86

In the case of **12a,a'**, single crystals of the *trans* isomer, suitable for X-ray diffraction measurements, could be grown from the saturated dichloromethane solution of the isomeric mixture (*cis/trans* ratio: 1:0.3) (Figure 5.9). Selected bond lengths and angles are given in Table 5.4. Of particular note is the almost planar conformation of the central 1,4-dihydro-1,4-diphosphinine ring in comparison to the boat-type conformation in *cis*-**11d** and *trans* isomer of disulfide 1,4-diphenyl-1,4-dihydro-1,4-diphosphinine reported by Avarvari¹³⁴ with folding along

the P1–P2 hinge by $11.5(5)^\circ$ and $18.6(1)^\circ$, respectively; also, both TTFs units are strongly folded around the S1–S2 and S5–S6 axes ($27.8(1)^\circ$), compared to *cis-11d* (with corresponding folding angles of $16.7(4)^\circ$ and $12.3(4)^\circ$).

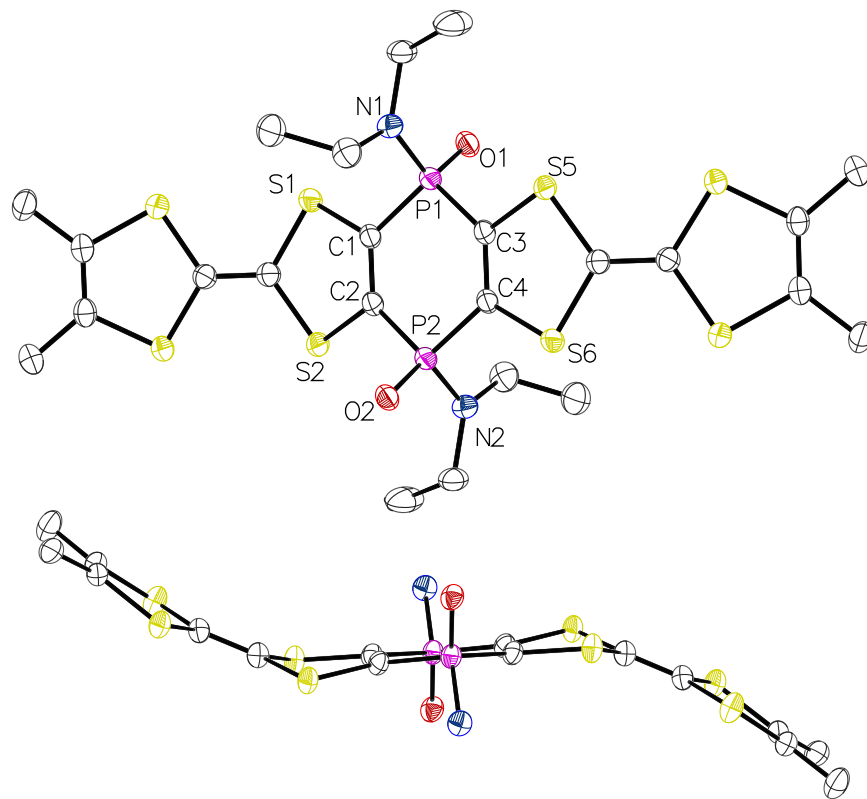


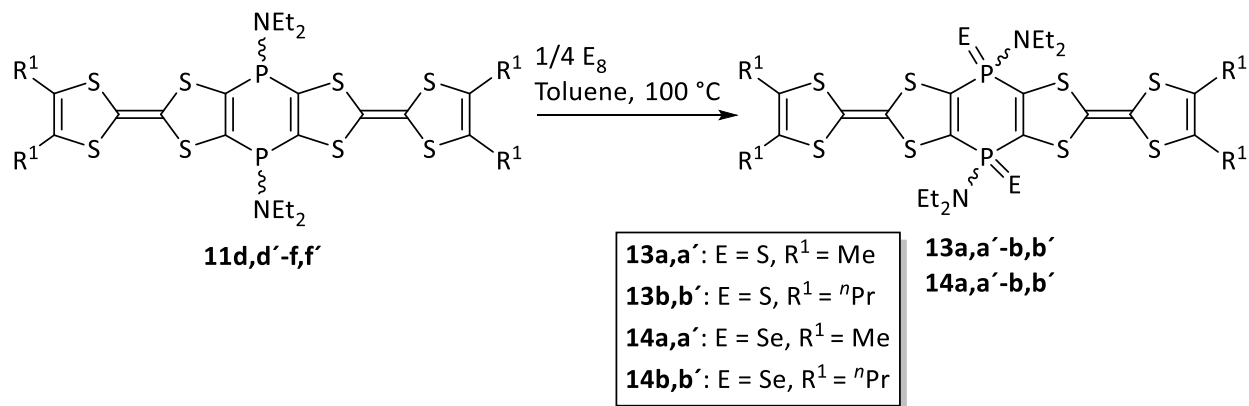
Figure 5.9. Top: ORTEP drawing of the molecular structure of *trans-12a* in the solid state (ellipsoids are set at 50% probability level and hydrogen atoms are omitted for clarity); bottom: Side view of the ORTEP drawing of the molecular structure of *trans-12a* in the solid state (ellipsoids are set at 50% probability level, hydrogen atoms and ethyl groups are omitted for clarity).

Table 5.4. Selected bond lengths and angles for *trans*-**12a**.

Bond lengths/Å		Bond angles/°	
P1–C1	1.800(2)	N1–P1–C1	108.28(11)
P1–C3	1.802(2)	N1–P1–C3	107.61(11)
P1–N1	1.629(2)	N1–P1–O1	113.18(10)
P1–O1	1.490(5)	C1–P1–C3	103.45(11)
P2–C2	1.802(0)	N2–P2–C2	107.61(10)
P2–C4	1.799(9)	N2–P2–C4	108.27(70)
P2–N2	1.629(3)	N2–P2–O2	113.17(60)
P2–O2	1.490(5)	C2–P2–C4	103.45(30)

5.3.2 Oxidation of the *P*-centers in **11d,f** using elemental sulfur and selenium

To synthesize the *P,P'*-disulfides and *P,P'*-diselenides, toluene solutions of the *cis/trans* isomeric mixtures of **11d,d'** and **11f,f'** (*cis/trans* ratio: 0.32:1 and 1:0.89 respectively) were reacted with the slight excess of elemental sulfur or selenium at 100 °C (Scheme 5.4).

**Scheme 5.4.** Oxidation reactions of **11d,d'** and **11f,f'** with elemental sulfur and selenium.

These reactions were monitored via ³¹P{¹H} NMR spectroscopy and in all cases, after 3 hours, the starting material was completely consumed while two new resonances appeared, corresponding

to the *cis/trans* isomers of the desired products (Table 5.5). These products were obtained after the removal of the unreacted sulfur or selenium by filtration and evaporation of the solvent in *vacuo* (8×10^{-3} mbar) and fully characterized by various analytical techniques such as multinuclear NMR, MS and Elemental analysis.

For *P,P'*-diselenide compounds, $^{31}\text{P}\{^1\text{H}\}$ NMR spectra showed coupling between phosphorus and selenium atoms with the coupling constant around 800 Hz (Table 5.5) which is in good agreement with the previously reported similar compound by the Streubel group having a phosphorus selenium double bond.¹⁰⁰ Also the changes in the relative position of resonances related to the isomers in $^{31}\text{P}\{^1\text{H}\}$ NMR spectra for **13** and **14** (Table 5.5), in comparison to the starting materials ($\Delta\delta$ for **11d,d'** and **11f,f'** = 2.8 ppm), are noteworthy (Figure 5.10).

Table 5.5. $^{31}\text{P}\{^1\text{H}\}$ NMR data (in CDCl_3), isomeric ratio (isolated) and yields for compounds **13,14a,a'-b,b'**.

Compound	δ $^{31}\text{P}\{^1\text{H}\}$ /ppm	$\Delta\delta$ /ppm	Isomeric ratio	Yield%
13a,a'	25.17, 25.24	0.07	0.8:1	59
13b,b'	25.2, 25.4	0.2	1:0.8	81
14a,a'	15.7 ($^1J_{\text{P,Se}} = 816$ Hz), 15.8 ($^1J_{\text{P,Se}} = 804$ Hz)	0.1	1:0.9	61
14b,b'	15.7 ($^1J_{\text{P,Se}} = 804$ Hz), 15.9 ($^1J_{\text{P,Se}} = 812$ Hz)	0.2	1:0.85	92

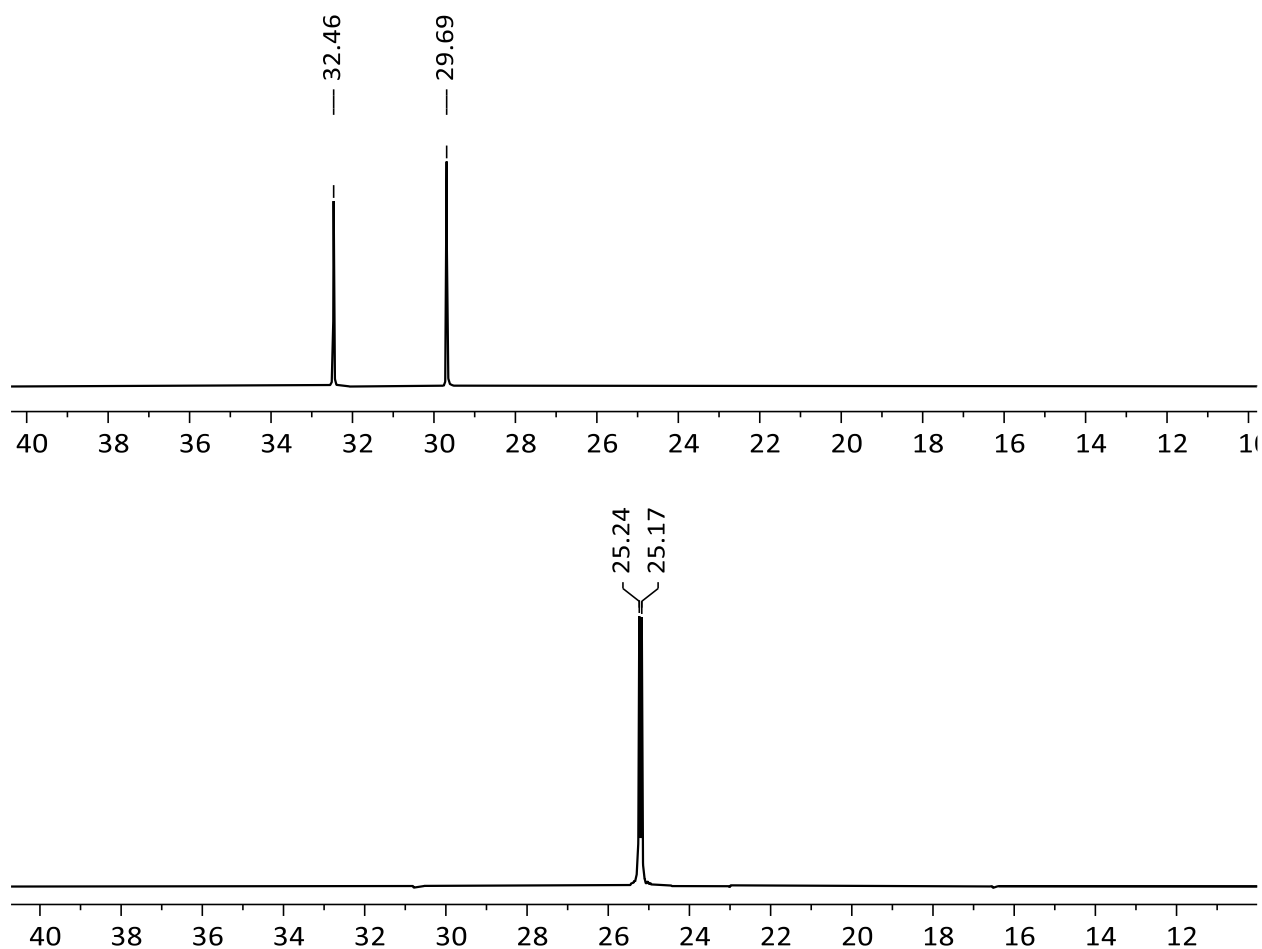


Figure 5.10. Comparison of $^{31}\text{P}\{^1\text{H}\}$ NMR spectra of compounds **11f,f'** (top) and **13b,b'** (bottom).

For **14b,b'**, single crystals of the *cis* isomer, suitable for X-ray diffraction measurements, could be obtained from the saturated dichloromethane solution of the isomeric mixture with a ratio of 1:0.85. It is crystallized in a monoclinic lattice with space group $P2_1/n$ (Figure 5.11); selected structural parameters are given in Table 5.6. Central 1,4-dihydro-1,4-diphosphinine ring possess a boat-type conformation with a folding angle of $29.3(5)^\circ$ along the P1–P2 hinge which is bigger than the corresponding angle in *cis*-**11d** ($11.5(5)^\circ$) and disulfide 1,4-dihydro-1,4-diphosphinine ($18.6(1)^\circ$) reported by Avarvari.¹³⁴ It is worthwhile noting the folding angle along the S1–S2 ($16.9(4)^\circ$) and S5–S6 axes ($27.1(5)^\circ$) in two TTF units are different (Figure 5.11) and comparable to the corresponding folding angles in *cis*-**11d** and *trans*-**12a**, respectively.

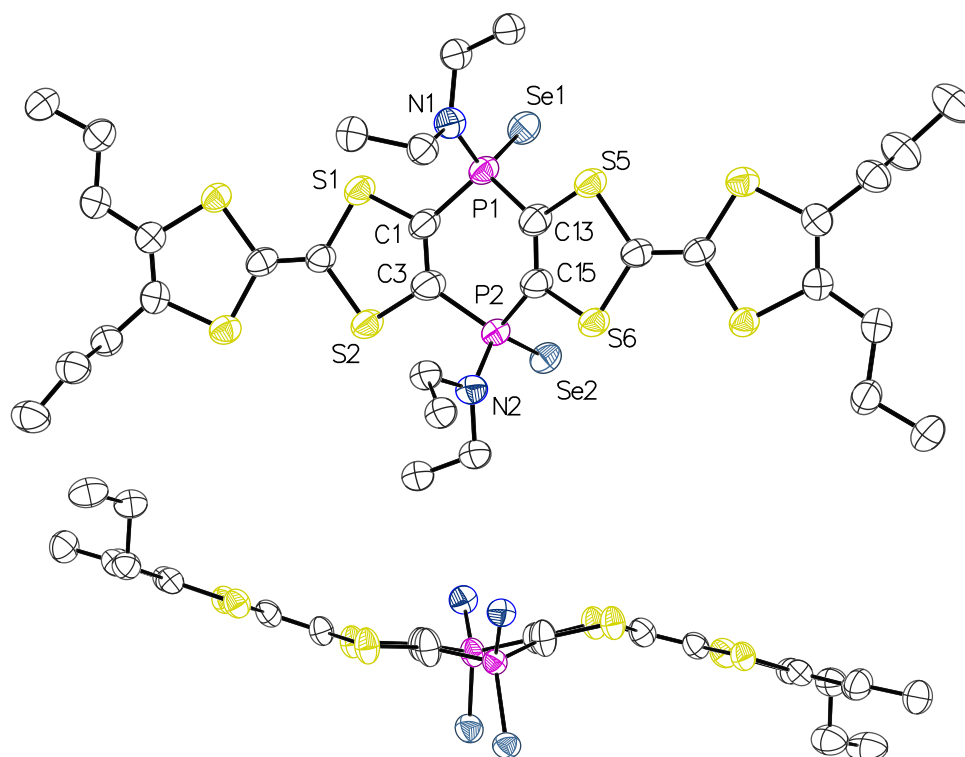


Figure 5.11. Top: ORTEP drawing of the molecular structure of *cis-14b* in the solid state (ellipsoids are set at 50% probability level and hydrogen atoms are omitted for clarity); bottom: Side view of the ORTEP drawing of the molecular structure of *cis-14b* in the solid state (ellipsoids are set at 50% probability level, hydrogen atoms and ethyl groups are omitted for clarity).

Table 5.6. Selected bond lengths and angles for *cis-14b*.

Bond lengths/Å		Bond angles/°	
P1–C1	1.806(7)	N1–P1–C1	105.0(3)
P1–C13	1.813(6)	N1–P1–C13	105.7(3)
P1–N1	1.651(6)	N1–P1–Se1	115.2(2)
P1–Se1	2.081(2)	C1–P1–C13	101.5(3)
P2–C3	1.824(7)	N2–P2–C3	106.0(4)
P2–C15	1.793(6)	N2–P2–C15	102.0(3)
P2–N2	1.652(7)	N2–P2–Se2	115.5(2)
P2–Se2	2.079(2)	C3–P2–C15	100.5(3)

5.3.3 Cyclic voltammetry studies of oxidized 1,4-dihydro-1,4-diphosphinines

The electrochemical properties of compounds **12–14** were investigated by employing cyclic voltammetry studies in dichloromethane. For these compounds, as their precursors, four redox waves, attributed to the sequential formation of the related radical cation and then dication followed by further oxidation to the tri and tetracationic species were expected in the positive region, but cyclic voltammograms exhibited three distinct redox waves in all cases (Figure 5.12, A35, A39 and A43). $E_{1/2}$, ΔE_p and I_p values for these processes are given in Table 5.7 and The differences between the first and second redox potentials are in good agreement with compounds **11d,d'–f,f'**. For **12a,a'–b,b'** the third and fourth oxidations were recorded in a single potential (note the increase in the related anodic current in Table 5.7), but in the other cases, the last two processes were not distinguishable and recorded as a broad redox wave (with ΔE_p values between 146 to 166 mV). This observation which was also reported by Avarvari for his compounds¹³⁴, can be attributed to the lower solubility of the oxidized species which causes adsorption phenomena, and also proximity of the redox potentials to each other and to the solvent limit. The higher oxidation potentials, compare to the precursor compounds by almost 200 mV, due to the chemical oxidation at the *P*-centers, is also noteworthy. Based on the obtained data, the first two oxidation processes could be considered quasi-reversible, but since the third and fourth oxidations are recorded either at the same potential or as a broad wave, ΔE_p values for these processes deviated from the Nernst equation. In addition to these oxidation processes, which are occurring at the TTF units, these compounds showed one (**12a,a'–b,b'** and **13b,b'**) or two (**13a,a'** and **14a,a'–b,b'**) reduction waves (Figure 5.13), which could be attributed to the reduction of the *P*-centers. The second reduction process for **12** and **13b,b'** is likely occurring at a lower potential than the solvent limit and hence was not observed. For compounds **12a,a'** and **12b,b'** a return oxidation wave was also observed (Figure 5.13) and based on the obtained ΔE_p and I_p^a/I_p^c from the voltammograms (Table 5.8) this reduction process is quasi-reversible, but for compounds **13** and **14** due to the proximity of the potentials to the solvent limit, a clear examination of the reversibility of these processes was not possible. However, E_p^c and I_p^c for these processes are given in Table 5.8. Also, scan rate dependency studies were performed by measuring CVs at various scan rates (50, 100, 200, 400 and 800 mVs⁻¹) (see the

appendix) and the plots of the cathodic peak current versus the square root of the scan rates were depicted for the first reduction waves (Figure 5.14), which show the linear increase of the peak currents concerning the square root of the scan rate, based on the Randles–Ševčík equation (Equation 3.1), and prove this process is diffusion-controlled.

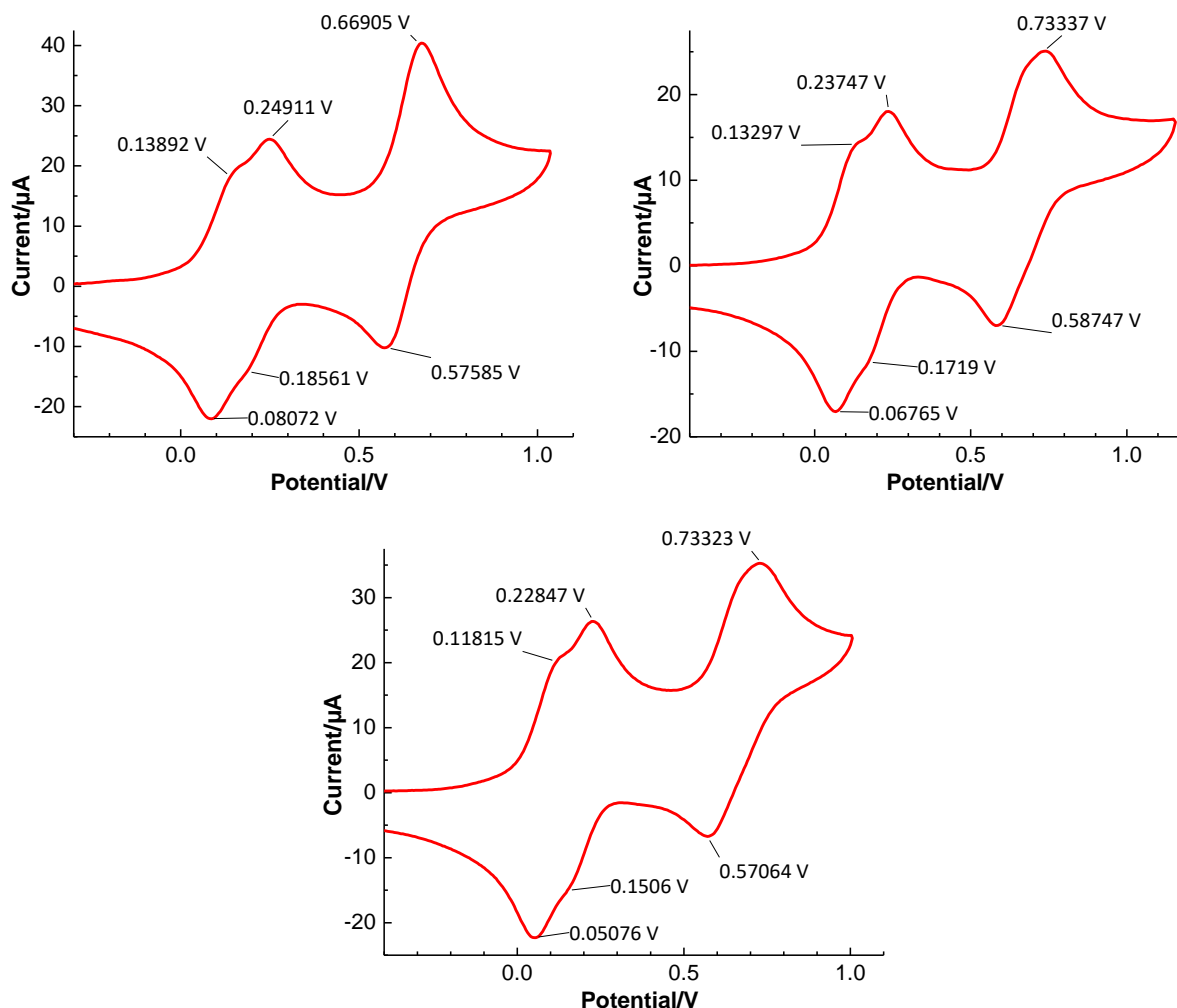


Figure 5.12. Cyclic voltammograms (oxidation processes) of **12a,a'** (top left), **13a,a'** (top right) and **14a,a'** (bottom) vs. $\text{Fc}^{0/+}$ (0.4 M $n\text{Bu}_4\text{PF}_6$ in DCM, 200 mVs^{-1}).

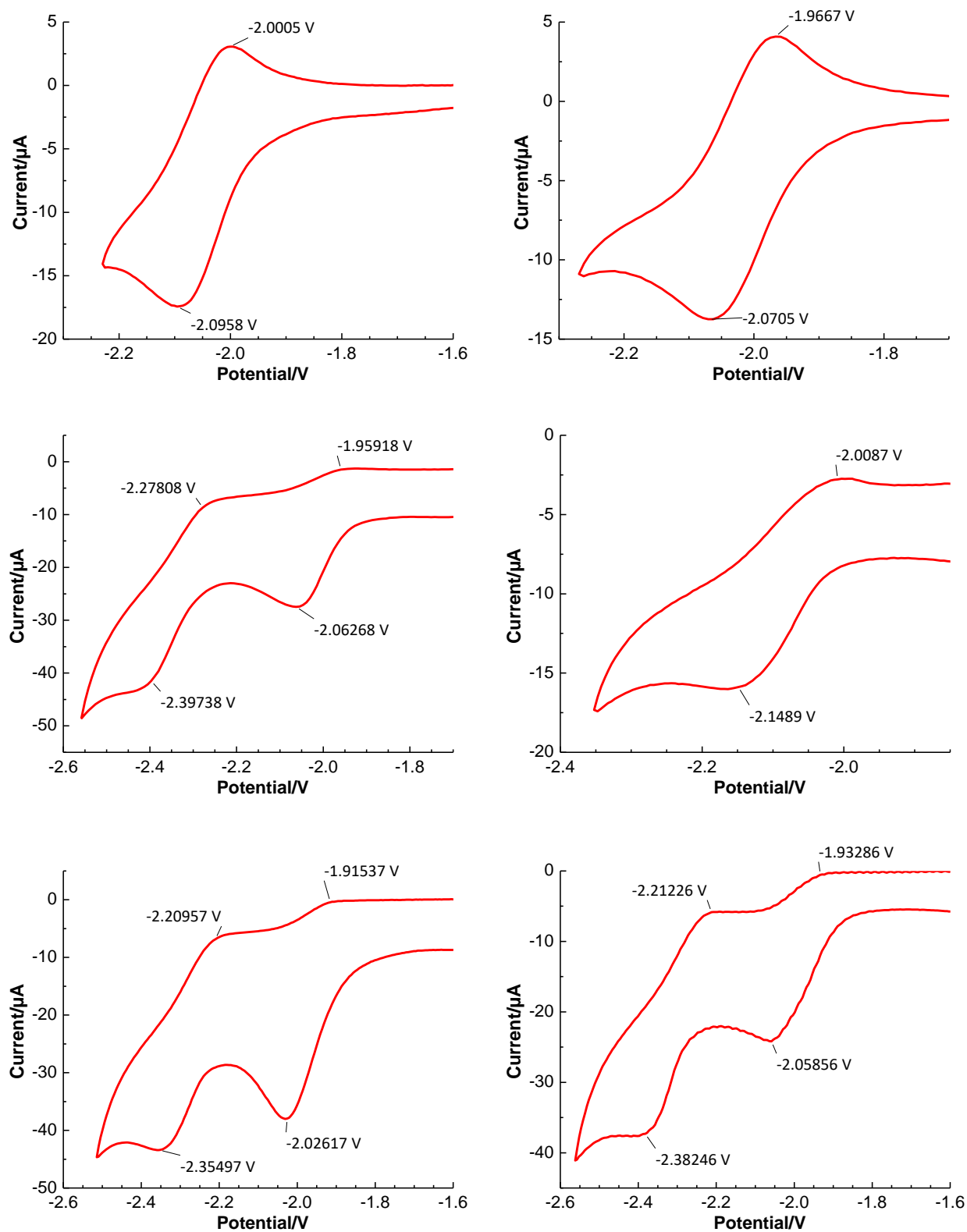


Figure 5.13. Cyclic voltammograms (reduction processes) of **12a,a'** (top left), **12b,b'** (top right), **13a,a'** (middle left), **13b,b'** (middle right), **14a,a'** (bottom left) and **14b,b'** (bottom right) Vs. $\text{Fc}^{0/+}$ (0.4 M $n\text{Bu}_4\text{PF}_6$ in DCM, 200 mVs^{-1}).

Table 5.7. Half wave potentials (Vs. $\text{Fc}^{0/+}$), $\Delta E_{1/2}$, cathodic and anodic currents for oxidation processes of compounds **12–14** (0.4 M $n\text{Bu}_4\text{PF}_6$ in DCM, 200 mVs^{-1}).

Compound	$E_{1/2}^1/\text{V}$ ($\Delta E_p/\text{mV}$)	$E_{1/2}^{1'}/\text{V}$ ($\Delta E_p/\text{mV}$)	$\Delta E_{1/2}^{1,1'}/\text{mV}$	$E_{1/2}^2/\text{V}$ ($\Delta E_p/\text{mV}$)
	$[I_p^a: I_p^c/\mu\text{A}]$	$[I_p^a: I_p^c/\mu\text{A}]$		$[I_p^a: I_p^c/\mu\text{A}]$
12a,a'	0.11 (58.2) [17.9:18.2]	0.22 (63.5) [14.0:14.7]	110	0.62 (93.2) [24.3:18.8]
12b,b'	0.09 (56.9) [15.4:16.3]	0.20 (65.4) [12.2:11.6]	110	0.60 (104.5) [18.9:16.1]
13a,a'	0.10 (65.3) [13.2:12.7]	0.20 (65.6) [11.3:10.7]	100	0.66 (145.9) [13.8:13.3]
13b,b'	0.09 (65.1) [8.5:8.3]	0.20 (80.4) [8.4:6.7]	110	0.66 (165.8) [8.7:7.1]
14a,a'	0.08 (67.4) [19.9:18.3]	0.19 (77.9) [17.4:14.4]	110	0.65 (162.6) [18.5:15.4]
14b,b'	0.08 (68.2) [18.6:19.7]	0.18 (73.3) [17.6:15.1]	100	0.65 (159) [21.5:19.7]

Table 5.8. Half wave potentials (Vs. $\text{Fc}^{0/+}$), $\Delta E_{1/2}$, cathodic and anodic currents for reduction processes of compounds **12–14** (0.4 M $n\text{Bu}_4\text{PF}_6$ in DCM, 200 mVs^{-1}).

Compound	E_p^{c1}/V ($I_p^{c1}/\mu\text{A}$)	E_p^{a1}/V ($I_p^{a1}/\mu\text{A}$)	E_p^{c2}/V ($I_p^{c2}/\mu\text{A}$)	E_p^{a2}/V ($I_p^{a2}/\mu\text{A}$)
12a,a'	-2.09 (14.3)	-2.00 (16.0)	–	–
12b,b'	-2.07 (11.3)	-1.97 (13.2)	–	–
13a,a'	-2.06 (16.5)	-1.96	-2.40 (18.1)	-2.28
13b,b'	-2.15 (7.8)	-2.01	–	–
14a,a'	-2.03 (18.3)	-1.91	-2.35 (14.1)	-2.21
14b,b'	-2.06 (17.2)	-1.93	-2.38 (14.7)	-2.21

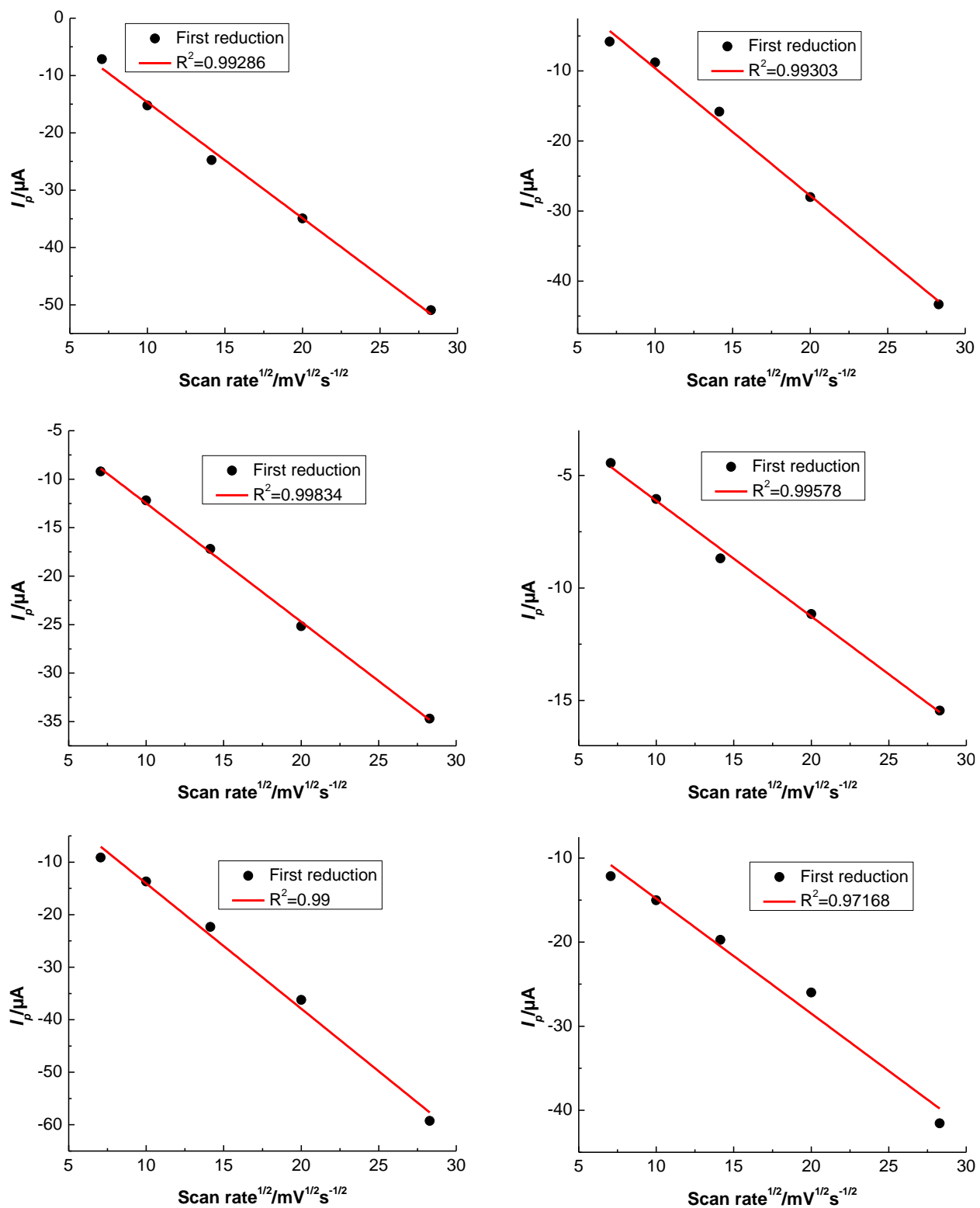


Figure 5.14. Dependency of the cathodic peak current (first reduction process) on the scan rate for **12a,a'** (top left), **12b,b'** (top right), **13a,a'** (middle left), **13b,b'** (middle right), **14a,a'** (bottom left) and **14b,b'** (bottom right).

5.4 Scrambling reaction of 11d,d' and 11f,f' with PCl₃

After getting access to 1,4-bis(diethylamino)-1,4-dihydro-1,4-diphosphinines (**11d,d'** and **11f,f'**) our next objective was to synthesize 1,4-diphosphinines fused to two TTF units. As it was discussed in the introduction, even though the chemistry of phosphinines and related compounds has been developed for more than half a century, the only example of a 1,4-diphosphinine **LXXVIII** was reported by Kobayashi⁸² (Figure 5.15), until the first isolated 1,4-diphosphinine having an imidazole-2-thione backbone **LXXXIV** (Figure 5.15), was introduced by the Streubel group in 2017.⁷⁸ Since then, several lines of research, using different backbones, were followed by our group to exploit 1,4-diphosphinine chemistry and our goal was establishing it as a linker between two TTF units, thus enabling new P-functional redox systems.

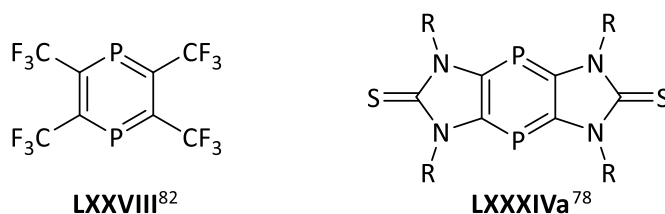
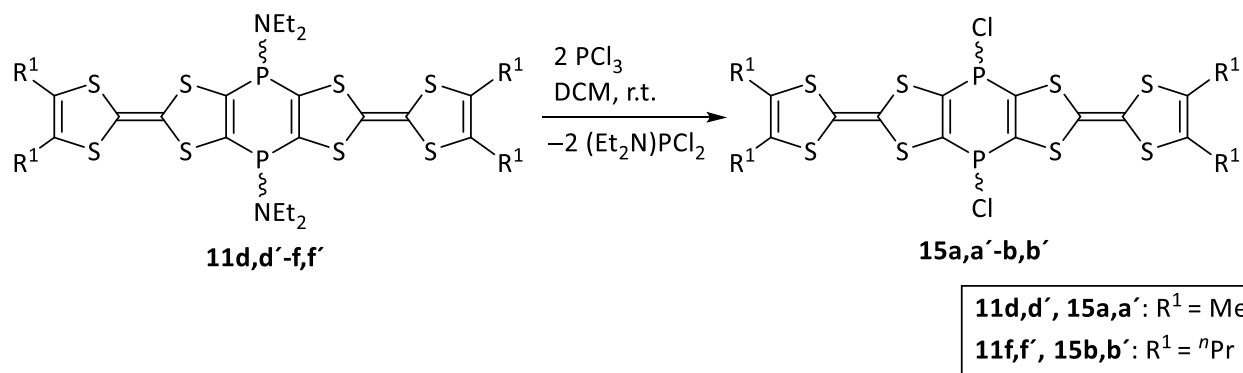


Figure 5.15. First example of a 1,4-diphosphinine **LXXVIII**⁸² and first isolated 1,4-diphosphinines **LXXXIV**.⁷⁸

To achieve our target, in the first step, the scrambling reaction between P-N and P-Cl bonds was performed with isomeric mixtures of 1,4-bis(diethylamino)-1,4-dihydro-1,4-diphosphinines (**11d,d'** and **11f,f'**). Therefore, these compounds were treated with PCl₃ in dichloromethane (Scheme 5.5).



Scheme 5.5. Scrambling reaction of **11d,d'-f,f'**.

In the case of **11d,d'**, after the addition of PCl_3 , a rapid color change from dark red to brown followed by the formation of a dark brown precipitate was observed and the $^{31}\text{P}\{^1\text{H}\}$ NMR spectrum of the reaction mixture showed two signals at 216 ppm and 162 ppm, assigned to the unreacted PCl_3 and Et_2NPCl_2 , respectively, but no other resonances for the product (Figure 5.16). After evaporation of all volatiles, different solvents were used to dissolve the residue, but it was not soluble in common organic solvents and resulted in all cases in an “empty” $^{31}\text{P}\{^1\text{H}\}$ NMR spectrum.

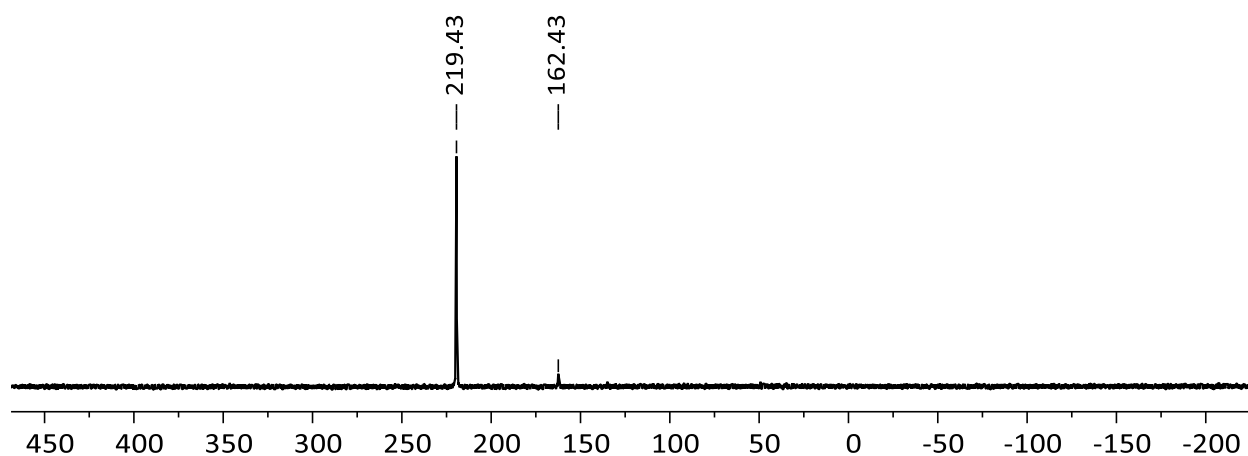


Figure 5.16. $^{31}\text{P}\{^1\text{H}\}$ NMR spectrum of the reaction of **11d,d'** with PCl_3 (reaction mixture).

$^{31}\text{P}\{^1\text{H}\}$ NMR monitoring revealed for the reaction of **11f,f'** with PCl_3 one broad resonance at 35 ppm with FWHM of 191 Hz (Figure 5.17), in addition to the previously mentioned signals for the unreacted PCl_3 and Et_2NPCl_2 . After removal of all volatiles in *vacuo* (8×10^{-3} mbar) and washing the residue with petrol ether, the $^{31}\text{P}\{^1\text{H}\}$ NMR spectrum of the product showed two singlet resonance signals at 35 and 38.2 ppm (ratio 1:0.15) (Figure 5.17). This broadening of the resonance in the ^{31}P NMR spectrum and relatively small change in chemical shift, compared to the starting material, is somehow consistent with the previously reported 1,4-dichloro-1,4-dihydro-1,4-diphosphinines by the Streubel group.^{78,85} The EI-MS spectrum of **15b,b'**, did not show any signal corresponding to the molecular ion peak, but the signals found at m/z 634.0 and 70.0 could be attributed to the related 1,4-diphosphinine $[\text{M}-\text{Cl}_2]^+$ fragment and Cl_2 radical cation, respectively.

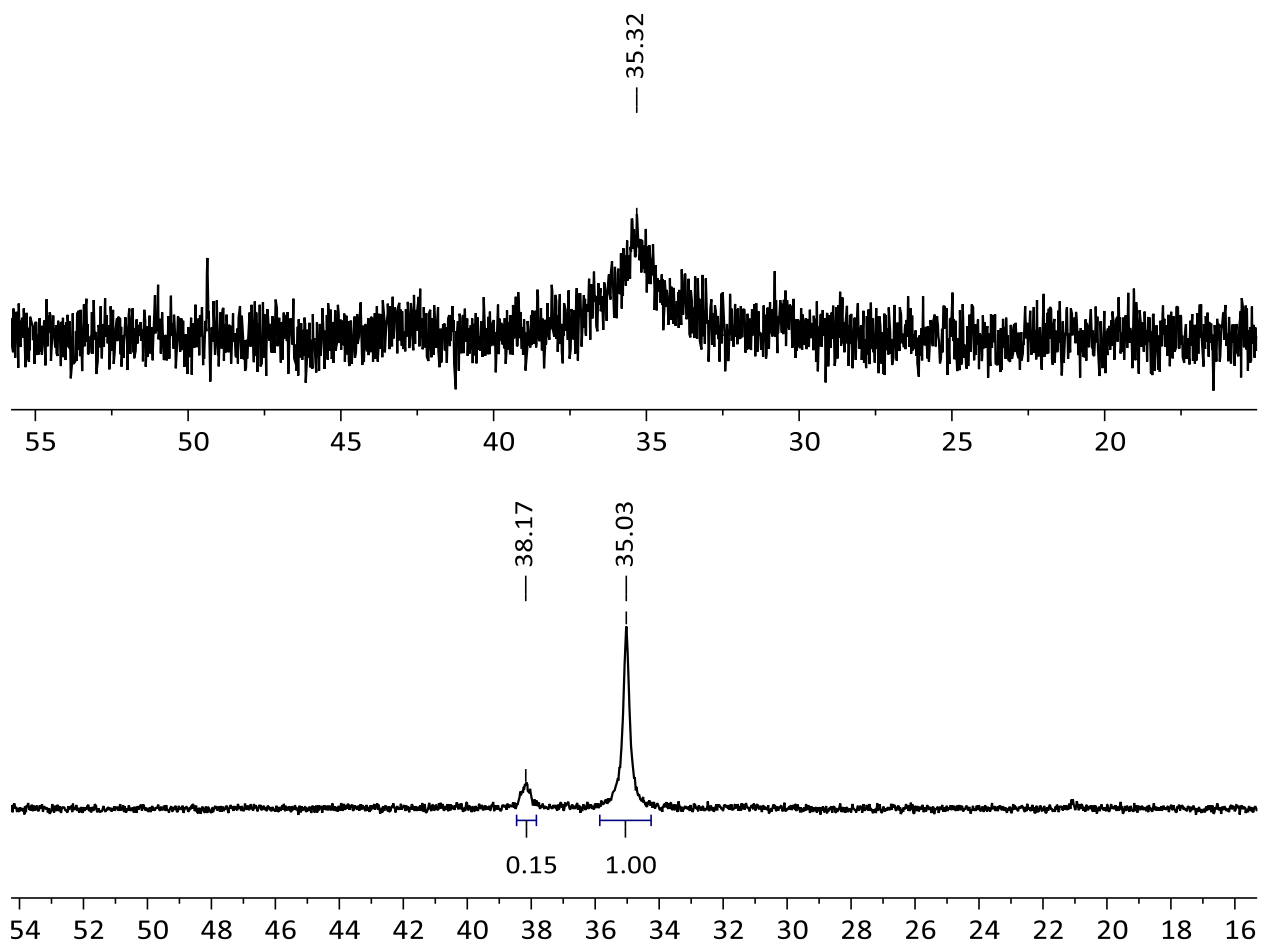


Figure 5.17. A cut out of $^{31}\text{P}\{^1\text{H}\}$ NMR spectrum of **15b,b'** from the reaction mixture (top) and after work up in CD_2Cl_2 (bottom).

Calculations by Kalisch, show two energetically close isomers ($\Delta G_{cis/trans} = 0.7$ kcal/mol) for 1,4-dichloro-1,4-dihydro-1,4-diphosphinines. In contrast to one expected ^{31}P NMR resonance for the *cis* isomer, the *trans* isomer is expected to exhibit two signals for axial and equatorial P–Cl bonds (Figure 5.18). This is in good agreement with model compounds ($\delta_{trans}/\text{ppm} = 37.6$ (eq), 9.1 (ax), $\delta_{cis}/\text{ppm} = 32.0$), calculated by Espinosa Ferao⁸⁰, which also revealed very fast coalescence of axial and equatorial positions ($\Delta G^\ddagger = 0.25$ kcal/mol). The latter could also explain the broad ^{31}P NMR resonance signal for **15b,b'** in solution.

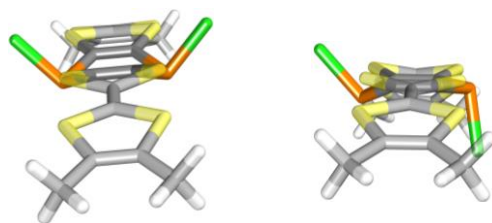
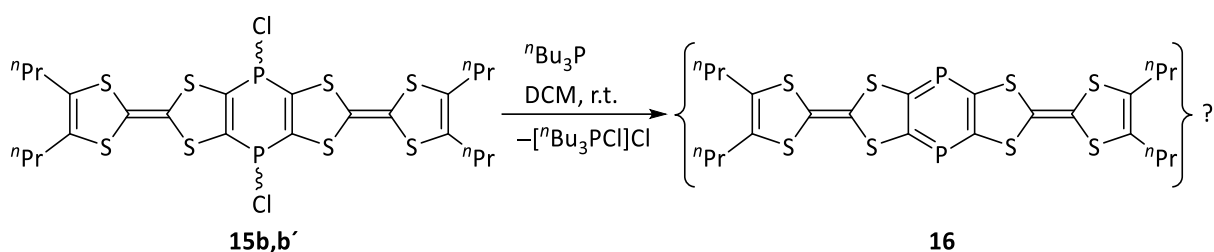


Figure 5.18. Calculated geometries for *cis/trans*-1,4-dichloro-1,4-dihydro-1,4-diphosphinine; Level of theory: TPSS-D3/def2-TZVP (CPCM THF)//PW6B95-D3/def2-QZVP (CPCM THF).

5.5 Reducing the *P*-Cl substituted 1,4-dihydro-1,4-diphosphinine **15**

To get access to the desired 1,4-diphosphinine fused to two TTF units an isomeric mixture of **15b,b'** was treated with ${}^n\text{Bu}_3\text{P}$ (Scheme 5.6), following the established protocol^{78,81,85}.



Scheme 5.6. Attempted synthesis of 1,4-diphosphinine **16**.

Despite the formation of the expected phosphonium salt $[\text{}^n\text{Bu}_3\text{PCl}]\text{Cl}$, the ${}^{31}\text{P}\{^1\text{H}\}$ NMR spectrum of the dark brown reaction mixture did not exhibit any resonance which could be attributed to the desired product based on the calculated ${}^{31}\text{P}$ NMR shift (by Kalisch): 183.0 ppm; referenced to thiazole-2-thione-based diphosphinine; level of theory: B97-D3(CPCM_{THF})/def2-TZVP), also formation of precipitate was not observed. Different temperatures ($-80\text{ }^\circ\text{C}$, $-40\text{ }^\circ\text{C}$ and $0\text{ }^\circ\text{C}$) and solvents (THF, Toluene) were used, but the outcome remained almost the same and led to an unselective reaction having resonances between -75 to 65 ppm in ${}^{31}\text{P}\{^1\text{H}\}$ NMR spectrum (Figure 5.19); including high field AB-spin systems with coupling constants around 11 and 26 Hz (Figure 5.19).

DFT calculations of **16** (by Kalisch) revealed a considerably smaller HOMO/LUMO gap (2.5 eV) compared to the tricyclic 1,4-diphosphinines, reported earlier by the Streubel group (Table 5.9). Despite this small HOMO/LUMO gap, based on the results of the calculations by Nyulászi and Kelemen, **16** is a closed-shell singlet and the triplet state is less stable by 30.2 kcal/mol; also any

attempts to find an open shell singlet remained unsuccessful. These calculations also showed a *trans*-bent structure for **16** (Figure 5.20), which lowers the aromaticity of the central ring (NICS(1) = -5.2) in comparison to previously described 1,4-diphosphinines (Table 5.9) while the related dication possess a planar structure (Figure 5.20).

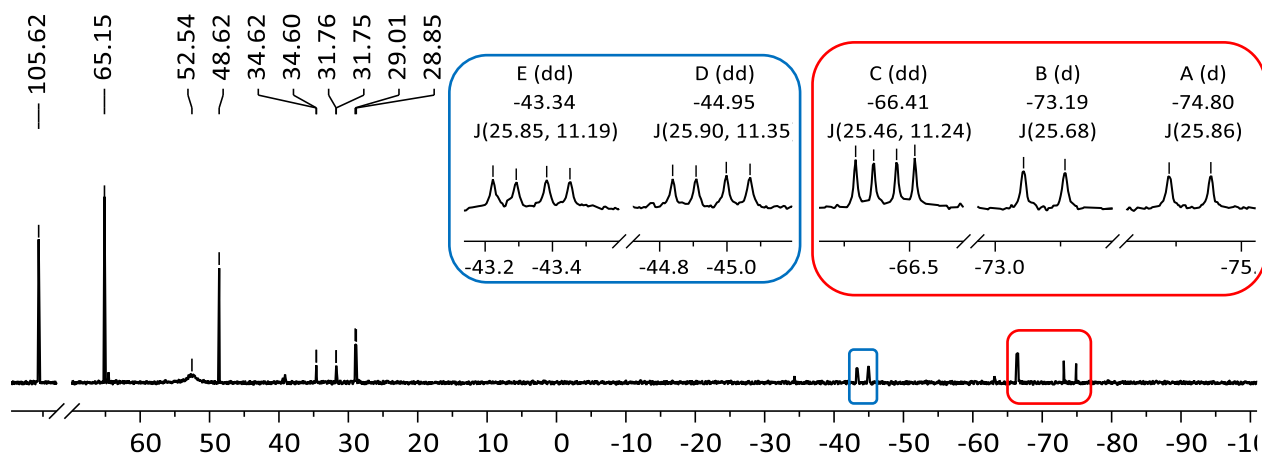


Figure 5.19. $^{31}\text{P}\{^1\text{H}\}$ NMR spectrum of the reaction of **15b,b'** with $^t\text{Bu}_3\text{P}$.

Table 5.9. NICS(1) values and HOMO/LUMO gaps for 1,4-diphosphinines; level of theory for optimization/energy: TPSS-D3/def2-TZVP (CPCM_{THF})/PW6B95-D3/def2-QZVP (CPCM_{THF}); level of theory for NICS(1) values: B3LYP-D3/def2-TZVPPD.

Annulated ring of 1,4-Diphosphinine	NICS(1)	HOMO/LUMO gap (eV)
Imidazole-2-thione	-8.1	3.3
Imidazole-2-selone	-8.1	3.1
Thiazole-2-thione	-7.2	3.4
Dithiole-2-thione	-6.2	3.6
TTF	-5.2	2.5
TTF dication	-3.5	0.8

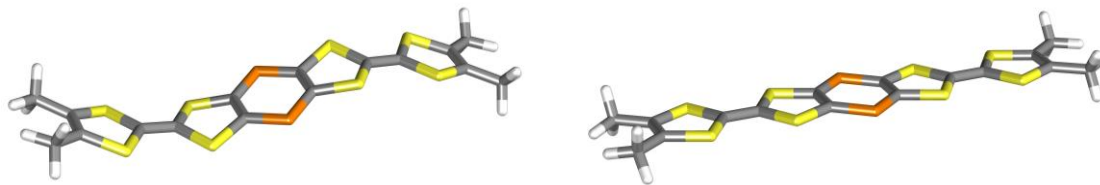


Figure 5.20. Calculated structures for 1,4-diphosphinine (left) and related dication (right); level of theory: TPSS-D3/def2-TZVP (CPCM_{THF})/PW6B95-D3/def2-QZVP (CPCM_{THF}).

Considering the smaller HOMO/LUMO gap and lower aromaticity, suggested by DTF calculations and their possible effect on the reactivity and/or sensitivity of the desired 1,4-diphosphinine, reaction with ⁿBu₃P was performed in the dark. This reaction resulted in a more selective ³¹P{¹H} NMR spectrum with fewer resonances, but still no sign of the expected resonance of the desired, new 1,4-diphosphinine derivative. Different solvents were examined to make sure that this observation was not due to the lack of solubility of the product, but the outcome remained the same (Figure 5.21).

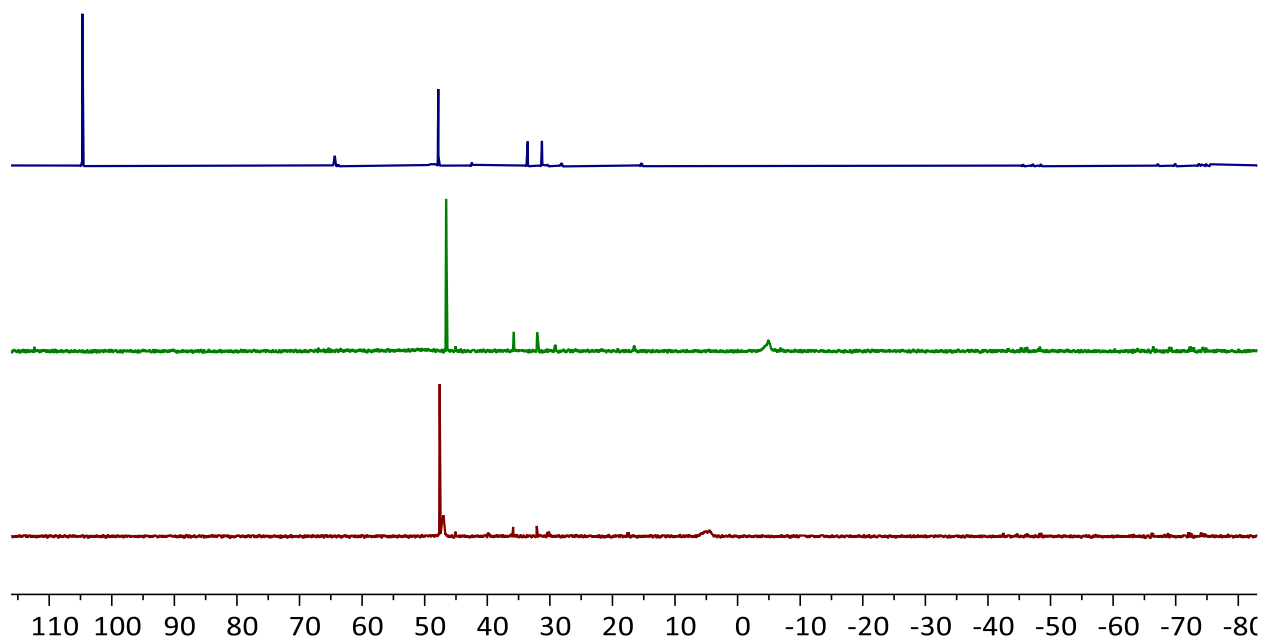
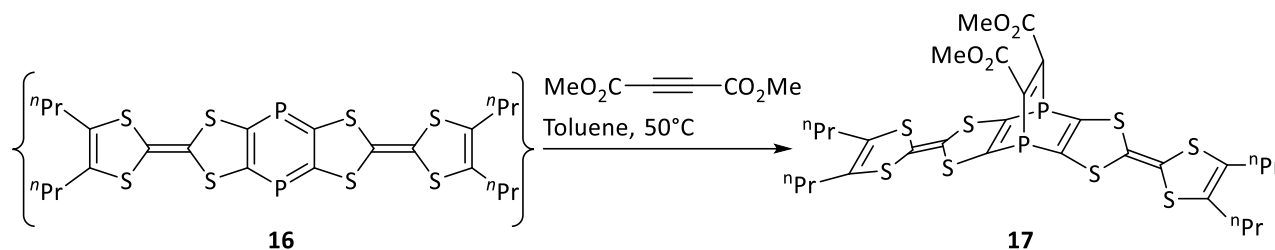


Figure 5.21. ³¹P{¹H} NMR spectrum of the reaction of **15b,b'** with ⁿBu₃P in dark, in DCM (top), toluene (middle) and THF (bottom).

5.6 Trapping of a TTF-fused 1,4-diphosphinine

To probe the assumption that the product mixture of the reaction of **15b,b'** with $n\text{Bu}_3\text{P}$ contained the targeted 1,4-diphosphinine **16**, the raw product mixture was heated with dimethylacetylene dicarboxylate (DMAD) in toluene at elevated temperature to achieve the [4+2]-cycloaddition reaction (Scheme 5.7).



Scheme 5.7. Conversion of crude 1,4-diphosphinine **16** via reaction with DMAD.

After one day a signal at -70.3 ppm was observed in the $^{31}\text{P}\{^1\text{H}\}$ NMR spectrum (Figure 5.22), which was well in the range of the phosphorus chemical shifts for the previously reported 1,4-diphosphabarrelenes having a dimethyl (or diethyl) ethylene dicarboxylate as bridging unit (-87.3 to -73.5 ppm).^{80,88,89} But the intensity of the signal was too low and after stirring the reaction mixture for a longer time, it disappeared (Figure 5.22).

The DFT calculations for the molecular orbitals of **16** showed that the HOMO is mainly located on the TTF units, while the LUMO is localized on the central 1,4-diphosphinine ring (Figure 5.23). These results, together with the slow and unselective reaction of DMAD as an electron-deficient alkyne with **16**, revealed that electron-rich alkyne and/or alkene would be a better choice to achieve [4+2]-cycloaddition reaction with our system. In addition to these qualities, a terminal alkene and/or alkyne could result in an asymmetric product and, hence, a higher solubility. Apart from this assignment of the ^{31}P and ^1H NMR resonances might be facilitated. Therefore, 1-hexene was chosen as the trapping reagent in a slightly modified reaction.

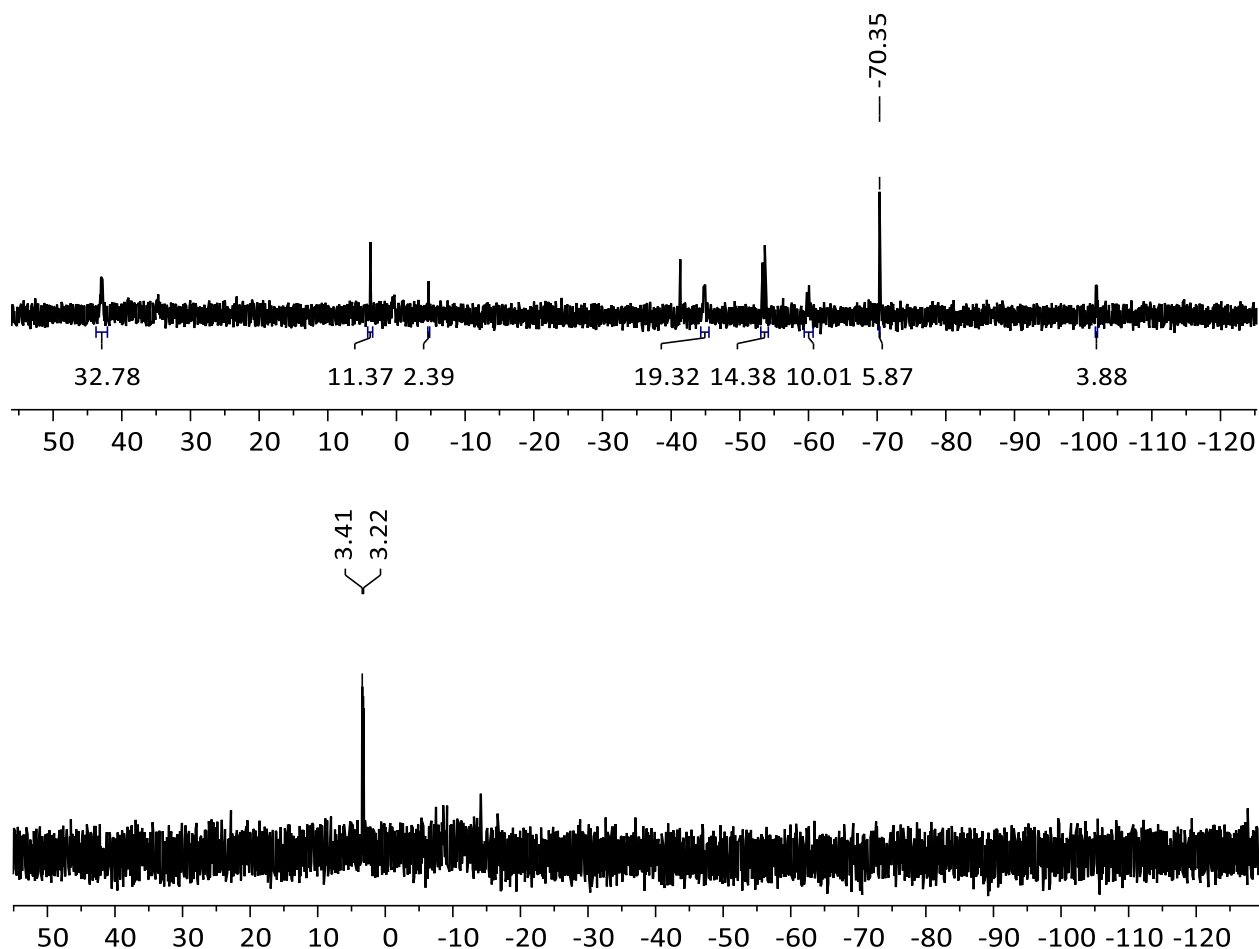


Figure 5.22. $^{31}\text{P}\{^1\text{H}\}$ NMR spectrum of the reaction of **16** with DMAD, after 1 day (top) and after 4 days (bottom).

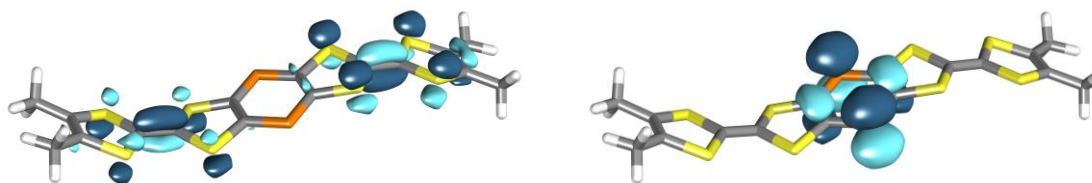
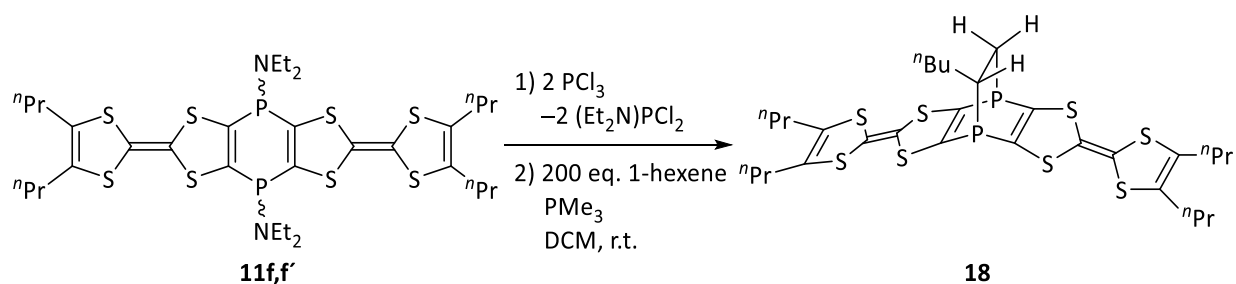


Figure 5.23. HOMO (left) and LUMO (right) for **16**; Level of theory: TPSS-D3/def2-TZVP (CPCM_{THF})/PW6B95-D3/def2-QZVP (CPCM_{THF}).

The best outcome was achieved in the reaction of freshly formed 1,4-dichloro-1,4-dihydro-1,4-diphosphinine with Me_3P , after removal of the Et_2NPCl_2 in *vacuo* (8×10^{-3} mbar), using a huge excess of 1-hexene (200 eq) (Scheme 5.8). After 3 days, the $^{31}\text{P}\{^1\text{H}\}$ NMR spectrum showed an almost selective conversion into the desired 1,4-diphosphabarrelene **18** (Figure 5.24). The product (**18**) could be obtained after the removal of all volatiles in *vacuo* (8×10^{-3} mbar) and extraction with n-pentane and was fully characterized by various analytical techniques such as

multinuclear NMR spectroscopy, MS spectrometry and elemental analysis. $^{31}\text{P}\{^1\text{H}\}$ NMR spectrum exhibits two sets of doublets at -71.7 and -67.7 with a ratio of 1:0.9 and coupling constant of 32.4 Hz; Also the two phosphorus atoms can be distinguished via ^{31}P NMR spectroscopy where a signal resonance (doublet of triplet) at -71.7 ppm with the coupling constants of 32.4 ($^3J_{\text{P,P}}$) and 8.1 ($^2J_{\text{P,H}}$) Hz can be attributed to the phosphorus atom attached to the terminal CH_2 while the other phosphorus atom appears as a multiplet resonance at -67.7 . The EI-MS spectrum of **18**, in addition to the molecular ion peak (m/z 718.036), shows a signal at m/z 633.942 $[\text{M}-\text{C}_6\text{H}_{12}]^+$ which matches the calculated m/z value (633.943) of the related 1,4-diphosphinine **16**.



Scheme 5.8. Synthesis of 1,4-diphosphabarrelene fused to two TTF units **18**.

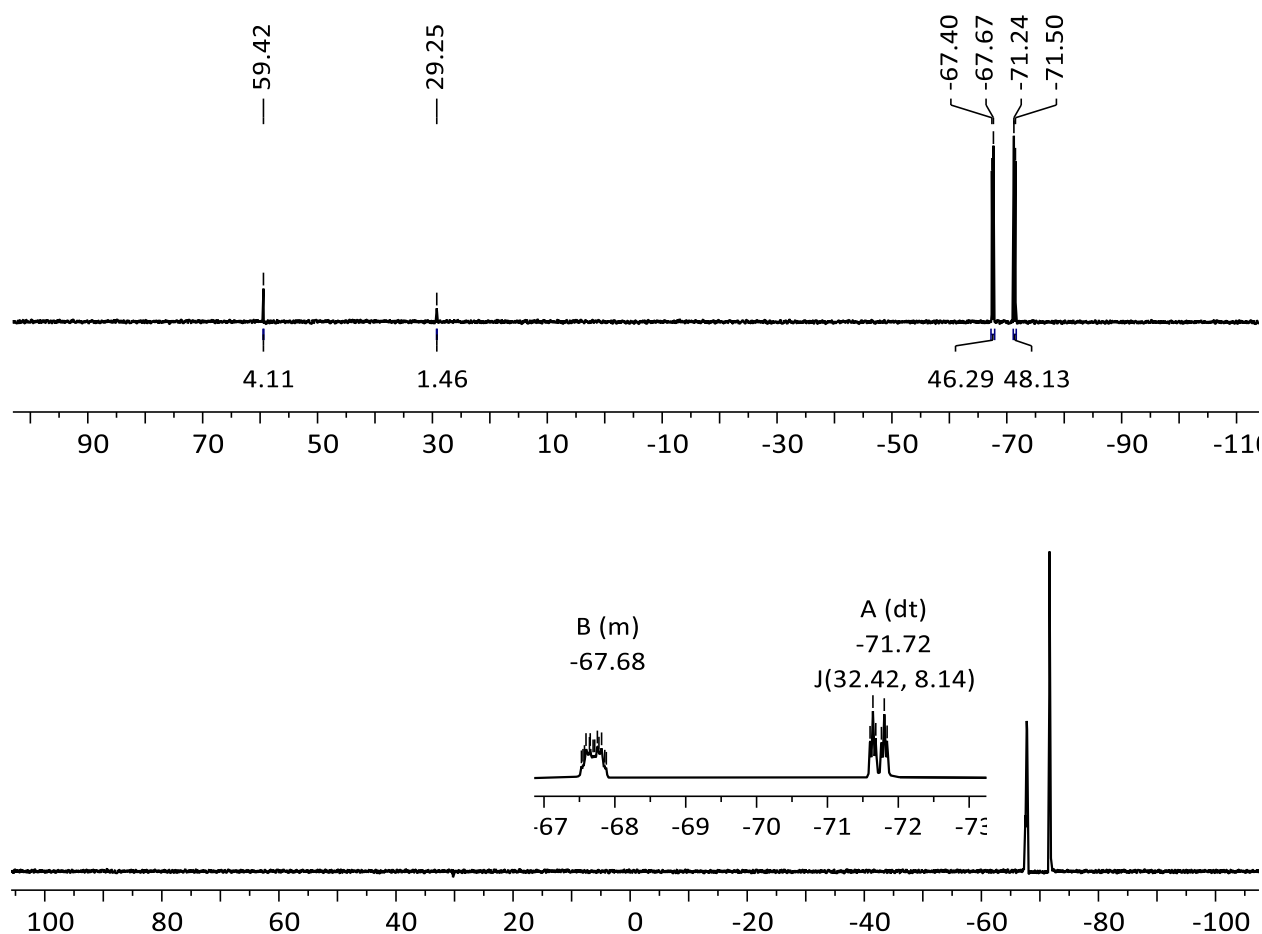


Figure 5.24. $^{31}\text{P}\{^1\text{H}\}$ NMR spectrum of the reaction mixture (top) and ^{31}P NMR spectrum of the isolated 1,4-diphosphabarrelene **18** (bottom).

5.6.1 Cyclic voltammetry study of 1,4-diphosphabarrelene **18**

To investigate the electrochemical properties of **18**, cyclic voltammetry studies were performed in dichloromethane. For this compound, same as for the previous compounds containing two TTF motifs, four sequential, one-electron transfer processes yielding a tetracation species were expected, but the cyclic voltammogram showed only three oxidation processes (Figure 5.25). Likely due to the lower solubility of the oxidized species which causes adsorption phenomena, and also proximity of the redox potentials to each other and to the solvent limit, the last two processes were not distinguishable and recorded as a broad redox wave, with ΔE_p values of 145 mV (Table 5.10). However, the separation between the first and second redox potentials (Table 5.10), as a measure of the degree of communication between two TTF units, is in good agreement with the previous compounds described beforehand. Based on the obtained $E_{1/2}$, ΔE_p and I_p

values (Table 5.10), the first two oxidation processes could be considered quasi-reversible, but since the third and fourth oxidations are recorded as a broad wave, ΔE_p value deviated from the Nernst equation. Also, CVs were recorded at various scan rates (50, 100, 200, 400 and 800 mVs^{-1}) (see the appendix) and the plots of the anodic peak current versus the square root of the scan rates were depicted for the first and second redox waves (Figure 5.25). The linear increase of the peak currents with respect to the square root of the scan rate, based on the Randles–Ševčík equation (Equation 3.1), proves the diffusion-controlled origin of these redox processes.

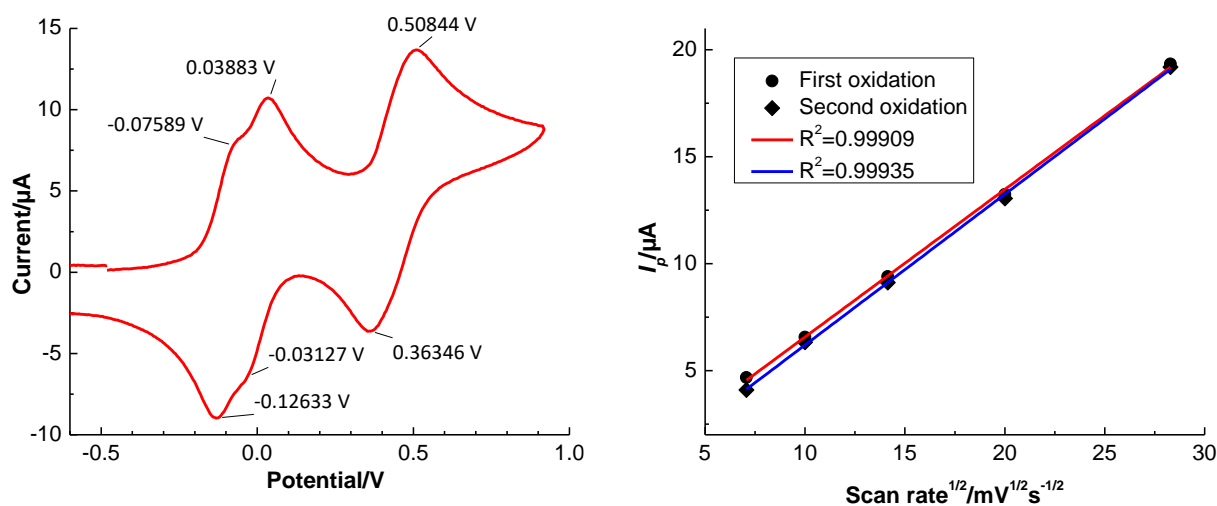


Figure 5.25. Cyclic voltammograms of **18** (left) Vs. $\text{Fc}^{0/+}$ (0.4 M $n\text{Bu}_4\text{PF}_6$ in DCM, 100 mVs^{-1}) and dependency of the anodic peak currents (first and second redox processes) on the scan rate for **18** (right).

Table 5.10. Half wave potentials (Vs. $\text{Fc}^{0/+}$), $\Delta E_{1/2}$, cathodic and anodic currents for compounds **18** (0.4 M $n\text{Bu}_4\text{PF}_6$ in DCM, 100 mVs^{-1}).

Compound	$E_{1/2}^1/\text{V}$ ($\Delta E_p/\text{mV}$)	$E_{1/2}^{1'}/\text{V}$ ($\Delta E_p/\text{mV}$)	$\Delta E_{1/2}^{1,1'}/\text{mV}$	$E_{1/2}^2/\text{V}$ ($\Delta E_p/\text{mV}$)
	$[I_p^a: I_p^c/\mu\text{A}]$	$[I_p^a: I_p^c/\mu\text{A}]$		$[I_p^a: I_p^c/\mu\text{A}]$
18	-0.10 (50.4) [7.3:6.7]	0.00 (70.1) [6.9:6.3]	100	0.44 (144.9) [7.2:7.5]

6 Oligomers containing TTF units linked by 1,4-dihydro-1,4-diphosphinine rings

The incorporation of tetrathiafulvalene units into a polymeric structure was first reported in the late 70s and early 80s, *e.g.* polyurethanes¹³⁵, polyamides¹³⁶, polyesters¹³⁷ and polysulfonates.¹³⁸ Unlike the monomeric TTF derivatives, these polymers could form resilient and processable charge transfer complexes. The developments in the synthesis of new TTF derivatives, such as stepwise lithiation and electrophilic substitution protocol^{139–141}, enabled the easy preparation of various TTF-based building blocks in high yields, in which the oxidation potentials can be finely tuned by using electron-donating or electron-withdrawing substituents. These building blocks were employed in supramolecular structures with applications in various fields such as sensors, catalysts or switches at the molecular level.^{8,23,142–144} Polymers comprising a TTF unit can be classified into two main types: i) TTF incorporated into polymer side-chains **CIII–CV**^{145–147} and ii) TTF-introduced polymer main chain systems **CVI, CVII**^{148,149} (Figure 6.1).

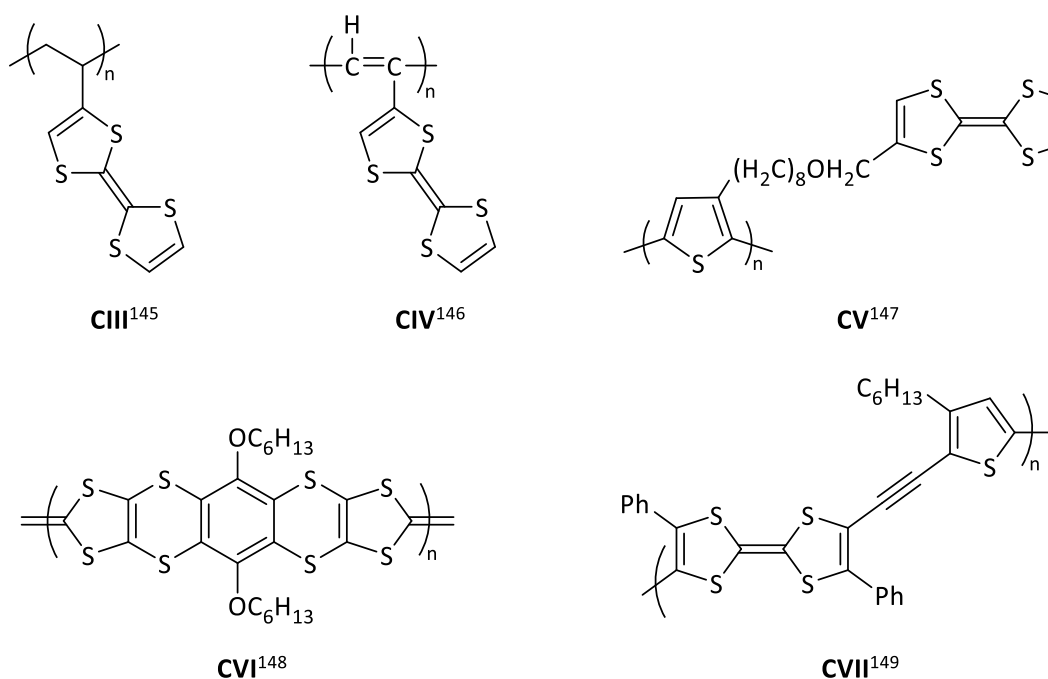
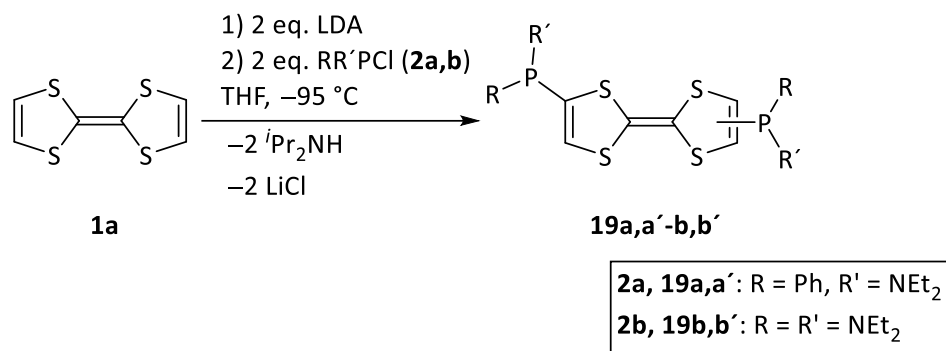


Figure 6.1. Some examples of polymers containing TTF units.^{145–149}

To achieve oligomeric and/or polymeric structures having a 1,4-dihydro-1,4-diphosphinine ring as linker between TTF units, two different synthetic approaches can be employed. First, using doubly-phosphanylated TTF as the precursor for the ring-closing reaction on both sides of the molecule, which can lead to the formation of oligomeric products. Second, the desulfurization of 1,4-dihydro-1,4-diphosphinines, annulated to two 1,3-dithiole-2-thiones, was also tested.

6.1 Doubly-phosphanylated TTFs as precursor for oligomeric products

As it was mentioned in chapter 3, doubly-phosphanylated TTFs were formed as side-products in the reaction of tetrathiafulvalene with 1 equivalent of LDA and (mono) chlorophosphanes. These compounds could be used as a starting point for synthesizing oligomeric products, containing 1,4-dihydro-1,4-diphosphinine rings bridging between TTF moieties. In order to achieve the selective formation of the desired products **19**, tetrathiafulvalene was lithiated by using two equivalents of base and subsequently reacted with chlorophosphanes **2a,b** (Scheme 6.1).



Scheme 6.1. Synthesis of doubly-phosphanylated TTFs.

The progress of each reaction was monitored by $^{31}\text{P}\{^1\text{H}\}$ NMR spectroscopy which showed new resonance signals while the starting phosphane signal had disappeared. After the removal of volatiles in *vacuo* (8×10^{-3} mbar) and the LiCl salt via filtration, compounds **19a,a'-b,b'** could be isolated in moderate yields (Table 6.1). These compounds were fully characterized by various analytical techniques such as multinuclear NMR spectroscopy and MS spectrometry. For the reaction with bis(diethylamino)chlorophosphane, the product showed two resonances at 84.65 and 84.70 with a ratio of 1:0.8 in the $^{31}\text{P}\{^1\text{H}\}$ NMR spectrum (Figure 6.2), due to the formation of pseudo-*E/Z* isomers. But in the case of chloro(diethylamino)phenylphosphane, three phosphorus

resonances were observed at 52.76, 52.85 and 52.92 ppm with a 0.5:0.5:1 respective ratio (Figure 6.2). This could be explained by the two possible configurations, concerning the positions of the substituents at the phosphorus atoms for the pseudo-Z isomer. The extreme proximity of the phosphorus chemical shifts for these isomers to each other, and also to the monophosphanylated compounds **3a,b**, proves that substitution had happened at the opposite sites of the TTF molecule.

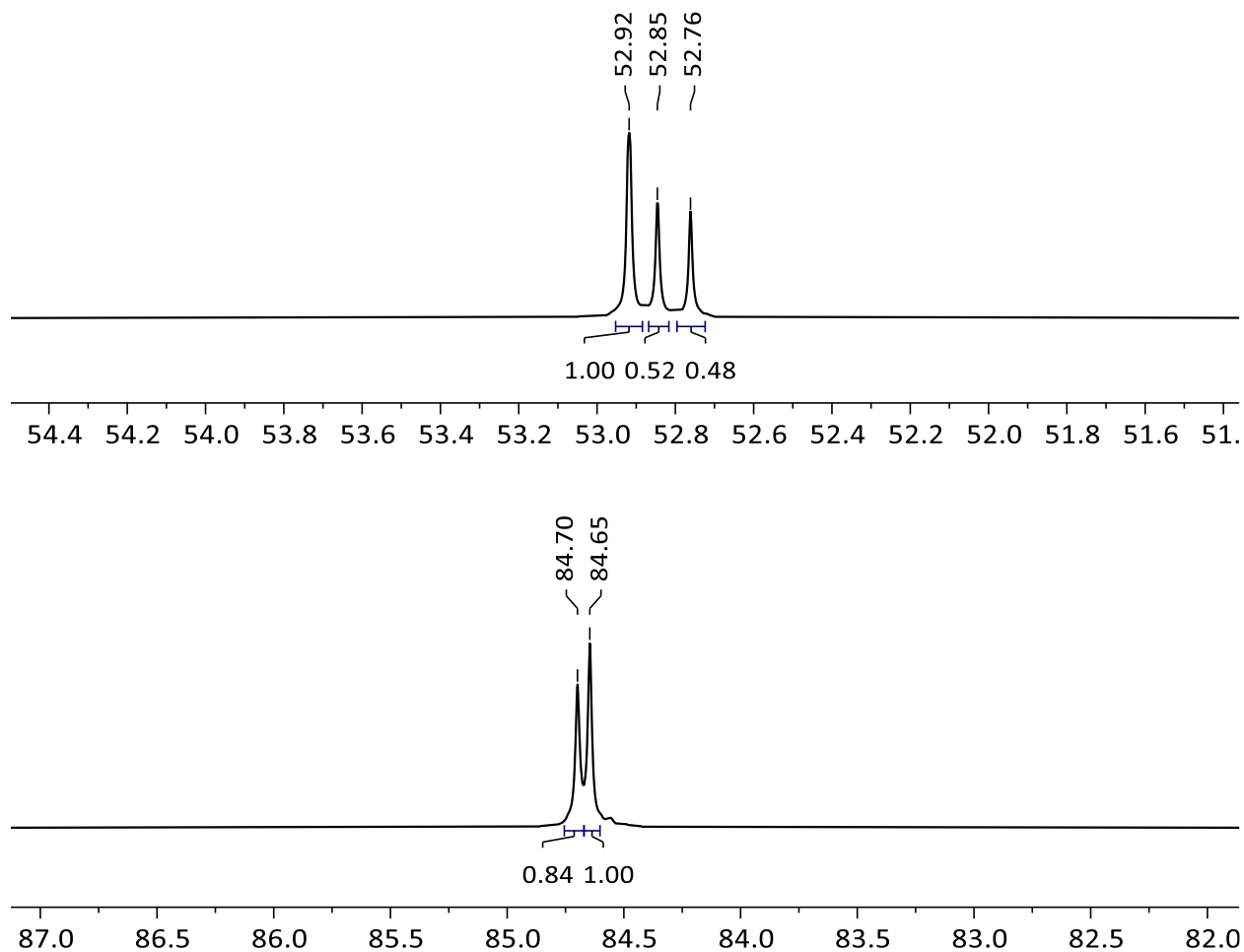


Figure 6.2. $^{31}\text{P}\{^1\text{H}\}$ NMR spectrum of **19a,a'** (top) and **19b,b'** (bottom) in CDCl_3 .

Table 6.1. Selected NMR data (in CDCl₃) and yields for compounds **19a,a'**-**b,b'**.

Compound	$\delta^{31}\text{P}\{^1\text{H}\}/\text{ppm}$	$\delta^1\text{H}/\text{ppm}$ (C ⁵ -H)	$\delta^{13}\text{C}\{^1\text{H}\}/\text{ppm}$ (C ⁴)	Yield%
19a,a'	52.76, 52.85 and 52.92	6.61 (<i>m</i>)	138.8 (<i>m</i>)	58
19b,b'	84.65 and 84.70	6.09 (<i>2d</i> , $^3J_{\text{P,H}} = 1.8$ Hz)	140.2 and 140.5 (<i>2d</i> , $^1J_{\text{P,C}} = 18$ Hz)	65

For **19b**, single crystals of the pseudo-*E* isomer, suitable for X-ray crystallographic measurements, could be obtained from the saturated diethylether solution of the isomeric mixture and was crystallized in a monoclinic lattice with space group P2₁/c (Figure 6.3); selected structural parameters are given in Table 6.2.

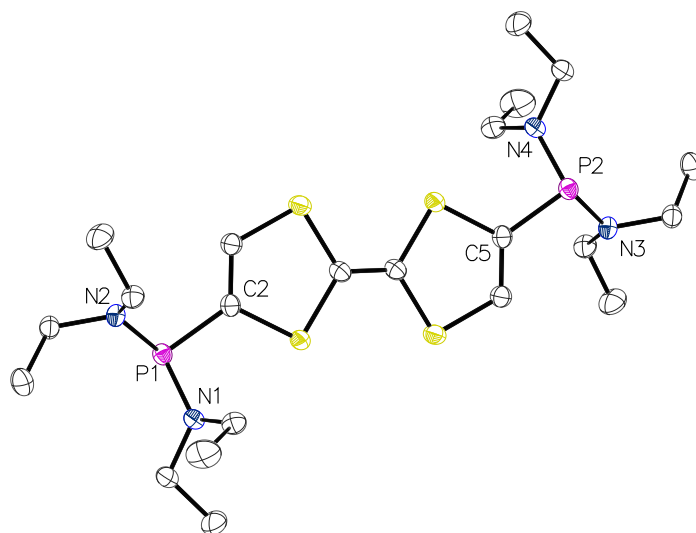
**Figure 6.3.** ORTEP drawings of the molecular structure of pseudo-*E*-**19b** in the solid state (ellipsoids are set at 50% probability level and hydrogen atoms are omitted for clarity).

Table 6.2. Selected bond lengths and angles for pseudo-*E*-**19b**.

Bond lengths/Å		Bond angles/°	
P1–C2	1.8283(17)	$\Sigma(\angle P1)$	312.7
P1–N1	1.6943(14)	$\Sigma(\angle N1)$	357.9
P1–N2	1.6907(14)	$\Sigma(\angle N2)$	353.5
P2–C5	1.8283(4)	$\Sigma(\angle P2)$	312.4
P2–N3	1.6907(3)	$\Sigma(\angle N3)$	358.1
P2–N4	1.69431(18)	$\Sigma(\angle N4)$	354.0

6.1.1 Cyclic voltammetry studies of doubly-phosphanylated tetrathiafulvalenes

The redox properties of **19a,a'-b,b'** were investigated by means of cyclic voltammetry in dichloromethane. For these compounds, two distinct redox waves were observed in the oxidation region as expected (Figure 6.4) which are corresponding to the sequential one-electron step processes, forming the related TTF radical cation and then the dication. $E_{1/2}$, ΔE_p and I_p values for these redox waves, are given in Table 6.3. Comparing the obtained data for **19a,a'-b,b'** with the mono-phosphanylated compounds **3c,d**, revealed that even though the half-wave potentials for the redox waves did not change significantly, the ΔE_p values for these processes are much bigger and, hence, deviate from the Nernst equation, especially for the second oxidation process. Cyclic voltammograms were also recorded at various scan rates (50, 100, 200, 400 and 800 mVs⁻¹) (see the appendix) and the anodic peak currents for the redox waves versus the square root of the scan rates were plotted (Figure 6.5). For both oxidation, the peak current linearly increased with respect to the square root of the scan rate based on the Randles–Ševčík equation (Equation 3.1), indicating these processes are diffusion controlled.

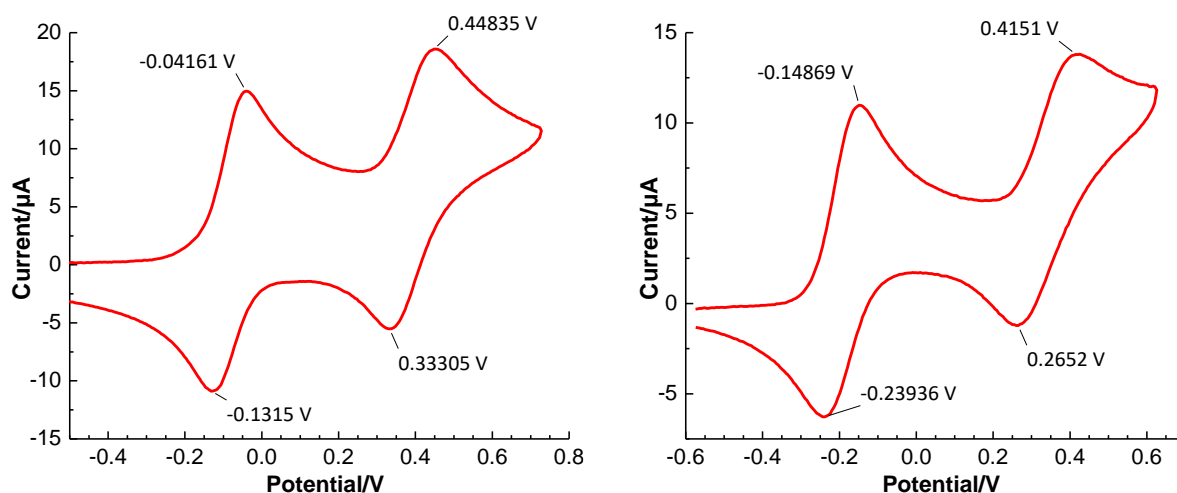


Figure 6.4. Cyclic voltammograms of **19a,a'** (left), **19b,b'** (right) Vs. $\text{Fc}^{0/+}$ (0.4 M $n\text{Bu}_4\text{PF}_6$ in DCM, 100 mVs^{-1}).

Table 6.3. Half wave potentials (Vs. $\text{Fc}^{0/+}$), ΔE_p , cathodic and anodic currents for **3c,d** and **19a,a'-b,b'** (0.4 M $n\text{Bu}_4\text{PF}_6$ in DCM, 100 mVs^{-1}).

Compound	$E_{1/2}^1/\text{V}$	$\Delta E_p/\text{mV}$	$I_p^a/\mu\text{A}$	$I_p^c/\mu\text{A}$	$E_{1/2}^2/\text{V}$	$\Delta E_p/\text{mV}$	$I_p^a/\mu\text{A}$	$I_p^c/\mu\text{A}$
3c	-0.15	64.7	5.4	4.4	0.36	69.4	4.7	4.4
3d	-0.20	78.3	9.5	7.8	0.33	77.1	8.3	7.6
19a,a'	-0.09	89.9	14.4	9.1	0.39	115.3	10.4	8.8
19b,b'	-0.19	90.7	10.9	8.1	0.34	149.9	8.1	9.8

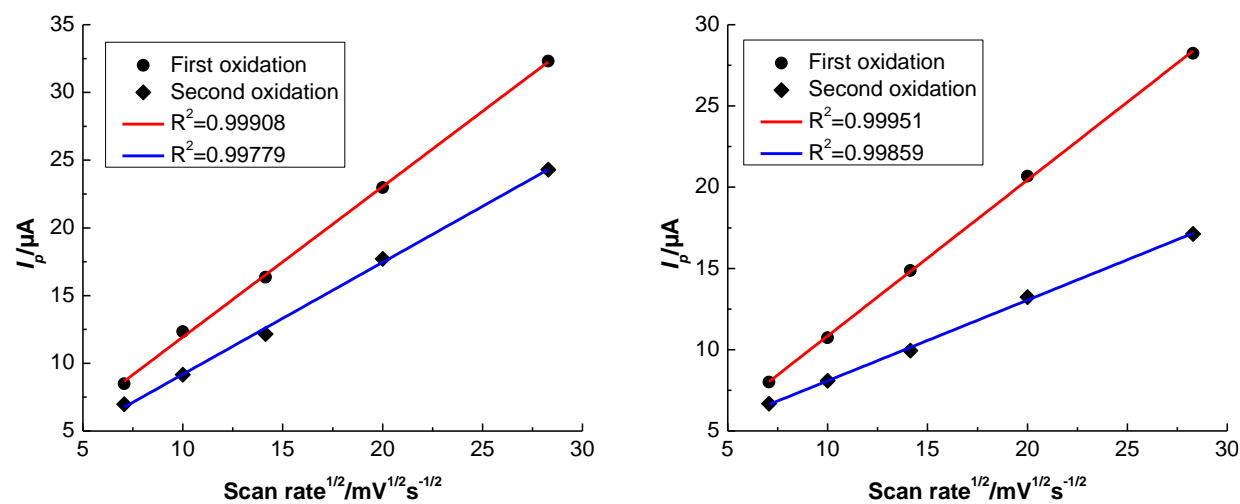
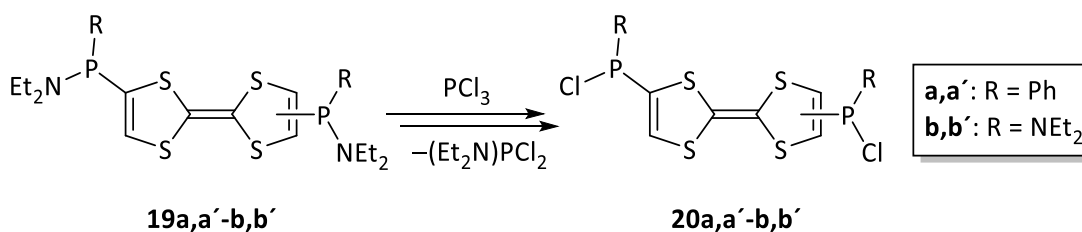


Figure 6.5. Dependency of the anodic peak currents on the scan rate for **19a,a'** (left) and **19b,b'**.

6.1.2 Bis(chlorophosphanyl)tetrathiafulvalenes

To synthesize bis(chlorophosphanyl)tetrathiafulvalenes as the precursor for the ring-closing/oligomerization reaction, pseudo-*E/Z* isomeric mixtures of **19a,a'** and **19b,b'** with the ratio of 1:1 and 1:0.8 respectively, were subjected to a scrambling reaction (σ bond metathesis) using PCl_3 (Scheme 6.2). In the case of **19a,a'** reaction was performed in dichloromethane at room temperature and $^{31}\text{P}\{^1\text{H}\}$ NMR monitoring showed the selective formation of the desired product by the appearance of new resonance signals at around 64 ppm, while the precursor signal had vanished. For **19b,b'** reaction was performed in diethylether at low temperature to avoid the possibility of exchanging both diethylamino groups for two chlorine atoms and $^{31}\text{P}\{^1\text{H}\}$ NMR monitoring revealed that reaction was completed after 1 hour at -90°C . After removal of volatiles in *vacuo* (8×10^{-3} mbar), compounds **20a,a'-b,b'** were extracted from the crude, using diethylether, and could be obtained in excellent yields (Table 6.4). These compounds were characterized by multinuclear NMR and MS analysis.



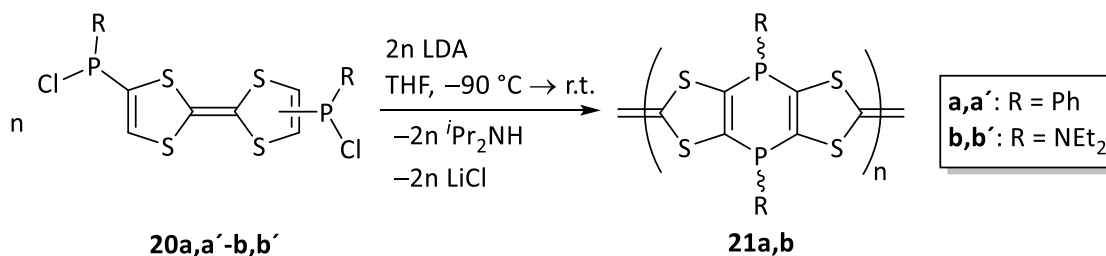
Scheme 6.2. The scrambling reaction of **19a,a'-b,b'** with PCl_3 .

Table 6.4. Selected NMR data (in CDCl_3) and yields for compounds **20a,a'-b,b'**.

Compound	$\delta^{31}\text{P}\{^1\text{H}\}/\text{ppm}$ (ratio)	$\delta^1\text{H}/\text{ppm}$ ($\text{C}^5\text{-H}$)	$\delta^{13}\text{C}\{^1\text{H}\}/\text{ppm}$ (C^4)	Yield%
20a,a'	63.4 and 63.6 (1:0.9)	6.93 (2t, 2H, $\text{C}^5\text{-H}$, $^3J_{\text{P,H}} = 10.38$ Hz)	136.8 (m)	94
20b,b'	117.6 and 117.7 (1:0.45)	6.72 and 6.73 (d, 2H, $\text{C}^5\text{-H}$, $^3J_{\text{P,H}} = 2.5$)	137.0 (m)	97

6.1.3 Ring-closing/oligomerization reaction

In the next step, compounds **20** were subjected to a similar ring-closing reaction as the one to form the related 1,4-dihydro-1,4-diphosphinines. But in this case, two equivalents of base was used to achieve the ring-closing reaction on both side of the molecule and form oligomeric products **21** (Scheme 6.3).



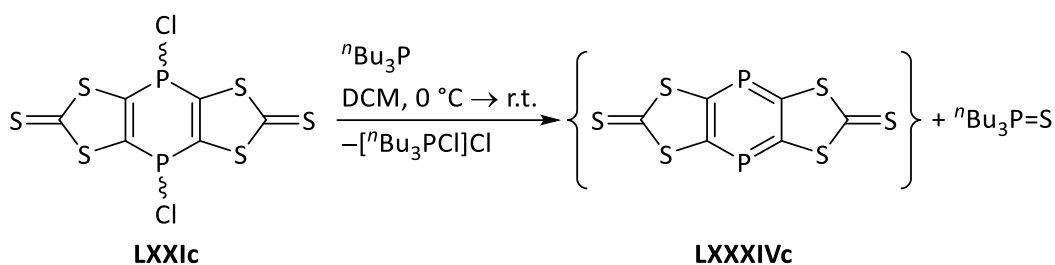
Scheme 6.3. The formation of oligomeric products of not determined weight and composition (**21**).

In both reactions, after the addition of base, a brown precipitate was formed immediately. The reaction mixtures were allowed to warm up slowly and stir overnight, then the solvent was removed via filtration and the residue was washed with THF, DCM and n-pentane to remove side products and impurities, and then dried in *vacuo* (8×10^{-3} mbar). Different solvents were examined, but the obtained products (dark brown powder) were not soluble in common organic solvents and, hence, NMR spectroscopy and mass spectrometry could not be used to characterize the products. Elemental analysis was performed for **21a,b**, but the obtained data revealed, even after washing the products with different solvents, some unidentified impurities which could not be removed. For example in the case of **21a**, the determined elemental analysis value showed that the submitted sample contains 0.64% nitrogen, thus indicating insoluble impurities alongside with the desired oligomeric products.

6.2 Desulfurization of tricyclic 1,4-dihydro-1,4-diphosphinines annulated to two 1,3-dithiole-2-thiones

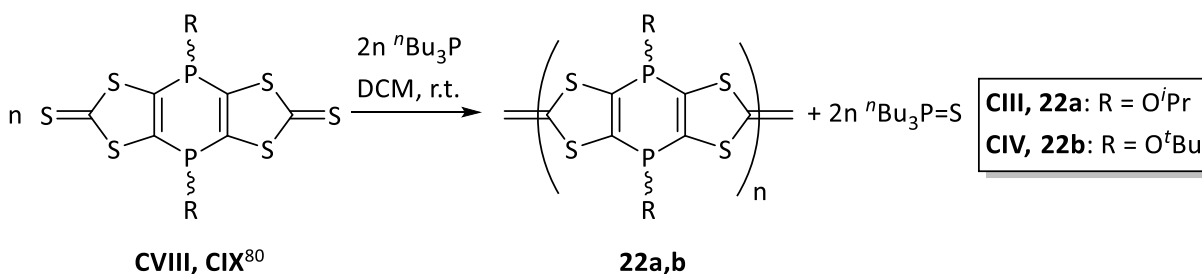
In previous studies Gese had tried to access a 1,3-dithiole-2-thione-based 1,4-diphosphine **LXXXIVc**^{80,150} via reaction of the appropriate 1,4-dichloro-1,4-dihydro-1,4-diphosphine derivative **LXXIc** with ⁿBu₃P in dichloromethane (Scheme 6.4). He had observed that in addition

to the resonance signal of the chlorophosphonium chloride [$n\text{Bu}_3\text{PCl}]\text{Cl}$, the $^{31}\text{P}\{^1\text{H}\}$ NMR spectrum of the reaction mixture showed the unexpected formation of $n\text{Bu}_3\text{P}=\text{S}$ at 48.5 ppm as a side product. He concluded that not only the targeted didechlorination to the 1,4-diphosphinine **LXXXIVc** took place but also desulfurization of the thione functionality had occurred in a competing reaction, leading to some oligomeric products which were not further analyzed. These conclusions were further supported by DFT calculations showing that both pathways have similar barriers and, hence, are feasible.⁸⁰



Scheme 6.4. Reported synthesis of the 1,4-diphosphinine **LXXXIVc**.⁸⁰

To eliminate the competing didechlorination reaction, and also have a better chance to get access to a soluble product, the related 1,4-di-*iso*-propoxy-1,4-dihydro-1,4-diphosphinine **CVIII** and 1,4-di-*tert*-butoxy-1,4-dihydro-1,4-diphosphinine **CIX**⁸⁰ were subjected to the reaction with $n\text{Bu}_3\text{P}$ under ambient conditions (Scheme 6.5). In both cases, precipitates were formed and the resonance signal of the starting materials had vanished after 3 hours, and the $^{31}\text{P}\{^1\text{H}\}$ NMR spectra of the reaction mixtures showed just two resonances at -31.4 and 48.5 ppm related to the unreacted $n\text{Bu}_3\text{P}$ and $n\text{Bu}_3\text{P}=\text{S}$, respectively (Figure 6.6). With these data, it was concluded that indeed the desired reaction occurred and oligomeric products were formed. Unfortunately, they were not soluble, again, and, hence, the more soluble 1,4-bis(diethylamino)-1,4-dihydro-1,4-diphosphinine was used as starting material in the next attempt (below).



Scheme 6.5. Synthesis oligomeric products having *P*-alkoxy substituents.

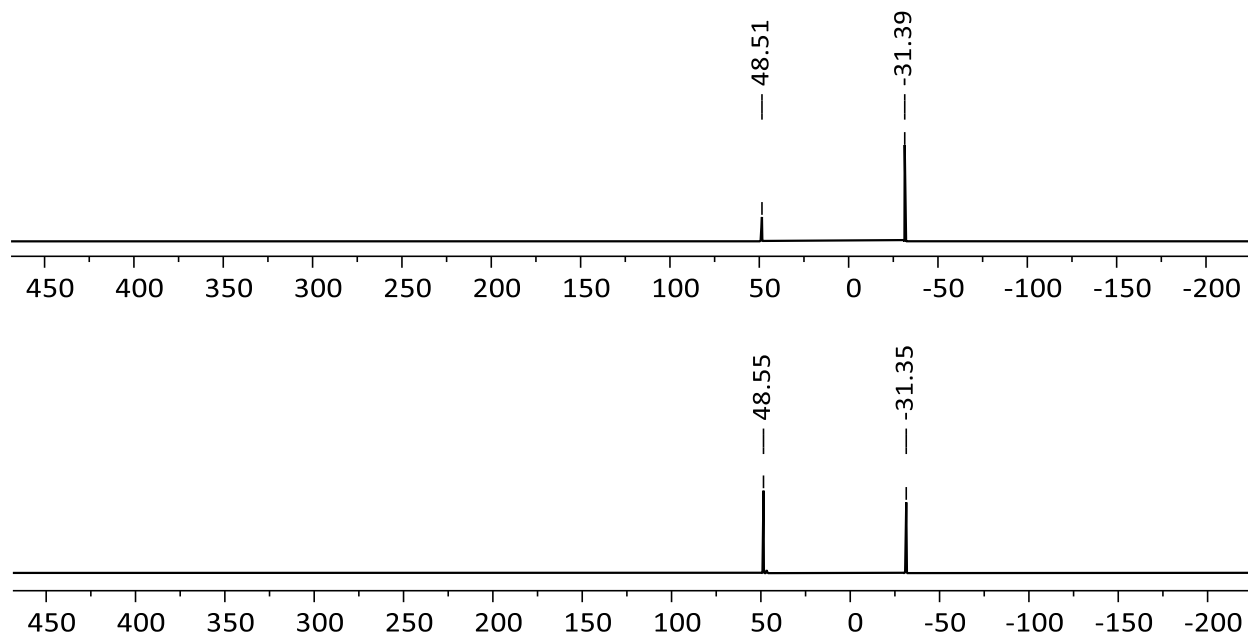
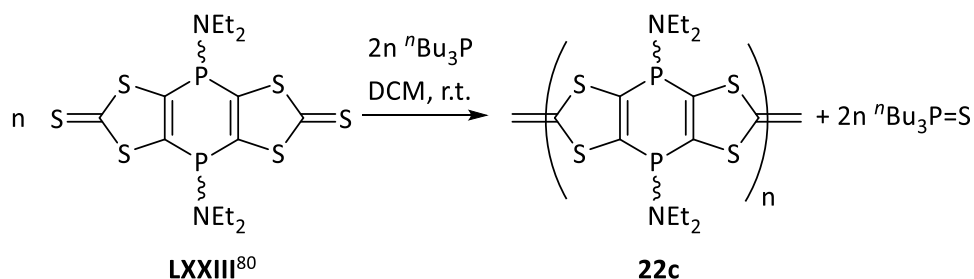


Figure 6.6. $^{31}\text{P}\{^1\text{H}\}$ NMR of the reaction of **CVIII** (top) and **CIX** (bottom) with $^n\text{Bu}_3\text{P}$ (reaction mixture).

In further efforts to increase the solubility of the product, the related 1,4-bis(diethylamino)-1,4-dihydro-1,4-diphosphinine **LXXIII**⁸⁰ was used in the desulfurization reaction (Scheme 6.6). Having *P*-diethylamino substituents could eventually also give the possibility of performing the scrambling reaction, finally leading to oligomers with aromatic 1,4-diphosphinine rings as linker between TTF units.



Scheme 6.6. Synthesis of a mixture of oligomeric products having *P*-diethylamino substituents.

In addition to the resonances related to $^n\text{Bu}_3\text{P}$ and $^n\text{Bu}_3\text{P}=\text{S}$, $^{31}\text{P}\{^1\text{H}\}$ NMR of the reaction mixture showed new signals in the region between 26 and 38 ppm. The pure product could be obtained after the removal of volatiles in *vacuo* (8×10^{-3} mbar) and washing the residue with petrol ether. By comparing the phosphorus chemical shifts of the product (Figure 6.7) with those of the starting material (two singlets at 23.5 and 30.5 ppm) and the 1,4-bis(diethylamino)-1,4-dihydro-

1,4-diphosphinines fused to two TTF units **11d,d'-f,f'** (two singlets at 29 and 32 ppm), it was concluded that the oligomeric products, having 1,4-dihydro-1,4-diphosphinines as linker between TTF units were formed. Due to the possibility of having different numbers of monomeric units in the oligomer, each with pseudo-*E/Z* configuration, a multitude of phosphorus chemical signals were observed in a rather narrow range of 25-40 ppm. A MALDI-MS experiment clearly showed *m/z* values for the products having three (1219.0), four (1625.0) and five (2031.0) monomeric units (406) in the oligomeric structure (Figure 6.8), including the typical fragmentation pattern, but oligomers having higher masses are conceivable, too.

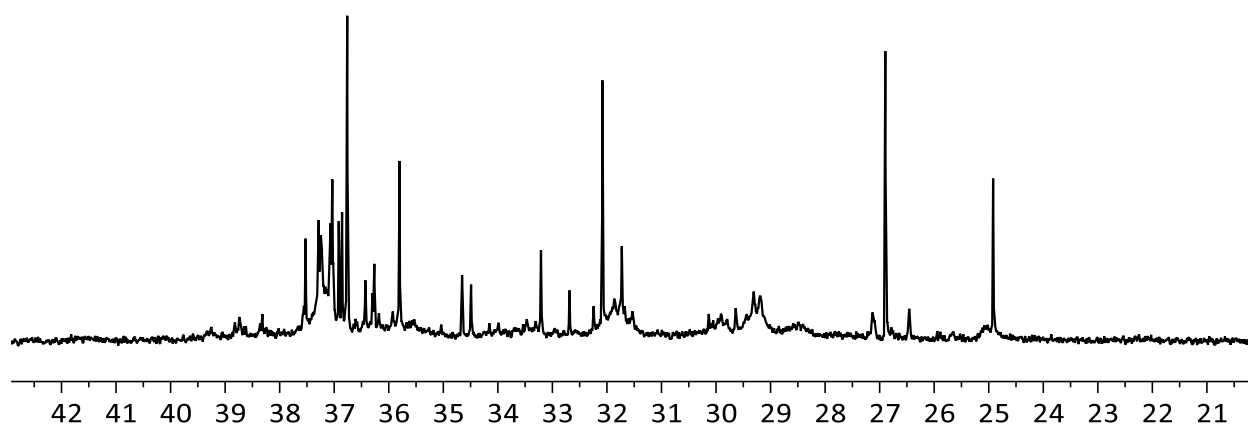


Figure 6.7. $^{31}\text{P}\{^1\text{H}\}$ NMR spectrum of **22c** in CD_2Cl_2 .

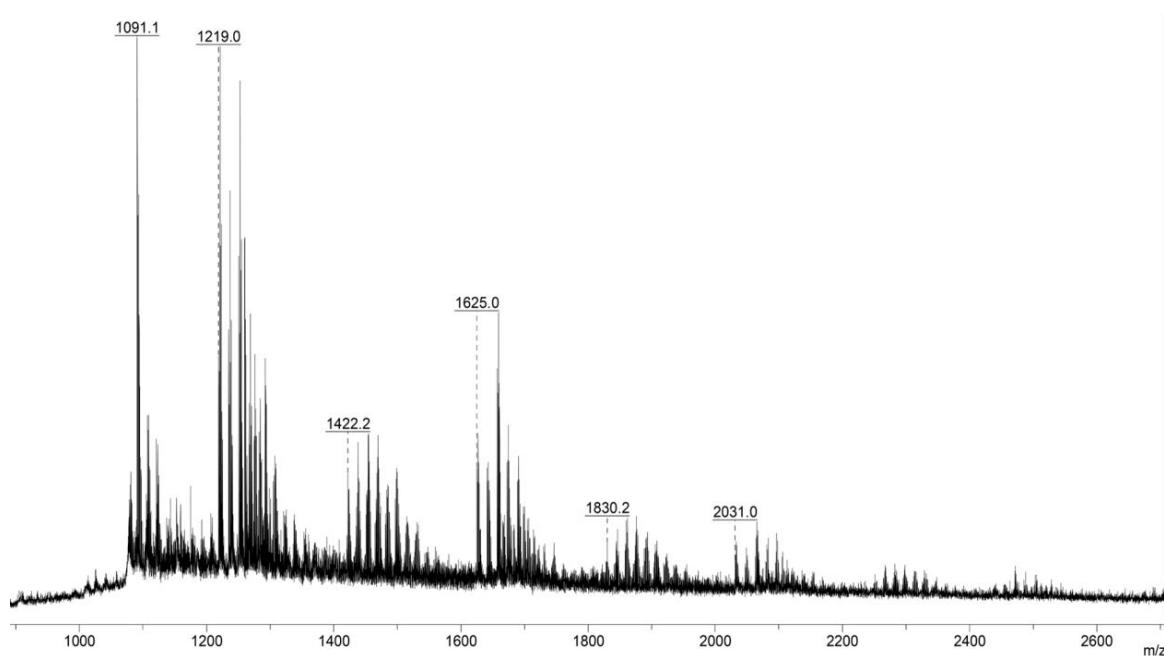
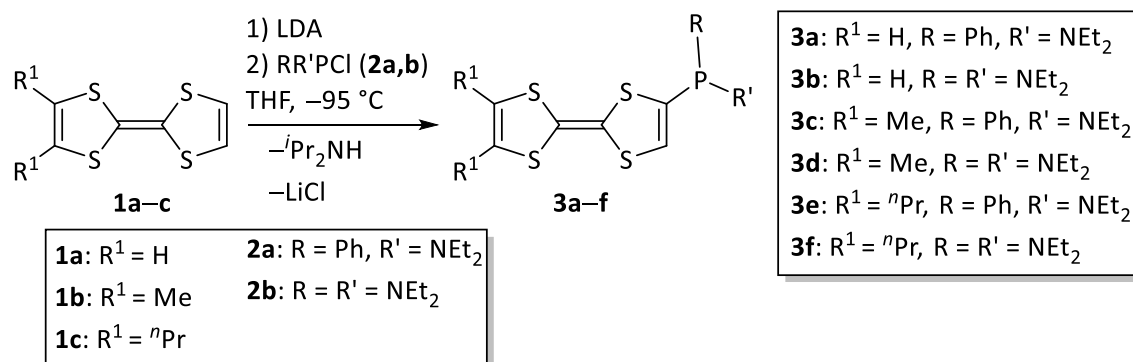


Figure 6.8. MALDI-MS spectrum of **22c**.

7 Summary

In this Ph.D. thesis results from investigations on the synthesis and reactivity of the first P-functional tetrathiafulvalenes are presented. A particular focus was on their transformation to new 1,4-dihydro-1,4-diphosphinines and 1,4-diphosphinines. Furthermore, first studies on the reactivity of chlorophosphanyl-substituted TTF and synthesis of oligomeric products having TTF units in their main chain were carried out. The electrochemical properties of isolated compounds were studied using cyclic voltammetry.

Chapter 3 describes the synthesis and characterization of phosphanylated tetrathiafulvalenes **3a-f** (Scheme 7.1) using the reaction of *in situ* generated lithiated TTFs with chloro(diethylamino)phenylphosphane (**2a**) and bis(diethylamino)chlorophosphane (**2b**).

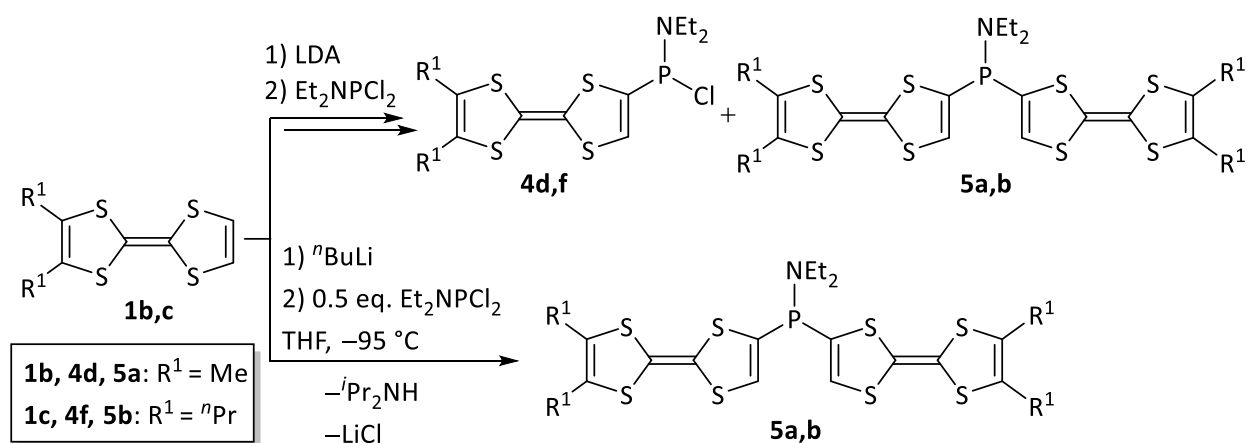


Scheme 7.1. Synthesis of phosphanylated TTFs **3a-f**.

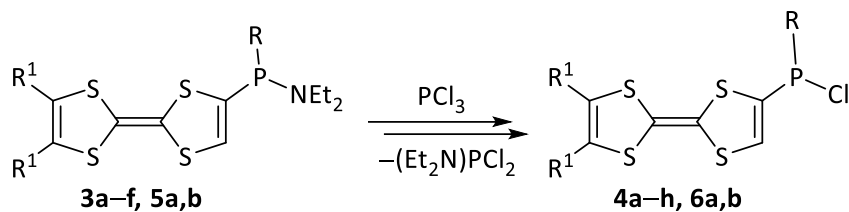
In the case of **1b,c**, the desired products were formed selectively and isolated in moderate to good yields. This was starkly contrasted for the case of **1a** due to the possibility of a lithiation on both sides of the unsubstituted TTF molecule and, hence, completely selective lithiation and phosphanylation were not obtained even after trying various reaction conditions. In these cases (for **3a,b**) The purification attempts such as room and low-temperature column chromatography, also sublimation using an ultrahigh vacuum pump (1×10^{-5} mbar) to remove side-products (unreacted TTF and doubly-phosphanylated TTF) were met with limited success and pure compounds couldn't be obtained. However, multinuclear NMR spectroscopic and mass

spectrometric data confirmed the formation of **3a,b**. Cyclic voltammetry studies of **3c-f** exhibit two distinct quasi-reversible redox processes in the oxidation region which are corresponding to the sequential one-electron step processes, forming the related TTF radical cation and then dication.

Chapter 4 describes the chemistry of chlorophosphanylated TTFs. The initial attempt to achieve one-pot synthesis of these derivatives via lithiation of *ortho*-substituted TTFs **1b,c** followed by reaction with one equivalent of Et_2NPCI_2 resulted in a mixture of the desired product **4d,f** and the related *P*- NEt_2 bridged compounds having two TTF units **5a,b** (Scheme 7.2). Later **5a,b** were selectively formed by using half equivalent of Et_2NPCI_2 after the lithiation step (Scheme 7.2) and selective formation of the chlorophosphanyl-substituted tetrathiafulvalenes was achieved via reaction of compounds **3a-f** and **5a,b** with one or two equivalents of PCl_3 (Scheme 7.3). The electrochemical properties of **4c-f** and **5a,b** were investigated by employing cyclic voltammetry. **4c-f**, same as their precursors, exhibit two distinct quasi-reversible redox processes in the oxidation region, but in the case of **4d,e,f** irreversible reductions, corresponding to the reduction of the *P*-Cl bond were also observed. For compounds **5a,b**, due to the presence of two TTF units in their structure, four sequential oxidation processes were expected, resulting in the related tetracationic species. For **5b** These four distinct oxidation processes were observed, while due to the lower solubility of the oxidized species for **5a** and adsorption/precipitation phenomena at the surface of the electrodes, the last two processes for **5a** were recorded in the same potential.



Scheme 7.2. Proposed products for the reaction of **1b,c** with LDA and 1 eq. of dichloro(diethylamino)phosphane (top) and selective synthesis of mono-bridged compounds **5a,b** (bottom).



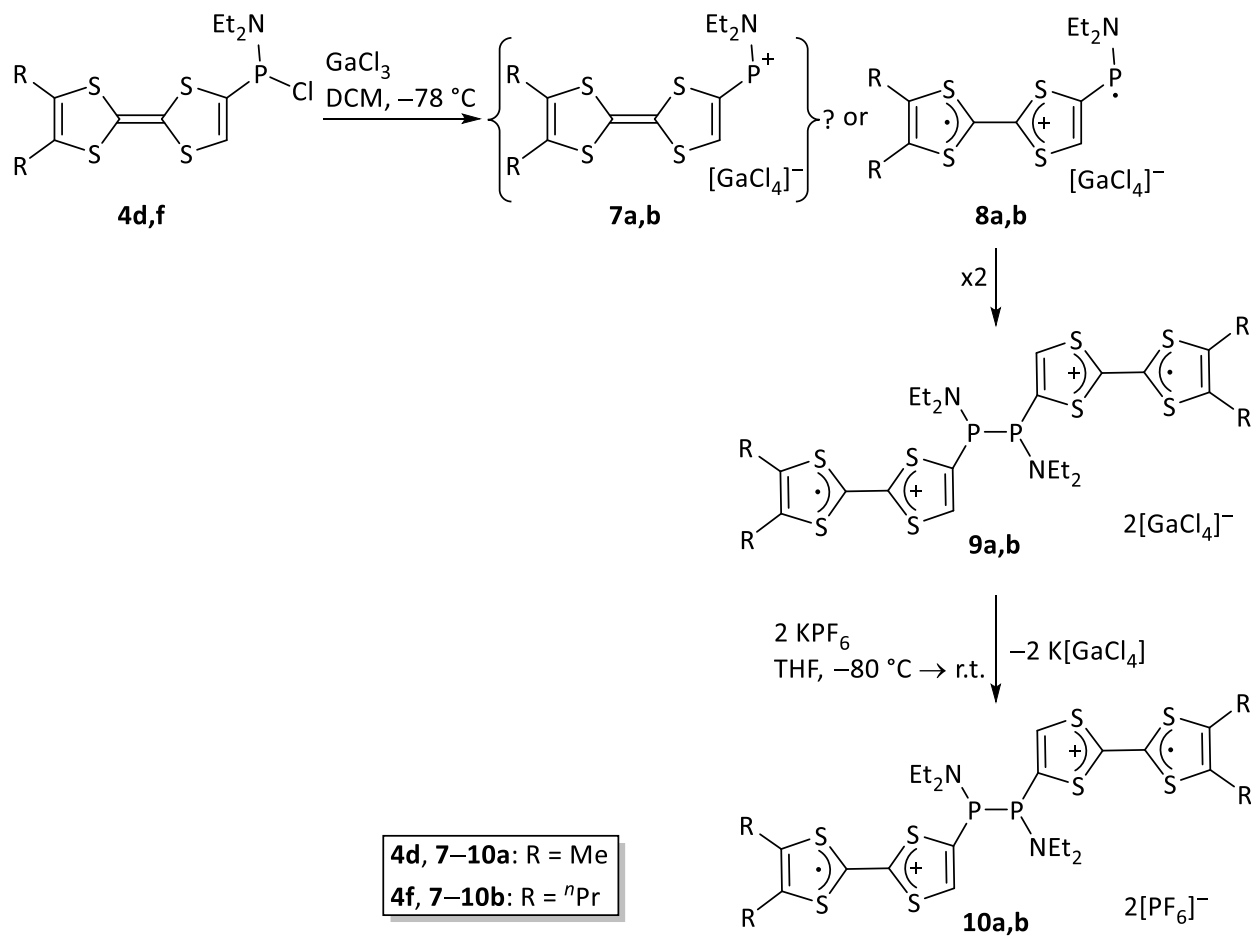
3a, 4a: R ¹ = H, R = Ph	4g: R ¹ = Me, R = Cl
3b, 4b: R ¹ = H, R = NEt ₂	4h: R ¹ = ⁿ Pr, R = Cl
3c, 4c: R ¹ = Me, R = Ph	5a, 6a: R ¹ = Me, R = <i>o</i> -DMTTF
3d, 4d: R ¹ = Me, R = NEt ₂	5b, 6b: R ¹ = ⁿ Pr, R = <i>o</i> - ⁿ Pr ₂ TTF
3e, 4e: R ¹ = ⁿ Pr, R = Ph	
3f, 4f: R ¹ = ⁿ Pr, R = NEt ₂	

Scheme 7.3. Selective formation of chlorophosphanyl-substituted TTFs.

Next, the chemical reduction of **4d,g** was aimed to obtain the related diphosphane or cyclophosphane having two or four TTF units, respectively, linked by phosphorus atoms; but despite using various reagents a selective reaction to the desired products could not be achieved.

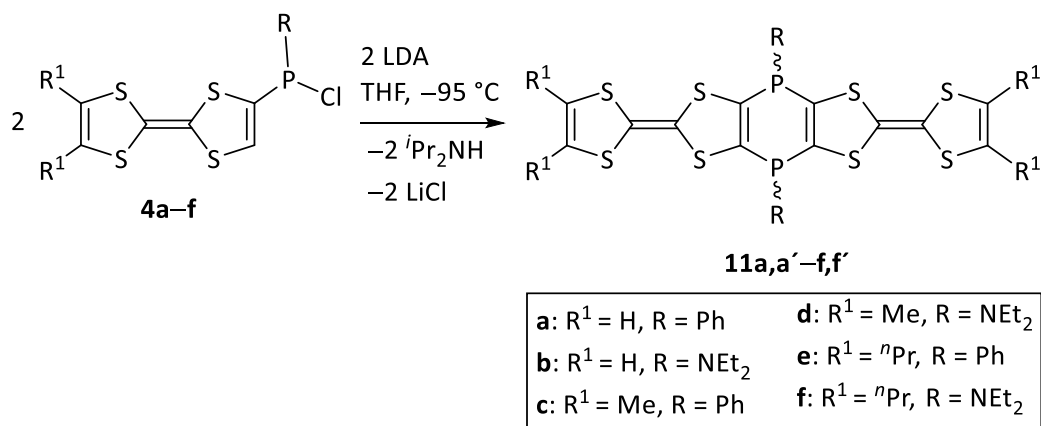
In the next step, chloride abstraction reaction from **4d,f** using GaCl₃ was performed to achieve a heterolytic P–Cl bond cleavage and formation of the related phosphonium compounds (Scheme 7.4). However, the ³¹P NMR spectrum of the reaction mixture showed no signals and the EPR spectrum revealed an open-shell species with *g* values equal to 2.008 and 2.007 for the reactions of **4d** and **4f** with GaCl₃, respectively. This observation can be explained by an intramolecular one-electron transfer from the tetrathiafulvalene moiety to the cationic phosphorus center in **7a,b** resulting in the formation of the biradical cationic species **8a,b**, followed by dimerization to form compounds **9a,b** (Scheme 7.4). DFT calculations revealed a small energy difference (7.4 kcal/mol) between the singlet (phosphenium cation) to the triplet (biradical cation) states, while the related dimer is more stable by 37.7 kcal/mol compared to the monomeric biradical cation. These calculations also showed almost no spin density contribution on the phosphorus center which is in good agreement with the results of EPR spectroscopy, showing a singlet signal with no hyperfine coupling. Anion exchange reaction of **9a,b** was tried using potassium hexafluorophosphate (Scheme 7.4), which resulted in a color change from dark green (starting material solution) to orange, but no signal was found in ³¹P NMR spectra. **9a,b** and **10a,b** were

subjected to reduction using one and two equivalents of decamethylcobaltocene and KC_8 , respectively, but again no product signal appeared in the ^{31}P NMR spectra of the reaction mixtures.



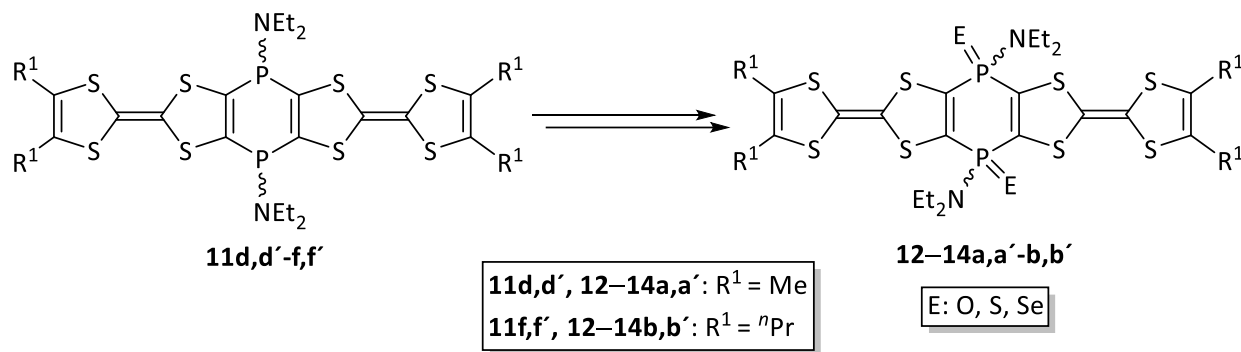
Scheme 7.4. Proposed mechanism to form **9a,b** and anion exchange reaction of **9a,b** using KPF_6 .

Chapter 5 describes the synthesis and reactivity studies of new 1,4-dihydro-1,4-diphosphinines fused to two tetrathiafulvalene units. The ring-closing reaction was achieved using **4a–f** and LDA at low temperature leading to the 1,4-dihydro-1,4-diphosphinines **11**, obtained as isomeric mixtures (Scheme 7.5). In the cases of **4c–f**, a clean conversion was observed by $^{31}\text{P}\{^1\text{H}\}$ NMR spectroscopy, and **11d,d'–f,f'** could be isolated in moderate to excellent yields. But for **4a,b**, ring-closing reactions (with different bases and reaction conditions) were not selective, due to the accessibility of protons at the opposing ring (side) in the TTF unit and, therefore, the desired 1,4-dihydro-1,4-diphosphinines were obtained only as minor products.



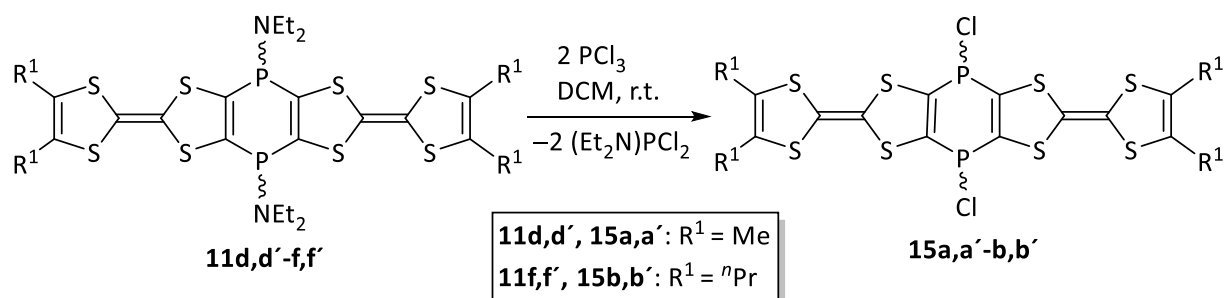
Scheme 7.5. Synthesis of 1,4-dihydro-1,4-diphosphinines **11** fused to two TTF units.

The P-centers of 1,4-bis(diethylamino)-1,4-dihydro-1,4-diphosphinines **11d,d'-f,f'** could be oxidized via reaction with H_2O_2 -urea adduct, elemental sulfur and selenium to form the related P(V)/P(V) dichalcogenides **12-14** (Scheme 7.6).



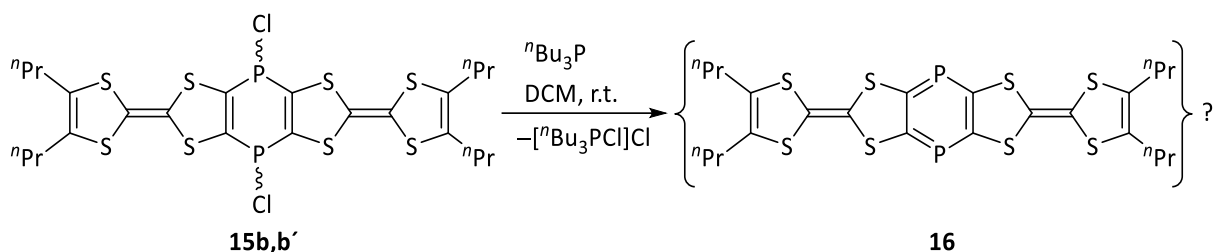
Scheme 7.6. Oxidation and scrambling reactions of **11d,d'** and **11f,f'** using chalcogens.

Also, the exchange of the amino groups for chloride (scrambling reaction), as a crucial step towards the synthesis of the related 1,4-diphosphinines, was performed (Scheme 7.7). In the case of **11d,d'**, and after the addition of PCl_3 , formation of a dark brown precipitate was observed which was not soluble in common organic solvents. Reaction of **11f,f'** with PCl_3 resulted in a product with $^{31}\text{P}\{^1\text{H}\}$ NMR resonances at 35 and 38.2 ppm (ratio 1:0.15). Although the EI-MS spectrum of **15b,b'**, did not show any signal corresponding to the molecular ion peak, signals at m/z 634.0 and 70.0 can be attributed to the related 1,4-diphosphinine $[\text{M}-\text{Cl}_2]^+$ fragment and the Cl_2 radical cation, respectively.



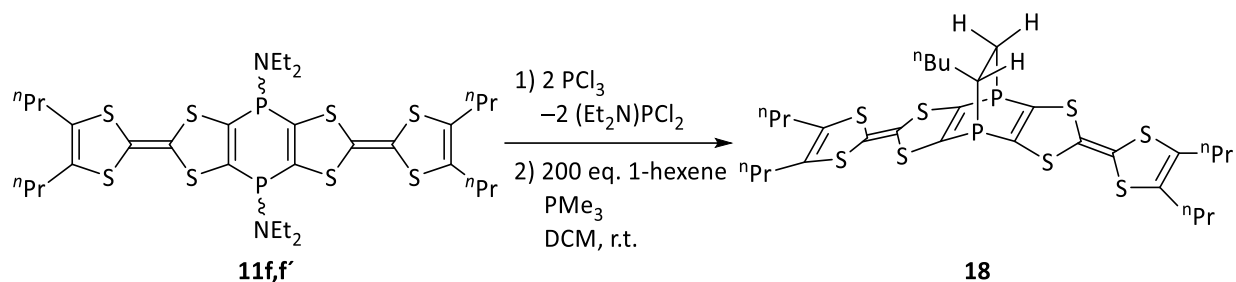
Scheme 7.7. Scrambling reaction of **11d,d'** and **11f,f'**.

Treatment of an isomeric mixture of **15b,b'** with ⁿBu₃P (Scheme 7.8) did not lead to 1,4-diphosphine **16**, observable in the ³¹P{¹H} NMR spectrum of the reaction mixture, despite the formation of the salt [ⁿBu₃PCl]Cl and no resonance could be safely assigned to the desired product using DFT-based NMR calculations. The latter also suggested a smaller HOMO/LUMO gap (2.5 eV) and lower aromaticity for **16** (NICS (1) = -5.2) compared to previously described 1,4-diphosphinines. Considering a possible effect on reactivity and/or sensitivity of **16**, reaction with ⁿBu₃P was performed in different temperatures and solvents, including reaction in the dark, but still, no NMR signal corresponding to the desired, new 1,4-diphosphine derivative could be observed.



Scheme 7.8. Attempted synthesis of 1,4-diphosphine **16**.

The assumption that the reaction of **15b,b'** has led to transient 1,4-diphosphine **16** was probed, and two changes were made: a) an excess of 1-hexene was chosen as trapping reagent in a [4+2]-cycloaddition reaction and b) PMe₃ as the reducing agent. Under these conditions the ³¹P{¹H} NMR spectrum showed a selective conversion into the desired 1,4-diphosphabarrelene **18** (Scheme 7.9). EI-MS spectrum of **18** showed the molecular ion peak (m/z 718.036) and a signal at m/z 633.942 which was assigned to the radical cation fragment of the 1,4-diphosphine **16** after cleavage of the C₂-bridge ([M-C₆H₁₂]^{•+}).



Scheme 7.9. Synthesis of 1,4-diphospha-barrelene fused to two TTF units **18**.

For the new 1,4-dihydro-1,4-diphosphinines **11d,d'-f,f'**, cyclic voltammetry showed four sequential, one-electron transfer processes yielding tetracation species, finally (Figure 7.1). An important aspect of the electrochemical properties of these new doubly-bridged TTF compounds is the separation between the first and second, and also third and fourth redox potentials as a measure of the degree of communication between two TTF units. These differences for **11d,d'-f,f'** are in good agreement with the previously by Avarvari reported compound, having a non-aromatic 1,4-dihydro-1,4-diphosphinine ring, i.e., two PPh groups as bridge between two TTF moieties (120 mV)³¹, but smaller than the cases where the two redox-active units are connected via an aromatic linker (160–260 mV).¹⁰⁶ For compounds **12–14** and **18** four redox waves were also expected but for **12a,a'** and **12b,b'** the third and fourth oxidations were recorded at a single potential and in the other cases, the last two processes were not distinguishable and recorded as a broad redox wave, with ΔE_p values between 146 to 166 mV. This can be attributed to the lower solubility of the oxidized species which causes adsorption phenomena, and also proximity of the redox potentials to each other and to the solvent limit. The differences between the first and second redox potentials are in good agreement with **11d,d'-f,f'**, but the oxidation potentials for **12–14** compare to the precursor compounds are higher by almost 200 mV, which is due to the change of the oxidation state at the P-centres. In addition to these oxidation processes, occurring at the TTF units, compounds **12–14** showed one (**12a,a'-b,b'** and **13b,b'**) or two (**13a,a'** and **14a,a'-b,b'**) reduction waves which can be attributed to the reduction of the P-centres. The second reduction process for **12a,a'-b,b'** and **13b,b'** is likely occurring at a lower potential than the solvent limit and hence was not observed. For compounds **12a,a'** and **12b,b'** a return oxidation wave was also observed and based on the obtained ΔE_p and I_p^a/I_p^c the reduction process can be considered quasi-reversible, but for compounds **13** and **14** due to the proximity of the

potentials to the solvent limit, a clear examination of the reversibility of these processes was not possible.

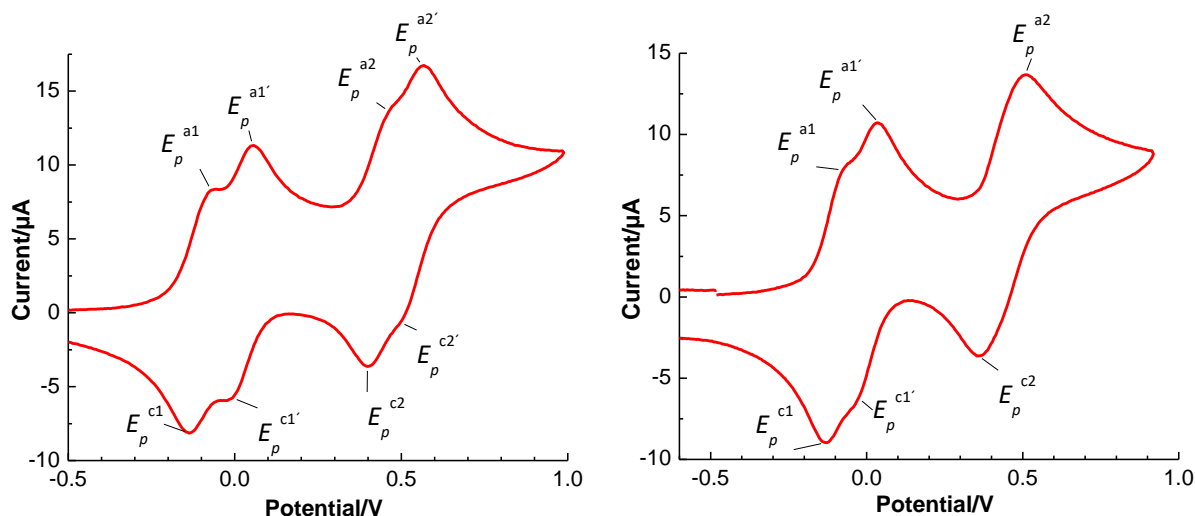
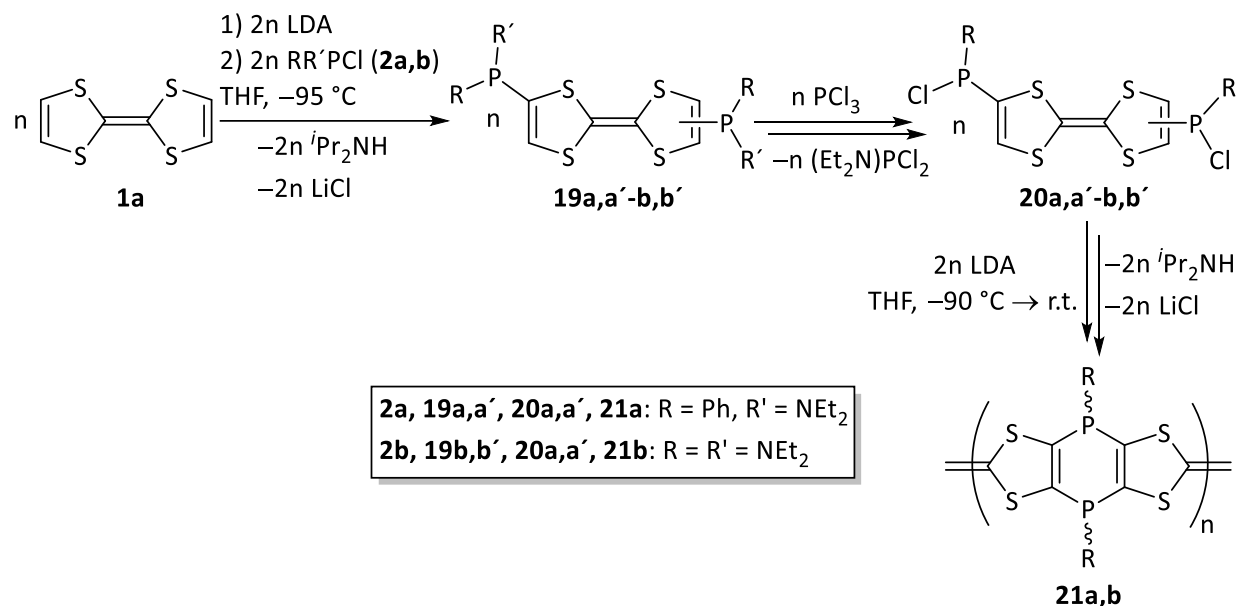


Figure 7.1. Cyclic voltammograms of **11d,d'** (left) and **18** (right) Vs. $Fc^{0/+}$ (0.4 M nBu_4PF_6 in DCM, 100 mVs^{-1}).

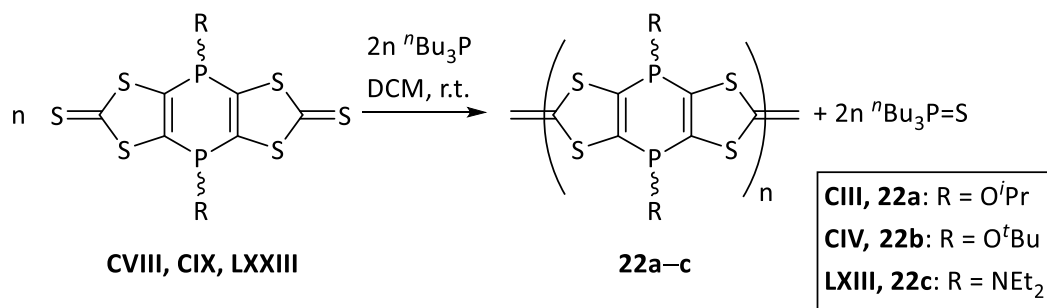
Chapter six describes preliminary results of the synthesis of oligomeric and/or polymeric structures having a 1,4-dihydro-1,4-diphosphinine ring as linker between TTF units. To achieve this goal two different synthetic approaches were employed.

First, doubly-phosphanylated TTFs **19**, observed firstly as side-products in the synthesis of **3a,b**, were employed as precursor for ring-closing reaction on both sides, using a more selective synthetic protocol (Scheme 7.10). This was followed by σ -bond metathesis using PCl_3 to get bis(chlorophosphanyl)tetrathiafulvalenes **20**. Application of the same ring-closing reaction protocol, using two equivalents of base, resulted in a mixture of oligomeric products **21** as dark brown powder, not soluble in common organic solvents.

In an alternative approach, 1,4-dihydro-1,4-diphosphinines, annulated to two 1,3-dithiole-2-thiones (**CVIII**, **CIX** and **LXXIII**) were subjected to a desulfurization reaction using nBu_3P to achieve the oligomeric products **22** (Scheme 7.11).



Scheme 7.10. The synthesis of oligomeric products of not determined weight and composition **21**.



Scheme 7.11. Synthesis of oligomeric products **22** via desulfurization pathway.

In the cases of **CVIII** and **CIX**, insoluble precipitates were formed and the ³¹P{¹H} NMR spectra of the reaction mixtures showed just two resonances at -31.4 and 48.5 ppm related to unreacted ⁿBu₃P and ⁿBu₃P=S, respectively. But in case of **LXXIII** the reaction with ⁿBu₃P led to soluble products having a multitude of broad resonances between 26 and 38 ppm in the ³¹P{¹H} NMR spectrum. The multitude and broadness of the signals point to a mixture of compounds having different numbers of monomeric units in the oligomer, each with *cis* and *trans* configuration. The MALDI-MS experiment showed the typical repetitive pattern of oligomers, i.e., with *m/z* values products (or fragments) having three (1219.0), four (1625.0) and five (2031.0) monomeric units (406) in the oligomeric structure (Figure 7.2).

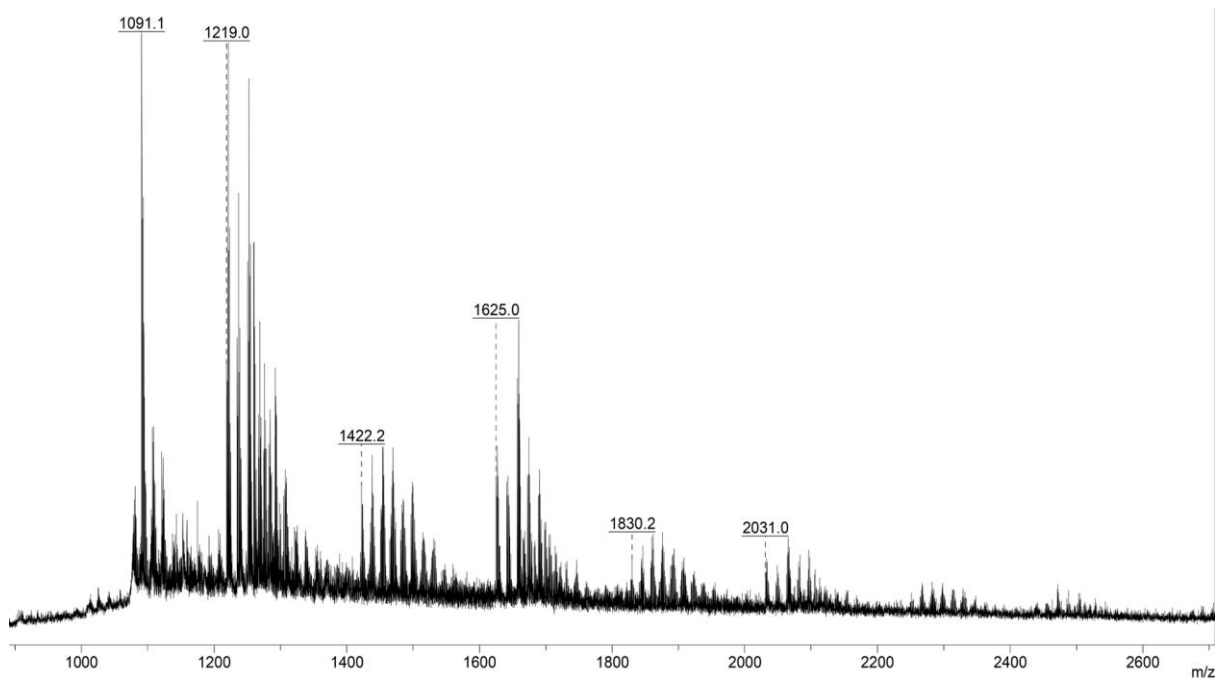


Figure 7.2. MALDI-MS spectrum of **22c**.

8 Experimental section

8.1 General techniques

All reactions and manipulations were carried out under an atmosphere of deoxygenated (pre-heated BTS catalyst at 100–130 °C) and dried (phosphorus pentoxide and silica gel) argon gas, using standard Schlenk techniques or glove box techniques with conventional glassware. All air and/or moisture sensitive chemicals were stored in either Schlenk flasks/tubes or handled in the glovebox. Solvents were dried and distilled according to standard procedures¹⁵¹ and were used freshly from distills. For air-sensitive reactions, Schlenk glasswares were evacuated, heated in *vacuo* and filled with argon gas before use. All the glass joints were lubricated with OKS grease type 1112. High-temperature reactions were carried out in an oil bath. In the case of low-temperature reactions, ethanol and liquid nitrogen was employed as coolant. To remove salts, formed in the reaction mixture, common 3G frits having two Schlenk joints, along with a silica gel bed (Merck 60–200) were used. Cannulas with Whatman glass microfiber filters (GF/B, d = 25 mm) connected to one end with Teflon band were used for filtrations, washings and extractions with pressure gradient of the argon gas. For transferring solvents, stainless steel double needles were used, which were pre-heated and dried in the oven at 75 °C. Whatman filter papers and/or glass microfiber filter papers were used for filtration purposes under air. All the used glassware was soaked overnight in a KOH/isopropanol bath and then dipped into an HCl-water bath for the sake of neutralization before washing with soap water. Then the cleaned glassware was rinsed with de-ionized water and acetone simultaneously before drying at 110 °C in the oven overnight. The chemical waste disposal was performed on the basis of the latest “Gefahrstoffverordnung”. Organic and inorganic wastes were separated from each other and collected in the designed container before disposing. Other dry chemical wastes along with column waste were collected together and disposed of. All the dangerous and reactive reagent leftovers were destroyed according to the literature reported protocols¹⁵² and taken care of. All the waste was submitted to the Department 4.2 “Arbeits- und Umweltschutz” of the University of Bonn for further processing.

8.1.1 Melting point determination

The melting points (or decomposition temperatures) were recorded on a Büchi 535 Type S melting point apparatus, where the samples were placed inside both-sided closed glass capillary tubes; the values are not corrected.

8.1.2 Elemental analysis

The samples for the elemental analyses were prepared in a tin or silver (for halogen containing compounds) boat using a glove box. Elemental analyses were performed using an elementary vario EL analytical gas chromatograph. The mean values of three or four independent measurements are given in each case.

8.1.3 NMR spectroscopy

NMR spectra of all the compounds were recorded on Bruker Avance DMX-300, DPX-300, DPX-400 or DMX-500 spectrometers. Deuterated solvents (CDCl_3 , CD_2Cl_2 or THF-d_8) were dried using literature procedures and used for the multinuclear NMR characterizations. The chemical resonances are given relative to the residual protons of the deuterated solvents (^1H , ^{13}C) or 85% H_3PO_4 (^{31}P NMR). The chemical shifts are expressed in parts per million, ppm. Coupling constants are abbreviated as $^nJ_{X,Y}$, where X and Y denote the coupling nuclei (ordered by decreasing atomic number) and n is the number of bonds that separate X and Y. The following abbreviations were used for expression of the multiplicities of the resonance signals: *s* = singlet, *d* = doublet, *t* = triplet, *q* = quartet, *quin* = quintet, *sept* = septet, *m* = multiplet and *br* = broad signal. All the measurements were recorded at 298K unless some specific temperature is given. HSQC and HMBC experiments were used for purpose of assigning the ^1H NMR and ^{13}C NMR signals of all compounds.

8.1.4 EPR spectroscopy

The EPR spectra were recorded on a Bruker EMX-micro EPR spectrometer equipped with EMX standard resonator (4119 HS) both from Bruker. EPR spectra were collected with a microwave power of 1.739 mW, a modulation frequency of 100.00 KHz, a modulation amplitude of 1.0 G, a

microwave frequency of 9.402544 GHz, and 1429 points in the field interval 325.895–335.895 mT.

8.1.5 Mass spectrometry

Electron ionization mass spectra were recorded on a MAT 95 XL Finnigan using EI (70 eV). For ESI mass spectra a Thermo Fisher Scientific Orbitrap XL Mass spectrometer was used. LIFDI mass spectra were recorded on a Thermo Finnigan MAT 90 sector instrument equipped with a LIFDI ion source (Linden CMS). MALDI mass spectra were acquired from a Bruker Daltonik ultrafleXtreme TOF/TOF time-of-flight spectrometer. Only selected data are given for the detected ions (mass to charge ratio, relative intensity in percent). Standard deviation values are provided for electron ionization HR-MS data and for ESI-MS just the absolute values are given.

8.1.6 Cyclic voltammetry

Cyclic voltammograms (CVs) were measured under rigorous exclusion of the atmosphere by working in an argon-filled glove box. CVs were measured at Au and Pt electrodes "screen printed" onto patterned ceramic plates.

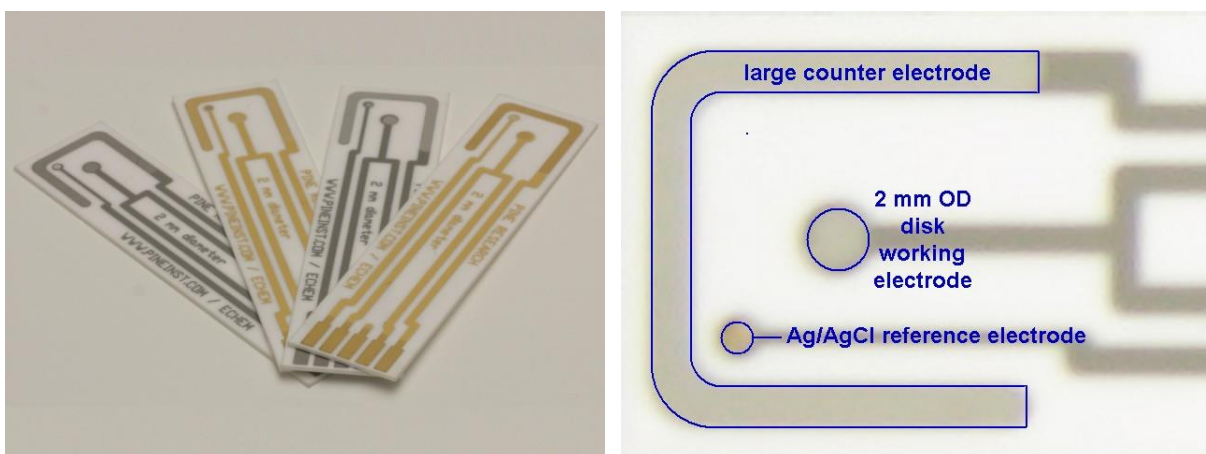


Figure 8.1. Screen-printed platinum and gold electrodes, fabricated on ceramic substrate with the built-in Ag/AgCl reference electrode.

The starting potentials were determined from an open circuit potential (OCP) experiment. Electrochemical samples were recorded with scan rates of 50–800 mVs⁻¹ at r.t. Cobaltocenium hexafluorophosphate was used as an internal reference to determine the potential. The

commercial [ⁿBu₄N]PF₆ was dried by heating for 24h at +80°C in *vacuo* (8×10⁻³ mbar). Solvents (DCM, THF and Acetonitrile) were prepared as follows:

CH₂Cl₂: Freshly distilled solvent (over CaH₂, under Ar atmosphere) was collected into a Young-valve-Schlenk over P₂O₅ and freeze-thaw degassed with 5 cycles of freezing and thawing, using a high vacuum source (8×10⁻³ mbar). Pure solvent was then vacuum transferred to a second Young-valve-Schlenk of similar volume and taken directly into the glove box.

THF: Freshly distilled solvent (over Na, under Ar atmosphere) was transferred to a Young-valve-Schlenk containing potassium. Then it was freeze-thaw degassed with 5 cycles of freezing and thawing, using a high vacuum source (8×10⁻³ mbar). It was then vacuum distilled into a second flask for transfer to the glove box.

CH₃CN: Freshly distilled solvent (over CaH₂, under Ar atmosphere), was re-distilled from P₂O₅ onto activated 4 Å molecular sieves, followed by 5 cycles of freeze-thaw degassing using a high vacuum source (8×10⁻³ mbar). Then it was taken into the glove box.

8.1.7 Single crystal X-ray diffraction studies

Single crystals were grown by evaporation of saturated solutions of the compounds or by diffusion technique. After crystal growing the single crystals were separated from the supernatant solution and were covered with Fomblin for protection from further decomposition. A suitable single crystal was selected under the microscope and loaded onto the diffractometer. The crystallographic data were collected on Bruker D8-Venture diffractometer, Bruker X8-KappaApexII, Bruker APEX-II CCD, Nonius KappaCCD or STOE IPDS 2T diffractometer equipped with a low-temperature device at 100.0 K using graphite monochromated Cu-K α radiation ($\lambda = 1.54178$ Å) or Cu-K α radiation ($\lambda = 1.54178$). The structures were solved by Patterson methods or Direct Methods (SHELXS-97)^{153,154} and refined by full-matrix least squares on F^2 (SHELXL-97)^{154,155}. All non-hydrogen atoms were refined anisotropically, the hydrogen atoms were included isotropically using the riding model on the bound carbon atoms. Data analyses and the picture preparation of the molecular structure for all the compounds were done using the Olex-2 program.

8.1.8 Chemicals

The following chemicals were commercially available and all chlorophosphanes were purified before use (producer/supplier name in brackets):

- Acetonitrile (Fisher Scientific)
- n-Butyllithium (Acros)
- Carbondisulfide (Sigmaaldrich)
- Chloroform (Fisher Scientific)
- Chloroform-d (Eurisotop)
- Diethylether (VWR)
- Dichloromethane (VWR)
- Diisopropylamine (Acros)
- Dimethylsulfoxide (Acros)
- Dimethylacetylenedicarboxylate (Acros)
- Ethanol (Hofmann)
- Lithium metal (Sigmaaldrich)
- Methanol (Aldrich)
- Methylamine (Sigmaaldrich)
- Potassium metal (Riedel de Haen)
- n-Pentane (VWR)
- Petrol ether 40/60 (Biesterfeld)
- Phosphorus trichloride (Acros)
- Sodium Metal (Riedel de Haen)
- Sodium hydroxide(Sigmaaldrich)
- Selenium (Acros)
- Sulfur (Acros)
- Sulfuric acid (Fluka)
- Tetrahydrofuran (Fisher Scientific)
- THF-d₈ (Eurisotop)

- Tri-n-butyl-phosphane (Acros)
- Triethylamine (Sigmaaldrich)
- Toluene (Fisher Scientific)
- Hydrogen peroxide (Acros)
- Hydrogen peroxide-urea adduct (Acros)
- Iodine (Grüssing)
- Isopropylamine (Sigmaaldrich)
- Isopropanol (Biesterfeld)
- Water-d₂ (Eurisotop)

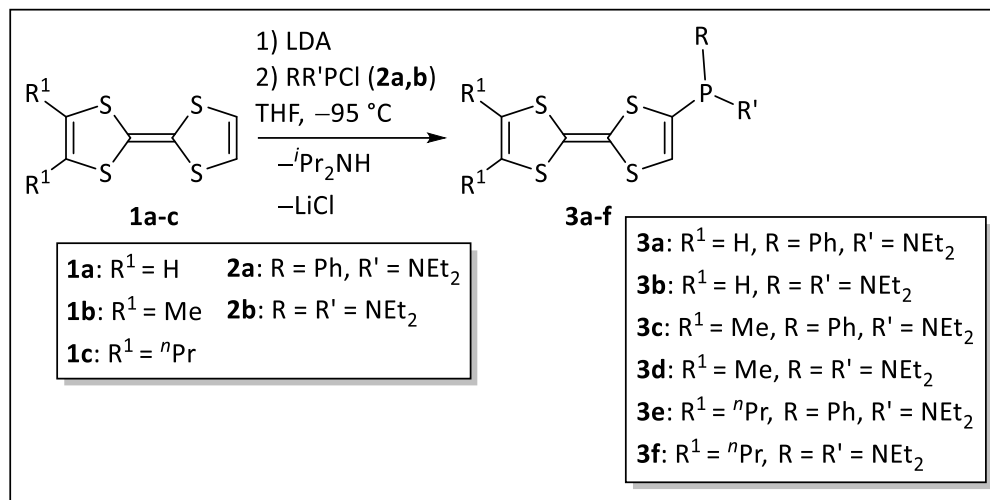
The following compounds were received from Dr. A. Gese:

- 4,8-Di-*iso*-propoxy-4,8-dihydro[1,4]diphosphinine[2,3-d:5,6-d']bisdithiole-2,6-dithione (**CVIII**)
- 4,8-Di-*tert*-butoxy-4,8-dihydro[1,4]diphosphinine[2,3-d:5,6-d']bisdithiole-2,6-dithione (**CIX**)

The following compounds were synthesized according to published procedures:

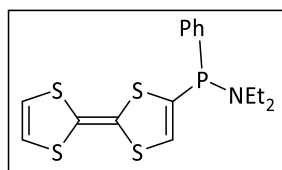
- Tetrathiafulvalene (**1a**)⁹¹
- 2-(1,3-Dithiol-2-ylidene)-4,5-dimethyl-1,3-dithiole (*ortho*-dimethyl-tetrathiafulvalene) (**1b**)^{14,95}
- 2-(1,3-Dithiol-2-ylidene)-4,5-dipropyl-1,3-dithiole (**1c**)⁹⁵
- Chloro(diethylamino)phenylphosphane (**2a**)¹⁵⁶
- Bis(diethylamino)chlorophosphane (**2b**)¹⁵⁷
- Dichloro(diethylamino)phosphane (**2c**)¹⁵⁸
- 4,8-Bis(diethylamino)-4,8-dihydro[1,4]diphosphinine[2.3-d:5.6-d']bisdithiole-2,6-dithione (**LXXIII**)⁸⁰

8.2 Synthesis of C-phosphanylated tetrathiafulvalenes 3a–f



Compound **1** was dissolved in dry THF in a Schlenk flask and cooled to -95 °C. A solution of LDA (1.05 eq for **1a,b**, 1.1 eq for **1c-f**) in dry THF was prepared and cooled to -95 °C, then added dropwise to the TTF solutions and each reaction mixture was stirred for 90 minutes (**1a,b**), 3 hours (**1c,d**) or 105 minutes (**1e,f**). During this time temperature was kept between -95 °C and -75 °C. Then **2a,b** (1.05–1.1 eq) was added dropwise (T = -95 °C) and the reaction mixture was warmed slowly and stirred for 3 hours. Then the solution was concentrated in *vacuo* (8×10⁻³ mbar) and the residue was taken up in dry dichloromethane and filtered over a 3G-frit having a celite® pad and silica gel to remove the formed lithium chloride. The filtrate was collected and the solvent was removed in *vacuo* (8×10⁻³ mbar) and then dried. In the case of **3a** and **3b** the residue was subjected to a low-temperature column chromatography to remove doubly substituted side-products. The unreacted TTF was partially removed via sublimation using an ultrahigh vacuum pump (1×10⁻⁵ mbar) over 8 hours. However, in these cases the pure product couldn't be obtained.

8.2.1 4-Diethylamino(phenyl)phosphanyl-2,2'-bis(1,3-dithiolylidene) (3a)



	Amount (gr or mL)	mmol
1a	1.2 gr	5.9
LDA	660 mg	6.2
Et₂N(Ph)PCI	1.18 mL	6.1
THF	55 mL	

Reaction code: SHK-333

Column chromatography: h = 10 cm, \varnothing = 1.5 cm, T = -20 °C, Stationary phase: SiO₂, Eluent: Petroleum ether/Et₂O (95:5)

Appearance: Orange-yellow oil of the raw product (content of **3a**: 82%)

Elemental composition: C₁₆H₁₈NPS₄ **Molecular weight:** 383.54 g/mol

NMR code: 21P5a041.21

¹H NMR (500.1 MHz, CDCl₃): δ = 1.09 (*t*, 6H, ³J_{H,H} = 7.0 Hz, N-CH₂-CH₃), 3.12 (*m*, 4H, N-CH₂-CH₃), 6.28 and 6.30 (*d*, 2H, ³J_{H,H} = 6.4 Hz, C^{4'}, C^{5'}-H), 6.31 (*s*, s.m.), 6.63 (*d*, 1H, ³J_{P,H} = 9 Hz, C⁵-H), 7.31 (*m*, 1H, *para*-C₆H₅), 7.37 (*m*, 2H, *meta*-C₆H₅), 7.43 (*m*, 2H, *ortho*-C₆H₅).

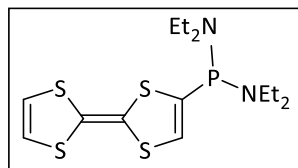
¹³C NMR (125.8 MHz, CDCl₃): δ = 14.5 (*d*, ³J_{P,C} = 3.4 Hz, N-CH₂-CH₃), 44.6 (*d*, ²J_{P,C} = 15 Hz, N-CH₂-CH₃), 109.8 and 112.6 (*s*, C², C^{2'}), 119.1 and 119.2 (*s*, C^{4'} and C^{5'}), 119.3 (*s*, s.m.), 127.5 (*d*, ²J_{P,C} = 42 Hz, C⁵), 128.5-128.6 (*para*, *meta*-C₆H₅), 130.7 (*d*, ²J_{P,C} = 18 Hz, *ortho*-C₆H₅), 138.4 (*d*, ¹J_{P,C} = 13.2 Hz, *ipso*-C₆H₅), 138.6 (*d*, ¹J_{P,C} = 48.2 Hz, C⁴).

³¹P{¹H} NMR (202.5 MHz, CDCl₃): δ = 52.9 (*s*).

³¹P NMR (202.5 MHz, CDCl₃): δ = 52.9 (*m*).

MS (EI, 70 eV): m/z (%) = 415 (38) [M+O₂]⁺, 383.1 (88) [M]⁺, 312 (34) [M-NEt₂+H]⁺, 204 (25) [M-PPh(NEt₂)+H]⁺, 180 (54) [PPh(NEt₂)]⁺, 109 (38) [P-C₆H₅+H]⁺.

HR-MS (EI, 70 eV): Calculated: 383.0059, Found: 383.0058 (standard deviation: 0.63 ppm).

8.2.2 4-Bis(diethylamino)phosphanyl-2,2'-bis(1,3-dithiolylidene) (**3b**)

	Amount (gr or mL)	mmol
1a	1 gr	4.9
LDA	550 mg	5.1
(Et₂N)₂PCI	1.13 mL	5.3
THF	50 mL	

Reaction code: SHK-334

Column chromatography: h = 8 cm, \varnothing = 2 cm, T = -20 °C, Stationary phase: SiO₂, Eluent: Petroleum ether (40/65)

Appearance: Yellow-orange oil of the raw product (content of **3b**: 78%)

Elemental composition: C₁₄H₂₃N₂PS₄ **Molecular weight:** 378.57 g/mol

NMR code: 21P5a042.21

¹H NMR (500.1 MHz, CDCl₃): δ = 1.08 (*t*, 12H, ³J_{H,H} = 7.2 Hz, N-CH₂-CH₃), 3.10 (*m*, 8H, N-CH₂-CH₃), 6.10 (*d*, 1H, ³J_{P,H} = 1.7 Hz, C⁵-H), 6.28 and 6.29 (*d*, 2H, ³J_{H,H} = 6.5 Hz, C^{4'}, C^{5'}-H), 6.31 (*s*, s.m.).

¹³C NMR (125.8 MHz, CDCl₃): δ = 14.7 (*d*, ³J_{P,C} = 3.3 Hz, N-CH₂-CH₃), 42.9 (*d*, ²J_{P,C} = 17.7 Hz, N-CH₂-CH₃), 109 and 113.4 (*s*, C², C^{2'}), 119.1 (*d*, ²J_{P,C} = 17.9 Hz, C⁵), 119.3 and 119.4 (*s*, C^{4'} and C^{5'}), 119.5 (*s*, s.m.), 140.3 (*d*, ¹J_{P,C} = 18.3 Hz, C⁴).

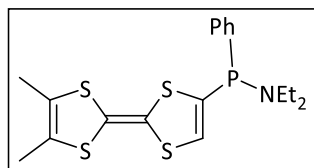
³¹P{¹H} NMR (202.5 MHz, CDCl₃): δ = 84.4 (*s*).

³¹P NMR (202.5 MHz, CDCl₃): δ = 84.4 (*m*).

MS (EI, 70 eV): m/z (%) = 410 (8) [M+O₂]⁺, 378.1 (6) [M]⁺, 204 (100) [M-P(NEt₂)₂+H]⁺.

HR-MS (EI, 70 eV): Calculated: 378.0481, Found: 378.0480 (standard deviation: 0.71 ppm).

8.2.3 4-Diethylamino(phenyl)phosphanyl-4',5'-dimethyl-2,2'-bis(1,3-dithiolylidene) (3c)



	Amount (gr or mL)	mmol
1b	300 mg	1.29
LDA	152 mg	1.42
Et₂N(Ph)PCl	0.27 mL	1.4
THF	35 mL	

Reaction code: SHK-297

Appearance: Orange oil **Yield:** 427 mg (1.04 mmol, 80%)

Elemental composition: C₁₈H₂₂NPS₄ **Molecular weight:** 411.59 g/mol

NMR code: 03t4b007.21

¹H NMR (400.1 MHz, CDCl₃): δ = 1.08 (*t*, 6H, ³J_{H,H} = 7.3 Hz, N-CH₂-CH₃), 1.92 and 1.93 (*br*, 6H, C^{4'}, C^{5'}-Me), 3.10 (*m*, 4H, N-CH₂-CH₃), 6.61 (*d*, 1H, ³J_{P,H} = 8.9 Hz, C⁵-H), 7.30 (*m*, 1H, *para*-C₆H₅), 7.36 (*m*, 2H, *meta*-C₆H₅), 7.42 (*m*, 2H, *ortho*-C₆H₅).

¹³C NMR (100.6 MHz, CDCl₃): δ = 13.8 (*s*, C^{4'}, C^{5'}-Me), 14.5 (*d*, ³J_{P,C} = 3.5 Hz, N-CH₂-CH₃), 44.6 (*d*, ²J_{P,C} = 14.9 Hz, N-CH₂-CH₃), 108.4 and 111.7 (*s*, C², C^{2'}), 122.9 and 123.1 (*s*, C^{4'} and C^{5'}), 127.6 (*d*, ²J_{P,C} = 42.2 Hz, C⁵), 128.4-128.5 (*para*, *meta*-C₆H₅), 130.7 (*d*, ²J_{P,C} = 18.1 Hz, *ortho*-C₆H₅), 138.4 (*d*, ¹J_{P,C} = 39.1 Hz, C⁴), 138.6 (*d*, ¹J_{P,C} = 22.2 Hz, *ipso*-C₆H₅).

³¹P{¹H} NMR (162.0 MHz, CDCl₃): δ = 52.9 (*s*).

³¹P NMR (162.0 MHz, CDCl₃): δ = 52.9 (*m*).

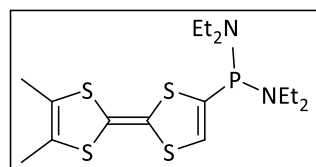
MS (EI, 70 eV): *m/z* (%) = 442.9 (3) [M+O₂]⁺, 411 (27) [M]⁺, 339.9 (8) [M-NEt₂+H]⁺, 231.9 (54) [M-PPh(NEt₂)+H]⁺.

HR-MS (EI, 70 eV): Calculated: 411.0372, Found: 411.0368 (standard deviation: 0.27 ppm).

EA (%): Calculated/Found **C:** 52.53/51.15, **H:** 5.39/5.67, **N:** 3.40/2.92, **S:** 31.16/28.90.

Crystal structure identification code: GSTR711 (structural data can be found in appendix).

8.2.4 4-Bis(diethylamino)phosphanyl-4',5'-dimethyl-2,2'-bis(1,3-dithiolylidene) (3d)



	Amount (gr or mL)	Mmol
1b	600 mg	2.58
LDA	305 mg	2.85
(Et₂N)₂PCI	0.6 mL	2.85
THF	40 mL	

Reaction code: SHK-296

Appearance: Orange oil **Yield:** 579 mg (1.4 mmol, 50%)

Elemental composition: C₁₆H₂₇N₂PS₄ **Molecular weight:** 406.62 g/mol

NMR code: 03t4b006.21

¹H NMR (400.1 MHz, CDCl₃): δ = 1.07 (t, 12H ³J_{H,H} = 7.1 Hz, N-CH₂-CH₃), 1.93 (s, 6H, C^{4'}, C^{5'}-Me), 3.09 (m, 8H, N-CH₂-CH₃), 6.09 (d, 1H, ³J_{P,H} = 1.7 Hz, C⁵-H).

¹³C NMR (100.6 MHz, CDCl₃): δ = 13.8 and 13.9 (s, C^{4'}, C^{5'}-Me), 14.7 (d, ³J_{P,C} = 3.2 Hz, N-CH₂-CH₃), 43 (d, ²J_{P,C} = 17.7 Hz, N-CH₂-CH₃), 107.5 and 112.5 (s, C², C^{2'}), 119.5 (d, ²J_{P,C} = 14.5 Hz, C⁵), 122.8 and 123.1 (s, C^{4'} and C^{5'}), 140.4 (d, ¹J_{P,C} = 18.4 Hz, C⁴).

³¹P{¹H} NMR (162.0 MHz, CDCl₃): δ = 84.7 (s).

³¹P NMR (162.0 MHz, CDCl₃): δ = 84.7 (m).

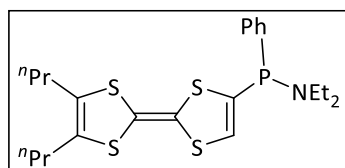
MS (EI, 70 eV): m/z (%) = 438 (6) [M+O₂]⁺, 406.0 (36) [M]⁺, 231.9 (100) [M-P(NEt₂)₂+H]⁺.

HR-MS (EI, 70 eV): Calculated: 406.0794, Found: 406.0791 (standard deviation: 0.32 ppm).

EA (%): Calculated/Found **C:** 47.26/46.35, **H:** 6.69/6.73, **N:** 6.89/5.84, **S:** 31.54/29.98.

Crystal structure identification code: GSTR776 (structural data can be found in appendix).

8.2.5 4-Diethylamino(phenyl)phosphanyl-4',5'-di-*n*-propyl-2,2'-bis(1,3-dithiolylidene) (3e)



	Amount (gr or mL)	Mmol
1c	350 mg	1.2
LDA	143 mg	1.33
Et₂N(Ph)PCI	0.26 mL	1.36
THF	30 mL	

Reaction code: SHK-464

Appearance: Orange oil **Yield:** 497 mg (1.06 mmol, 88%)

Elemental composition: C₂₂H₃₀NPS₄ **Molecular weight:** 467.70 g/mol

NMR code: 20p5a033.22

¹H NMR (500.1 MHz, CDCl₃): δ = 0.93 (*t*, 6H, ³J_{H,H} = 7.35 Hz, C^{4'}, C^{5'}-CH₂-CH₂-CH₃), 1.09 (*t*, 6H, ³J_{H,H} = 7.08 Hz, N-CH₂-CH₃), 1.53 (*m*, 4H, C^{4'}, C^{5'}-CH₂-CH₂-CH₃), 2.31 (*m*, 4H, C^{4'}, C^{5'}-CH₂-CH₂-CH₃), 3.11 (*m*, 4H, N-CH₂-CH₃), 6.60 (*d*, 1H, ³J_{P,H} = 9 Hz, C⁵-H), 7.30 (*m*, 1H, *para*-C₆H₅), 7.36 (*m*, 2H, *meta*-C₆H₅), 7.42 (*m*, 2H, *ortho*-C₆H₅).

¹³C NMR (125.8 MHz, CDCl₃): δ = 13.8 (2*s*, C^{4'}, C^{5'}-CH₂-CH₂-CH₃), 14.6 (*d*, ³J_{P,C} = 3.37 Hz, N-CH₂-CH₃), 23.1 (2*s*, C^{4'}, C^{5'}-CH₂-CH₂-CH₃), 30.9 (*s*, C^{4'}, C^{5'}-CH₂-CH₂-CH₃), 44.6 (*d*, ²J_{P,C} = 14.79 Hz, N-CH₂-CH₃), 108.6 and 110.8 (*s*, C², C^{2'}), 119.2 (*s*, C^{4'} and C^{5'}), 127.6 (*d*, ²J_{P,C} = 42.22 Hz, C⁵), 128.4-129 (*para*, *meta*-C₆H₅), 130.7 (*d*, ²J_{P,C} = 17.91 Hz, *ortho*-C₆H₅), 138.4 (*d*, ¹J_{P,C} = 40.7 Hz, C⁴), 138.6 (*d*, ¹J_{P,C} = 19.5 Hz, *ipso*-C₆H₅).

³¹P{¹H} NMR (202.5 MHz, CDCl₃): δ = 52.9 (*s*).

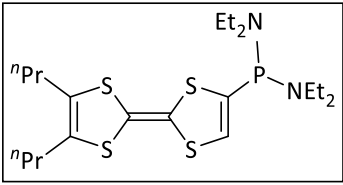
³¹P NMR (202.5 MHz, CDCl₃): δ = 52.9 (*m*).

MS (EI, 70 eV): *m/z* (%) = 499.1 (8) [M+O₂]⁺, 467.1 (30) [M]⁺, 396.0 (5) [M-NEt₂]⁺, 288 (100) [M-P(NEt₂)Ph+H]⁺, 230.0 (30) [M-P(NEt₂)Ph-2C₂H₅+2H]⁺, 180.1 (10) [P(NEt₂)Ph]⁺.

HR-MS (EI, 70 eV): Calculated: 467.0999, Found: 467.1008 (standard deviation: 0.17 ppm).

EA (%): Calculated/Found C: 56.50/56.44, H: 6.47/6.21, N: 2.99/3.30, S: 27.42/30.13.

8.2.6 4-Bis(diethylamino)phosphanyl-4',5'-di-*n*-propyl-2,2'-bis(1,3-dithiolylidene) (3f)

	Amount (gr or mL)	Mmol	
	1c	1.531 gr	5.3
	LDA	630 mg	5.88
	(Et₂N)₂PCl	1.25 mL	5.94
	THF	80 mL	

Reaction code: SHK-463

Appearance: Orange oil Yield: 1.718 gr (3.71 mmol, 70%)

Elemental composition: C₂₀H₃₅N₂PS₄ Molecular weight: 462.73 g/mol

NMR code: 20p5a032.22

¹H NMR (500.1 MHz, CDCl₃): δ = 0.93 (t, 6H, ³J_{H,H} = 7.36 Hz, C^{4'}, C^{5'}-CH₂-CH₂-CH₃), 1.07 (t, 12H, ³J_{H,H} = 7.05 Hz, N-CH₂-CH₃), 1.53 (m, 4H, C^{4'}, C^{5'}-CH₂-CH₂-CH₃), 2.31 (t, 4H, ³J_{H,H} = 7.52 Hz, C^{4'}, C^{5'}-CH₂-CH₂-CH₃), 3.09 (m, 8H, N-CH₂-CH₃), 6.09 (d, 1H, ³J_{P,H} = 1.8 Hz, C⁵-H).

¹³C NMR (125.8 MHz, CDCl₃): δ = 13.8 (s, C^{4'}, C^{5'}-CH₂-CH₂-CH₃), 14.7 (d, ³J_{P,C} = 3.22 Hz, N-CH₂-CH₃), 23.1 (2s, C^{4'}, C^{5'}-CH₂-CH₂-CH₃), 30.9 (2s, C^{4'}, C^{5'}-CH₂-CH₂-CH₃), 43 (d, ²J_{P,C} = 17.59 Hz, N-CH₂-CH₃), 107.9 (s, C^{2'}), 111.7 (d, ³J_{P,C} = 2.93 Hz, C²), 119.6 (d, ²J_{P,C} = 14.61 Hz, C⁵), 128.7 and 129 (s, C^{4'} and C^{5'}), 140.4 (d, ¹J_{P,C} = 18.13 Hz, C⁴).

³¹P{¹H} NMR (202.5 MHz, CDCl₃): δ = 84.7 (s).

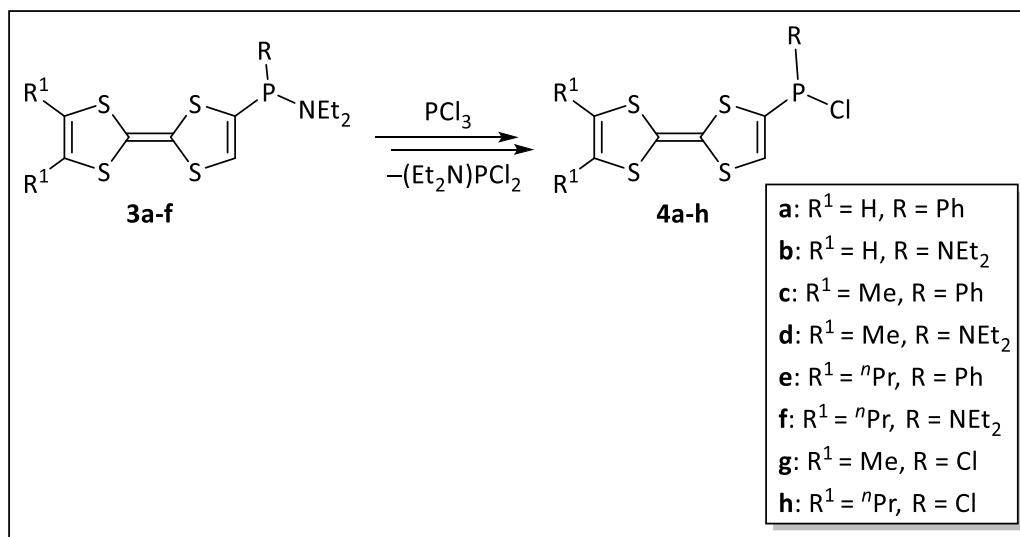
³¹P NMR (202.5 MHz, CDCl₃): δ = 84.7 (m).

MS (EI, 70 eV): m/z (%) = 494.1 (35) [M+O₂]⁺, 462.1 (92) [M]⁺, 390.0 (10) [M-NEt₂]⁺, 319.0 (5) [M-2(NEt₂)+H]⁺, 287 (10) [M-P(NEt₂)₂]⁺, 230.0 (95) [M-P(NEt₂)₂-2C₂H₅+2H]⁺, 175.1 (100) [P(NEt₂)₂]⁺.

HR-MS (EI, 70 eV): Calculated: 462.1421, Found: 462.1435 (standard deviation: 1.29 ppm).

EA (%): Calculated/Found **C:** 51.91/52.09, **H:** 7.62/7.23, **N:** 6.05/6.06, **S:** 27.71/36.00.

8.3 Synthesis of 4-chlorophosphanyl-tetrathiafulvalenes 4a–h



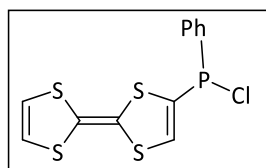
General procedure I: **3a,c,e** were each dissolved in dry dichloromethane in a Schlenk tube, then PCl₃ (1 eq) was added dropwise, and the reaction mixture was stirred for 1 hour (**3a**), 2 (**3c**) or 3 hours (**3e**) at r.t. The reaction mixture was concentrated in *vacuo* (8×10⁻³ mbar), and the residue was then dissolved in dry diethylether. The solution was filtered, concentrated and dried in *vacuo* (8×10⁻³ mbar).

General procedure II: **3b,d,f** were each dissolved in dry diethylether in a Schlenk tube and cooled to -90 °C, then PCl₃ (1 eq) was added dropwise, and the reaction mixture was warmed up slowly and stirred for 1 h. The reaction mixture was concentrated in *vacuo* (8×10⁻³ mbar), and the residue was then dissolved in dry diethylether. The solution was filtered, concentrated and dried in *vacuo* (8×10⁻³ mbar).

General procedure III: **3d,f** were each dissolved in dry dichloromethane in a Schlenk tube, then PCl₃ (2.2 eq) was added dropwise, and the reaction mixture was stirred for 3 h. The reaction mixture was concentrated in *vacuo* (8×10⁻³ mbar), and the residue was then

dissolved in dry diethylether. The solution was filtered, concentrated and dried in *vacuo* (8×10^{-3} mbar) resulting.

8.3.1 4-Chloro(phenyl)phosphanyl-2,2'-bis(1,3-dithiolylidene) (4a)



	Amount (gr or mL)	mmol
3a	805 mg	2.1
PCl₃	0.2 mL	2.3
DCM	30 mL	

Reaction code: SHK-340

Appearance: Red oil of the raw product (content of **4a**: 85%)

Elemental composition: C₁₂H₈ClPS₄ **Molecular weight:** 346.86 g/mol

NMR code: 21P5a043.21

¹H NMR (500.1 MHz, CDCl₃): δ = 6.28 and 6.29 (*d*, 2H, $^3J_{H,H}$ = 6.8 Hz, C^{4'},C^{5'}-H), 6.31 (*s*, TTF), 6.96 (*d*, 1H, $^3J_{P,H}$ = 10.8 Hz, C⁵-H), 7.46 (*m*, 3H, *para, meta*-C₆H₅), 7.71 (*m*, 2H, *ortho*-C₆H₅).

¹³C NMR (125.8 MHz, CDCl₃): δ = 109.4 and 113.2 (*s*, C²,C^{2'}), 119 and 119.2 (*s*, C^{4'} and C^{5'}), 119.3 (*s*, C^{4,4'},C^{5,5'}-TTF), 128.9, 129 and 130.7 (*para,meta*- C₆H₅), 131 (*d*, $^2J_{P,C}$ = 13.1 Hz, *ortho*-C₆H₅), 132.3 (*d*, $^2J_{P,C}$ = 52 Hz, C⁵), 135.9 (*d*, $^1J_{P,C}$ = 28.9 Hz, *ipso*-C₆H₅), 136.7 (*d*, $^1J_{P,C}$ = 61.2 Hz, C⁴).

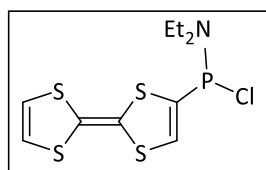
³¹P{¹H} NMR (202.5 MHz, CDCl₃): δ = 63.9 (*s*, with chlorine shoulder).

³¹P NMR (202.5 MHz, CDCl₃): δ = 63.9 (*m*).

MS (EI, 70 eV): *m/z* (%) = 345.8 (4) [M]⁺, 311.8 (16) [M-Cl+H]⁺, 203.8 (100) [M-PhPCI+H]⁺.

HR-MS (EI, 70 eV): Calculated: 345.8935, Found: 345.8935 (Standard deviation: 0.67 ppm).

8.3.2 4-Chloro(diethylamino)phosphanyl-2,2'-bis(1,3-dithiolylidene) (**4b**)



	Amount (gr or mL)	Mmol
3b	1.2 gr	3.17
PCl₃	0.28 mL	3.2
Et₂O	40 mL	

Reaction code: SHK-341

Appearance: Yellow-orange oil of the raw product (content of **4b**: 95%)

Elemental composition: C₁₀H₁₃ClNPS₄ **Molecular weight:** 341.88 g/mol

NMR code: 21P5a056.21

¹H NMR (500.1 MHz, CDCl₃): δ = 1.17 (*t*, 6H, ³J_{H,H} = 7.4 Hz, N-CH₂-CH₃), 3.20 (*m*, 4H, N-CH₂-CH₃), 6.30 and 6.32 (*d*, 2H, ³J_{H,H} = 6.5 Hz, C^{4'}, C^{5'}-H), 6.31 (*s*, TTF), 6.73 (*d*, 1H, ³J_{P,H} = 2.6 Hz, C⁵-H).

¹³C NMR (125.8 MHz, CDCl₃): δ = 14.1 (*d*, ³J_{P,C} = 6.2 Hz, N-CH₂-CH₃), 43.9 (*d*, ²J_{P,C} = 14.8 Hz, N-CH₂-CH₃), 110.6 and 112.1 (*s*, C², C^{2'}), 119.1 and 119.3 (*s*, C^{4'} and C^{5'}), 126.4 (*d*, ²J_{P,C} = 18.5 Hz, C⁵), 136.9 (*d*, ¹J_{P,C} = 50.9 Hz, C⁴).

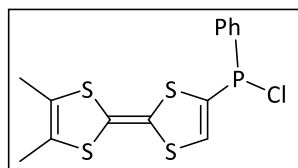
³¹P{¹H} NMR (202.5 MHz, CDCl₃): δ = 117.9 (*s*).

³¹P NMR (202.5 MHz, CDCl₃): δ = 117.9 (*s*).

MS (EI, 70 eV): m/z (%) = 372.9 (30) [M+O₂]⁺, 340.9 (90) [M]⁺, 203.9 (78) [M-P(NEt₂)₂+H]⁺.

HR-MS (EI, 70 eV): Calculated: 340.9357, Found: 340.9352 (standard deviation: 0.44 ppm).

8.3.3 4-Chloro(phenyl)phosphanyl-4',5'-dimethyl-2,2'-bis(1,3-dithiolylidene) (4c)



	Amount (gr or mL)	mmol
3c	329 mg	0.8
PCl₃	0.07 mL	0.8
DCM	20 mL	

Reaction code: SHK-299

Appearance: Red powder **Yield:** 271 mg (0.72 mmol, 90%) **Melting point:** 104 °C

Elemental composition: C₁₄H₁₂ClPS₄ **Molecular weight:** 374.91 g/mol

NMR code: 03p5a052.21

¹H NMR (500.1 MHz, CDCl₃): δ = 1.91 (*m*, 6H, C^{4'}, C^{5'}-Me), 6.95 (*d*, 1H, ³J_{P,H} = 10.7 Hz, C⁵-H), 7.46 (*m*, 3H, *para*, *meta*-C₆H₅), 7.71 (*m*, 2H, *ortho*-C₆H₅).

¹³C NMR (125.8 MHz, CDCl₃): δ = 13.8 (*s*, C^{4'}, C^{5'}-Me), 108.4 and 111.9 (*s*, C², C^{2'}), 122.8 and 123.1 (*s*, C^{4'} and C^{5'}), 128.9, 130 and 130.7 (*para*, *meta*-C₆H₅), 131 (*d*, ²J_{P,C} = 6.2 Hz, *ortho*-C₆H₅), 132.5 (*d*, ²J_{P,C} = 52.1 Hz, C⁵), 136 (*d*, ¹J_{P,C} = 27.8 Hz, *ipso*-C₆H₅), 136.6 (*d*, ¹J_{P,C} = 60.6 Hz, C⁴).

³¹P{¹H} NMR (202.5 MHz, CDCl₃): δ = 64 (*s*, with chlorine shoulder).

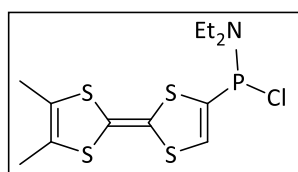
³¹P NMR (202.5 MHz, CDCl₃): δ = 64 (*m*).

MS (EI, 70 eV): m/z (%) = 373.9 (100) [M]⁺, 339.9 (38) [M-Cl+H]⁺, 231.9 (62) [M-PhPCI+H]⁺.

HR-MS (EI, 70 eV): Calculated: 373.9248, Found: 373.9243 (standard deviation: 0.37 ppm).

EA (%): Calculated/Found **C:** 44.85/45.96, **H:** 3.23/3.89, **S:** 34.21/32.69.

8.3.4 4-Chloro(diethylamino)phosphanyl-4',5'-dimethyl-2,2'-bis(1,3-dithiolyli- dene) (4d)



	Amount (gr or mL)	mmol
3d	477 mg	1.17
PCl₃	0.1 mL	1.15
Et₂O	25 mL	

Reaction code: SHK-298

Appearance: Orange-red oil **Yield:** 410 mg (1.1 mmol, 95%)

Elemental composition: C₁₂H₁₇ClNPS₄ **Molecular weight:** 369.94 g/mol

NMR code: 03p5a054.21

¹H NMR (500.1 MHz, CDCl₃): δ = 1.17 (*t*, 6H, ³J_{H,H} = 7.2 Hz, N-CH₂-CH₃), 1.94 (*s*, 6H, C^{4'}, C^{5'}-Me), 3.20 (*m*, 4H, N-CH₂-CH₃), 6.72 (*d*, 1H, ³J_{P,H} = 2.7 Hz, C⁵-H).

¹³C NMR (125.8 MHz, CDCl₃): δ = 13.9 (*s*, C^{4'}, C^{5'}-Me), 14.1 (*d*, ³J_{P,C} = 5.9 Hz, N-CH₂-CH₃), 43.9 (*d*, ²J_{P,C} = 15 Hz, N-CH₂-CH₃), 109.6 and 110.8 (*s*, C², C^{2'}), 122.9 and 123.1 (*s*, C^{4'} and C^{5'}), 126.5 (*d*, ²J_{P,C} = 18.6 Hz, C⁵), 136.8 (*d*, ¹J_{P,C} = 51 Hz, C⁴).

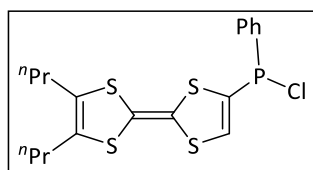
³¹P{¹H} NMR (202.5 MHz, CDCl₃): δ = 118.2 (*s*).

³¹P NMR (202.5 MHz, CDCl₃): δ = 118.2 (*m*).

MS (EI, 70 eV): *m/z* (%) = 368.9 (26) [M]⁺, 231.9 (86) [M-(Et₂N)PCl+H]⁺.

HR-MS (EI, 70 eV): Calculated: 368.9670, Found: 368.9663 (standard deviation: 0.57 ppm).

8.3.5 4-Chloro(phenyl)phosphanyl-4',5'-di-*n*-propyl-2,2'-bis(1,3-dithiolylidene) (4e)



	Amount (gr or mL)	mmol
3e	401 mg	0.86
PCl₃	0.08 mL	0.9
DCM	30 mL	

Reaction code: SHK-466

Appearance: Red oil **Yield:** 362 mg (0.84 mmol, 98%)

Elemental composition: C₁₈H₂₀ClPS₄ **Molecular weight:** 431.02 g/mol

NMR code: 20p5a056.22

¹H NMR (500.1 MHz, CDCl₃): δ = 0.92 (*m*, 6H, C^{4'}, C^{5'}-CH₂-CH₂-CH₃), 1.51 (*m*, 4H, C^{4'}, C^{5'}-CH₂-CH₂-CH₃), 2.30 (*m*, 4H, C^{4'}, C^{5'}-CH₂-CH₂-CH₃), 6.95 (*d*, 1H, ³J_{P,H} = 10.73 Hz, C⁵-H), 7.46 (*m*, 3H, *para*, *meta*-C₆H₅), 7.71 (*m*, 2H, *ortho*-C₆H₅).

¹³C NMR (125.8 MHz, CDCl₃): δ = 13.8 (*s*, C^{4'}, C^{5'}-CH₂-CH₂-CH₃), 23.1 (2*s*, C^{4'}, C^{5'}-CH₂-CH₂-CH₃), 30.8 (2*s*, C^{4'}, C^{5'}-CH₂-CH₂-CH₃), 107.7 and 112.2 (*s*, C², C^{2'}), 129 (*s*, C^{4'} and C^{5'}), 128.8 - 131 (*para*, *meta*, *ortho*-C₆H₅), 132.6 (*d*, ²J_{P,C} = 52.24 Hz, C⁵), 136 (*d*, ¹J_{P,C} = 28.08 Hz, *ipso*-C₆H₅), 136.6 (*d*, ¹J_{P,C} = 60.43 Hz, C⁴).

³¹P{¹H} NMR (202.5 MHz, CDCl₃): δ = 64.1 (*s*, with chlorine shoulder).

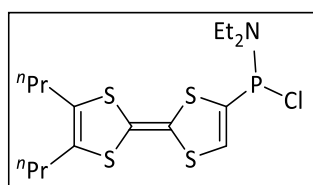
³¹P NMR (202.5 MHz, CDCl₃): δ = 64.1 (*m*).

MS (LIFDI): *m/z* (%) = 430.0 (100) [M]⁺

HR-MS (ESI-pos): [M-Cl+OH]⁺ (100%) Calculated: 412.0207, Found: 412.0207.

EA (%): Calculated/Found **C:** 50.16/51.01, **H:** 4.68/4.99, **S:** 29.75/30.48.

8.3.6 4-Chloro(diethylamino)phosphanyl-4',5'-di-*n*-propyl-2,2'-bis(1,3-dithiolylidene) (4f)



	Amount (gr or mL)	mmol
3f	1.615 gr	3.49
PCl₃	0.31 mL	3.55
Et₂O	50 mL	

Reaction code: SHK-465

Appearance: Red oil **Yield:** 1.487 gr (3.49 mmol, 100%)

Elemental composition: C₁₆H₂₅ClNPS₄ **Molecular weight:** 426.05 g/mol

NMR code: 20p5a040.22

¹H NMR (500.1 MHz, CDCl₃): δ = 0.94 (2t, 6H, $^3J_{H,H}$ = 7.34 Hz, C^{4'}, C^{5'}-CH₂-CH₂-CH₃), 1.16 (t, 6H, $^3J_{H,H}$ = 7.16 Hz, N-CH₂-CH₃), 1.53 (m, 4H, C^{4'}, C^{5'}-CH₂-CH₂-CH₃), 2.32 (m, 4H, C^{4'}, C^{5'}-CH₂-CH₂-CH₃), 3.20 (m, 4H, N-CH₂-CH₃), 6.72 (d, 1H, $^3J_{P,H}$ = 2.61 Hz, C⁵-H).

¹³C NMR (125.8 MHz, CDCl₃): δ = 13.8 (s, C^{4'}, C^{5'}-CH₂-CH₂-CH₃), 14.1 (d, $^3J_{P,C}$ = 6.08 Hz, N-CH₂-CH₃), 23.1 (2s, C^{4'}, C^{5'}-CH₂-CH₂-CH₃), 30.9 (s, C^{4'}, C^{5'}-CH₂-CH₂-CH₃), 43.9 (d, $^2J_{P,C}$ = 14.7 Hz, N-CH₂-CH₃), 108.9 (d, $^4J_{P,C}$ = 2.88 Hz, C^{2'}), 111.2 (s, C²), 126.6 (d, $^2J_{P,C}$ = 18.57 Hz, C⁵), 128.9 and 129 (s, C^{4'} and C^{5'}), 136.8 (d, $^1J_{P,C}$ = 50.81 Hz, C⁴).

³¹P{¹H} NMR (202.5 MHz, CDCl₃): δ = 118.4 (s).

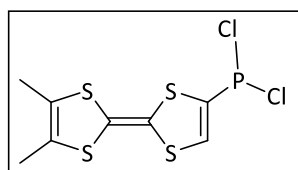
³¹P NMR (202.5 MHz, CDCl₃): δ = 118.4 (p, $^3J_{P,H}$ = 12.29 Hz)

MS (LIFDI): m/z (%) = 425.1 (100) [M]⁺

HR-MS (ESI-pos): [M-Cl]⁺ (5%) Calculated: 390.0602, Found: 390.0598, [M-Cl+OH]⁺ (100%) Calculated: 407.0629, Found: 407.0625.

EA (%): Calculated/Found **C:** 45.11/45.06, **H:** 5.91/6.02, **N:** 3.29/3.54, **S:** 30.10/31.89.

8.3.7 4-Dichlorophosphanyl-4',5'-dimethyl-2,2'-bis(1,3-dithiolylidene) (4g)



	Amount (gr or mL)	mmol
3d	212 mg	0.52
PCl₃	0.1 mL	1.15
DCM	15 mL	

Reaction code: SHK-412

Appearance: Red powder **Yield:** 170 mg (0.51 mmol, 98%) **Melting point:** 83 °C

Elemental composition: C₈H₇Cl₂PS₄ **Molecular weight:** 333.26 g/mol

NMR code: 28t4a033.22

¹H NMR (500.1 MHz, CDCl₃): δ = 1.95 and 1.96 (*s, br*, 6H, C^{4'}, C^{5'}-Me), 7.12 (*d*, 1H, ³J_{P,H} = 12.84 Hz, C⁵-H).

¹³C NMR (125.8 MHz, CDCl₃): δ = 13.9 (*s*, C^{4'}, C^{5'}-Me), 114.6 (*s*, C², C^{2'}), 122.9 and 123.3 (*s*, C^{4'} and C^{5'}), 134 (*d*, ²J_{P,C} = 64.61 Hz, C⁵), 138.7 (*d*, ¹J_{P,C} = 77.24 Hz, C⁴).

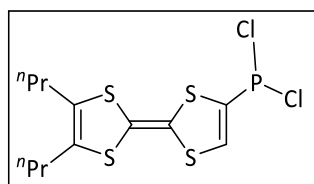
³¹P{¹H} NMR (202.5 MHz, CDCl₃): δ = 134.2 (*s*).

³¹P NMR (202.5 MHz, CDCl₃): δ = 134.2 (*d*, ³J_{P,H} = 12.67 Hz).

MS (EI, 70 eV): m/z (%) = 331.8 (52) [M]⁺, 231.9 (44) [M-PCl₂+H]⁺, 231.9 (62) [M-PhPCI+H]⁺.

HR-MS (EI, 70 eV): Calculated: 331.8545, Found: 331.8535 (standard deviation: 0.21 ppm).

8.3.8 4-Dichlorophosphanyl-4',5'-di-n-propyl-2,2'-bis(1,3-dithiolylidene) (4h)



	Amount (gr or mL)	mmol
3f	158 mg	0.34
PCl₃	0.07 mL	0.8
DCM	20 mL	

Reaction code: SHK-483

Appearance: Red oily/sticky solid **Yield:** 122 mg (0.31 mmol, 92%)

Elemental composition: C₁₂H₁₅Cl₂PS₄ **Molecular weight:** 389.37 g/mol

NMR code: 24m3a005.22 and 28p5a009.22

¹H NMR (500.1 MHz, CDCl₃): δ = 0.94 (*m*, 6H, C^{4'}, C^{5'}-CH₂-CH₂-CH₃), 1.54 (*m*, 4H, C^{4'}, C^{5'}-CH₂-CH₂-CH₃), 2.34 (*m*, 4H, C^{4'}, C^{5'}-CH₂-CH₂-CH₃), 7.12 (*d*, 1H, ³J_{P,H} = 12.86 Hz, C⁵-H).

¹³C NMR (125.8 MHz, CDCl₃): δ = 13.8 (2*s*, C^{4'}, C^{5'}-CH₂-CH₂-CH₃), 23.1 (2*s*, C^{4'}, C^{5'}-CH₂-CH₂-CH₃), 30.8 (2*s*, C^{4'}, C^{5'}-CH₂-CH₂-CH₃), 105.3 (*d*, ³J_{P,C} = 2.10 Hz, C²), 115 (*s*, C^{2'}), 128.9 and 129.2 (*s*, C^{4'} and C^{5'}), 134.1 (*d*, ²J_{P,C} = 64.66 Hz, C⁵), 138.7 (*d*, ¹J_{P,C} = 77.07 Hz, C⁴).

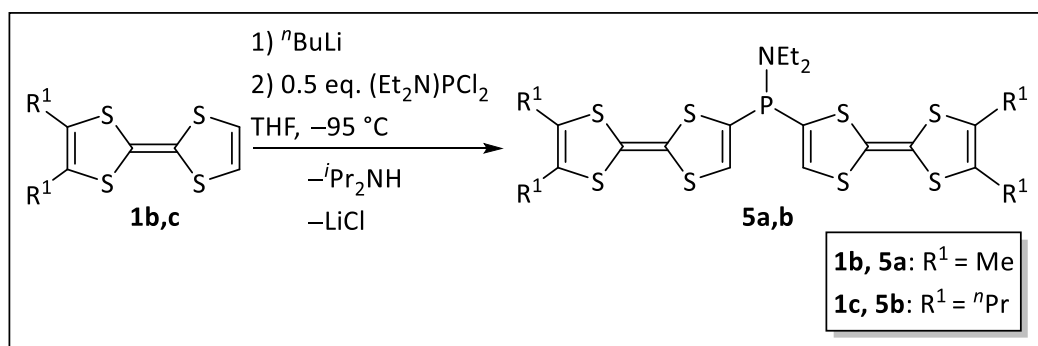
³¹P{¹H} NMR (202.5 MHz, CDCl₃): δ = 134.3 (*s*).

³¹P NMR (202.5 MHz, CDCl₃): δ = 134.3 (*d*, ³J_{P,H} = 13.02 Hz).

MS (EI, 70 eV): *m/z* (%) = 288 (20) [M-PCl₂+H]⁺, 200.1 (56) [M-C₉H₁₄S₂]⁺, 187.0 (100) [C₉H₁₄S₂+H]⁺, 131.0 (12) [M-C₉H₁₄S₂-Cl₂]⁺.

MS (LIFDI): *m/z* (%) = 387.9 (100) [M]⁺.

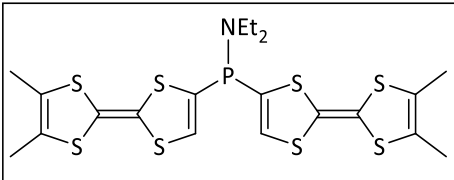
8.4 Synthesis of bis(tetrathiafulvalenyl)aminophosphanes 5a,b



1b,c were each dissolved in dry THF in a Schlenk flask and cooled down to -95 °C. Then ⁿBuLi (1.6 M in Hexane, 1.1 eq) was added dropwise to the TTF solution and the reaction mixture was stirred for 3 hours and 30 minutes. During this time temperature was kept

between $-95\text{ }^{\circ}\text{C}$ and $-75\text{ }^{\circ}\text{C}$. Then Et_2NPCI_2 (0.5 eq) was added dropwise ($T = -95\text{ }^{\circ}\text{C}$) and the reaction mixture was warmed up slowly and stirred over night. Then the solution was concentrated in *vacuo* (8×10^{-3} mbar) and the residue was taken up in dry dichloromethane and filtered over a 3G-frit having a celite[®] pad and silica gel to remove the formed lithium chloride. The filtrate was collected and the solvent was removed in *vacuo* (8×10^{-3} mbar) and then dried.

8.4.1 Bis[2-(4,5-dimethyl-1,3-dithiol-2-ylidene)-1,3-dithiol-4-yl]diethylamino-phosphane (5a)

	Amount (gr or mL)	Mmol
		
1b	125 mg	0.54
<i>n</i>BuLi (1.6 M)	0.37 mL	0.59
Et₂NPCI₂	0.039 mL	0.27
THF	25 mL	

Reaction code: SHK-495

Appearance: Orange oily/sticky solid of the raw product (content of **5a**: 92%)

Elemental composition: $\text{C}_{20}\text{H}_{24}\text{NPS}_8$ **Molecular weight:** 565.87 g/mol

NMR code: 27p5a030.22

^1H NMR (500.1 MHz, CDCl_3): $\delta = 1.09$ (*t*, 6H, $^3J_{\text{H,H}} = 7.07$ Hz, N-CH₂-CH₃), 1.94 (*s*, 12H, C^{4'}, C^{5'}-Me), 3.08 (*m*, 4H, N-CH₂-CH₃), 6.29 (*s*, s.m.), 6.52 (*d*, 2H, $^3J_{\text{P,H}} = 6.96$ Hz, C⁵-H).

^{13}C NMR (125.8 MHz, CDCl_3): $\delta = 13.9$ (2*s*, C^{4'}, C^{5'}-Me), 14.4 (*d*, $^3J_{\text{P,C}} = 3.56$ Hz, N-CH₂-CH₃), 44.5 (*d*, $^2J_{\text{P,C}} = 15.41$ Hz, N-CH₂-CH₃), 109.5 and 110.5 (*s*, C², C^{2'}), 122.9 and 123.1 (*s*, C^{4'} and C^{5'}), 125.9 (*d*, $^2J_{\text{P,C}} = 32.23$ Hz, C⁵), 136.2 (*d*, $^1J_{\text{P,C}} = 40.60$ Hz, C⁴).

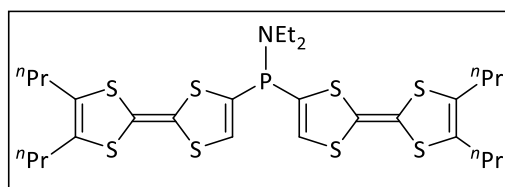
$^{31}\text{P}\{^1\text{H}\}$ NMR (202.5 MHz, CDCl_3): $\delta = 42$ (*s*).

^{31}P NMR (202.5 MHz, CDCl_3): $\delta = 42$ (*m*).

MS (EI, 70 eV): m/z (%) = 596.9 (8) $[M+O_2]^+$, 564.9 (24) $[M]^+$, 334.0 (30) $[M-DMTTF]^+$, 261.1 (58) $[M-DMTTF-NEt_2]^+$, 231.9 (42) $[M-DMTTF-P(NEt_2)+H]^+$, 201.0 (52) $[M-DMTTF-P(NEt_2)-2CH_3]^+$.

HR-MS (EI, 70 eV): Calculated: 564.9412, Found: 564.9418 (standard deviation: 0.23 ppm).

8.4.2 Bis[2-(4,5-di-*n*-propyl-1,3-dithiol-2-ylidene)-1,3-dithiol-4-yl]diethylamino-phosphane (**5b**)



	Amount (gr or mL)	mmol
1c	132 mg	0.46
<i>n</i>BuLi (1.6 M)	0.31 mL	0.5
Et₂NPCl₂	0.033 mL	0.23
THF	25	

Reaction code: SHK-496

Appearance: Orange oil of the raw product (content of **5b**: 92%)

Elemental composition: C₂₈H₄₀NPS₈ **Molecular weight:** 678.09 g/mol

NMR code: 27p5a029.22

¹H NMR (500.1 MHz, CDCl₃): δ = 0.93 (*t*, 12H, $^3J_{H,H}$ = 7.45 Hz, C^{4'}, C^{5'}-CH₂-CH₂-CH₃), 1.09 (*t*, 6H, $^3J_{H,H}$ = 7.07 Hz, N-CH₂-CH₃), 1.54 (*m*, 8H, C^{4'}, C^{5'}-CH₂-CH₂-CH₃), 2.32 (*m*, 8H, C^{4'}, C^{5'}-CH₂-CH₂-CH₃), 3.08 (*m*, 4H, N-CH₂-CH₃), 6.28 (*s*, s.m.), 6.52 (*d*, 2H, $^3J_{P,H}$ = 6.99 Hz, C⁵-H).

¹³C NMR (125.8 MHz, CDCl₃): δ = 13.8 (*s*, C^{4'}, C^{5'}-CH₂-CH₂-CH₃), 14.6 (*d*, $^3J_{P,C}$ = 3.55 Hz, N-CH₂-CH₃), 23.1 (2*s*, C^{4'}, C^{5'}-CH₂-CH₂-CH₃), 30.9 (2*s*, C^{4'}, C^{5'}-CH₂-CH₂-CH₃), 44.5 (*d*, $^2J_{P,C}$ = 15.30 Hz, N-CH₂-CH₃), 109.7 and 109.8 (*s*, C², C^{2'}), 126 (*d*, $^2J_{P,C}$ = 32.24 Hz, C⁵), 128.8 and 129 (*s*, C^{4'} and C^{5'}), 136.3 (*d*, $^1J_{P,C}$ = 40.59 Hz, C⁴).

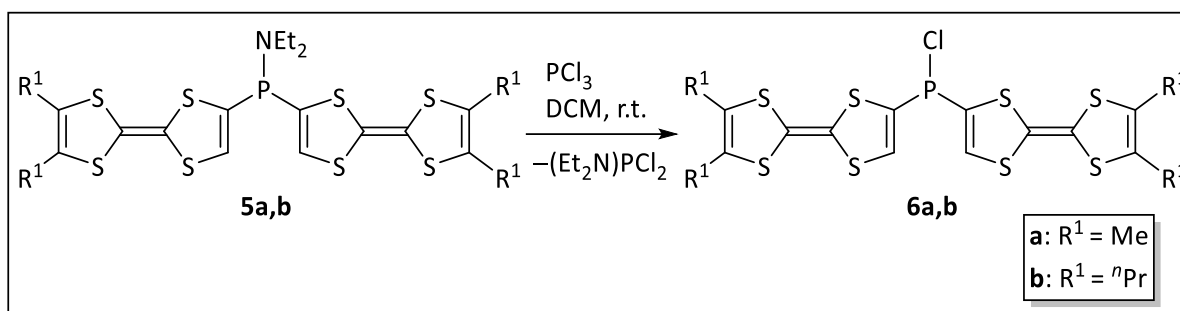
³¹P{¹H} NMR (202.5 MHz, CDCl₃): δ = 42.1 (*s*).

³¹P NMR (202.5 MHz, CDCl₃): δ = 42.1 (*m*).

MS (EI, 70 eV): m/z (%) = 709.0 (4) $[M+O_2]^+$, 677.0 (8) $[M]^+$, 491.9 (6) $[M-C_9H_{14}S_2+H]^+$, 288.0 (22) $[^nPr_2TTF]^+$, 187.0 (76) $[C_9H_{14}S_2+H]^+$.

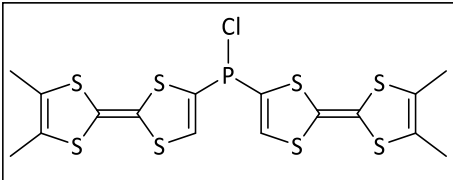
HR-MS (EI, 70 eV): Calculated: 677.0664, Found: 677.0647 (standard deviation: 0.35 ppm).

8.5 Synthesis of Bis(tetrathiafulvalenyl)chlorophosphanes 6a,b



5a,b were each dissolved in dry DCM in a Schlenk tube then PCl_3 (1.2 eq to 1.5 eq) was added dropwise, and the reaction mixture was stirred for 3 h. Then the reaction mixture was concentrated in *vacuo* (8×10^{-3} mbar) and the residue was dissolved in dry Toluene (**6a**) or diethylether (**6b**). The solution was filtered, concentrated and dried in *vacuo* (8×10^{-3} mbar).

8.5.1 Bis[2-(4,5-dimethyl-1,3-dithiol-2-ylidene)-1,3-dithiol-4-yl]chlorophosphane (6a)

	Amount (gr or mL)	mmol	
	5a	50 mg	0.09
	PCl₃	0.01 mL	0.11
	DCM	3 mL	

Reaction code: SHK-504

Appearance: Red sticky solid **Yield:** 34 mg (0.06 mmol, 71%) **Melting point:** 124 °C

Elemental composition: $C_{16}H_{14}ClPS_8$ **Molecular weight:** 529.19 g/mol

NMR code: 29p5a036.22

^1H NMR (500.1 MHz, CDCl_3): δ = 1.94 and 1.95 (2s(br), 12H, $\text{C}^{4'}$, $\text{C}^{5'}$ -Me), 6.92 (d, 2H, $^3J_{\text{P,H}}$ = 11.18 Hz, C^5 -H).

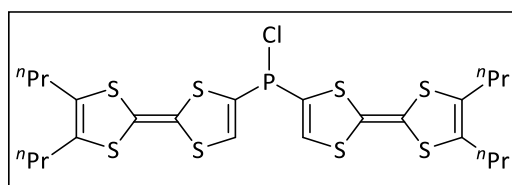
^{13}C NMR (125.8 MHz, CDCl_3): δ = 13.8 and 13.9 (s, $\text{C}^{4'}$, $\text{C}^{5'}$ -Me), 107.9 and 112.8 (s, C^2, C^2'), 122.8 and 123.3 (s, $\text{C}^{4'}$ and $\text{C}^{5'}$), 132.7 (d, $^2J_{\text{P,C}}$ = 51.23 Hz, C^5), 133.6 (d, $^1J_{\text{P,C}}$ = 54.61 Hz, C^4).

$^{31}\text{P}\{^1\text{H}\}$ NMR (202.5 MHz, CDCl_3): δ = 48.6 (s).

^{31}P NMR (202.5 MHz, CDCl_3): δ = 48.6 (t, $^3J_{\text{P,H}}$ = 11.32 Hz).

MS (LIFDI): m/z (%) = 527.9 (100) $[\text{M}]^+$, 985.1 (100) $[2\text{M}-2\text{Cl}]^+$.

8.5.2 Bis[2-(4,5-di-n-propyl-1,3-dithiol-2-ylidene)-1,3-dithiol-4-yl]chlorophosphane (6b)



	Amount (gr or mL)	mmol
5b	74 mg	0.11
PCl_3	0.015 mL	0.17
DCM	5 mL	

Reaction code: SHK-505

Appearance: Red oil of the raw product (content of **5b**: 80%)

Elemental composition: $\text{C}_{24}\text{H}_{30}\text{ClPS}_8$ Molecular weight: 641.41 g/mol

NMR code: 29p5a006.22

^1H NMR (500.1 MHz, CDCl_3): δ = 0.94 (m, 12H, $\text{C}^{4'}$, $\text{C}^{5'}$ - CH_2 - CH_2 - CH_3), 1.53 (m, 8H, $\text{C}^{4'}$, $\text{C}^{5'}$ - CH_2 - CH_2 - CH_3), 2.33 (m, 8H, $\text{C}^{4'}$, $\text{C}^{5'}$ - CH_2 - CH_2 - CH_3), 6.92 (d, 2H, $^3J_{\text{P,H}}$ = 11.23 Hz, C^5 -H).

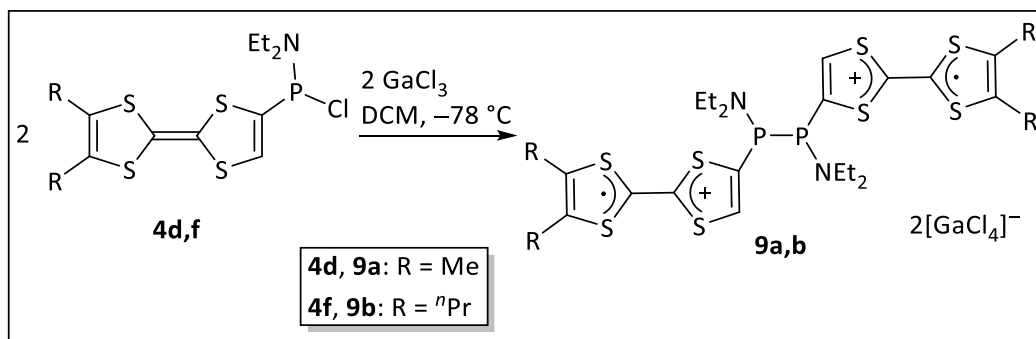
^{13}C NMR (125.8 MHz, CDCl_3): δ = 13.8 (2s, $\text{C}^{4'}$, $\text{C}^{5'}$ - CH_2 - CH_2 - CH_3), 23.1 and 23.2 (s, $\text{C}^{4'}$, $\text{C}^{5'}$ - CH_2 - CH_2 - CH_3), 30.8 and 30.9 (s, $\text{C}^{4'}$, $\text{C}^{5'}$ - CH_2 - CH_2 - CH_3), 107.3 and 113.2 (s, C^2, C^2'), 128.7 and 129.2 (s, $\text{C}^{4'}$ and $\text{C}^{5'}$), 132.8 (d, $^2J_{\text{P,C}}$ = 51.21 Hz, C^5), 133.6 (d, $^1J_{\text{P,C}}$ = 54.67 Hz, C^4).

$^{31}\text{P}\{^1\text{H}\}$ NMR (202.5 MHz, CDCl_3): δ = 48.8 (s).

^{31}P NMR (202.5 MHz, CDCl_3): $\delta = 48.8$ (t, $^3J_{\text{P,H}} = 11.21$ Hz).

MS (LIFDI): m/z (%) = 640.0 (100) $[\text{M}]^+$.

8.6 Chloride abstraction reaction of 4d,f

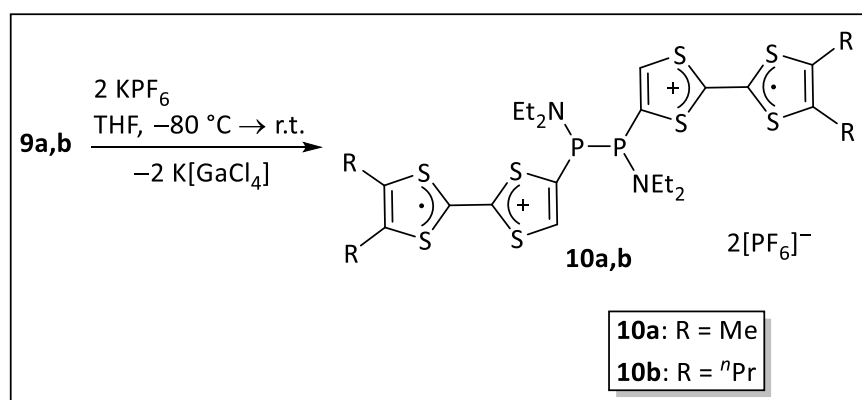


4d,f were dissolved in dry DCM (10 mL) in a Schlenk tube and cooled to $-80\text{ }^\circ\text{C}$. A solution of GaCl_3 (1 eq) in dry DCM (5 mL) was prepared and cooled to $-80\text{ }^\circ\text{C}$, then added dropwise to the solution of starting material and the orange reaction mixtures immediately turned dark red and then dark green; then solvent was removed and the residues were dried in *vacuo* (8×10^{-3} mbar).

Appearance: dark green sticky solid

Reaction code: SHK-511 and SHK-512.

8.7 Anion exchange reaction of 9a,b



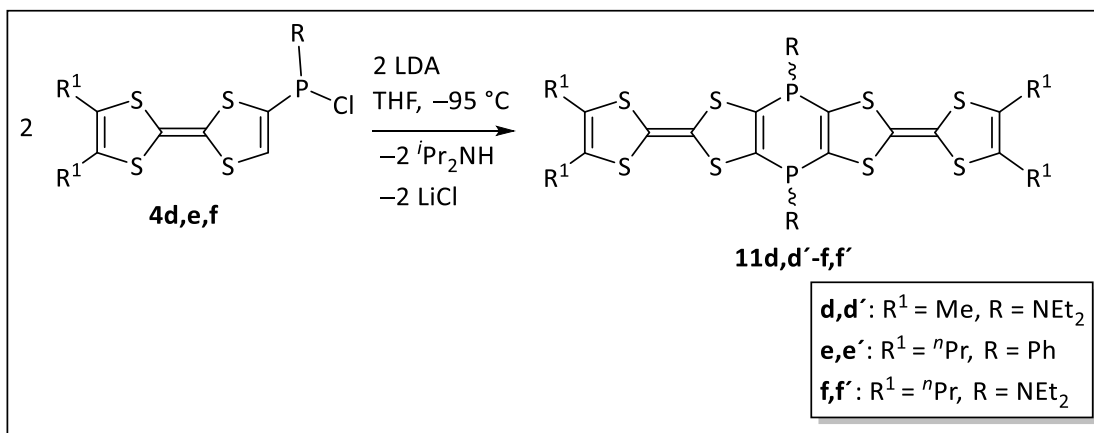
9a,b were dissolved in dry THF (3 mL) in a Schlenk tube and cooled to $-80\text{ }^\circ\text{C}$. A solution of KPF_6 (1 eq) in dry THF (2 mL) was prepared and cooled to $-80\text{ }^\circ\text{C}$, then added dropwise to the solution

of starting material and the reaction mixtures were allowed to warm up slowly and stir overnight. After this time the color of reaction mixtures changed from dark green to orange; then solvent was removed in *vacuo* (8×10^{-3} mbar). Product was extracted from the residues using diethylether (2x15 mL) and dried in *vacuo* (8×10^{-3} mbar).

Appearance: orange sticky solid/oil

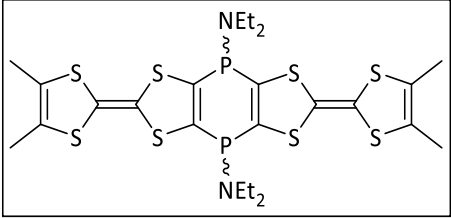
Reaction code: SHK-523 and SHK-524.

8.8 Synthesis of 1,4-bis(diethylamino)-1,4H-1,4-diphosphinines 11d,d'-f,f'



4d,e,f were each dissolved in dry THF and cooled down to $-95 \text{ }^\circ\text{C}$. A solution of LDA (1.1 eq) in dry THF was prepared and cooled down to $-95 \text{ }^\circ\text{C}$, then it was added dropwise to starting material. Then the reaction mixture was allowed to warm up slowly and stirred for 3 hours. After that the solvent was evaporated in *vacuo* (8×10^{-3} mbar). Then the residue was taken up in dry diethylether and filtered, the solution was concentrated and dried in *vacuo* (8×10^{-3} mbar).

8.8.1 2,6-Bis(4,5-dimethyl-1,3-dithiol-2-ylidene)-bis(1,3-dithiole)[2,3-d:5,6-d']-4,8-bis(diethylamino)-4,8H-4,8-diphosphinine (11d,d')

	Amount (gr or mL)	mmol	
	4d	300 mg	0.81
	LDA	95 mg	0.88
	THF	20 mL	

Reaction code: SHK-303

Appearance: Brown powder **Yield:** 162 mg (0.24 mmol, 60%) **Melting point:** 182 °C (decomp.)

Elemental composition: C₂₄H₃₂N₂P₂S₈ **Molecular weight:** 666.96 g/mol

Cis/trans ratio: 0.32:1.

NMR code: 03P5a053.21

¹H NMR (500.1 MHz, CDCl₃): δ = 1.11 and 1.16 (*t*, 12H, ³J_{H,H} = 7.1 Hz, N-CH₂-CH₃), 1.93 (*s*, 12H, C⁴,C⁴-Me), 2.98 and 3.05 (*m*, 8H, N-CH₂-CH₃).

¹³C NMR (125.8 MHz, CDCl₃): δ = 13.9 (*s*, C⁴, C⁵-Me), 14.9 (*br*, N-CH₂-CH₃), 44.8 (*br*, N-CH₂-CH₃), 110.8 and 111 (*s*, C²,C^{2'}), 123.1 and 123.1 (*s*, C⁴ and C⁵), 133.5 and 139 (*m*, C^{2,3,5,6}, central ring).

³¹P{¹H} NMR (202.5 MHz, CDCl₃): δ = 29.4 (*s*), 32.3 (*s*).

³¹P NMR (202.5 MHz, CDCl₃): δ = 29.4 (*m*), 32.3 (*m*).

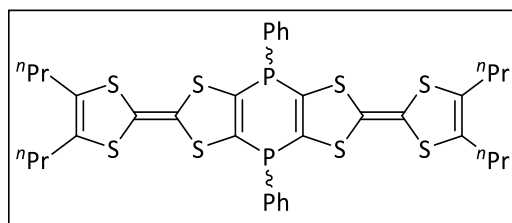
MS (EI, 70 eV): m/z (%) = 698 (8) [M+O₂]⁺, 666 (80) [M]⁺, 521.8 (35) [M-(Et₂N)₂PCI]⁺.

HR-MS (EI, 70 eV): Calculated: 665.9806, Found: 665.9819 (standard deviation: 0.56 ppm).

EA (%): Calculated/Found **C:** 43.22/44.49, **H:** 4.84/5.99, **N:** 4.20/3.09, **S:** 38.45/29.82.

Crystal structure identification code: GSTR689 (structural data can be found in appendix).

8.8.2 2,6-Bis(4,5-dipropyl-1,3-dithiol-2-ylidene)-bis(1,3-dithiole)[2,3-d:5,6-d']-4,8-diphenyl-4,8*H*-4,8-diphosphinine (11e,e')



	Amount (gr or mL)	mmol
4e	278 mg	0.64
LDA	76 mg	0.71
THF	25 mL	

Reaction code: SHK-469

Appearance: Brown powder **Yield:** 251 mg (0.31 mmol, 97%) **Melting point:** 131 °C

Elemental composition: C₃₆H₃₈P₂S₈ **Molecular weight:** 789.13 g/mol

Cis/trans ratio: 0.69:1.

NMR code: 21p5a014

¹H NMR (500.1 MHz, CDCl₃): δ = 0.9 (*m*, 12H, C^{4'}, C^{5'}-CH₂-CH₂-CH₃), 1.46 (*m*, 8H, C^{4'}, C^{5'}-CH₂-CH₂-CH₃), 2.26 (*m*, 8H, C^{4'}, C^{5'}-CH₂-CH₂-CH₃), 7.39-7.73 (*m*, 5H, *para*, *meta*, *ortho* -C₆H₅).

¹³C NMR (125.8 MHz, CDCl₃): δ = 13.7 (*s*, C^{4'}, C^{5'}-CH₂-CH₂-CH₃), 23.1 (*s*, C^{4'}, C^{5'}-CH₂-CH₂-CH₃), 30.8 (*s*, C^{4'}, C^{5'}-CH₂-CH₂-CH₃), 113.6 and 114 (*s*, C², C^{2'}), 128.7-135.1 (*m*, *para*, *meta*, *ortho*, *ipso* -C₆H₅), 134.2 (*m*, C^{2,3,5,6}, central ring).

³¹P{¹H} NMR (202.5 MHz, CDCl₃): δ = -21.9 (*s*), -26.2 (*s*).

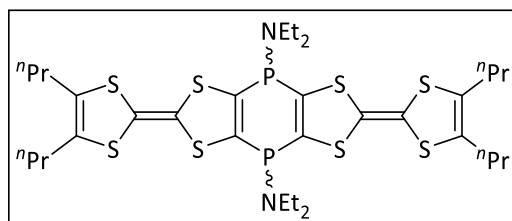
³¹P NMR (202.5 MHz, CDCl₃): δ = -21.9 (*m*), -26.2 (*m*).

MS (EI, 70 eV): *m/z* (%) = 788.2 (5) [M]⁺, 287.0 (32) [ⁿPr₂TTF], 230.1 (80) [DimethylTTF].

HR-MS (EI, 70 eV): Calculated: 788.0214, Found: 788.0220 (standard deviation: 0.26 ppm).

EA (%): Calculated/Found **C:** 54.79/55.50, **H:** 4.85/5.36, **S:** 32.5/31.47.

8.8.3 2,6-Bis(4,5-dipropyl-1,3-dithiol-2-ylidene)-bis(1,3-dithiole)[2,3-d:5,6-d']-4,8-bis(diethylamino)-4,8H-4,8-diphosphinine (11f,f')



	Amount (gr or mL)	mmol
4f	1.37 gr	3.21
LDA	380 mg	3.55
THF	60 mL	

Reaction code: SHK-468

Appearance: Brown powder **Yield:** 1.253 mg (3.21 mmol, 100%) **Melting point:** 118 °C

Elemental composition: C₃₂H₄₈N₂P₂S₈ **Molecular weight:** 779.18 g/mol

Cis/trans ratio: 1:0.89.

NMR code: 20p5a057

¹H NMR (500.1 MHz, CDCl₃): δ = 0.93 (*t*, 12H, ³J_{H,H} = 7.35 Hz, C^{4'}, C^{5'}-CH₂-CH₂-CH₃), 1.12 (*m* (2*t*), 12H, N-CH₂-CH₃), 1.53 (*m*, 8H, C^{4'}, C^{5'}-CH₂-CH₂-CH₃), 2.31 (*m*, 8H, C^{4'}, C^{5'}-CH₂-CH₂-CH₃), 2.99 (*m*, 8H, N-CH₂-CH₃).

¹³C NMR (125.8 MHz, CDCl₃): δ = 13.8 (*s*, C^{4'}, C^{5'}-CH₂-CH₂-CH₃), 14.9 (*s*, N-CH₂-CH₃), 23.1 (2*s*, C^{4'}, C^{5'}-CH₂-CH₂-CH₃), 30.9 (*s*, C^{4'}, C^{5'}-CH₂-CH₂-CH₃), 44.8 (*m* (2*d*), N-CH₂-CH₃), 110.9 and 111.3 (*s*, C², C^{2'}), 129 (2*s*, C^{4'} and C^{5'}), 133.5 and 139.1 (*m*, C^{2,3,5,6}, central ring).

³¹P{¹H} NMR (202.5 MHz, CDCl₃): δ = 29.7 (*s*), 32.5 (*s*).

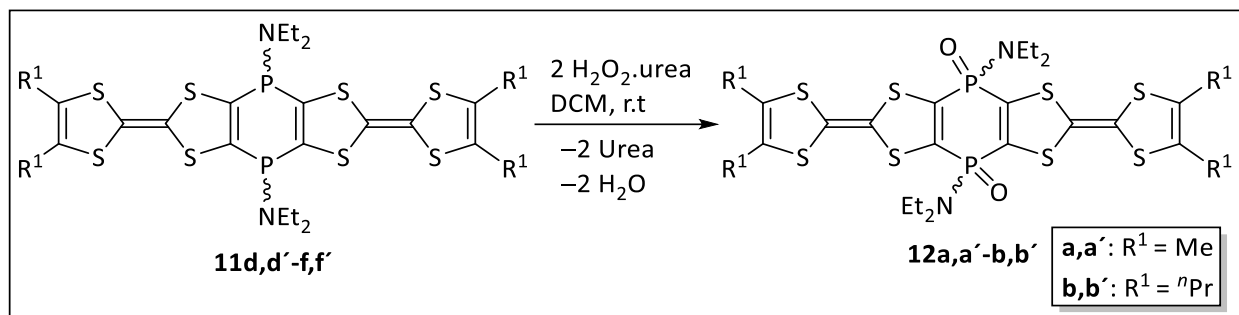
³¹P NMR (202.5 MHz, CDCl₃): δ = 29.7 (*m*), 32.5 (*m*).

MS (EI, 70 eV): m/z (%) = 778.1 (75) [M]⁺, 634.0 (10) [M-2NEt₂]⁺, 230.0 (100) [DimethylTTF].

HR-MS (EI, 70 eV): Calculated: 778.1058, Found: 778.1079 (standard deviation: 0.29 ppm).

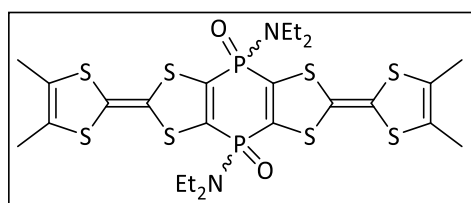
EA (%): Calculated/Found **C:** 49.33/49.46, **H:** 6.21/6.08, **N:** 3.60/3.63, **S:** 32.92/41.50.

8.9 Oxidation of the 1,4-bis(diethylamino)-1,4*H*-1,4-diphosphinines with hydrogen peroxide-urea adduct 12



The hydrogen peroxide-urea adduct was added to a Schlenk tube, containing the starting material, then DCM was added and the reaction mixture was stirred overnight at r.t. After this time, solvent was removed in *vacuo* (8×10^{-3} mbar). The residue was extracted with DCM (2x20 mL) and the solution was concentrated and dried in *vacuo* (8×10^{-3} mbar). In the case of **12a,a'**, the product was washed with n-pentane (2x10 mL) and dried in *vacuo* (8×10^{-3} mbar).

8.9.1 2,6-Bis(4,5-dimethyl-1,3-dithiol-2-ylidene)-bis(1,3-dithiole)[2,3-d:5,6-d']-4,8-bis(diethylamino)-4,8*H*-4,8-dioxide-4,8-diphosphinine (**12a,a'**)



	Amount (gr or mL)	mmol
11d,d'	40 mg	0.06
H₂O₂.urea	14 mg	0.15
DCM	3 mL	

Reaction code: SHK-499

Appearance: Brown powder

Yield: 31 mg (0.044 mmol, 74%)

Melting point: 207 °C

Elemental composition: C₂₄H₃₂N₂O₂P₂S₈

Molecular weight: 698.96 g/mol

Cis/trans ratio: 1:0.3.

NMR code: 26p5a017.22

¹H NMR (500.1 MHz, CDCl₃): δ = 1.17 (*m*(2*t*), 12H, N-CH₂-CH₃), 1.94 (*s*, 12H, C^{4'}, C^{5'}-CH₃), 3.14 (*m*, 8H, N-CH₂-CH₃).

¹³C NMR (125.8 MHz, CDCl₃): δ = 13.8 (*s*, N-CH₂-CH₃), 14.1 (*s*, C^{4'}, C^{5'}-CH₃), 38.2 (*d*, ²*J*_{P,C} = 10.76 Hz, N-CH₂-CH₃), 118.1 and 118.4 (*s*, C², C^{2'}), 123.1 and 123.2 (*s*, C^{4'} and C^{5'}), 140.6 (*m*, C^{2,3,5,6}, central ring).

³¹P{¹H} NMR (202.5 MHz, CDCl₃): δ = -2.1 (*s*), -0.8 (*s*).

³¹P NMR (202.5 MHz, CDCl₃): δ = -2.1 (*m*), -0.8 (*m*).

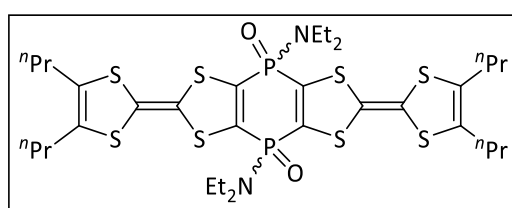
MS (ESI-pos): *m/z* (%) = 730.967 (30) [M+O₂+H]⁺, 713.965 (76) [M+O]⁺, 697.970 (100) [M]⁺.

HR-MS (ESI-pos): Calculated: 697.9699, Found: 697.9700.

EA (%): Calculated/Found **C:** 41.24/42.31, **H:** 4.61/5.21, **N:** 4.01/4.37, **S:** 36.96/35.30.

Crystal structure identification code: GSTR782 (structural data can be found in appendix).

8.9.2 2,6-Bis(4,5-dipropyl-1,3-dithiol-2-ylidene)-bis(1,3-dithiole)[2,3-d:5,6-d']-4,8-bis(diethylamino)-4,8H-4,8-dioxide-4,8-diphosphinine (12b,b')



	Amount (gr or mL)	Mmol
11f,f'	47 mg	0.06
H₂O₂.urea	13 mg	0.14
DCM	3 mL	

Reaction code: SHK-475

Appearance: Brown powder **Yield:** 42 mg (0.052 mmol, 86%) **Melting point:** 151 °C

Elemental composition: C₃₂H₄₈N₂O₂P₂S₈ **Molecular weight:** 811.18 g/mol

Cis/trans ratio: 1:0.67.

NMR code: 26p5a029.22

^1H NMR (500.1 MHz, CDCl_3): δ = 0.93 (2t, 12H, $^3J_{\text{H,H}} = 7.34$ Hz, $\text{C}^{4'}$, $\text{C}^{5'}$ - CH_2 - CH_2 - CH_3), 1.18 (m(2t), 12H, N- CH_2 - CH_3), 1.52 (m, 8H, $\text{C}^{4'}$, $\text{C}^{5'}$ - CH_2 - CH_2 - CH_3), 2.32 (m, 8H, $\text{C}^{4'}$, $\text{C}^{5'}$ - CH_2 - CH_2 - CH_3), 3.15 (m, 8H, N- CH_2 - CH_3).

^{13}C NMR (125.8 MHz, CDCl_3): δ = 13.7 (s, $\text{C}^{4'}$, $\text{C}^{5'}$ - CH_2 - CH_2 - CH_3), 14.1 (s, N- CH_2 - CH_3), 23.1 (s, $\text{C}^{4'}$, $\text{C}^{5'}$ - CH_2 - CH_2 - CH_3), 30.8 (s, $\text{C}^{4'}$, $\text{C}^{5'}$ - CH_2 - CH_2 - CH_3), 38.2 (m, N- CH_2 - CH_3), 118.3 and 118.9 (s, C^2 , C^2'), 129.1 (s, $\text{C}^{4'}$ and $\text{C}^{5'}$), 140.6 (m, $\text{C}^{2,3,5,6}$, central ring).

$^{31}\text{P}\{^1\text{H}\}$ NMR (202.5 MHz, CDCl_3): δ = -2.1 (s), -0.7 (s).

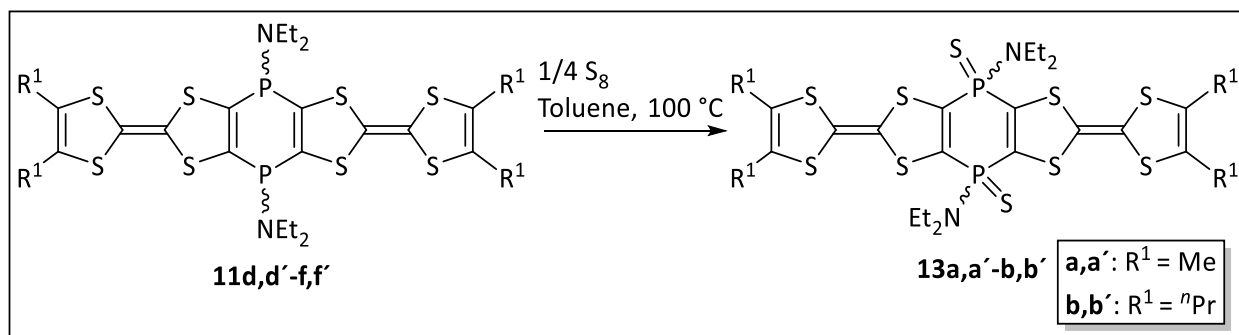
^{31}P NMR (202.5 MHz, CDCl_3): δ = -2.2 (m), -0.7 (m).

MS (ESI-pos): m/z (%) = 843.092 (29) $[\text{M}+\text{O}_2+\text{H}]^+$, 826.090 (65) $[\text{M}+\text{O}]^+$, 810.095 (100) $[\text{M}]^+$.

HR-MS (ESI-pos): Calculated: 810.0951, Found: 810.0953.

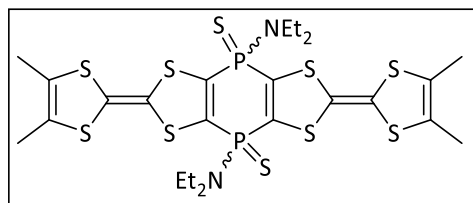
EA (%): Calculated/Found C: 47.38/47.68, H: 5.96/6.35, N: 3.45/4.09, S: 31.62/28.70.

8.10 Oxidation of the 1,4-bis(diethylamino)-1,4H-1,4-diphosphinines with elemental sulfur 13



Elemental sulfur was added to a Schlenk tube, containing the starting material, then toluene was added and the reaction mixture was stirred for 3 hours at 100 °C. After this time, solvent was removed in *vacuo* (8×10^{-3} mbar). The residue was extracted with DCM (2x20 mL) and the solution was concentrated and dried in *vacuo* (8×10^{-3} mbar). In the case of **13a,a'**, the product was washed with n-Pentane (2x10 mL) and dried in *vacuo* (8×10^{-3} mbar).

8.10.12,6-Bis(4,5-dimethyl-1,3-dithiol-2-ylidene)-bis(1,3-dithiole)[2,3-d:5,6-d']-4,8-bis(diethylamino)-4,8H-4,8-diphosphinine-4,8-disulfide (13a,a')



	Amount (gr or mL)	mmol
11d,d'	40 mg	0.06
S₈	6 mg	0.02
Toluene	3 mL	

Reaction code: SHK-497

Appearance: Brown powder **Yield:** 26 mg (0.035 mmol, 58%) **Melting point:** 238 °C

Elemental composition: C₂₄H₃₂N₂P₂S₁₀ **Molecular weight:** 731.08 g/mol

Cis/trans ratio: 0.79:1.

NMR code: 26p5a030.22

¹H NMR (500.1 MHz, CDCl₃): δ = 1.17 (*m*, 12H, N-CH₂-CH₃), 1.94 (*s*, 12H, C^{4'}, C^{5'}-CH₃), 3.27 (*m*, 8H, N-CH₂-CH₃).

¹³C NMR (125.8 MHz, CDCl₃): δ = 13.8 (*s*, N-CH₂-CH₃), 14.2 (*s*, C^{4'}, C^{5'}-CH₃), 39.3 (*s*, N-CH₂-CH₃), 117.7 (*2s*, C², C^{2'}), 123.2 (*2s*, C^{4'} and C^{5'}), 139.8 (*m*, C^{2,3,5,6}, central ring).

³¹P{¹H} NMR (202.5 MHz, CDCl₃): δ = 25.2 (*2s*).

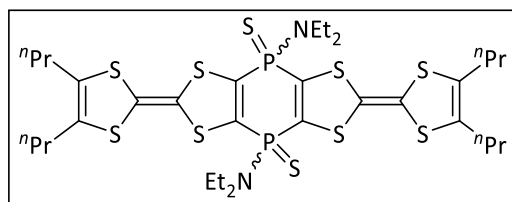
³¹P NMR (202.5 MHz, CDCl₃): δ = 25.2 (*m*).

MS (ESI-pos): *m/z* (%) = 762.921 (10) [M+O₂+H]⁺, 745.919 (48) [M+O]⁺, 729.924 (100) [M]⁺.

HR-MS (ESI-pos): Calculated: 729.9242, Found: 729.9243.

EA (%): Calculated/Found **C:** 39.43/38.48, **H:** 4.41/4.83, **N:** 3.83/3.15, **S:** 43.85/41.68.

8.10.22,6-Bis(4,5-dipropyl-1,3-dithiol-2-ylidene)-bis(1,3-dithiole)[2,3-d:5,6-d']-4,8-bis(diethylamino)-4,8H-4,8-diphosphinine-4,8-disulfide (13b,b')



	Amount (gr or mL)	mmol
11f,f'	47 mg	0.06
S₈	4 mg	0.015
Toluene	3 mL	

Reaction code: SHK-473

Appearance: Brown powder **Yield:** 41 mg (0.049 mmol, 81%) **Melting point:** 183 °C

Elemental composition: C₃₂H₄₈N₂P₂S₁₀ **Molecular weight:** 843.30 g/mol

Cis/trans ratio: 1:0.8.

NMR code: 21p5a042.22

¹H NMR (500.1 MHz, CDCl₃): δ = 0.93 (*t*, 12H, ³J_{H,H} = 7.40 Hz, C^{4'}, C^{5'}-CH₂-CH₂-CH₃), 1.16 and 1.19 (*t*, 12H, ³J_{H,H} = 7.1 Hz, N-CH₂-CH₃), 1.52 (*m*, 8H, C^{4'}, C^{5'}-CH₂-CH₂-CH₃), 2.32 (*m*, 8H, C^{4'}, C^{5'}-CH₂-CH₂-CH₃), 3.27 (*m*, 8H, N-CH₂-CH₃).

¹³C NMR (125.8 MHz, CDCl₃): δ = 13.7 (*s*, C^{4'}, C^{5'}-CH₂-CH₂-CH₃), 14.2 (*s*, N-CH₂-CH₃), 23.1 (*2s*, C^{4'}, C^{5'}-CH₂-CH₂-CH₃), 30.8 (*s*, C^{4'}, C^{5'}-CH₂-CH₂-CH₃), 39.4 (*s*, N-CH₂-CH₃), 117.6 and 117.9 (*s*, C², C^{2'}), 129.1 (*s*, C^{4'} and C^{5'}), 139.9 (*m*, C^{2,3,5,6}, central ring).

³¹P{¹H} NMR (202.5 MHz, CDCl₃): δ = 25.2 (*s*), 25.4 (*s*).

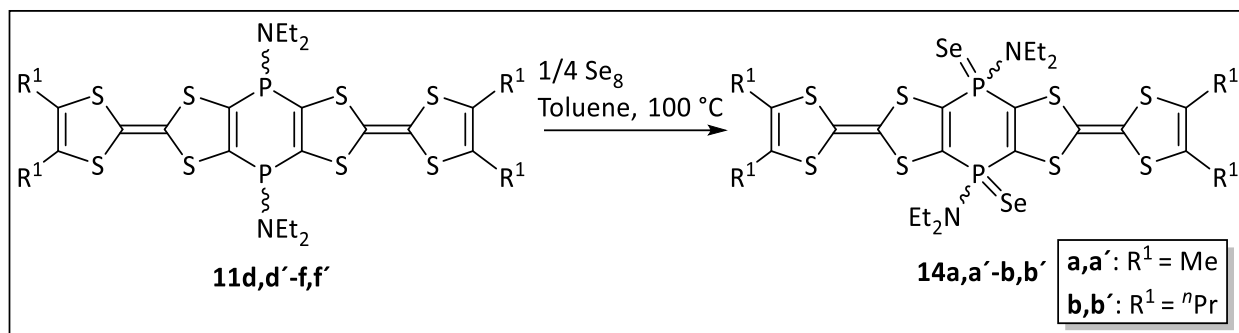
³¹P NMR (202.5 MHz, CDCl₃): δ = 25.3 (*m*).

MS (ESI-pos): *m/z* (%) = 875.046 (15) [M+O₂+H]⁺, 858.044 (51) [M+O]⁺, 842.049 (100) [M]⁺.

HR-MS (ESI-pos): Calculated: 842.0494, Found: 842.0491.

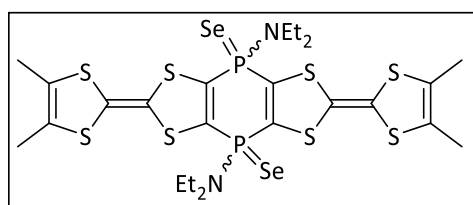
EA (%): Calculated/Found **C:** 45.58/43.85, **H:** 5.74/5.72, **N:** 3.33/3.07, **S:** 38.02/40.80.

8.11 Oxidation of the 1,4-bis(diethylamino)-1,4*H*-1,4-diphosphinines with elemental selenium 14



Selenium was added to a Schlenk tube, containing the starting material, then toluene was added and the reaction mixture was stirred for 3 hours at 100 °C. After this time, solvent was removed in *vacuo* (8×10^{-3} mbar). The residue was extracted with DCM (2x20 mL) and the solution was concentrated and dried in *vacuo* (8×10^{-3} mbar). In the case of **14a,a'**, the product was washed with n-Pentane (2x10 mL) and dried in *vacuo* (8×10^{-3} mbar).

8.11.12,6-Bis(4,5-dimethyl-1,3-dithiol-2-ylidene)-bis(1,3-dithiole)[2,3-d:5,6-d']-4,8-bis(diethylamino)-4,8*H*-4,8-diphosphinine-4,8-diselenide (**14a,a'**)



	Amount (gr or mL)	mmol
11d,d'	40 mg	0.06
Se₈	13 mg	0.02
Toluene	3 mL	

Reaction code: SHK-498

Appearance: Brown powder **Yield:** 30 mg (0.036 mmol, 61%) **Melting point:** 264 °C (decomp.)

Elemental composition: C₂₄H₃₂N₂P₂S₈Se₂ **Molecular weight:** 824.91 g/mol

Cis/trans ratio: 1:0.91.

NMR code: 26p5a031.22

¹H NMR (500.1 MHz, CDCl₃): δ = 1.16 and 1.19 (*t*, 12H, ³J_{H,H} = 7.1 Hz, N-CH₂-CH₃), 1.94 (*s*, 12H, C^{4'}, C^{5'}-CH₃), 3.32 (*m*, 8H, N-CH₂-CH₃).

¹³C NMR (125.8 MHz, CDCl₃): δ = 13.8 (*s*, N-CH₂-CH₃), 14.2 (*s*, C^{4'}, C^{5'}-CH₃), 40.2 (*d*, ²J_{P,C} = 16.72 Hz, N-CH₂-CH₃), 117.8 (*s*, C², C^{2'}), 123.2 (*2s*, C^{4'} and C^{5'}), 138.5 (*m*, C^{2,3,5,6}, central ring).

³¹P{¹H} NMR (202.5 MHz, CDCl₃): δ = 15.7 (*s*_{sat}, ¹J_{P,Se} = 816 Hz), 15.8 (*s*_{sat}, ¹J_{P,Se} = 804 Hz).

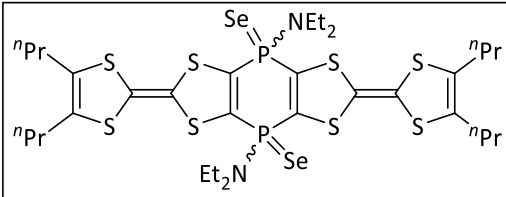
³¹P NMR (202.5 MHz, CDCl₃): δ = 15.7 (*m*).

MS (ESI-pos): m/z (%) = 841.807 (27) [M+O]⁺, 825.812 (100) [M]⁺.

HR-MS (ESI-pos): Calculated: 825.8127, Found: 825.8127.

EA (%): Calculated/Found C: 34.95/37.67, H: 3.91/4.52, N: 3.40/3.08, S: 31.09/30.18.

8.11.22,6-Bis(4,5-dipropyl-1,3-dithiol-2-ylidene)-bis(1,3-dithiole)[2,3-d:5,6-d']-4,8-bis(diethylamino)-4,8H-4,8-diphosphinine-4,8-diselenide (14b,b')

	Amount (gr or mL)	mmol
		
11f,f'	47 mg	0.06
Se₈	10 mg	0.016
Toluene	3 mL	

Reaction code: SHK-474

Appearance: Brown powder **Yield:** 52 mg (0.055 mmol, 92%) **Melting point:** 209 °C

Elemental composition: C₃₂H₄₈N₂P₂S₈Se₂ **Molecular weight:** 937.12 g/mol

Cis/trans ratio: 1:0.85.

NMR code: 21p5a043.22

^1H NMR (500.1 MHz, CDCl_3): δ = 0.93 (*t*, 12H, $^3J_{\text{H,H}}$ = 7.34 Hz, C^4 , $\text{C}^{5'}$ - CH_2 - CH_2 - CH_3), 1.16 and 1.19 (*t*, 12H, $^3J_{\text{H,H}}$ = 7.1 Hz, N-CH_2 - CH_3), 1.52 (*h*, 8H, $^3J_{\text{H,H}}$ = 7.41 Hz, C^4 , $\text{C}^{5'}$ - CH_2 - CH_2 - CH_3), 2.32 (*m*, 8H, C^4 , $\text{C}^{5'}$ - CH_2 - CH_2 - CH_3), 3.33 (*m*, 8H, N-CH_2 - CH_3).

^{13}C NMR (125.8 MHz, CDCl_3): δ = 13.7 (*s*, C^4 , $\text{C}^{5'}$ - CH_2 - CH_2 - CH_3), 14.2 (*d*, $^3J_{\text{P,C}}$ = 3.59 Hz, N-CH_2 - CH_3), 23.1 (*s*, C^4 , $\text{C}^{5'}$ - CH_2 - CH_2 - CH_3), 30.8 (*s*, C^4 , $\text{C}^{5'}$ - CH_2 - CH_2 - CH_3), 40.2 (*d*, $^2J_{\text{P,C}}$ = 21.51 Hz, N-CH_2 - CH_3), 117.7 and 117.9 (*s*, $\text{C}^2, \text{C}^{2'}$), 129.1 (*s*, C^4 and $\text{C}^{5'}$), 138.5 (*m*, $\text{C}^{2,3,5,6}$, central ring).

$^{31}\text{P}\{^1\text{H}\}$ NMR (202.5 MHz, CDCl_3): δ = 15.7 (*s*_{sat}, $^1J_{\text{P,Se}}$ = 804 Hz), 15.9 (*s*_{sat}, $^1J_{\text{P,Se}}$ = 812 Hz).

^{31}P NMR (202.5 MHz, CDCl_3): δ = 15.7 (*m*), 15.9 (*m*).

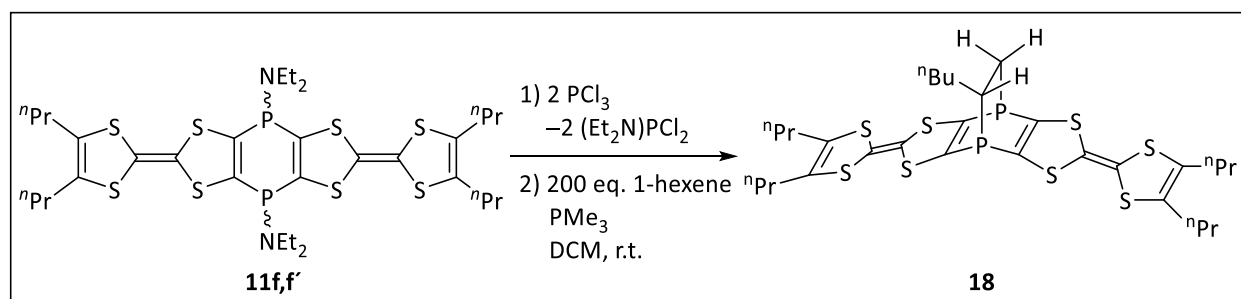
MS (ESI-pos): *m/z* (%) = 970.936 (18) [$\text{M}+\text{O}_2+\text{H}$]⁺, 953.934 (33) [$\text{M}+\text{O}$]⁺, 937.938 (100) [M]⁺.

HR-MS (ESI-pos): Calculated: 937.9381, Found: 937.9384.

EA (%): Calculated/Found C: 41.01/41.88, H: 5.16/5.45, N: 2.99/2.96, S: 27.37/26.23.

Crystal structure identification code: GSTR783 (structural data can be found in appendix).

8.12 Synthesis of 10-butyl-2,6-bis(4,5-dipropyl-1,3-dithiol-2-ylidene)-4,8-ethano[1,4]diphosphinino[2,3-d:5,6-d']bis([1,3]dithiole) 18



The starting material **11f,f'** was dissolved in dry DCM (10 mL), then PCl_3 (2.5 eq) was slowly added and the reaction mixture was stirred for 3 hours at r.t. After this time, all volatiles were evaporated in *vacuo* (8×10^{-3} mbar) and the residue was dissolved in dry DCM (5 mL). Then first 1-hexene (200 eq) and after that PMe_3 (1.3 eq) were added to the reaction mixture and it was stirred for 3 days. After that, all volatiles were evaporated in *vacuo*

(8×10^{-3} mbar). Then the product was extracted from the residue using dry n-Pentane (3x30 mL) and the solution was concentrated and dried in *vacuo* (8×10^{-3} mbar).

	Amount (gr or mL)	Mmol
11f,f'	177 mg	0.23
PCl₃	0.05 mL	0.57
1-Hexene	6 mL	48
PMe₃	0.03	0.29
DCM	15 mL	

Reactio code: SHK-470

Appearance: Orange-red oily/sticky solid **Yield:** 63 mg (0.088 mmol, 38%)

Elemental composition: C₃₀H₄₀P₂S₈ **Molecular weight:** 719.08 g/mol

Cis/trans ratio: 1:0.93.

NMR code: 21p5a021.22

¹H NMR (500.1 MHz, CDCl₃): δ = 0.89 (*t*, 3H, $^3J_{H,H}$ = 7.31 Hz, P-CH-CH₂-CH₂-CH₂-CH₃), 0.93 (*m*, 12H, C^{4'}, C^{5'}-CH₂-CH₂-CH₃), 1.18-1.46 (*m*, 7H, P-CH-CH₂-CH₂-CH₂-CH₃), 1.52 (*m*, 8H, C^{4'}, C^{5'}-CH₂-CH₂-CH₃), 1.99 (*m*, 2H, P-CH₂), 2.31 (*t*, 8H, $^3J_{H,H}$ = 6.46 Hz, C^{4'}, C^{5'}-CH₂-CH₂-CH₃).

¹³C NMR (125.8 MHz, CDCl₃): δ = 13.8 (*s*, P-CH-CH₂-CH₂-CH₂-CH₃), 14.1 (*s*, C^{4'}, C^{5'}-CH₂-CH₂-CH₃), 22.6 and 22.8 (*s*, P-CH-CH₂-CH₂-CH₂-CH₃), 23.1 (*s*, C^{4'}, C^{5'}-CH₂-CH₂-CH₃), 29.8 (*s*, P-CH-CH₂-CH₂-CH₂-CH₃), 30.8 (*s*, C^{4'}, C^{5'}-CH₂-CH₂-CH₃), 31.3 (*d*, $^1J_{P,C}$ = 15.21 Hz, P-CH-CH₂-CH₂-CH₂-CH₃), 34.9 (*d*, $^1J_{P,C}$ = 17.04 Hz, P-CH₂), 110.9 and 111.9 (*s*, C², C^{2'}), 129 (2*s*, C^{4'} and C^{5'}), 140-143.6 (*m*, C^{2,3,5,6}, central ring).

³¹P{¹H} NMR (202.5 MHz, CDCl₃): δ = -71.7 (*d*, $^3J_{P,P}$ = 32.3 Hz), -67.70 (*d*, $^3J_{P,P}$ = 32.3 Hz).

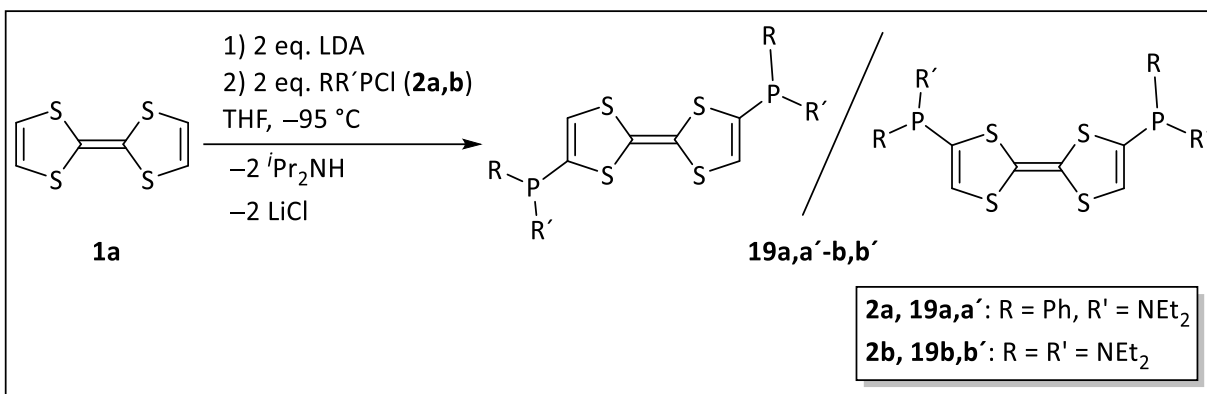
³¹P NMR (202.5 MHz, CDCl₃): δ = -71.7 (*dt*, $^3J_{P,P}$ = 32.3 Hz and $^2J_{P,H}$ = 8.14), -67.70 (*m*).

MS (ESI-pos): *m/z* (%) = 734.030 (3) [M+O]⁺, 718.036 (16) [M]⁺, 633.942 (3) [M-C₆H₁₂]⁺.

HR-MS (ESI-pos): Calculated: 718.0365, Found: 718.0363.

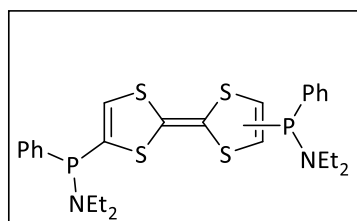
EA (%): Calculated/Found C: 50.11/53.77, H: 5.61/6.30, S: 35.67/39.76.

8.13 Synthesis of doubly-phosphanylated tetrathiafulvalenes 19



TTF was dissolved in dry THF in a Schlenk flask and cooled to -95 °C. A solution of LDA (2.2 eq) in dry THF was prepared and cooled to -95 °C, then added dropwise to the TTF solution and the reaction mixture was stirred for 2 hours. During this time temperature was kept between -95 °C and -80 °C. Then RR'PCI (2.2 eq) was added dropwise (T = -95 °C) and the reaction mixture was warmed slowly and stirred for 3 hours. Then the solution was concentrated in vacuo (8×10^{-3} mbar) and the residue was taken up in dry dichloromethane and filtered over a 3G-frit having a celite® pad and silica gel to remove the formed lithium chloride. The filtrate was collected and the solvent was removed in vacuo (8×10^{-3} mbar) and then dried.

8.13.1 Bis(diethylamino(phenyl)phosphanyl)-2,2'-bis(1,3-dithiolyliene) (19a,a')



	Amount (gr or mL)	mmol
1a	250 mg	1.22
LDA	288 mg	2.69
Et₂N(Ph)PCI	0.52 mL	2.71
THF	40 mL	
DCM	120 mL	

Reaction code: SHK-433

Appearance: Orange oily/sticky solid **Yield:** 400 mg (0.71 mmol, 58%)

Elemental composition: C₂₆H₃₂N₂P₂S₄ **Molecular weight:** 562.74 g/mol

Pseudo-E/Z ratio: 1:1.

NMR code: 13p5a007.22

¹H NMR (500.1 MHz, CDCl₃): δ = 1.08 (*m*, 12H, N-CH₂-CH₃), 3.10 (*m*, 8H, N-CH₂-CH₃), 6.61 (*m*, 2H, C⁵-H), 7.37 (*m*, 10H, *para*, *meta*, *ortho* -C₆H₅).

¹³C NMR (125.8 MHz, CDCl₃): δ = 14.6 (*pseudo-t*, ³J_{P,C} = 3 Hz, N-CH₂-CH₃), 44.5 and 44.6 (*2d*, ²J_{P,C} = 14.8 Hz, N-CH₂-CH₃), 112, 112.2 and 112.3 (*s*, C², C^{2'}), 127.5 (*m*, C⁵), 128.5 (*m*, *para*, *meta*-C₆H₅), 130.7 (*2d*, ²J_{P,C} = 18 Hz, *ortho*-C₆H₅), 138.4 (*m*, *ipso*-C₆H₅), 138.8 (*m*, C⁴).

³¹P{¹H} NMR (202.5 MHz, CDCl₃): δ = 52.7 (*s*), 52.8 (*s*), 52.9 (*s*).

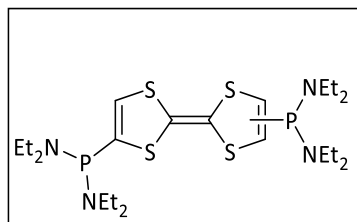
³¹P NMR (202.5 MHz, CDCl₃): δ = 52.9 (*m*).

MS (EI, 70 eV): *m/z* (%) = 562.2 (100) [M]⁺, 491.1 (5) [M-NEt₂]⁺, 383.1 (10) [M-P(NEt₂)Ph+H]⁺, 180.1 (75) [P(NEt₂)Ph]⁺, 109.0 (52) [PPh+H]⁺.

HR-MS (EI, 70 eV): Calculated: 562.0924, Found: 562.0945 (standard deviation: 0.12 ppm).

8.13.2 Bis(bis(diethylamino)phosphanyl)-2,2'-bis(1,3-dithiolylidene) (19b,b')

	Amount (gr or mL)	mmol
1a	250 mg	1.22
LDA	288 mg	2.69
(Et₂N)₂PCI	0.57 mL	2.71
THF	40 mL	
DCM	120 mL	



Reaction code: SHK-432

Appearance: Yellow-orange oily/sticky solid **Yield:** 440 mg (0.8 mmol, 65%)

Elemental composition: C₂₂H₄₂N₄P₂S₄ **Molecular weight:** 552.79 g/mol

Pseudo-*E/Z* ratio: 1:0.8.

NMR code: 13p5a008.22

¹H NMR (500.1 MHz, CDCl₃): δ = 1.07 (*t*, 24H, ³J_{H,H} = 7.06 Hz, N-CH₂-CH₃), 3.10 (*m*, 16H, N-CH₂-CH₃), 6.09 (*2d*, 2H, ³J_{P,H} = 1.79 Hz, C⁵-H).

¹³C NMR (125.8 MHz, CDCl₃): δ = 14.7 (*d*, ³J_{P,C} = 3.14 Hz, N-CH₂-CH₃), 42.9 (*d*, ²J_{P,C} = 17.61 Hz, N-CH₂-CH₃), 112.1 and 112.2 (*2d*, ³J_{P,C} = 2.91 Hz and 3.18 Hz, C²,C^{2'}), 119.4 and 119.7 (*2d*, ²J_{P,C} = 14.35 Hz and 14.45 Hz, C⁵), 140.2 and 140.5 (*2d*, ¹J_{P,C} = 17.96 Hz and 18.04 Hz, C⁴).

³¹P{¹H} NMR (202.5 MHz, CDCl₃): δ = 84.6 (*s*), 84.7 (*s*).

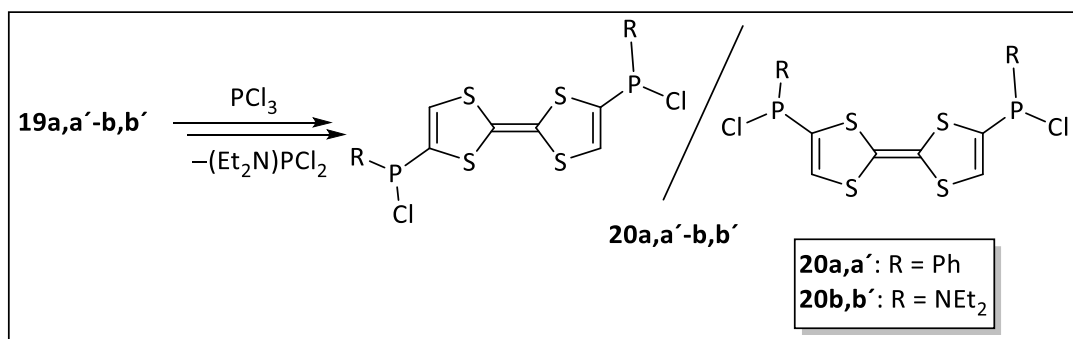
³¹P NMR (202.5 MHz, CDCl₃): δ = 84.7 (*m*).

MS (EI, 70 eV): *m/z* (%) = 552.3 (28) [M]⁺, 378.1 (35) [M-P(NEt₂)₂+H]⁺, 175.2 (100) [P(NEt₂)₂]⁺.

HR-MS (EI, 70 eV): Calculated: 552.1768, Found: 552.1773 (standard deviation: 0.14 ppm).

Crystal structure identification code: GSTR765 (structural data can be found in appendix).

8.14 Synthesis of Bis(chlorophosphanyl)tetrathiafulvalenes 20

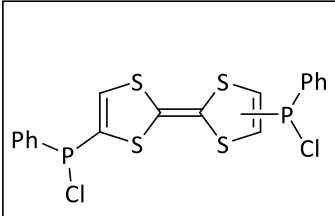


Procedure I: **19a,a'** (pseudo-*E/Z* ratio: 1:1) was dissolved in dry dichloromethane (20 mL) in a Schlenk tube, then PCl₃ (2.15 eq) was added dropwise, and the reaction mixture was stirred for 2 hours at r.t. The reaction mixture was concentrated in *vacuo* (8×10⁻³ mbar), and the

residue was then dissolved in dry diethylether (60 mL). The solution was filtered, concentrated and dried in *vacuo* (8×10^{-3} mbar).

Procedure II: **19b,b'** was dissolved in dry diethylether (15 mL) in a Schlenk tube and cooled to -95 °C, then PCl_3 (2.2 eq) was added dropwise, and the reaction mixture was warmed up slowly and stirred for 1 h. The reaction mixture was concentrated in *vacuo* (8×10^{-3} mbar), and the residue was then dissolved in dry diethylether (50 mL). The solution was filtered, concentrated and dried in *vacuo* (8×10^{-3} mbar).

8.14.1 Bis(chlorophenylphosphanyl)-2,2'-bis(1,3-dithiolylidene) (20a,a')

	Amount (gr or mL)	mmol	
	19a,a'	180 mg	0.32
	PCl₃	0.06 mL	0.69
	DCM	20 mL	
	Et₂O	60 mL	

Reaction code: SHK-461

Appearance: Red oily/sticky solid **Yield:** 169 mg (0.30 mmol, 94%)

Elemental composition: $\text{C}_{18}\text{H}_{12}\text{Cl}_2\text{P}_2\text{S}_4$ **Molecular weight:** 489.38 g/mol

Pseudo-E/Z ratio: 1:1.

NMR code: 27p5a028.22

^1H NMR (500.1 MHz, CDCl_3): δ = 6.28 (s, TTF), 6.93 (2t, 2H, $^3J_{\text{P,H}} = 10.38$ Hz, $\text{C}^5\text{-H}$), 7.46 (m, 6H, *para*, *meta*- C_6H_5), 7.68 (m, 4H, *ortho*- C_6H_5).

^{13}C NMR (125.8 MHz, CDCl_3): δ = 112.1, 112.3 and 112.5 (s, $\text{C}^2, \text{C}^{2'}$), 129 (m, *para*- C_6H_5), 130.7 (m, *meta*- C_6H_5), 130.9 (m, *ortho*- C_6H_5), 131.6 (d, $^2J_{\text{P,C}} = 16.19$ Hz, C^5), 132.1 (m, *ipso*- C_6H_5), 136.8 (m, C^4).

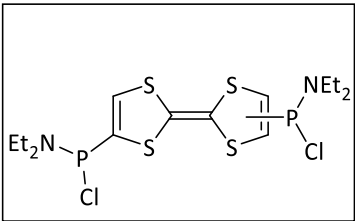
$^{31}\text{P}\{^1\text{H}\}$ NMR (202.5 MHz, CDCl_3): δ = 63.4 (2s), 63.6 (s), 63.7 (s), 63.9 (s).

^{31}P NMR (202.5 MHz, CDCl_3): δ = 63.4 (*m*), 63.6 (*m*)

MS (EI, 70 eV): m/z (%) = 488.0 (100) $[\text{M}]^+$, 346.0 (75) $[\text{M}-\text{PPhCl}+\text{H}]^+$.

HR-MS (EI, 70 eV): Calculated: 487.8674, Found: 487.8668 (standard deviation: 0.39 ppm).

8.14.2 Bis(chloro(diethylamino)phosphanyl)-2,2'-bis(1,3-dithiolylidene) (20b,b')

	Amount (gr or mL)	mmol	
	19b,b'	86 mg	0.15
	PCl_3	0.03 mL	0.34
	Et_2O	65 mL	

Reaction code: SHK-437

Appearance: Orange oily/sticky solid Yield: 70 mg (0.146 mmol, 97%)

Elemental composition: $\text{C}_{14}\text{H}_{22}\text{Cl}_2\text{N}_2\text{P}_2\text{S}_4$ Molecular weight: 479.43 g/mol

NMR code: 13p5a044.22

^1H NMR (500.1 MHz, CDCl_3): δ = 1.16 and 1.46 (*t*, 12H, $^3J_{\text{H,H}} = 7.17$ Hz and 7.29 Hz, N- CH_2 -CH₃), 3.18 (*m*, 8H, N-CH₂-CH₃), 6.72 and 6.73 (*d*, 2H, $^3J_{\text{P,H}} = 2.5$ Hz and 2.46 Hz, C^5 -H).

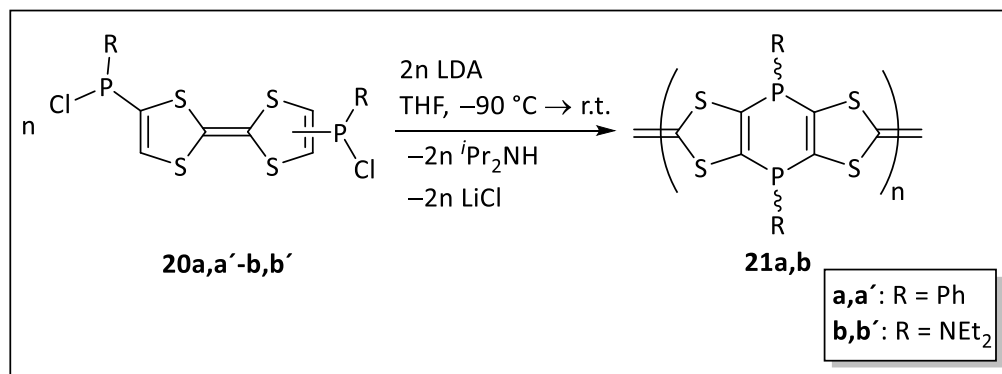
^{13}C NMR (125.8 MHz, CDCl_3): δ = 11.4 (*s*, N- CH_2 -CH₃), 14.1 (*d*, $^3J_{\text{P,C}} = 6.18$ Hz, N- CH_2 -CH₃), 42.3 (*s*, N-CH₂-CH₃), 43.9 (*d*, $^2J_{\text{P,C}} = 14.7$ Hz, N-CH₂-CH₃), 112.5 (*m*, $\text{C}^2, \text{C}^{2'}$), 126.3 (*m*, C^5), 137 (*m*, C^4).

$^{31}\text{P}\{^1\text{H}\}$ NMR (202.5 MHz, CDCl_3): δ = 117.6 (*s*), 117.7 (*s*).

^{31}P NMR (202.5 MHz, CDCl_3): δ = 117.6 (*m*).

MS (LIFDI): m/z (%) = 477.9 (100) $[\text{M}]^+$.

8.15 Synthesis of a mixture of oligomeric products containing TTF units via ring-closing reaction 21a,b

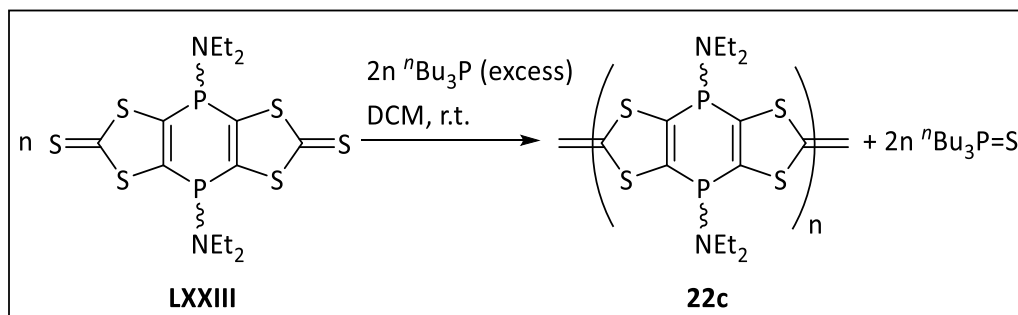


20a,a'-b,b' were dissolved in dry THF (10 mL) in a Schlenk tube and cooled to -90 °C. A solution of LDA (2.2 eq) in dry THF (5 mL) was prepared and cooled to -90 °C, then added dropwise to the solution of starting material and the reaction mixture was allowed to warm up slowly and stirred overnight. After this time, solvent was removed using a filter canula and the precipitate was washed using THF (3x15 mL), n-pentane (2x10 mL) and DCM (2x10 mL) and then dried in *vacuo* (8×10^{-3} mbar).

Appearance: Brown powder

Reaction code: SHK-439 and SHK-440.

8.16 Synthesis of a mixture of oligomeric products containing TTF units via desulfurization 22c



The starting material **LXXIII** (105 mg) was dissolved in dry DCM (10 mL) in a Schlenk tube and then ⁿBu₃P (2.2 eq) was added and the reaction mixture was stirred overnight. After removal of

all volatiles in *vacuo* (8×10^{-3} mbar) the residue was washed with Petroleum ether 40/65 (2x25mL) and then dried in *vacuo* (8×10^{-3} mbar).

Reaction code: SHK-368

Appearance: Red powder

NMR code: 39p5a041.22

^{31}P NMR (202.5 MHz, CD_2Cl_2): $\delta = 24.9\text{--}38.8$.

MS (MALDI): $m/z = 1219.0$ ($n = 3$), 1625.0 ($n = 4$), 2031.0 ($n = 5$).¹⁰⁹

References

- (1) Wudl, F.; Smith, G. M.; Hufnagel, E. J. *J. Chem. Soc. D Chem. Commun.* **1970**, 1453–1454.
- (2) Hurlley, W. R. H.; Smiles, S. *J. Chem. Soc.* **1926**, 129, 2263–2270.
- (3) Prinzbach, H.; Berger, H.; Lüttringhaus, A. *Angew. Chem. Int. Ed. Engl.* **1965**, 4, 435.
- (4) Wudl, F.; Wobschall, D.; Hufnagel, E. J. *J. Am. Chem. Soc.* **1972**, 94, 670–672.
- (5) Coleman, L. B.; Cohen, M. J.; Sandman, D. J.; Yamagishi, F. G.; Garito, A. F.; Heeger, A. J. *Solid State Commun.* **1973**, 12, 1125–1132.
- (6) Ferraris, J.; Cowan, D. O.; Walatka, V.; Perlstein, J. H. *J. Am. Chem. Soc.* **1973**, 95, 948–949.
- (7) Bryce, M. R. *Adv. Mater.* **1999**, 11, 11–23.
- (8) Segura, J. L.; Martín, N. *Angew. Chem. Int. Ed.* **2001**, 40, 1372–1409.
- (9) Hüchel, E. *Verlag Chem.* **1938**, 77–85.
- (10) Hargittai, I.; Brunvoll, J.; Kolonits, M.; Khodorkovsky, V. *J. Mol. Struct.* **1994**, 317, 273–277.
- (11) Katan, C. J. *Phys. Chem. A* **1999**, 103, 1407–1413.
- (12) Fourmigué, M.; Batail, P. *J. Chem. Soc., Chem. Commun.* **1991**, 1370–1372.
- (13) Fourmigué, M.; Batail, P. *Bull. Soc. Chim. Fr.* **1992**, 129, 29–36.
- (14) Gerson, F.; Lamprecht, A.; Fourmigué, M. *J. Chem. Soc., Perkin Trans. 2* **1996**, 1409–1414.
- (15) Yuan, M.; Ülgüt, B.; McGuire, M.; Takada, K.; DiSalvo, F. J.; Lee, S.; Abruña, H. *Chem. Mater.* **2006**, 18, 4296–4306.
- (16) Fourmigué, M.; Uzelmeier, C. E.; Boubekour, K.; Bartley, S. L.; Dunbar, K. R. *J. Organomet. Chem.* **1997**, 529, 343–350.
- (17) Delhaes, P. *Mol. Cryst. Liq. Cryst.* **1983**, 96, 229–262.
- (18) Cowan, D. O.; Kini, A.; Chiang, L.-Y.; Lerstrup, K.; Talham, D. R.; Poehler, T. O.; Bloch, A. N. *Mol. Cryst. Liq. Cryst.* **1982**, 86, 1–26.
- (19) Saito, G.; Ferraris, J. P. *Bull. Chem. Soc. Jpn.* **1980**, 53, 2141–2145.
- (20) Torrance, J. B. *Acc. Chem. Res.* **1979**, 12, 79–86.
- (21) Becker, J. Y.; Bernstein, J.; Ellern, A.; Gershtenman, H.; Khodorkovsky, V. *J. Mater. Chem.* **1995**, 5, 1557–1558.
- (22) Otsubo, T.; Aso, Y.; Takimiya, K. *Adv. Mater.* **1996**, 8, 203–211.
- (23) Iyoda, M.; Hasegawa, M.; Miyake, Y. *Chem. rev.* **2004**, 104, 5085–5114.
- (24) Izuoka, A.; Reijikumai; Tachikawa, T.; Sugawara, T. *Mol. Cryst. Liq. Cryst.* **1992**, 218, 213–218.

- (25) Bechgaard, K.; Lerstrup, K.; Jørgensen, M.; Johannsen, I.; Christensen, J.; Larsen, J. *Mol. Cryst. Liq. Cryst.* **1990**, *181*, 161–169.
- (26) Ferraro, J. R.; Williams, J. M. *Introduction to synthetic electrical conductors.*; Academic Press, San Diego, **1987**.
- (27) Kato, H.; Kobayashi, T. *Adv. Mater.* **1993**, *5*, 750–751.
- (28) Bryce, M. R.; Cooke, G.; Dhindsa, A. S.; Ando, D. J.; Hursthouse, M. B. *Tetrahedron Lett.* **1992**, *33*, 1783–1786.
- (29) Becker, J. Y.; Bernstein, J.; Bittner, S.; Sarma, J. A.; Shahal, L. *Tetrahedron Lett.* **1988**, *29*, 6177–6180.
- (30) Fourmigue, M.; Huang, Y. S. *Organometallics* **1993**, *12*, 797–802.
- (31) Avarvari, N.; Fourmigué, M. *Chem. Commun.* **2004**, 2794–2795.
- (32) Aqad, E.; Becker, J. Y.; Bernstein, J.; Ellern, A.; Khodorkovsky, V.; Shapiro, L. *J. Chem. Soc., Chem. Commun.* **1994**, 2775–2776.
- (33) Wang, C.; Ellern, A.; Becker, J. Y.; Bernstein, J. *Tetrahedron Lett.* **1994**, *35*, 8489–8492.
- (34) Wang, C.; Ellern, A.; Khodorkovsky, V.; Becker, J. Y.; Bernstein, J. *J. Chem. Soc., Chem. Commun.* **1994**, 2115.
- (35) Alkorta, I.; Elguero, J. *Magn. Reson. Chem.* **2010**, *48 Suppl 1*, S32-7.
- (36) Müller, C.; Broeckx, L. E. E.; Krom, I. de; Weemers, J. J. M. *Eur. J. Inorg. Chem.* **2013**, *2013*, 187–202.
- (37) Märkl, G.; Lieb, F.; Merz, A. *Angew. Chem. Int. Ed. Engl.* **1967**, *6*, 944–945.
- (38) Märkl, G. *Angew. Chem.* **1966**, *78*, 907–908.
- (39) Ashe, A. J. *J. Am. Chem. Soc.* **1971**, *93*, 3293–3295.
- (40) Maas, G.; Fink, J.; Wingert, H.; Blatter, K.; Regitz, M. *Chem. Ber.* **1987**, *120*, 819–824.
- (41) Blatter, K.; Rösch, W.; Vogelbacher, U.-J.; Fink, J.; Regitz, M. *Angew. Chem. Int. Ed. Engl.* **1987**, *26*, 85–86.
- (42) Märkl, G.; Heier, K.-H. *Angew. Chem. Int. Ed. Engl.* **1972**, *11*, 1017–1019.
- (43) Holand, S.; Ricard, L.; Mathey, F. *J. Org. Chem.* **1991**, *56*, 4031–4035.
- (44) Märkl, G.; Dörges, C.; Riedl, T.; Klärner, F.-G.; Ludwig, C. *Tetrahedron Lett.* **1990**, *31*, 4589–4592.
- (45) Hunter, R. A.; Whitby, R. J.; Light, M. E.; Hursthouse, M. B. *Tetrahedron Lett.* **2004**, *45*, 7633–7636.
- (46) Märkl, G.; Martin, C.; Weber, W. *Tetrahedron Lett.* **1981**, *22*, 1207–1210.
- (47) Ashe, A. J.; Smith, T. W. *Tetrahedron Lett.* **1977**, *18*, 407–410.
- (48) Märkl, G.; Heier, K. H. *Tetrahedron Lett.* **1974**, *15*, 4501–4504.
- (49) Märkl, G.; Martin, C. *Angew. Chem. Int. Ed. Engl.* **1974**, *13*, 408–409.
- (50) Märkl, G.; Merz, A. *Tetrahedron Lett.* **1971**, *12*, 1215–1218.

- (51) Märkl, G.; Merz, A. *Tetrahedron Lett.* **1969**, *10*, 1231–1234.
- (52) Streubel, R. Product Class 14: λ^5 -Phosphinines. In *Science of Synthesis Category 2, Heterocycles and Related Ring Systems*; Black, Ed.; Georg Thieme Verlag, **2005**; 1157–1179.
- (53) Black, D. S. C.; Ihmels, H.; Alvarez, M.; Bergsträßer, U.; Joule, J. A. *Science of Synthesis: Houben-Weyl Methods of Molecular Transformations Vol. 15: Six-Membered Heterocycles with One Nitrogen or Phosphorus Atom*; Thieme, **2014**.
- (54) Zhang, Y.; Tham, F. S.; Nixon, J. F.; Taylor, C.; Green, J. C.; Reed, C. A. *Angew. Chem.* **2008**, *120*, 3861–3864.
- (55) Dimroth, K. Delocalized phosphorus-carbon double bonds. In *Phosphorus-Carbon Double Bonds*; Fortschritte der Chemischen Forschung; Springer-Verlag, **1973**; 1–147.
- (56) Dimroth, K.; Städe, W. *Angew. Chem. Int. Ed. Engl.* **1968**, *7*, 881–882.
- (57) Pfeifer, G.; Ribagnac, P.; Le Goff, X.-F.; Wiecko, J.; Mézailles, N.; Müller, C. *Eur. J. Inorg. Chem.* **2015**, *2015*, 240–249.
- (58) Moores, A.; Cantat, T.; Ricard, L.; Mézailles, N.; Le Floch, P. *New J. Chem.* **2007**, *31*, 1493.
- (59) Moores, A.; Ricard, L.; Le Floch, P. *Angew. Chem.* **2003**, *115*, 5090–5094.
- (60) Märkl, G.; Lieb, F.; Martin, C. *Tetrahedron Lett.* **1971**, *12*, 1249–1252.
- (61) van den Winkel, Y.; van der Laarse, J.; Kanter, F. J. J. de; van der Does, T.; Bickelhaupt, F.; Smeets, W. J. J.; Spek, A. L. *Heteroatom Chem.* **1991**, *2*, 17–28.
- (62) Böhm, D.; Knoch, F.; Kummer, S.; Schmidt, U.; Zenneck, U. *Angew. Chem. Int. Ed. Engl.* **1995**, *34*, 198–201.
- (63) Jochem, G.; Schmidpeter, A. *Z. Naturforsch. B.* **1996**, *51*, 773–777.
- (64) Fluck, E.; Heckmann, G.; Gorbunowa, E.; Westerhausen, M.; Weller, F. *J. Organomet. Chem.* **1997**, *529*, 223–231.
- (65) Märkl, G. *Z. Naturforsch. B.* **1963**, *18*, 1136–1137.
- (66) Welideniya, D.; Ramachandran, M. R. K.; Kalisch, T.; Streubel, R. *Dalton Trans.* **2021**, *50*, 9345–9366.
- (67) Märkl, G.; Weber, W.; Weiß, W. *Chem. Ber.* **1985**, *118*, 2365–2395.
- (68) Bieger, K.; Heckmann, G.; Fluck, E.; Weller, F.; Peters, K.; Peters, E.-M. *Z. Anorg. Allg. Chem.* **1995**, *621*, 1981–1988.
- (69) Davis, M.; Mann, F. G. *J. Chem. Soc.* **1964**, 3770–3785.
- (70) Akutsu, H.; Ogasawara, M.; Saburi, M.; Kozawa, K.; Uchida, T. *Bull. Chem. Soc. Jpn.* **1996**, *69*, 1223–1226.
- (71) Cullen, W. R.; Wu, A. W. *J. Fluorine Chem.* **1976**, *8*, 183–187.

- (72) Uchiyama, Y.; Mazaki, Y. *Phosphorus, Sulfur Silicon Relat. Elem.* **2011**, *186*, 822–825.
- (73) Ren, Y.; Baumgartner, T. *Asian J. Chem.* **2010**, *5*, 1918–1929.
- (74) Uchiyama, Y.; Kawaguchi, T.; Kuroda, K. *Heteroat. Chem.* **2014**, *25*, 326–336.
- (75) Fenske, D.; Langer, E.; Heymann, M.; Becher, H. J. *Chem. Ber.* **1976**, *109*, 359–362.
- (76) Ivonin, S. P.; Tolmachev, A. A.; Chernega, A. N.; Pinchuk, A. M. *Heteroatom Chem.* **2002**, *13*, 46–52.
- (77) Huryeva, A. N.; Marchenko, A. P.; Koidan, G. N.; Yurchenko, A. A.; Zarudnitskii, E. V.; Pinchuk, A. M.; Kostyuk, A. N. *Heteroat. Chem.* **2010**, *21*, 103–118.
- (78) Koner, A.; Pfeifer, G.; Kelemen, Z.; Schnakenburg, G.; Nyulászi, L.; Sasamori, T.; Streubel, R. *Angew. Chem. Int. Ed.* **2017**, *56*, 9231–9235.
- (79) Begum, I.; Schnakenburg, G.; Streubel, R. *ChemistrySelect* **2020**, *5*, 5959–5964.
- (80) Gese, A.; Kermanshahian, S.; Schnakenburg, G.; Kelemen, Z.; Nyulaszi, L.; Ferao, A. E.; Streubel, R. K. *Inorg. Chem.* **2021**, *60*, 13029–13040.
- (81) Naz, N. R.; Schnakenburg, G.; Mikeházi, A.; Kelemen, Z.; Nyulászi, L.; Boéré, R. T.; Streubel, R. *Chem. Commun.* **2020**, *56*, 2646–2649.
- (82) Kobayashi, Y.; Kumadaki, I.; Ohsawa, A.; Hamana, H. *Tetrahedron Lett.* **1976**, *17*, 3715–3716.
- (83) Kobayashi, Y.; Fujino, S.; Kumadaki, I. *J. Am. Chem. Soc.* **1981**, *103*, 2465–2466.
- (84) Kobayashi, Y.; Hamana, H.; Fujino, S.; Ohsawa, A.; Kumadaki, I. *J. Am. Chem. Soc.* **1980**, *102*, 252–255.
- (85) Begum, I.; Schnakenburg, G.; Kelemen, Z.; Nyulászi, L.; Boéré, R. T.; Streubel, R. *Chem. Commun.* **2018**, *54*, 13555–13558.
- (86) Lukashev, N. V.; Fil'chikov, A. A.; Kazankova, M. A.; Beletskaya, I. P. *Heteroatom Chem.* **1993**, *4*, 403–407.
- (87) Majhi, P. K.; Koner, A.; Schnakenburg, G.; Kelemen, Z.; Nyulászi, L.; Streubel, R. *Eur. J. Inorg. Chem.* **2016**, *2016*, 3559–3573.
- (88) Koner, A.; Kelemen, Z.; Schnakenburg, G.; Nyulászi, L.; Streubel, R. *Chem. Commun.* **2018**, *54*, 1182–1184.
- (89) Begum, I.; Kalisch, T.; Schnakenburg, G.; Kelemen, Z.; Nyulászi, L.; Streubel, R. *Dalton Trans.* **2020**, *49*, 12776–12779.
- (90) Koner, A.; Gabidullin, B. M.; Kelemen, Z.; Nyulászi, L.; Nikonov, G. I.; Streubel, R. *Dalton Trans.* **2019**, *48*, 8248–8253.
- (91) Wudl, F.; Kaplan, M. L.; Hufnagel, E. J.; Southwick, E. W. *J. Org. Chem.* **1974**, *39*, 3608–3609.
- (92) Challenger, F.; Mason, E. A.; Holdsworth, E. C.; Emmott, R. *J. Chem. Soc.* **1953**, 292.

- (93) Takimiya, K.; Morikami, A.; Otsubo, T. *Synlett* **1997**, 1997, 319–321.
- (94) Fabre, J. M. *Chem. rev.* **2004**, *104*, 5133–5150.
- (95) Lincke, K.; Christensen, M. A.; Diederich, F.; Nielsen, M. B. *Helv. Chim. Acta* **2011**, *94*, 1743–1753.
- (96) Abad, A.; Arno, M.; Pedro, J. R.; Seoane, E. **1981**, *30*.
- (97) Sauerbrey, S.; Majhi, P. K.; Schnakenburg, G.; Arduengo, A. J.; Streubel, R. *Dalton Trans.* **2012**, *41*, 5368–5376.
- (98) Koner, A.; Kunz, M.; Schnakenburg, G.; Streubel, R. *Eur. J. Inorg. Chem.* **2018**, *2018*, 3778–3784.
- (99) Majhi, P. K. Ph.D. thesis, University of Bonn, Bonn, Germany, **2014**.
- (100) Begum Imtiaz. Ph.D. thesis, University of Bonn, Bonn, Germany, **2018**.
- (101) Rauf Naz Nabila. Ph.D. thesis, University of Bonn, Bonn, Germany, **2020**.
- (102) Hasegawa, M.; Iyoda, M. Tetrathiafulvalene: A Redox Unit for Functional Materials and a Building Block for Supramolecular Self-Assembly. In *Nishinaga (Ed.) 2016 – Organic Redox Systems: Synthesis, Properties, and Applications*; 89–129.
- (103) Zanello, P.; Biani, F. F. de; Nervi, C. *Inorganic electrochemistry: Theory, practice and application*, 2. ed.; RSC Publ, **2012**.
- (104) Allen J. Bard, Larry R. Faulkner. *Electrochemical Methods: Fundamentals and Applications*, 2nd Edition; John Wiley & Sons, Inc., **2000**.
- (105) Polcyn, D. S.; Shain, I. *Anal. Chem.* **1966**, *38*, 370–375.
- (106) Lahlil, K.; Moradpour, A.; Bowlas, C.; Menou, F.; Cassoux, P.; Bonvoisin, J.; Launay, J.-P.; Dive, G.; Dehareng, D. *J. Am. Chem. Soc.* **1995**, *117*, 9995–10002.
- (107) Connelly, N. G.; Geiger, W. E. *Chem. rev.* **1996**, *96*, 877–910.
- (108) Olaru, M.; Mebs, S.; Beckmann, J. *Angew. Chem. Int. Ed. Engl.* **2021**, *60*, 19133–19138.
- (109) Gudat, D. Low-Coordinate Main Group Compounds – Group 15. In *Comprehensive Inorganic Chemistry II*; Elsevier, **2013**; 587–621.
- (110) Burck, S.; Gudat, D.; Nättinen, K.; Nieger, M.; Niemeyer, M.; Schmid, D. *Eur. J. Inorg. Chem.* **2007**, *2007*, 5112–5119.
- (111) Gudat, D.; Haghverdi, A.; Hupfer, H.; Nieger, M. *Chem. Eur. J.* **2000**, *6*, 3414–3425.
- (112) Nieger, M.; Niecke, E.; Detsch, R. *Z. Kristallogr.* **1995**, *210*, 971–972.
- (113) Cowley, A. H.; Kemp, R. A. *Chem. rev.* **1985**, *85*, 367–382.
- (114) Thomas, M. G.; Schultz, C. W.; Parry, R. W. *Inorg. Chem.* **1977**, *16*, 994–1001.
- (115) Niecke, E.; Kröher, R. *Angew. Chem. Int. Ed. Engl.* **1976**, *15*, 692–693.
- (116) Dimroth, K.; Hoffmann, P. *Angew. Chem. Int. Ed. Engl.* **1964**, *3*, 384.

- (117) Walling, C.; Pearson, M. S. *Top. Phosphorus Chem.* **1966**, *3*, 1–56.
- (118) Schmidt, U.; Kabitzke, K.; Markau, K.; Müller, A. *Chem. Ber.* **1966**, *99*, 1497–1501.
- (119) Kochi, J. K.; Krusic, P. J. *J. Am. Chem. Soc.* **1969**, *91*, 3944–3946.
- (120) Gynane, M. J. S.; Hudson, A.; Lappert, M. F.; Power, P. P. *J. Chem. Soc., Chem. Commun.* **1976**, 623–624.
- (121) Ishida, S.; Hirakawa, F.; Iwamoto, T. *J. Am. Chem. Soc.* **2011**, *133*, 12968–12971.
- (122) Back, O.; Donnadiou, B.; Hopffgarten, M. von; Klein, S.; Tonner, R.; Frenking, G.; Bertrand, G. *Chem. Sci.* **2011**, *2*, 858–861.
- (123) Agarwal, P.; Piro, N. A.; Meyer, K.; Müller, P.; Cummins, C. C. *Angew. Chem. Int. Ed. Engl.* **2007**, *46*, 3111–3114.
- (124) Back, O.; Celik, M. A.; Frenking, G.; Melaimi, M.; Donnadiou, B.; Bertrand, G. *J. Am. Chem. Soc.* **2010**, *132*, 10262–10263.
- (125) Dumitrescu, A.; Rudzevich, V. L.; Romanenko, V. D.; Mari, A.; Schoeller, W. W.; Bourissou, D.; Bertrand, G. *Inorg. Chem.* **2004**, *43*, 6546–6548.
- (126) Bezombes, J.-P.; Borisenko, K. B.; Hitchcock, P. B.; Lappert, M. F.; Nycz, J. E.; Rankin, D. W. H.; Robertson, H. E. *Dalton Trans.* **2004**, 1980–1988.
- (127) Bezombes, J.-P.; Hitchcock, P. B.; Lappert, M. F.; Nycz, J. E. *Dalton Trans.* **2004**, 499–501.
- (128) Hinchley, S. L.; Morrison, C. A.; Rankin, D. W.; Macdonald, C. L.; Wiacek, R. J.; Voigt, A.; Cowley, A. H.; Lappert, M. F.; Gundersen, G.; Clyburne, J. A.; Power, P. P. *J. Am. Chem. Soc.* **2001**, *123*, 9045–9053.
- (129) Hinchley, S. L.; Morrison, C. A.; Rankin, D. W. H.; Macdonald, C. L. B.; Wiacek, R. J.; Cowley, A. H.; Lappert, M. F.; Gundersen, G.; Clyburne, J. A. C.; Power, P. P. *Chem. Commun.* **2000**, 2045–2046.
- (130) Gynane, M. J. S.; Hudson, A.; Lappert, M. F.; Power, P. P.; Goldwhite, H. *J. Chem. Soc., Dalton Trans.* **1980**, 2428–2433.
- (131) Sheberla, D.; Tumanskii, B.; Tomasik, A. C.; Mitra, A.; Hill, N. J.; West, R.; Apeloig, Y. *Chem. Sci.* **2010**, *1*, 234.
- (132) Roberts, B. P. *Adv. Free-Radical Chem.* **1980**, *6*, 225–289.
- (133) Koner, A.; Sauerbrey, S.; Schnakenburg, G.; Bauzá, A.; Frontera, A.; Streubel, R. *Eur. J. Inorg. Chem.* **2018**, *2018*, 904–916.
- (134) Danila, I.; Biaso, F.; Sidorenkova, H.; Geoffroy, M.; Fourmigué, M.; Levillain, E.; Avarvari, N. *Organometallics* **2009**, *28*, 3691–3699.
- (135) Hertler, W. R. *J. Org. Chem.* **1976**, *41*, 1412–1416.
- (136) Pittman, C. U.; Narita, M.; Liang, Y. F. *Macromolecules* **1976**, *9*, 360–361.

- (137) Koßmehl, G.; Rohde, M. *Makromol. Chem.* **1982**, *183*, 2077–2084.
- (138) Pittman, C. U.; Liang, Y.-F.; Ueda, M. *Macromolecules* **1979**, *12*, 541–546.
- (139) Iyoda, M.; Kuwatani, Y.; Ueno, N.; Oda, M. *J. Chem. Soc., Chem. Commun.* **1992**, 158–159.
- (140) Bryce, M. R.; Skabara, P. J.; Moore, A. J.; Batsanov, A. S.; Howard, J. A.; Hoy, V. J. *Tetrahedron* **1997**, *53*, 17781–17794.
- (141) Garín, J.; Orduna, J.; Uriel, S.; Moore, A. J.; Bryce, M. R.; Wegener, S.; Yufit, D. S.; Howard, J. A. K. *Synthesis* **1994**, *1994*, 489–493.
- (142) Jeppesen, J. O.; Nielsen, M. B.; Becher, J. *Chem. rev.* **2004**, *104*, 5115–5132.
- (143) Nielsen, M. B.; Lomholt, C.; Becher, J. *Chem. Soc. Rev.* **2000**, *29*, 153–164.
- (144) Bryce, M. R. *J. Mater. Chem.* **2000**, *10*, 589–598.
- (145) Thobie-Gautier, C.; Gorgues, A.; Jubault, M.; Roncali, J. *Macromolecules* **1993**, *26*, 4094–4099.
- (146) Shimizu, T.; Yamamoto, T. *Chem. Commun.* **1999**, 515–516.
- (147) Green, D. C.; Allen, R. W. *J. Chem. Soc., Chem. Commun.* **1978**, 832–833.
- (148) Yamamoto, T.; Shimizu, T. *J. Mater. Chem.* **1997**, *7*, 1967–1968.
- (149) Frenzel, S.; Baumgarten, M.; Müllen, K. *Synth. Met.* **2001**, *118*, 97–103.
- (150) Gese, A. Ph.D. thesis, University of Bonn, Bonn, Germany, **2020**.
- (151) Perrin, D. D.; Armarego, W. L. F.; Perrin, D. R. *Purification of Laboratory Chemicals*; Pergamon Press Oxford, **1988**.
- (152) Lunn, G.; Sansone, E. B. *Destruction of Hazardous Chemicals in the Laboratory*; John Wiley & Sons, Inc., **2012**.
- (153) Sheldrick, G. M. *SHELXL-97: Program for the Refinement of Crystal Structures*; University of Göttingen, **1997**.
- (154) Sheldrick, G. M. *Acta Crystallogr A Found Crystallogr* **1990**, *46*, 467–473.
- (155) Sheldrick, G. M. *Acta Crystallogr A Found Crystallogr* **2008**, *64*, 112–122.
- (156) Bestmann, H. J.; Lienert, J.; Heid, E. *Chem. Ber.* **1982**, *115*, 3875–3879.
- (157) Chantrell, P. G.; Pearce, C. A.; Toyer, C. R.; Twaits, R. *J. Appl. Chem.* **1964**, *14*, 563–564.
- (158) King, R. B.; Sadanani, N. D. *Synth. React. Inorg. Met. -Org. Chem.* **1985**, *15*, 149–153.

Abbreviations

Xa,a' = a mixture of two isomers (*cis/trans*); where **X**=compound number and **a,a'** are two isomers

Å	Ångström (1×10^{-10} m)
°	angle in degree
Ar	Aromatic substituent
ATR	Attenual Total Reflexion
au	Atomic Unit
br	broad signal
ⁿ Bu	ⁿ butyl
calc.	calculated
°C	degree Celsius
CDCl ₃	deuterated chloroform
CD ₂ Cl ₂	deuterated dichloromethane
cm	Centimeter
CSD	Cambridge Structural Database
CV	Cyclic voltammetry
D	Days
dec.	decomposition
DEPT	Distortionless Enhancement by Polarization
DMAD	Dimethyl acetylenedicarboxylate
DMTF	<i>ortho</i> -Dimethytetrathiafulvalene
δ	chemical shift in ppm

$\Delta\delta$	chemical shift difference
EI	Electron Impact ionization
ESI	Electrospray Ionization
Et	ethyl
Et ₂ O	diethyl ether
eq.	Equivalent
FWHM	Full Width at Half Maximum
g	gram
H	Hour
HR-MS	High Resolution Mass Spectrometry
Hz	Hertz
IR	infrared
ⁿ J _{X,Y}	coupling constant (between the elements X,Y over n bonds) in Hz
K	Kelvin
KHMDS	Potassium hexamethyldisilazide
L	ligand
LIFDI	Liquid Injection Field Desorption Ionization
m	multiplet
mg	milligram
mL	millilitre
MLn	transition metal fragment bearing n ligands min minutes
mmol	millimole
MS	mass spectrometry

m/z	mass to charge ratio
nm	nanometre
NMR	Nuclear Magnetic Resonance
PE	petrol ether (40/60)
Ph	phenyl (C ₆ H ₅)
ppm	parts per million
ⁿ Pr	ⁿ Propyl
q	Quartet
quin	quintet
R, R', R ¹	organic substituent
r.t.	room temperature
s	singlet
T	temperature
THF	tetrahydrofuran
THF-d ₈	deuterated tetrahydrofuran
TMEDA	Tetramethylethylenediamine
Toluene-d ₈	deuterated toluene
TTF	tetrathiafulvalene
∅	diameter
VT-NMR	Variable Temperature NMR
X	halogen or leaving group

Appendix

Cyclic voltammograms

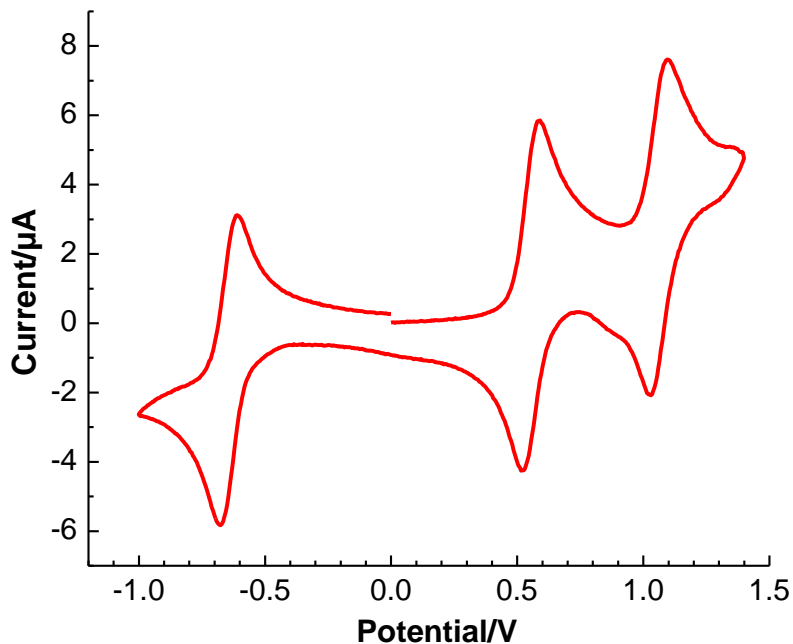


Figure A.1. Cyclic voltammogram of **3c** with Cobaltocenium hexafluorophosphate as internal reference (0.4 M $n\text{Bu}_4\text{PF}_6$ in DCM, 100 mVs^{-1}).

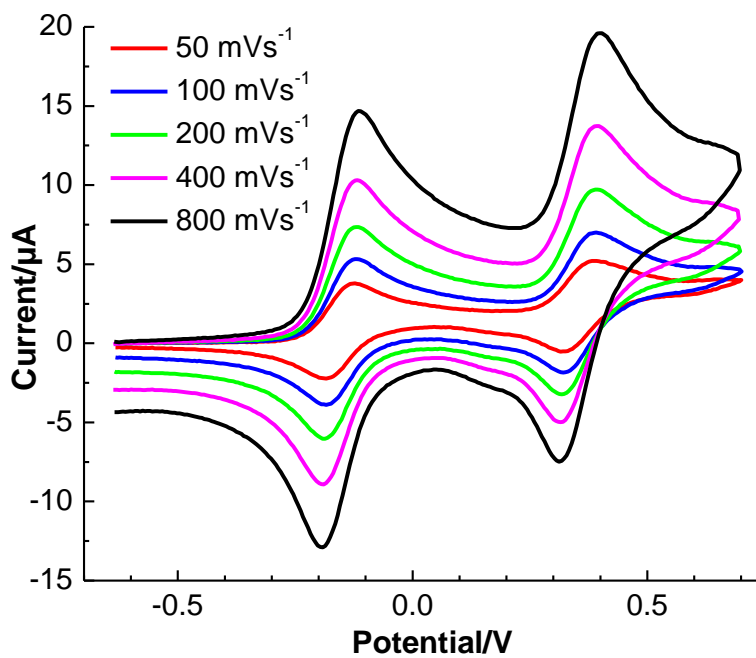


Figure A.2. Scan rate dependency (SRD) study for **3c**.

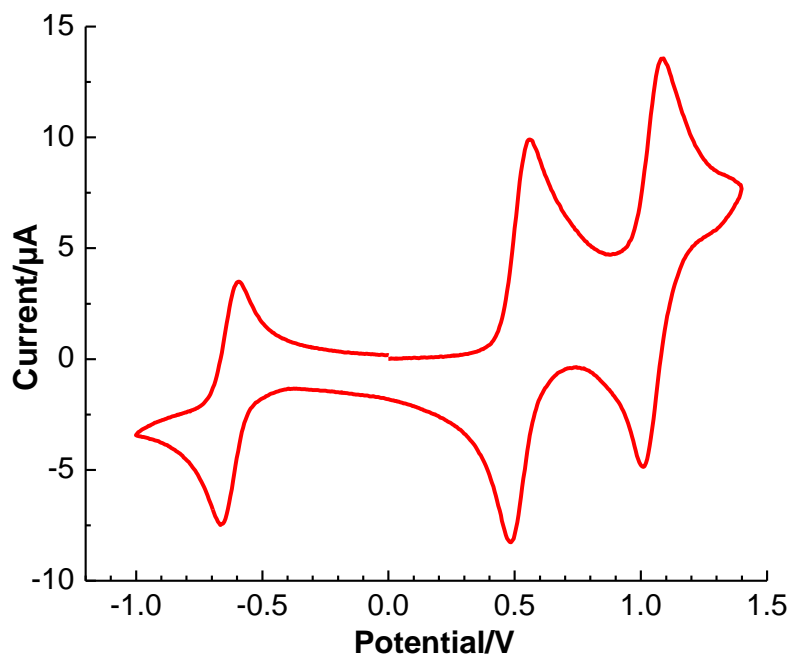


Figure A.3. Cyclic voltammogram of **3d** with Cobaltocenium hexafluorophosphate as internal reference (0.4 M ${}^n\text{Bu}_4\text{PF}_6$ in DCM, 100 mVs^{-1}).

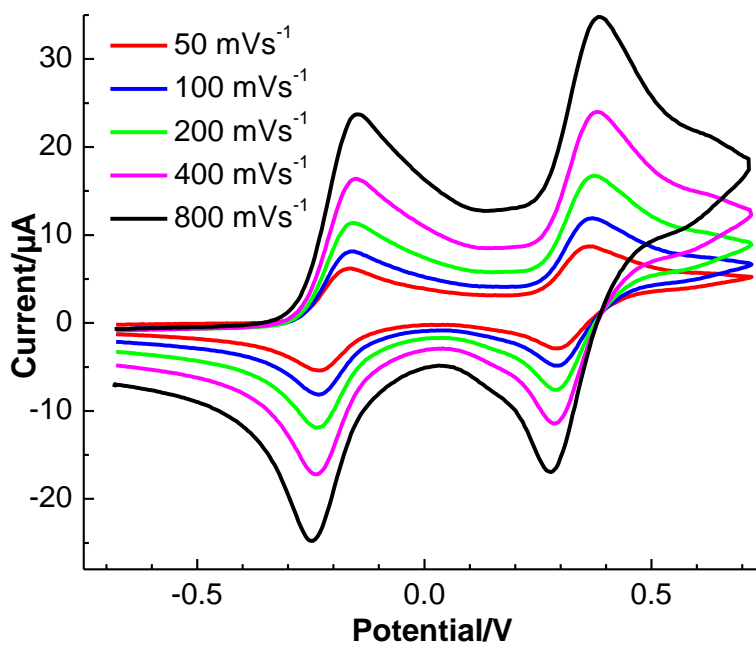


Figure A.4. Scan rate dependency (SRD) study for **3d**.

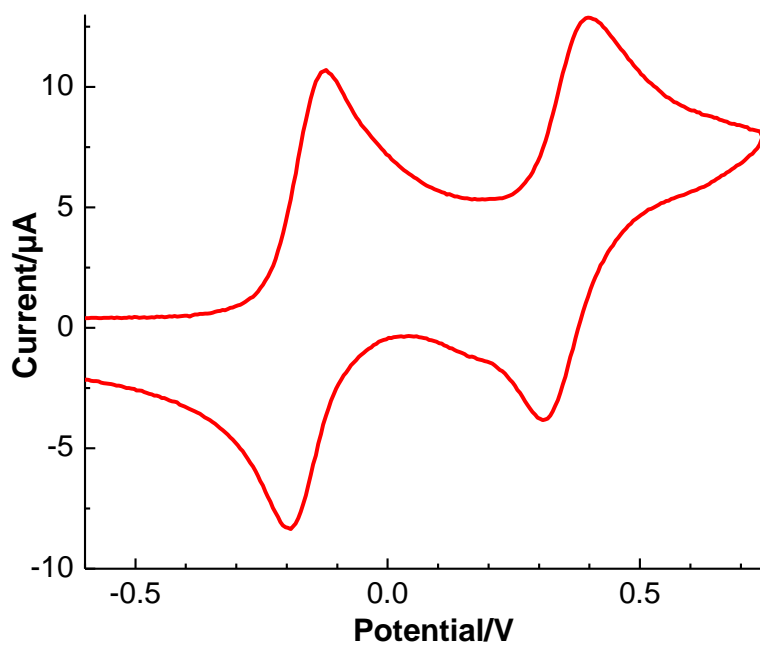


Figure A.5. Cyclic voltammograms of **3e** Vs. $\text{Fc}^{0/+}$ (0.4 M $n\text{Bu}_4\text{PF}_6$ in DCM, 100 mVs^{-1}).

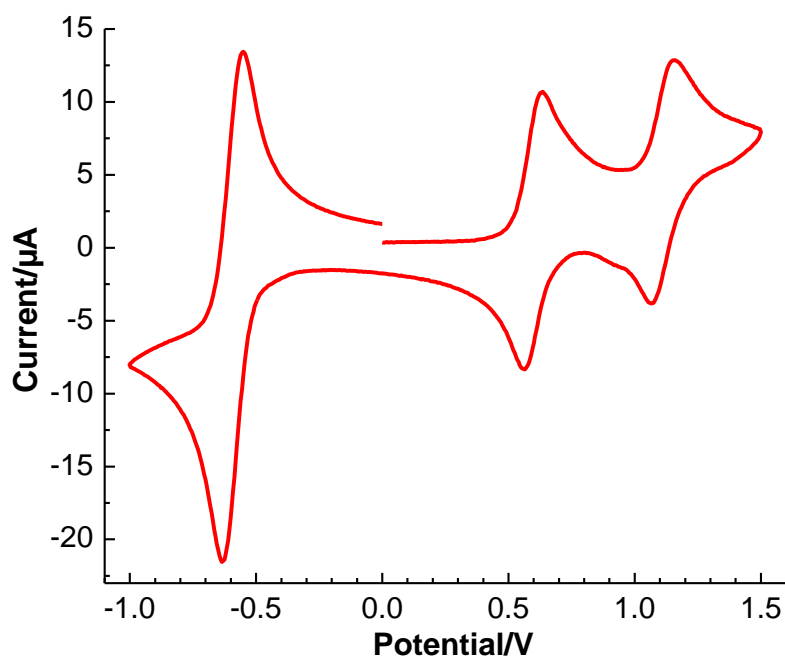


Figure A.6. Cyclic voltammogram of **3e** with Cobaltocenium hexafluorophosphate as internal reference (0.4 M $n\text{Bu}_4\text{PF}_6$ in DCM, 100 mVs^{-1}).

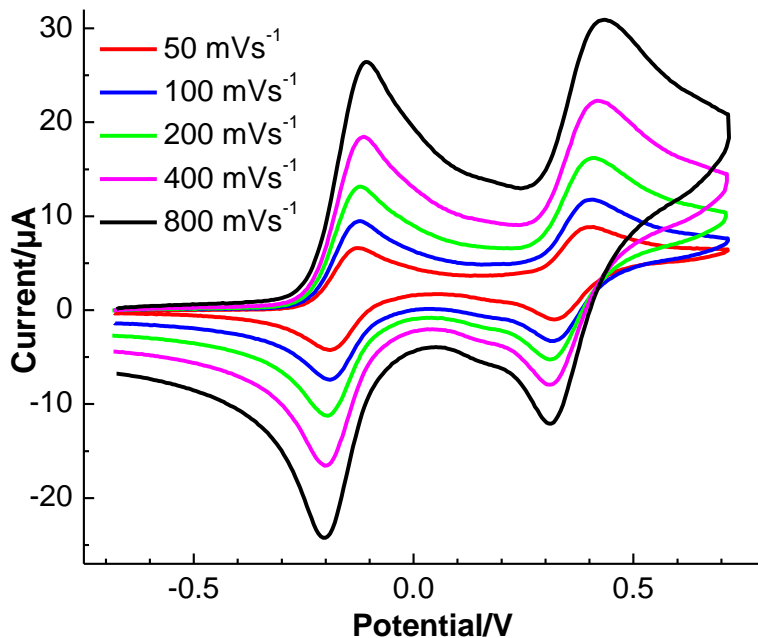


Figure A.7. Scan rate dependency (SRD) study for 3e.

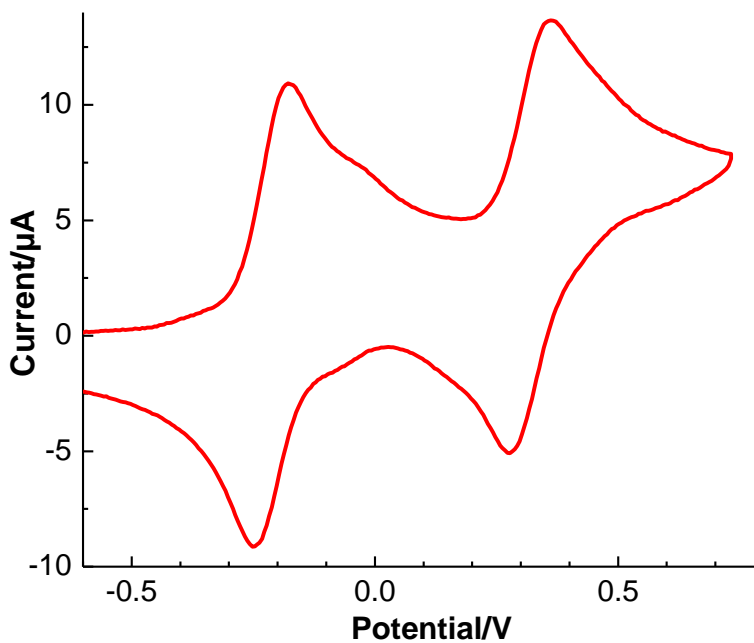


Figure A.8. Cyclic voltammograms of 3e Vs. $\text{Fc}^{0/+}$ (0.4 M $n\text{Bu}_4\text{PF}_6$ in DCM, 100 mVs^{-1}).

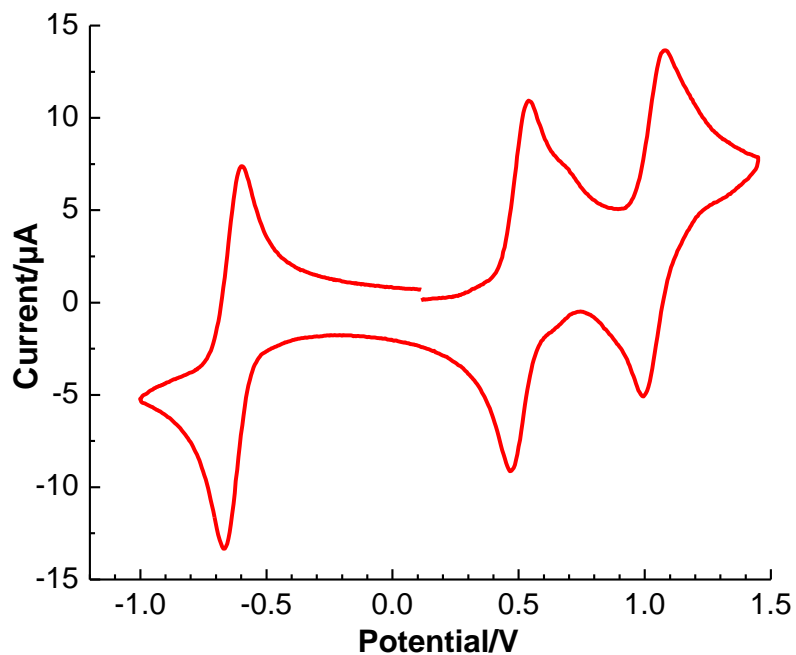


Figure A.9. Cyclic voltammogram of **3f** with Cobaltocenium hexafluorophosphate as internal reference (0.4 M $n\text{Bu}_4\text{PF}_6$ in DCM, 100 mVs^{-1}).

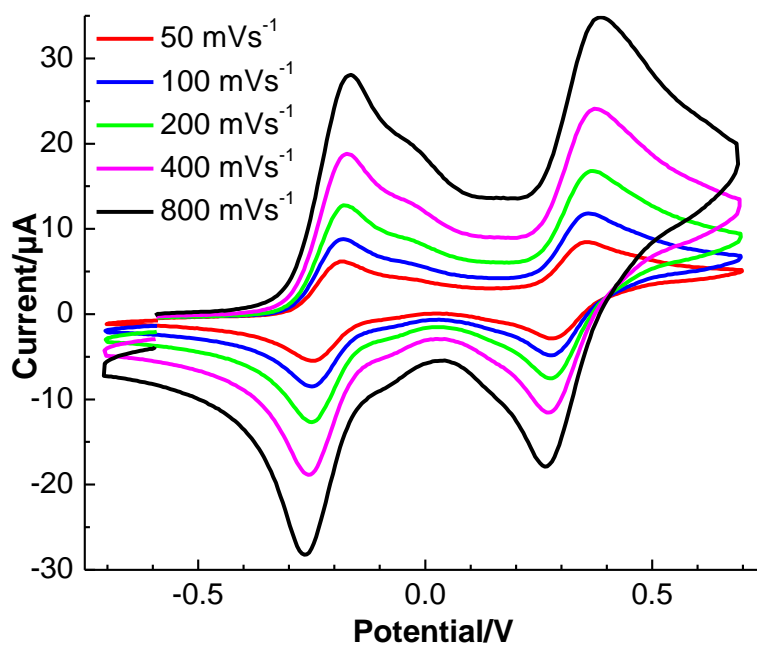


Figure A.10. Scan rate dependency (SRD) study for **3f**.

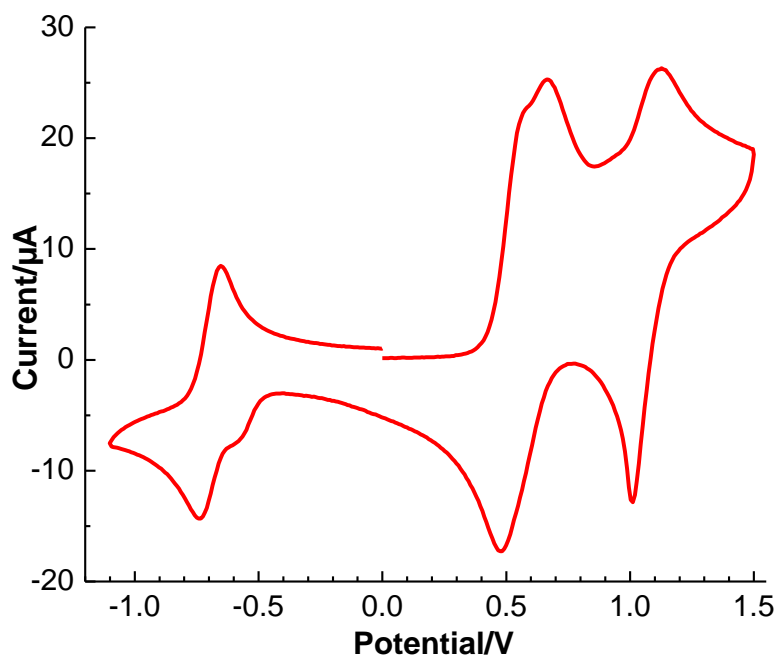


Figure A.11. Cyclic voltammogram of **5a** with Cobaltocenium hexafluorophosphate as internal reference (0.4 M $n\text{Bu}_4\text{PF}_6$ in DCM, 200 mVs^{-1}).

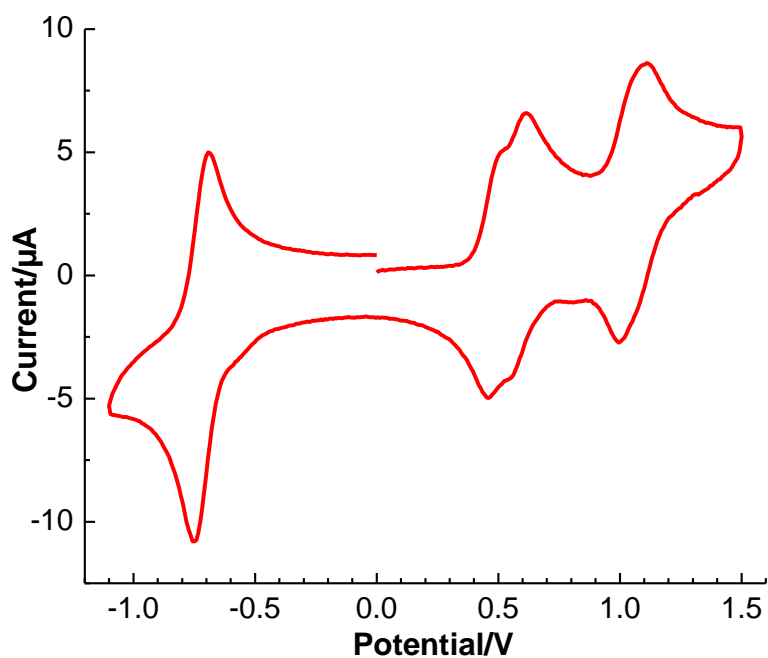


Figure A.12. Cyclic voltammogram of **5b** with Cobaltocenium hexafluorophosphate as internal reference (0.4 M $n\text{Bu}_4\text{PF}_6$ in DCM, 200 mVs^{-1}).

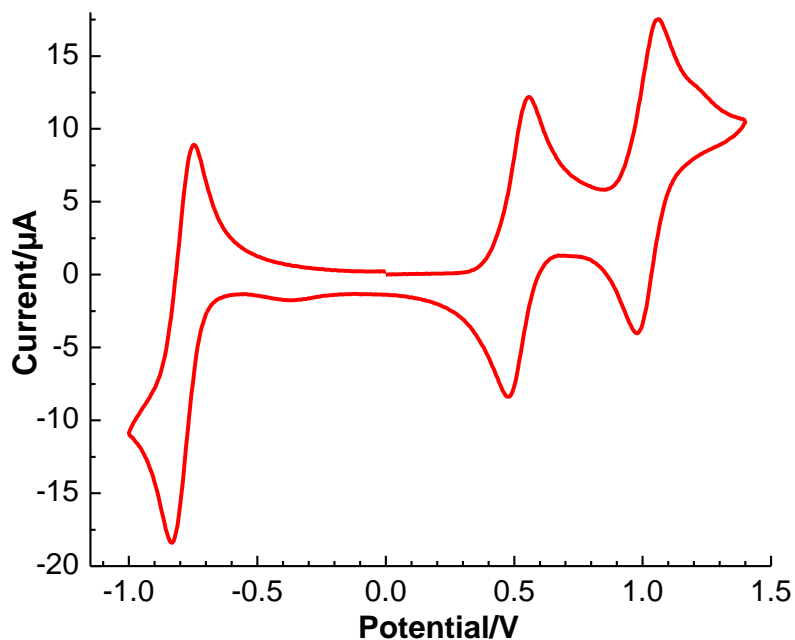


Figure A.13. Cyclic voltammogram of **4c** with Cobaltocenium hexafluorophosphate as internal reference (0.4 M $n\text{Bu}_4\text{PF}_6$ in DCM, 200 mVs^{-1}).

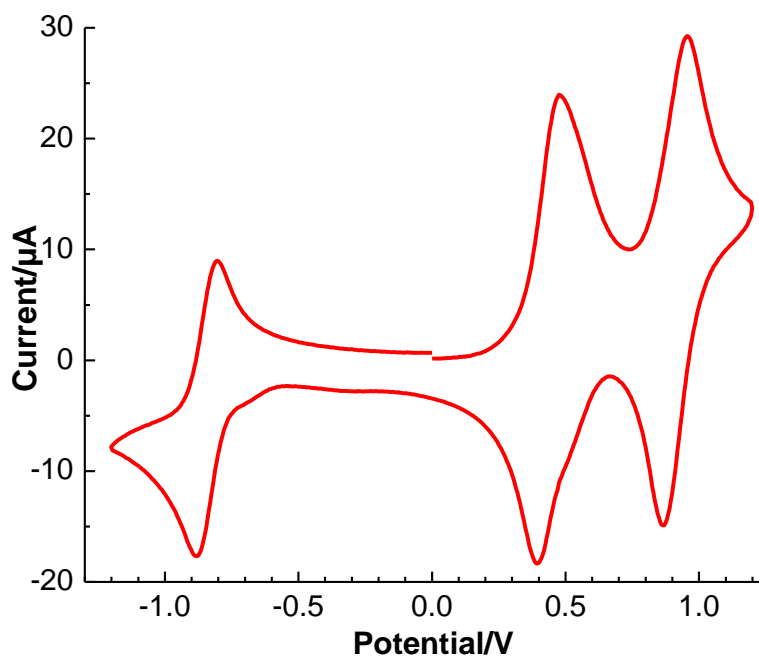


Figure A.14. Cyclic voltammogram of **4d** with Cobaltocenium hexafluorophosphate as internal reference (0.4 M $n\text{Bu}_4\text{PF}_6$ in DCM, 200 mVs^{-1}).

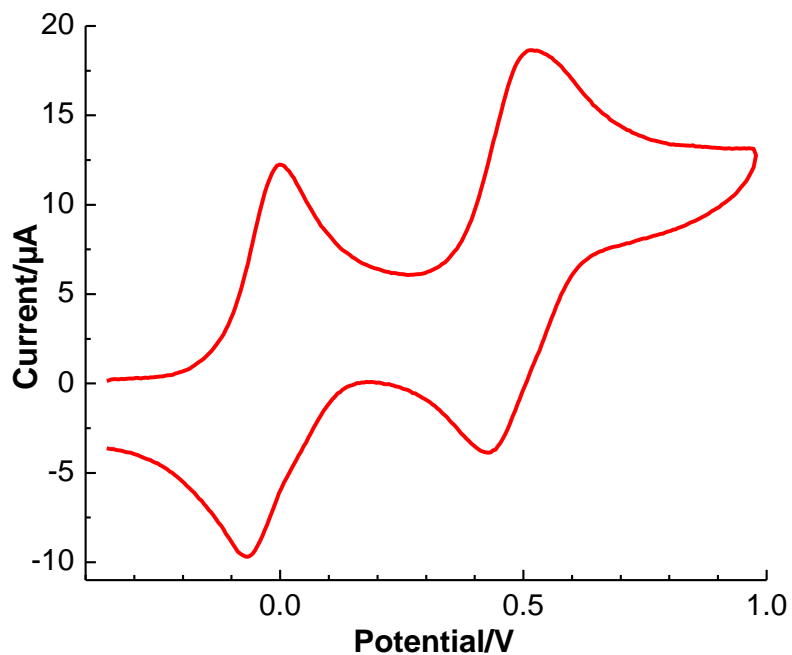


Figure A.15. Cyclic voltammograms of **4e** Vs. $\text{Fc}^{0/+}$ (0.4 M ${}^n\text{Bu}_4\text{PF}_6$ in DCM, 200 mVs^{-1}).

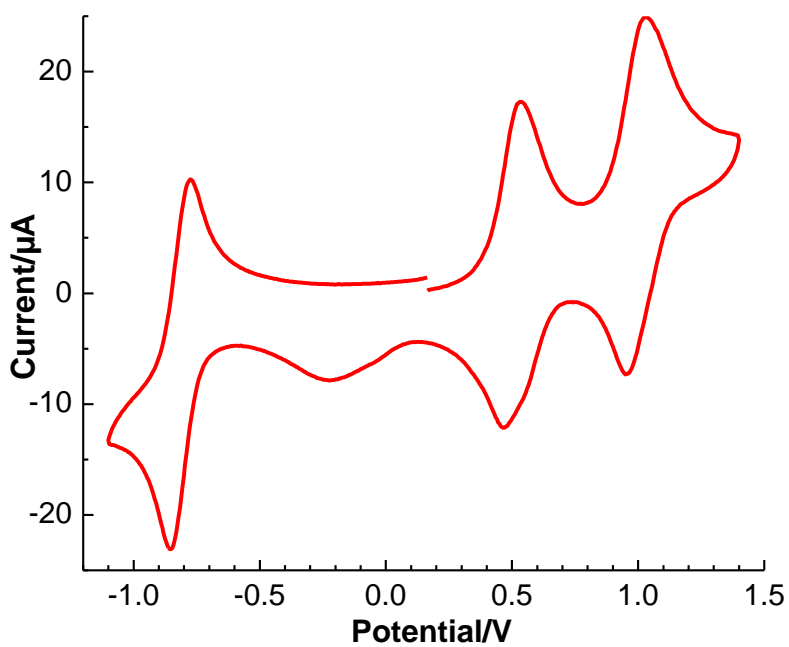


Figure A.16. Cyclic voltammogram of **4e** with Cobaltocenium hexafluorophosphate as internal reference (0.4 M ${}^n\text{Bu}_4\text{PF}_6$ in DCM, 200 mVs^{-1}).

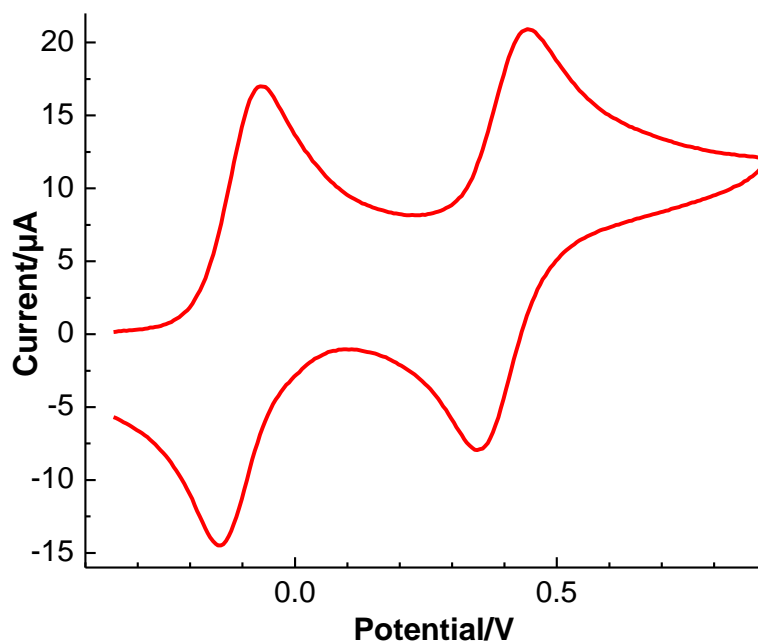


Figure A.17. Cyclic voltammograms of **4f** Vs. $\text{Fc}^{0/+}$ (0.4 M ${}^n\text{Bu}_4\text{PF}_6$ in DCM, 200 mVs^{-1}).

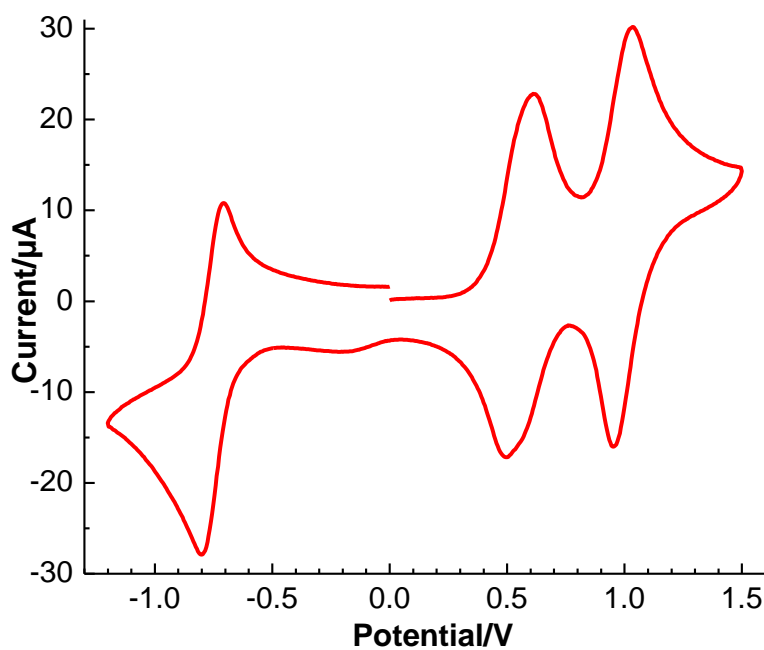


Figure A.18. Cyclic voltammogram of **4f** with Cobaltocenium hexafluorophosphate as internal reference (0.4 M ${}^n\text{Bu}_4\text{PF}_6$ in DCM, 200 mVs^{-1}).

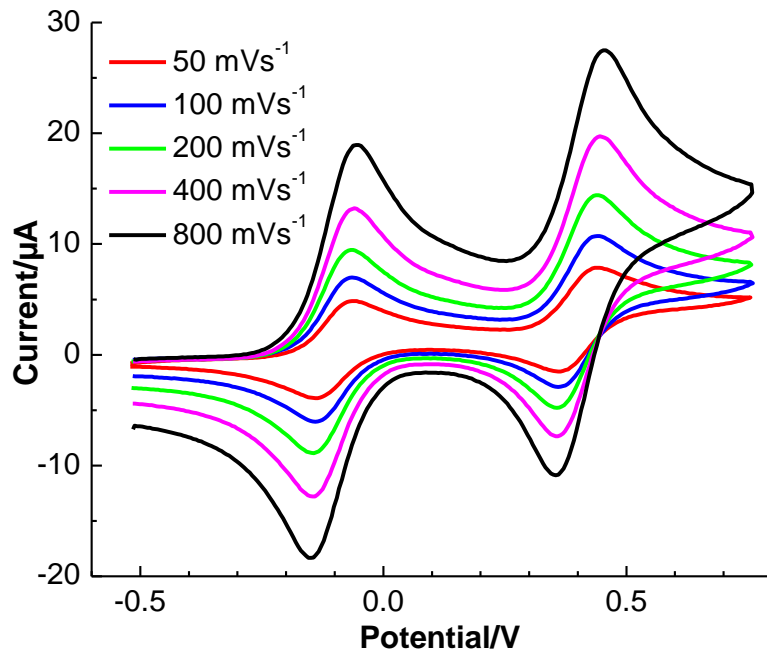


Figure A.19. Scan rate dependency (SRD) study for 4c.

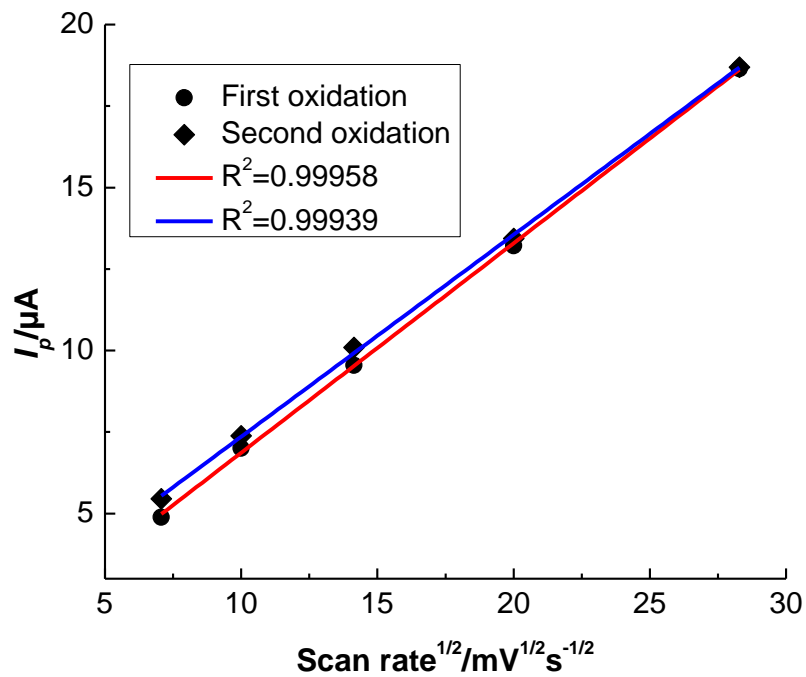


Figure A.20. Dependency of the anodic peak currents on the scan rate for 4c.

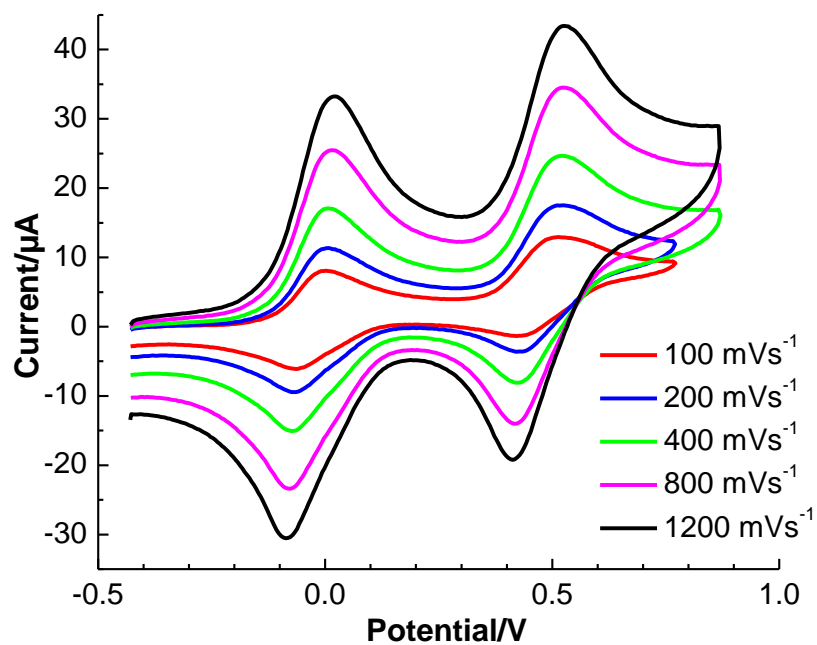


Figure A.21. Scan rate dependency (SRD) study for 4e.

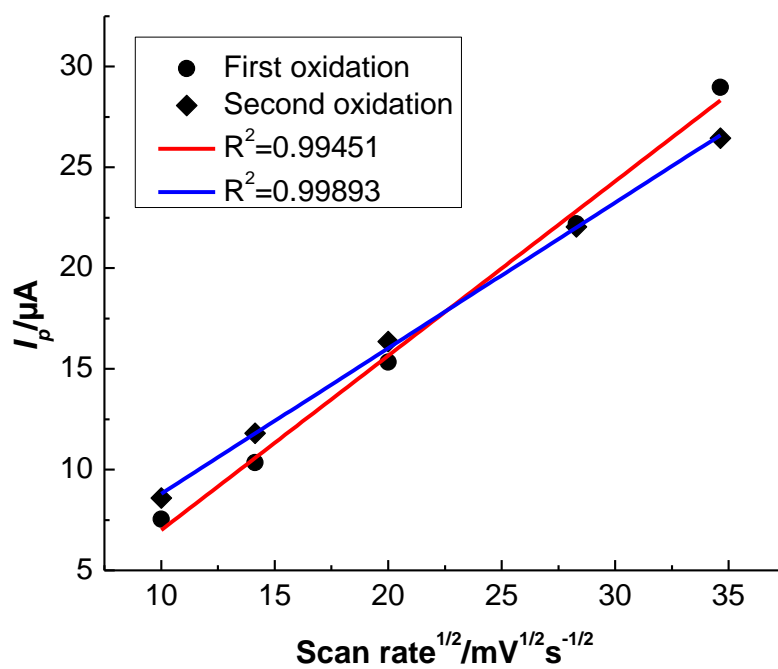


Figure A.22. Dependency of the anodic peak currents on the scan rate for 4e.

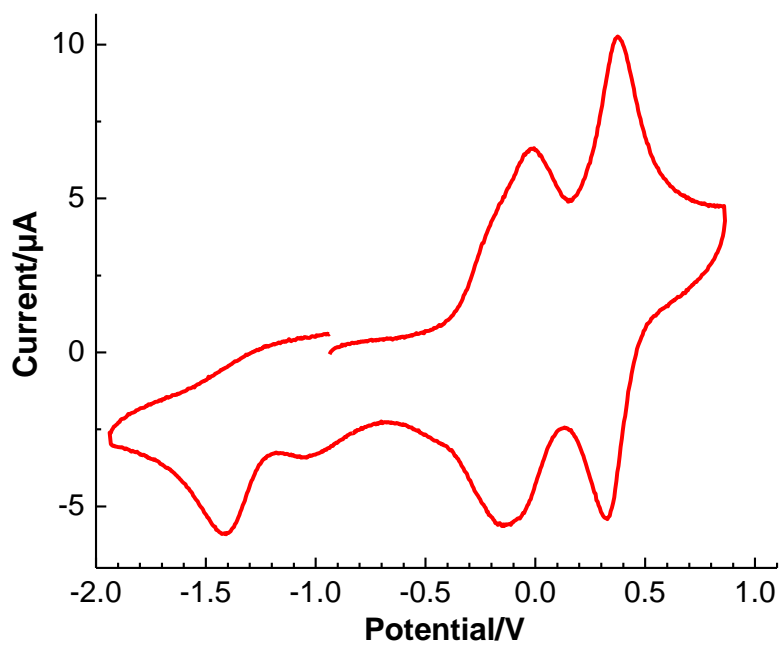


Figure A.23. Cyclic voltammogram of **4d** (wide range) Vs. $\text{Fc}^{0/+}$ (0.1 M $n\text{Bu}_4\text{PF}_6$ in MeCN, 200 mVs^{-1}).

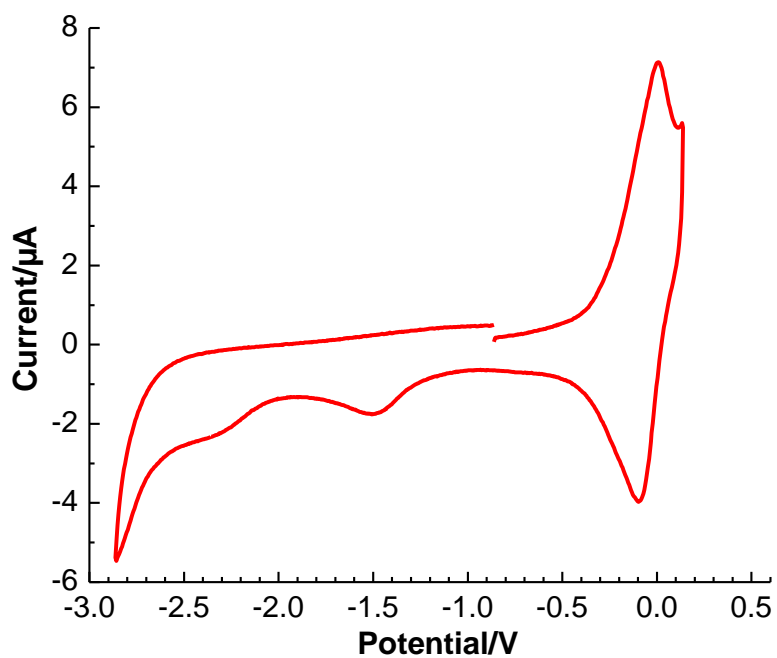


Figure A.24. Cyclic voltammogram of **4d** (wide range) Vs. $\text{Fc}^{0/+}$ (0.2 M $n\text{Bu}_4\text{PF}_6$ in THF, 200 mVs^{-1}).

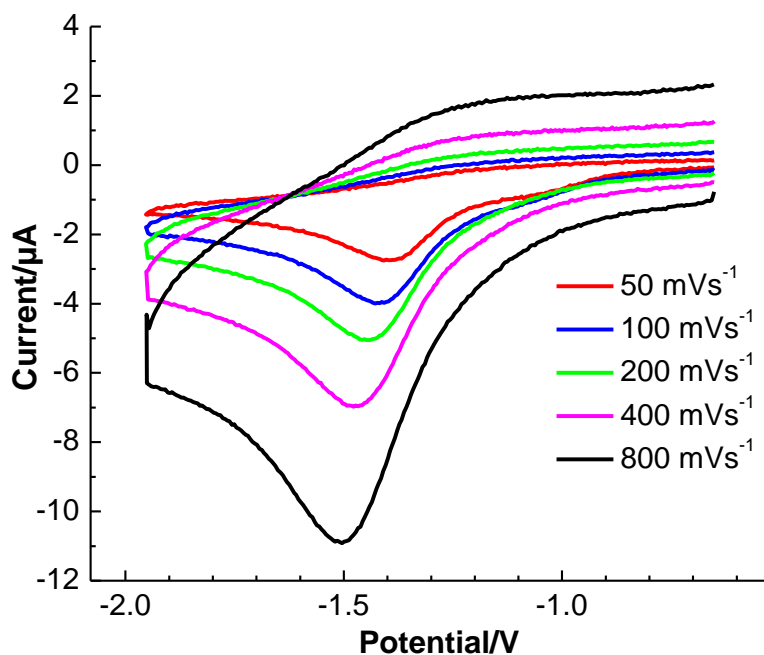


Figure A.25. Scan rate dependency (SRD) study for the second reduction of **4d** in MeCN.

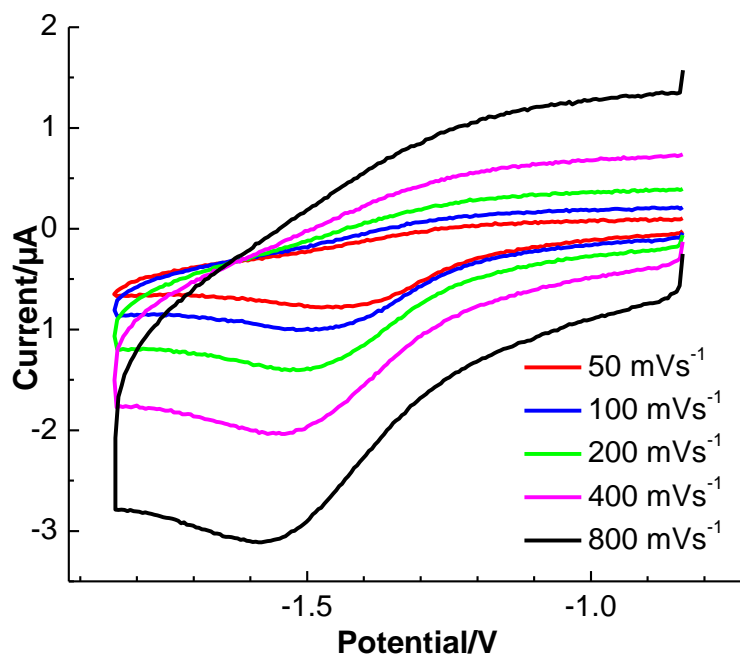


Figure A.26. Scan rate dependency (SRD) study for the first reduction of **4d** in THF.

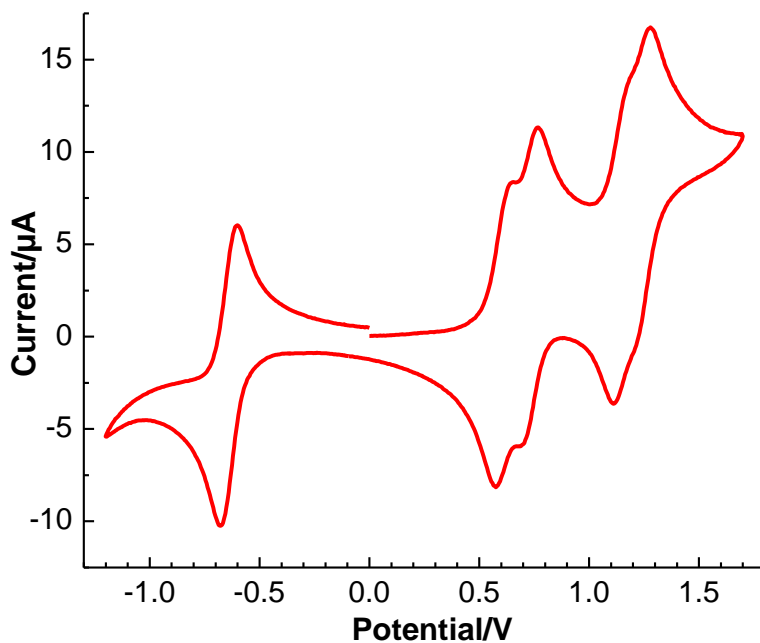


Figure A.27. Cyclic voltammogram of **11d,d'** with Cobaltocenium hexafluorophosphate as internal reference (0.4 M $n\text{Bu}_4\text{PF}_6$ in DCM, 100 mVs^{-1}).

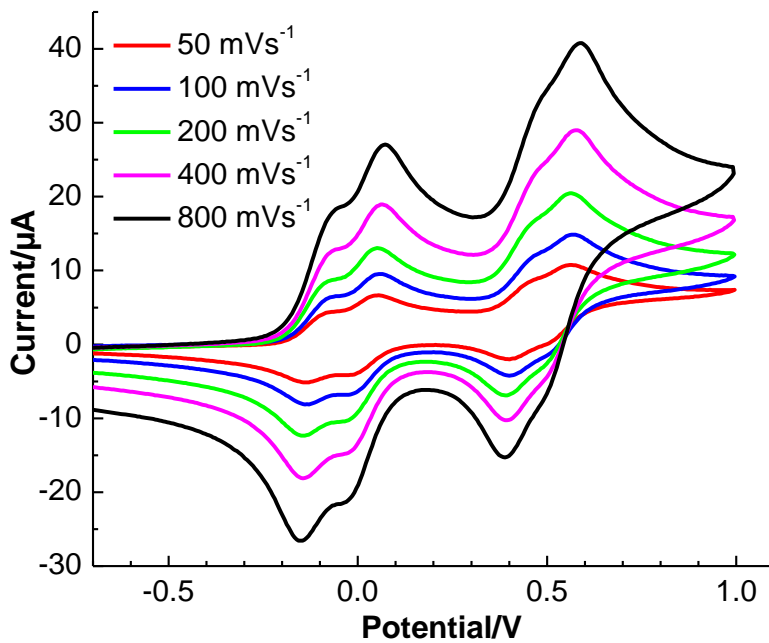


Figure A.28. Scan rate dependency (SRD) study for **11d,d'**.

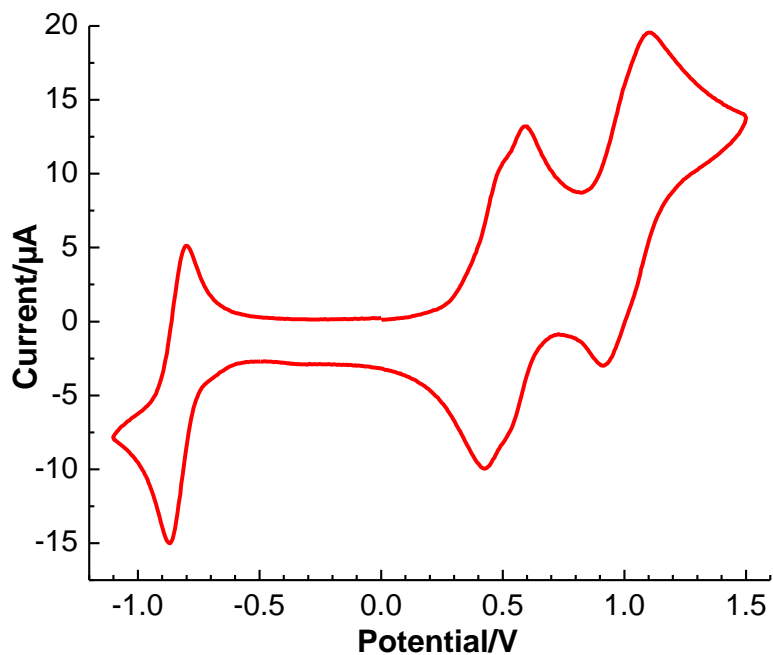


Figure A.29. Cyclic voltammogram of **11e,e'** with Cobaltocenium hexafluorophosphate as internal reference (0.4 M ${}^n\text{Bu}_4\text{PF}_6$ in DCM, 100 mVs^{-1}).

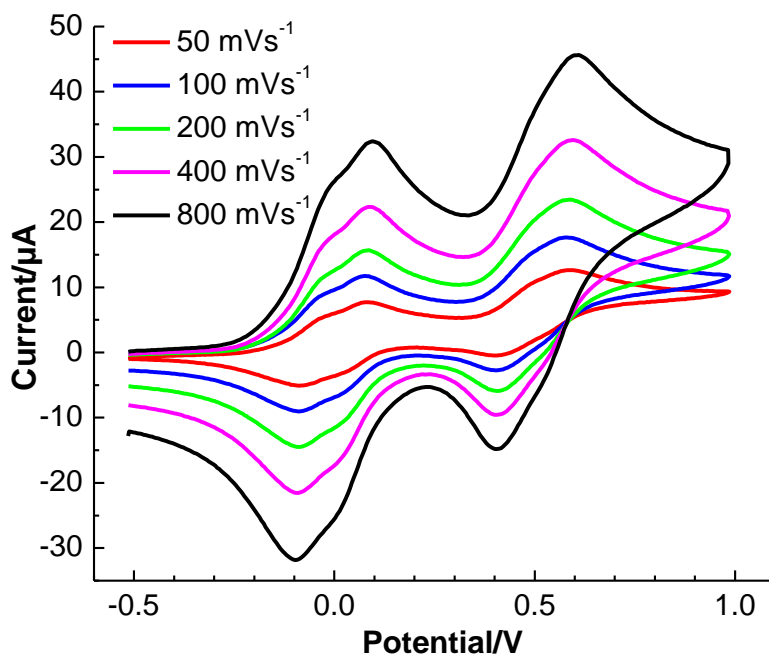


Figure A.30. Scan rate dependency (SRD) study for **11e,e'**.

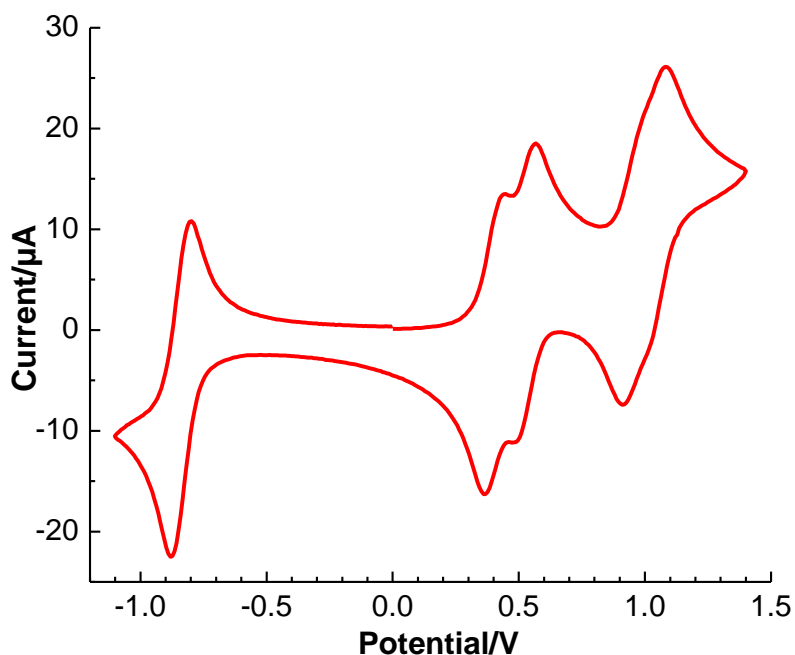


Figure A.31. Cyclic voltammogram of **11f,f'** with Cobaltocenium hexafluorophosphate as internal reference (0.4 M ${}^n\text{Bu}_4\text{PF}_6$ in DCM, 100 mVs^{-1}).

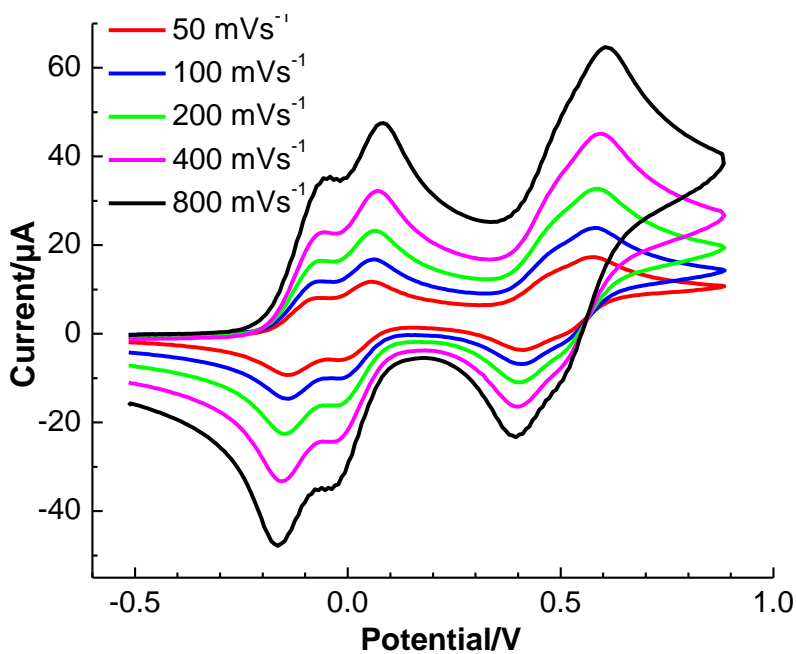


Figure A.32. Scan rate dependency (SRD) study for **11f,f'**.

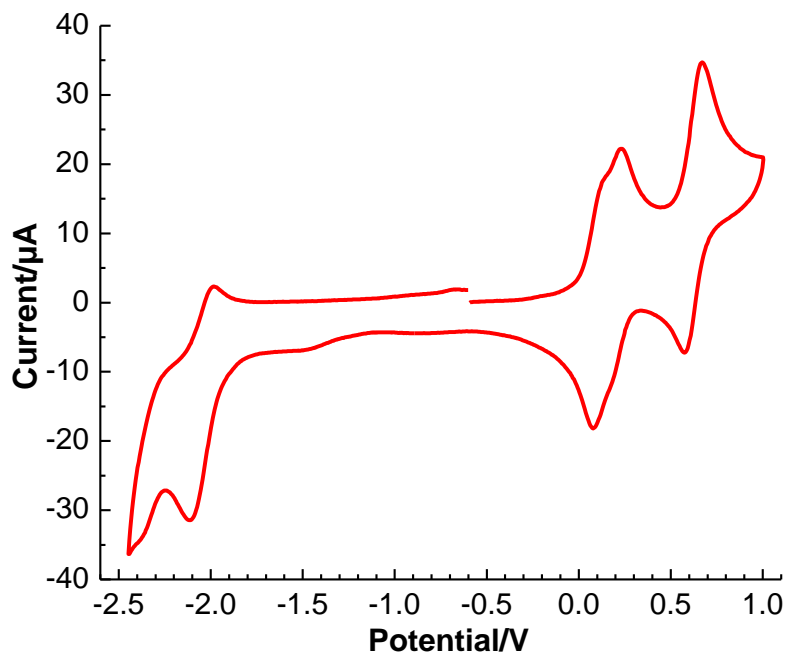


Figure A.33. Cyclic voltammogram of **12a,a'** (wide range) Vs. $\text{Fc}^{0/+}$ (0.4 M $n\text{Bu}_4\text{PF}_6$ in DCM, 200 mVs^{-1}) (the small reduction wave at around -1.5 V is due to the presence of the trace of oxygen in the solvent).

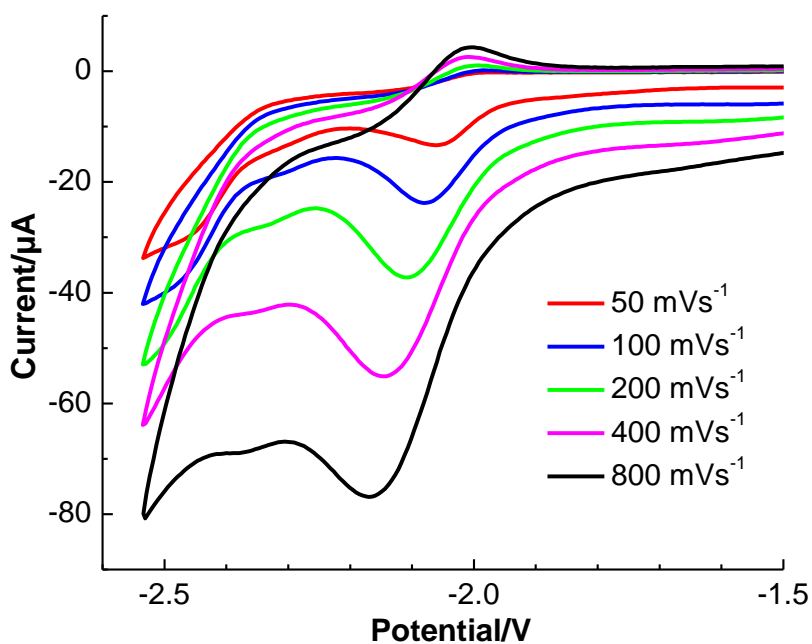


Figure A.34. Scan rate dependency (SRD) study for **12a,a'**.

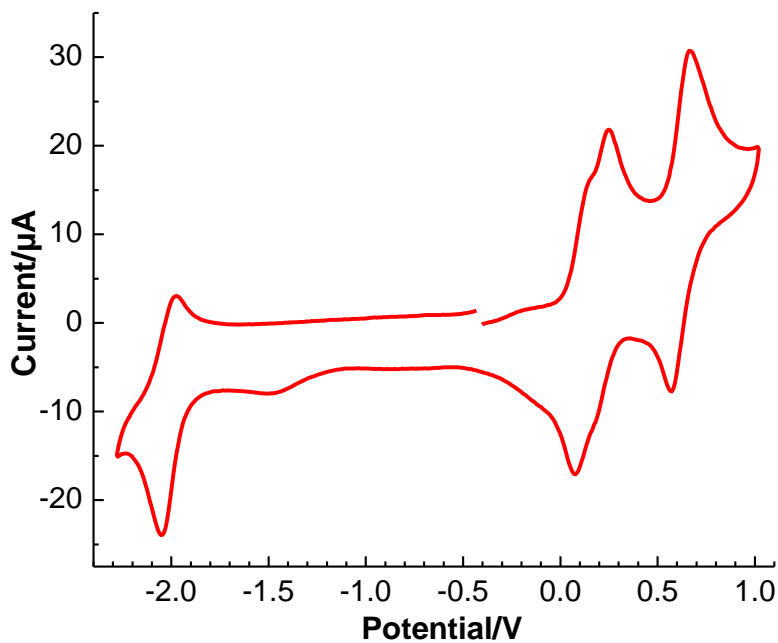


Figure A.35. Cyclic voltammogram of **12b,b'** (wide range) Vs. $\text{Fc}^{0/+}$ (0.4 M $n\text{Bu}_4\text{PF}_6$ in DCM, 200 mVs^{-1}) (the small reduction wave at around -1.5 V is due to the presence of the trace of oxygen in the solvent).

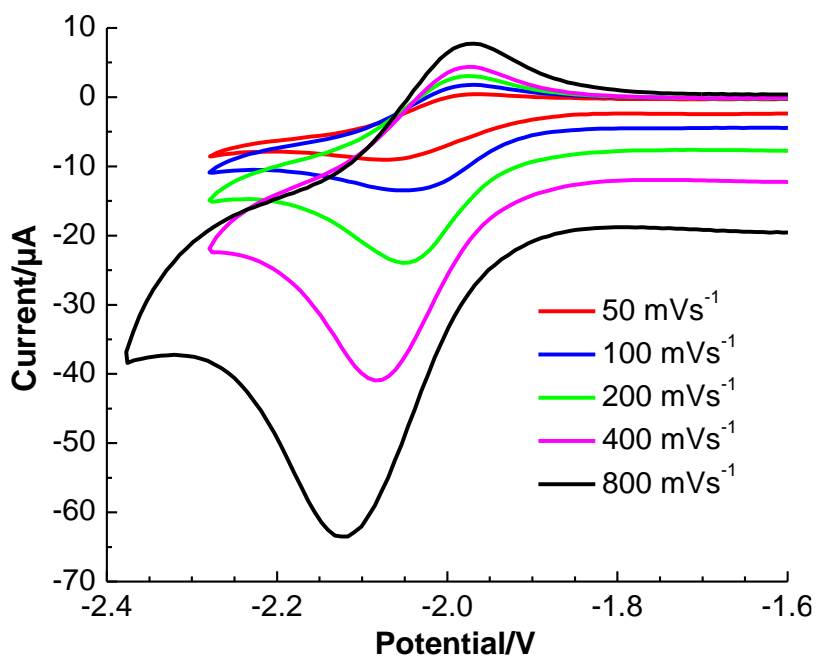


Figure A.36. Scan rate dependency (SRD) study for **12b,b'**.

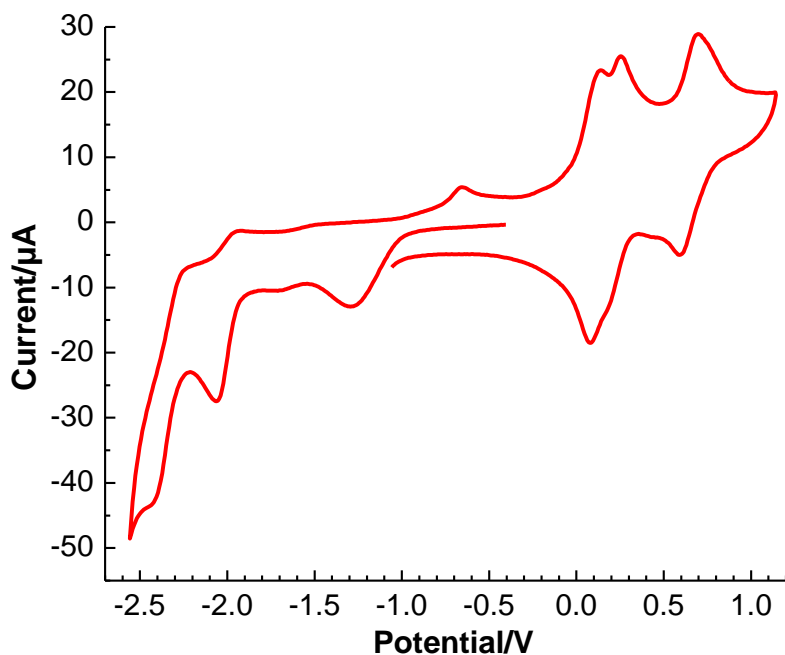


Figure A.37. Cyclic voltammogram of **13a,a'** (wide range) Vs. $\text{Fc}^{0/+}$ ($0.4 \text{ M } ^n\text{Bu}_4\text{PF}_6$ in DCM, 200 mVs^{-1}) (the reduction wave at around -1.3 V is due to the presence of the trace of oxygen in the solvent).

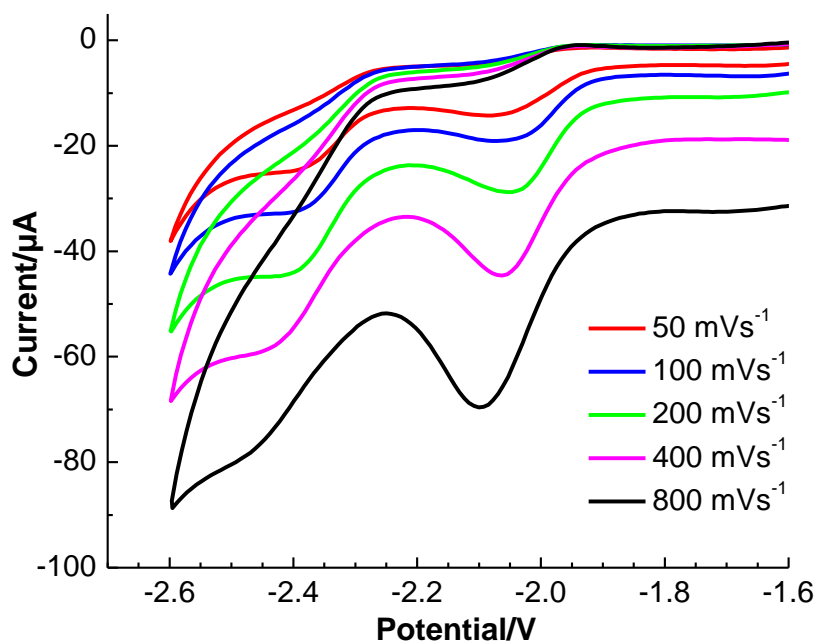


Figure A.38. Scan rate dependency (SRD) study for **13a,a'**.

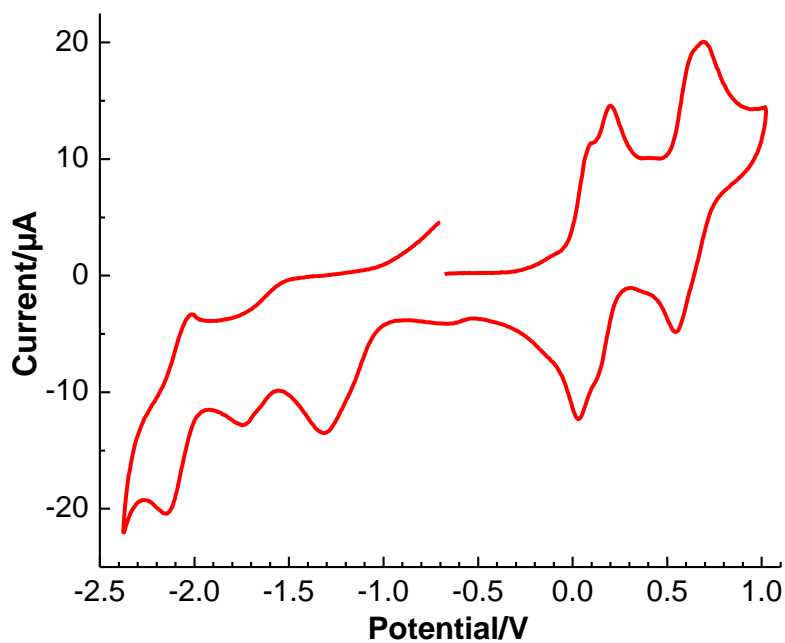


Figure A.39. Cyclic voltammogram of **13b,b'** (wide range) Vs. $\text{Fc}^{0/+}$ (0.4 M ${}^n\text{Bu}_4\text{PF}_6$ in DCM, 200 mVs^{-1}). (the reduction waves at around -1.3 and -1.7 V are due to the presence of oxygen in the solvent).

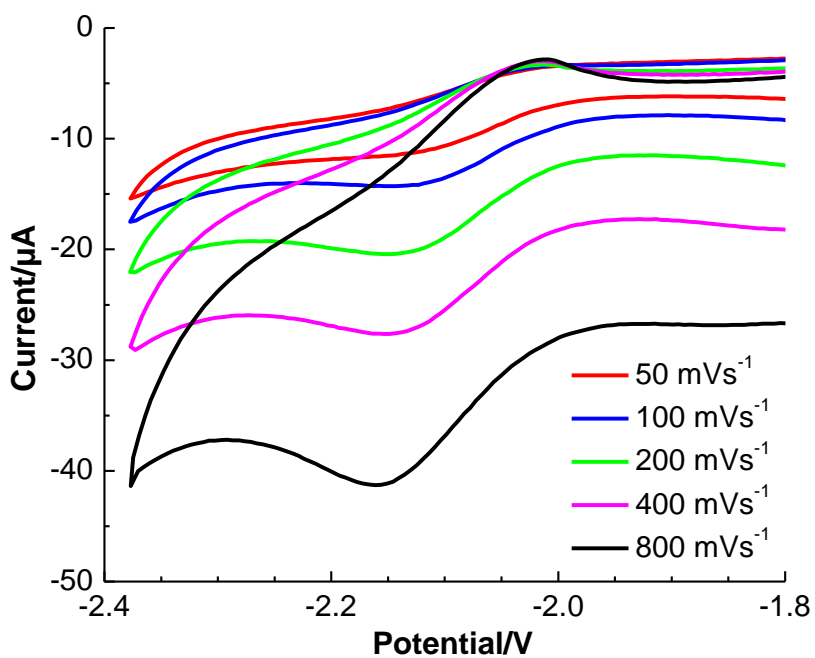


Figure A.40. Scan rate dependency (SRD) study for **13b,b'**.

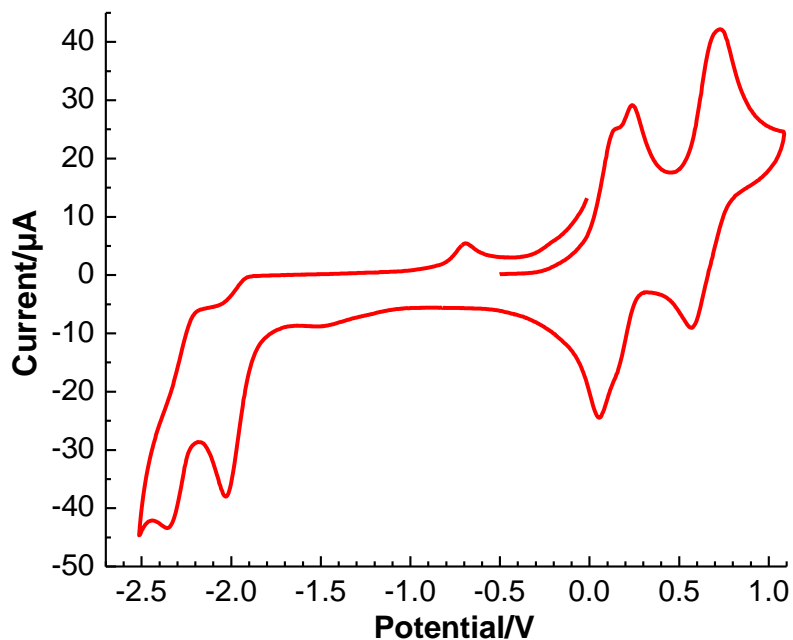


Figure A.41. Cyclic voltammogram of **14a,a'** (wide range) Vs. $\text{Fc}^{0/+}$ ($0.4 \text{ M } n\text{Bu}_4\text{PF}_6$ in DCM, 200 mVs^{-1}) (the small reduction wave at around -1.5 V is due to the presence of the trace of oxygen in the solvent).

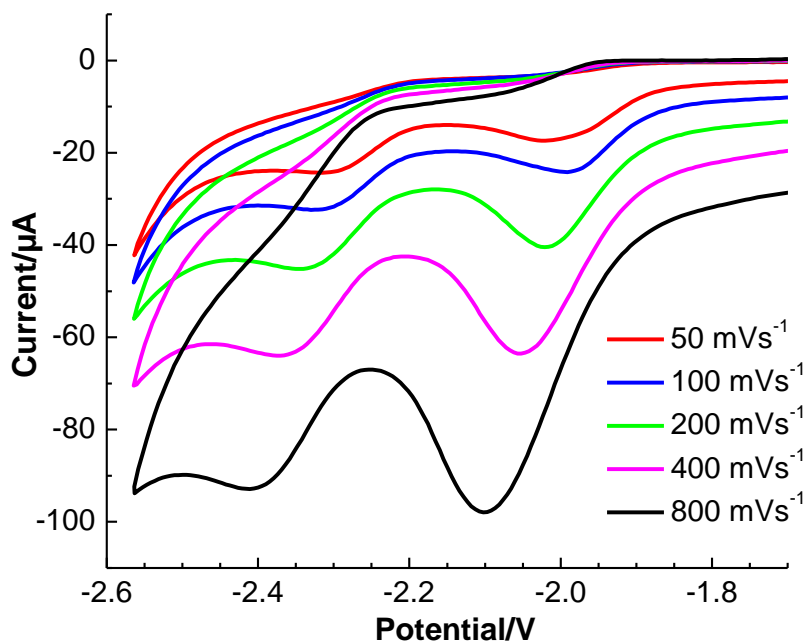


Figure A.42. Scan rate dependency (SRD) study for **14a,a'**.

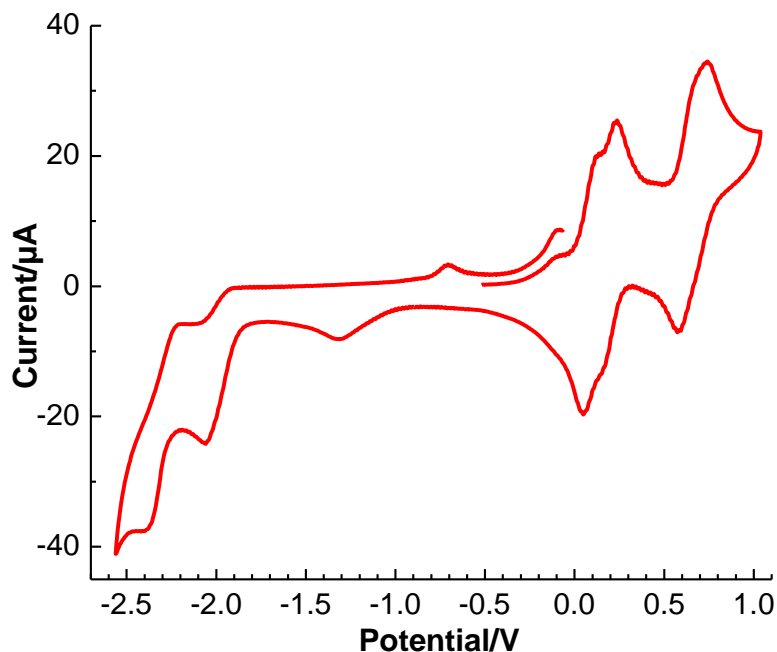


Figure A.43. Cyclic voltammogram of **14b,b'** (wide range) Vs. $\text{Fc}^{0/+}$ (0.4 M $n\text{Bu}_4\text{PF}_6$ in DCM, 200 mVs^{-1}) (the small reduction wave at around -1.3 V is due to the presence of the trace of oxygen in the solvent).

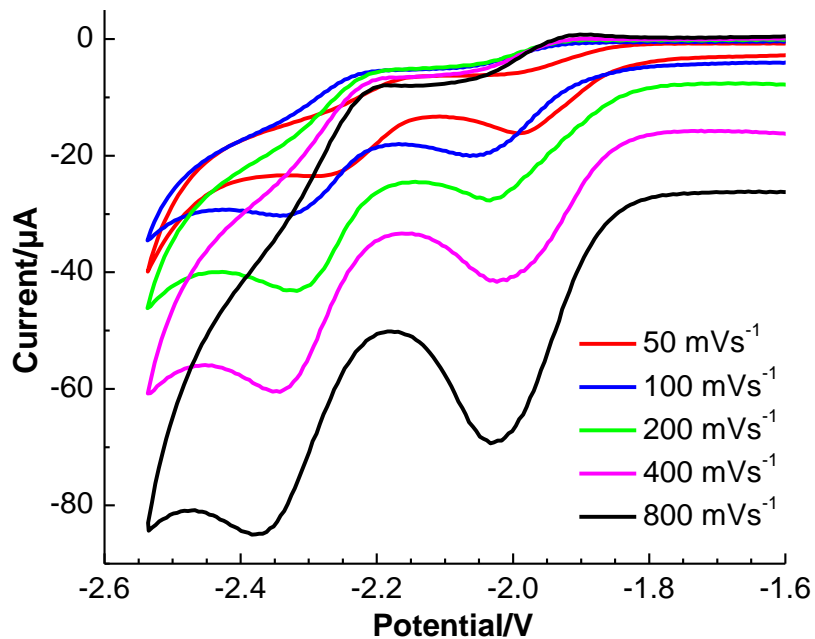


Figure A.44. Scan rate dependency (SRD) study for **14b,b'**.

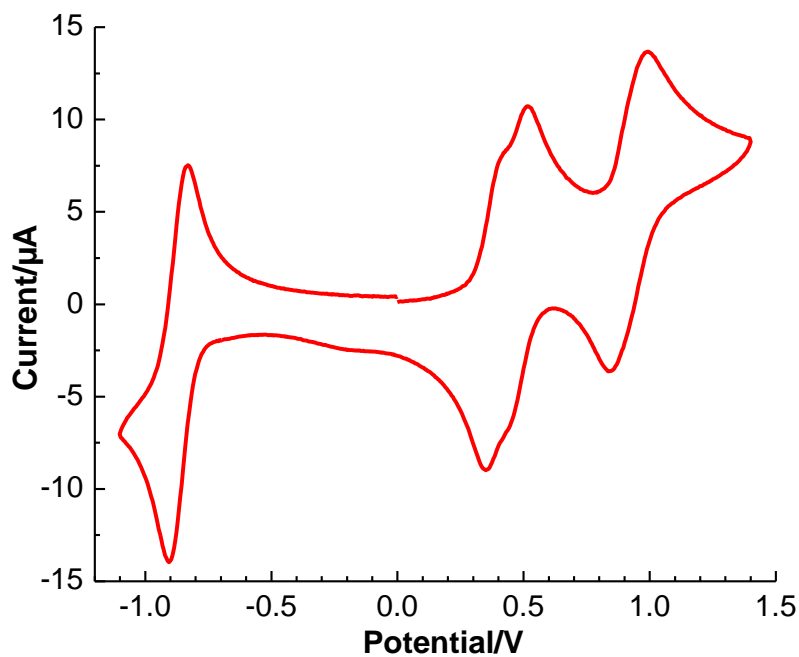


Figure A.45. Cyclic voltammogram of **18** with Cobaltocenium hexafluorophosphate as internal reference (0.4 M ${}^n\text{Bu}_4\text{PF}_6$ in DCM, 100 mVs^{-1}).

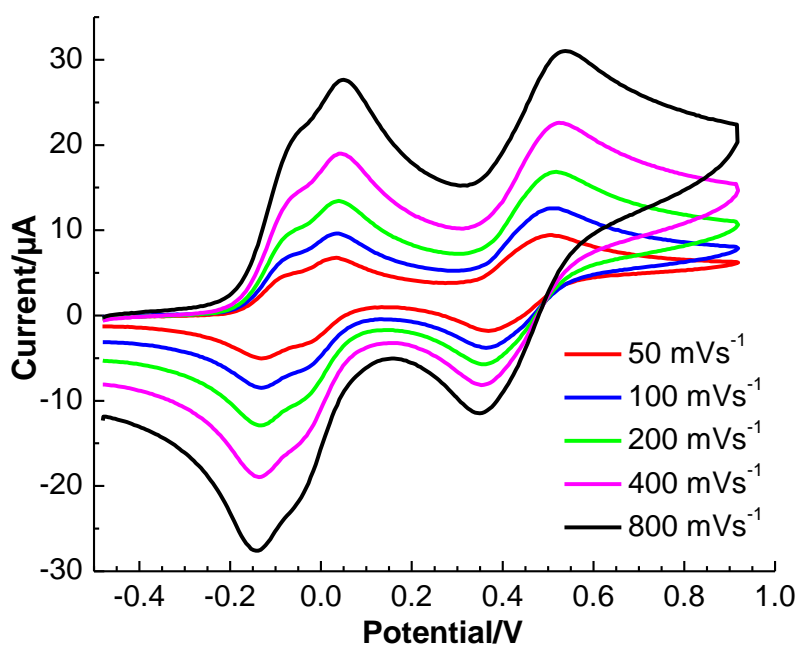


Figure A.46. Scan rate dependency (SRD) study for **18**.

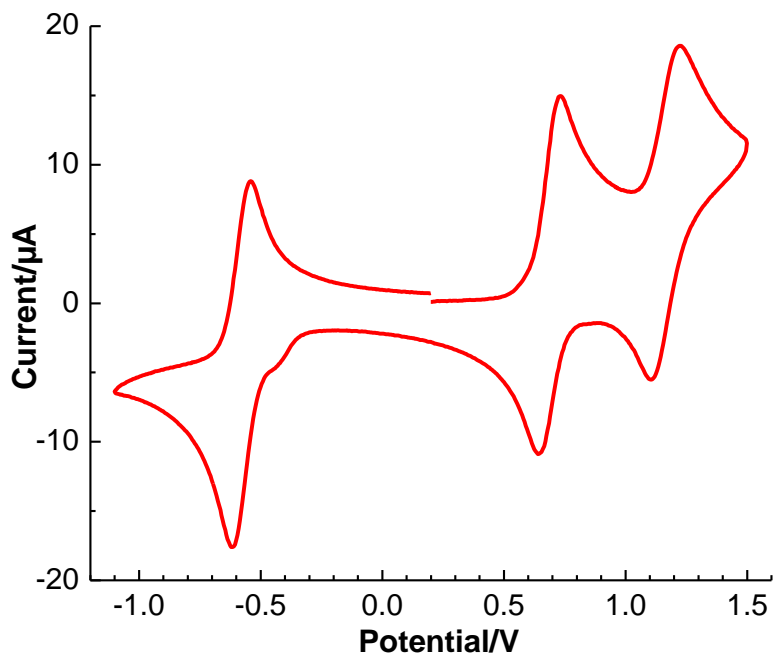


Figure A.47. Cyclic voltammogram of **19a,a'** with Cobaltocenium hexafluorophosphate as internal reference (0.4 M $n\text{Bu}_4\text{PF}_6$ in DCM, 100 mVs^{-1}).

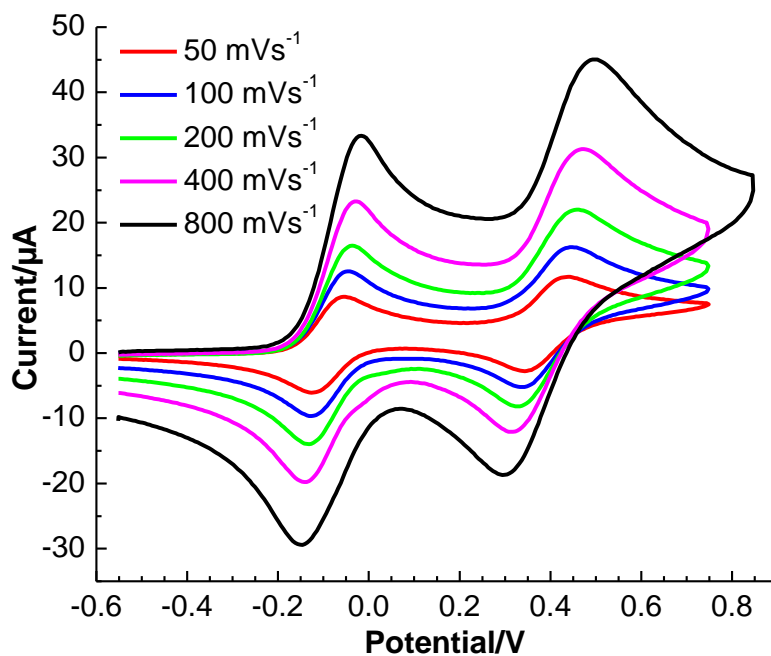


Figure A.48. Scan rate dependency (SRD) study for **19a,a'**.

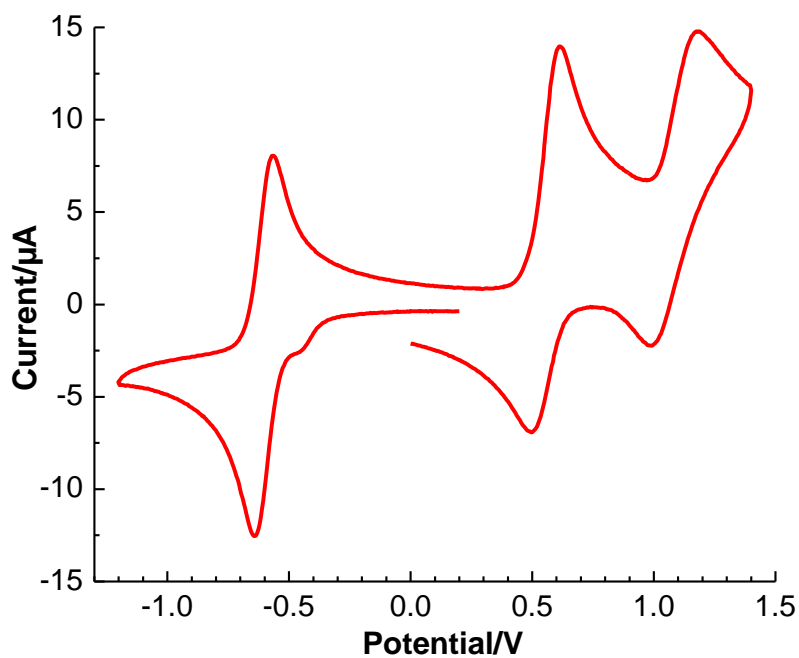


Figure A.49. Cyclic voltammogram of **19b,b'** with Cobaltocenium hexafluorophosphate as internal reference (0.4 M $n\text{Bu}_4\text{PF}_6$ in DCM, 100 mVs^{-1}).

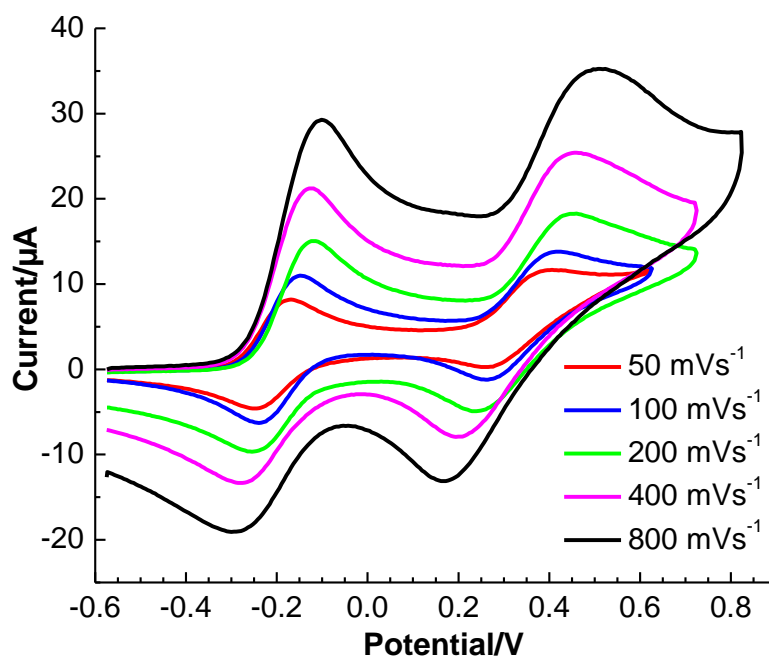


Figure A.50. Scan rate dependency (SRD) study for **19b,b'**.

EPR spectrum

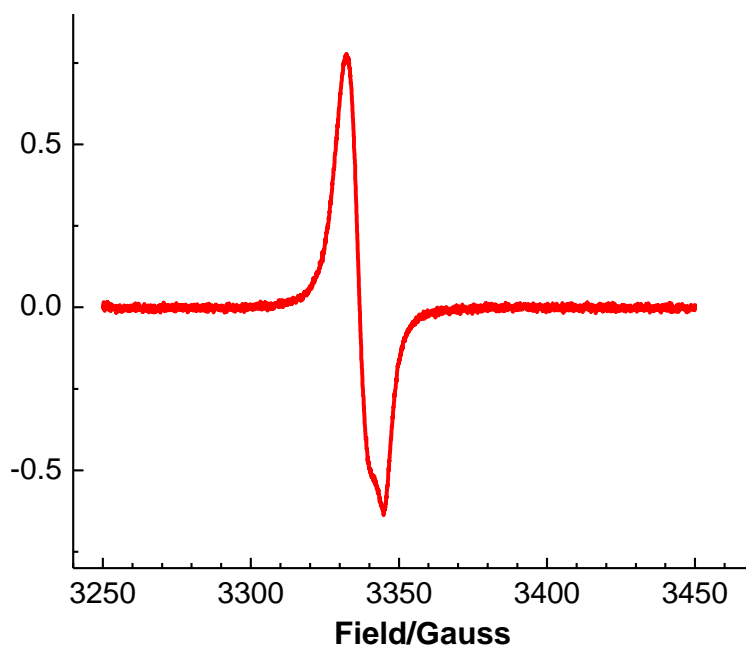


Figure A.51. CW EPR spectra from the reaction mixtures of **4d** with GaCl₃.

Frontier molecular orbitals

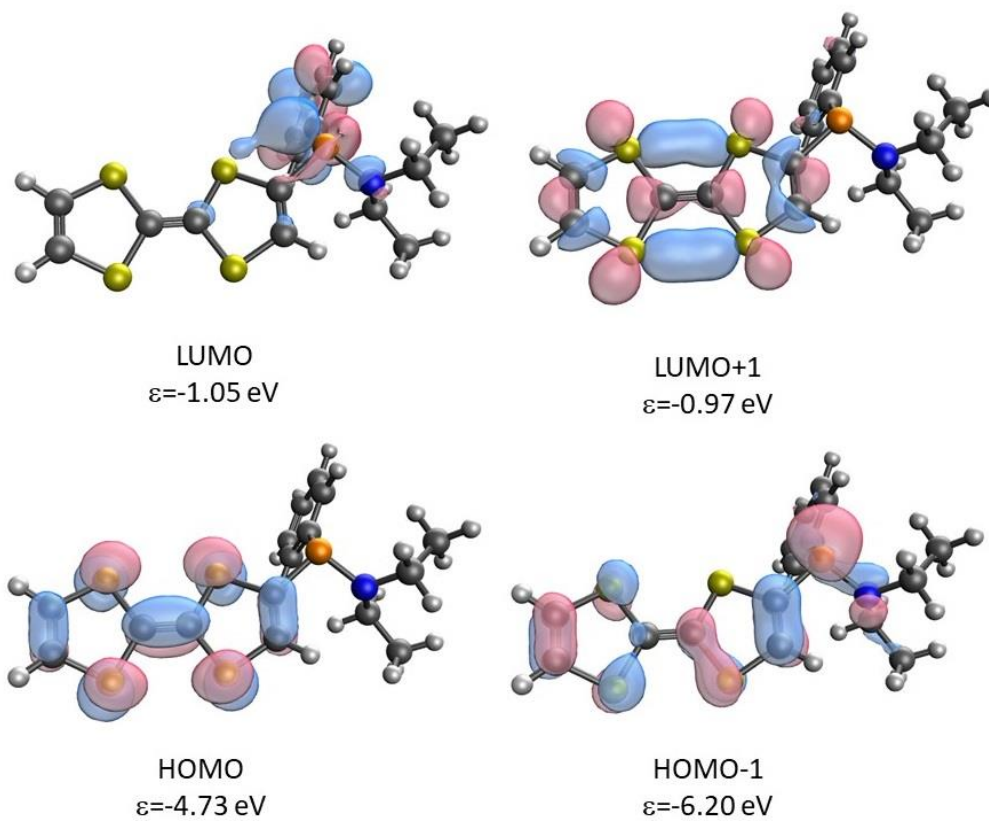


Figure A.52. Kohn-Salm molecular orbitals of **3a** at B3LYP/6-311+G**//M06-2X/6-311+G** level of theory.

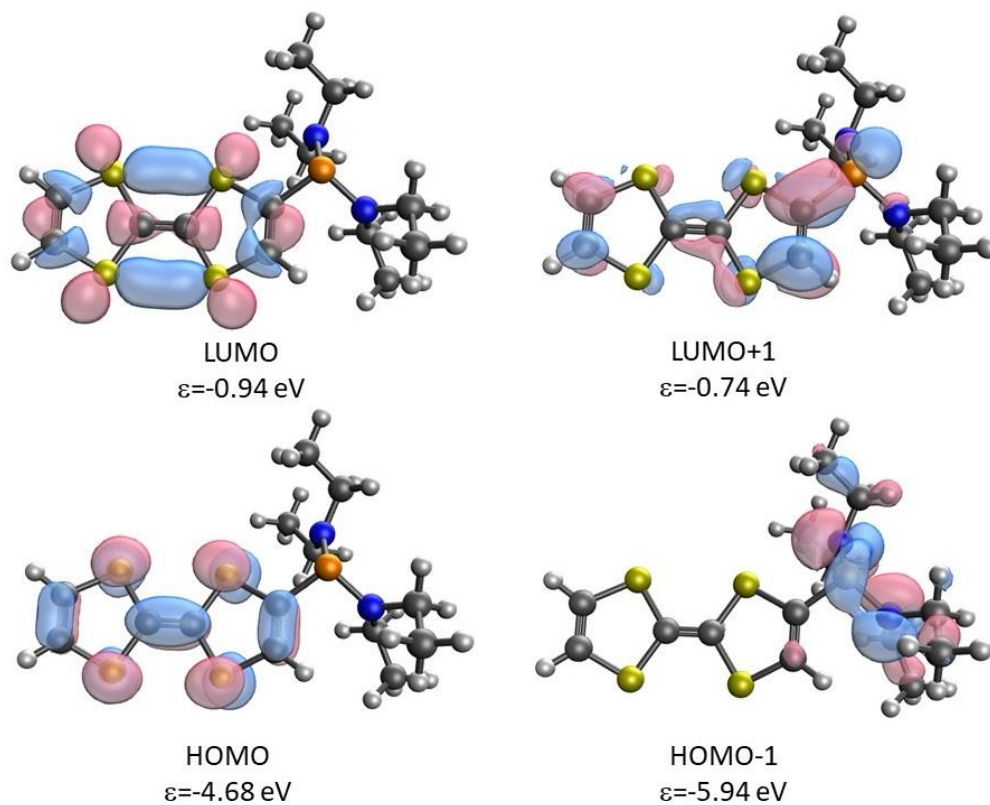


Figure A.53. Kohn-Sham molecular orbitals of **3b** at B3LYP/6-311+G**//M06-2X/6-311+G** level of theory.

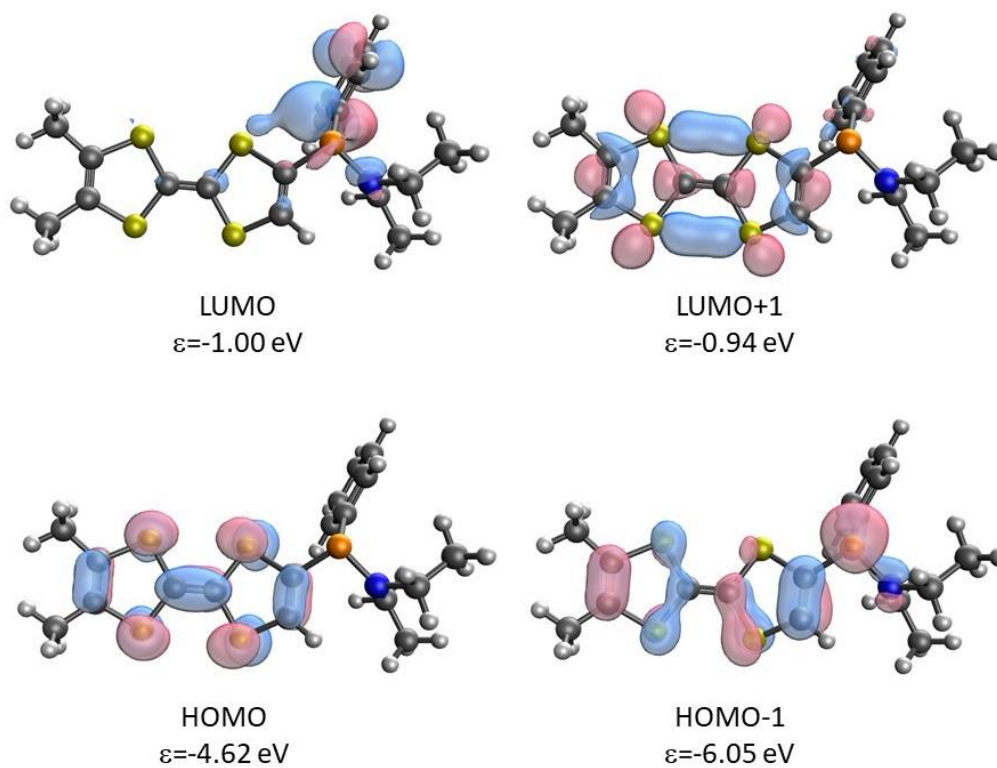


Figure A.54. Kohn-Sham molecular orbitals of **3c** at B3LYP/6-311+G**//M06-2X/6-311+G** level of theory.

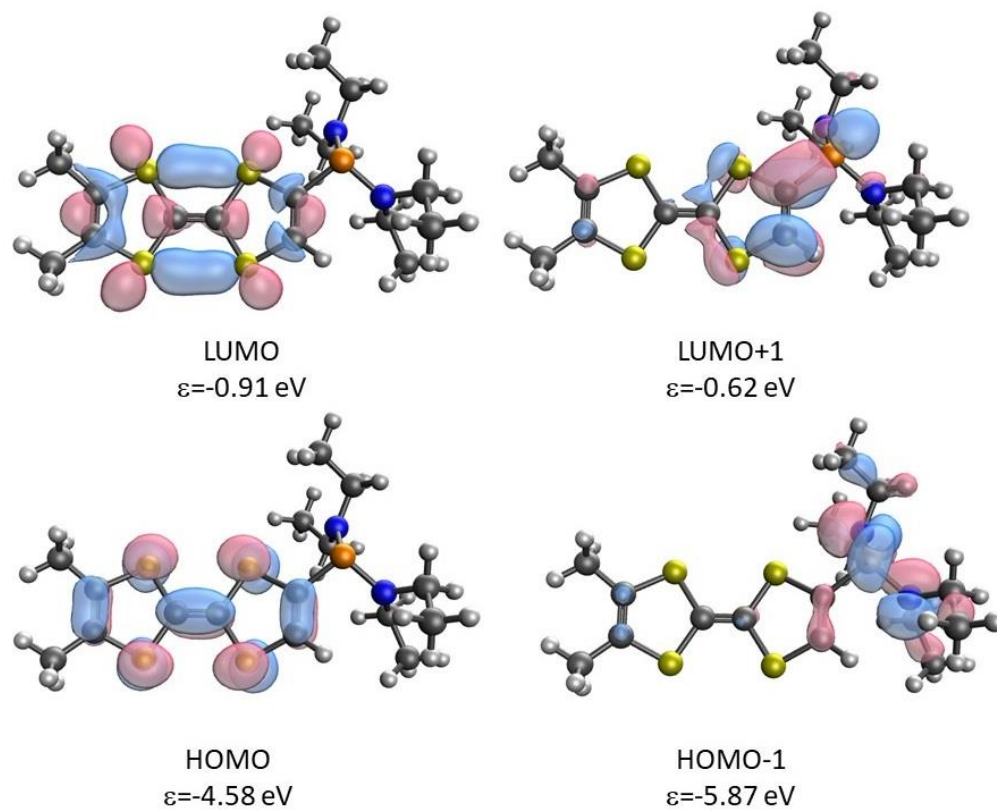
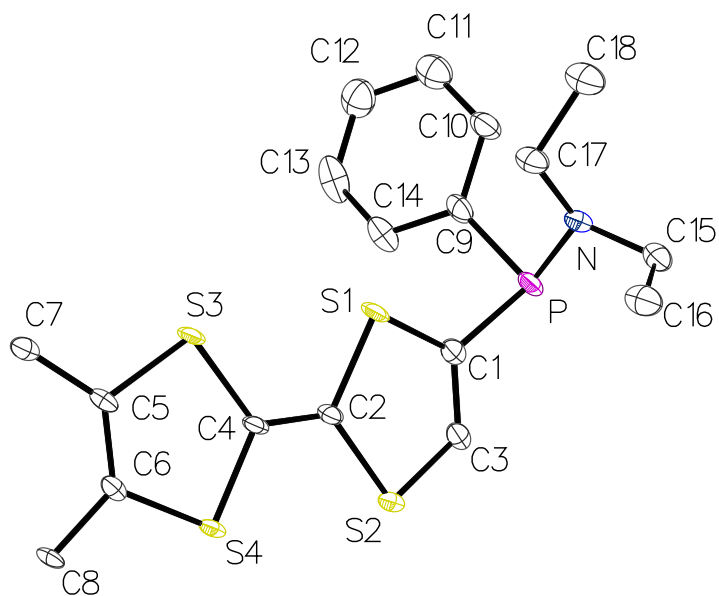


Figure A.55. Kohn-Sham molecular orbitals of **3d** at B3LYP/6-311+G**//M06-2X/6-311+G** level of theory.

Crystal data and structure refinement for compound 3c



Identification code	GSTR711, SHK-297 // GXraycu_6477f
Crystal Habitus	clear yellow plate
Device Type	Bruker D8 Venture
Empirical formula	C ₁₈ H ₂₂ NPS ₄
Moiety formula	C ₁₈ H ₂₂ N P S ₄
Formula weight	411.57
Temperature/K	100.0
Crystal system	monoclinic
Space group	P2 ₁ /n
a/Å	6.8055(3)
b/Å	7.6486(4)
c/Å	37.8273(16)
α/°	90
β/°	92.938(2)
γ/°	90
Volume/Å ³	1966.42(16)
Z	4
ρ _{calc} /cm ³	1.390
μ/mm ⁻¹	5.200
F(000)	864.0

Crystal size/mm ³	0.12 × 0.09 × 0.05
Absorption correction	empirical
Tmin; Tmax	0.4144; 0.7536
Radiation	CuKα (λ = 1.54178)
2θ range for data collection/°	4.678 to 135.438°
Completeness to theta	0.984
Index ranges	-7 ≤ h ≤ 8, -9 ≤ k ≤ 9, -40 ≤ l ≤ 45
Reflections collected	15066
Independent reflections	3506 [R _{int} = 0.0683, R _{sigma} = 0.0534]
Data/restraints/parameters	3506/6/221
Goodness-of-fit on F ²	1.066
Final R indexes [I >= 2σ (I)]	R ₁ = 0.0620, wR ₂ = 0.1725
Final R indexes [all data]	R ₁ = 0.0720, wR ₂ = 0.1852
Largest diff. peak/hole / e Å ⁻³	0.63/-0.78

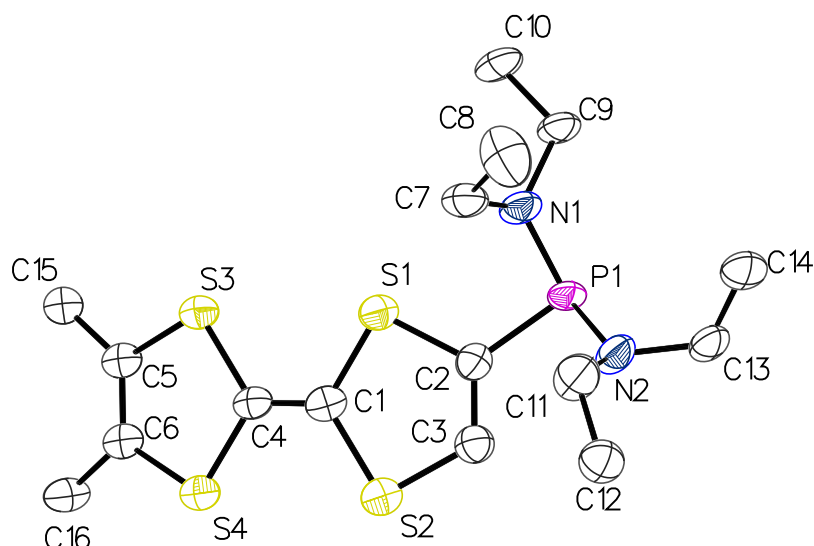
Bond Lengths

Atom	Atom	Length/Å	Atom	Atom	Length/Å
S1	C1	1.765(4)	C1	C3	1.329(6)
S1	C2	1.762(4)	C2	C4	1.340(6)
S2	C2	1.770(4)	C5	C6	1.336(6)
S2	C3	1.752(4)	C5	C7	1.501(6)
S3	C4	1.754(4)	C6	C8	1.493(5)
S3	C5	1.763(4)	C9	C10	1.410(6)
S4	C4	1.756(4)	C9	C14	1.399(6)
S4	C6	1.763(4)	C10	C11	1.388(7)
P	N	1.695(4)	C11	C12	1.386(7)
P	C1	1.833(4)	C12	C13	1.386(7)
P	C9	1.832(5)	C13	C14	1.374(7)
N	C15	1.479(6)	C15	C16	1.514(7)
N	C17	1.458(6)	C17	C18	1.523(6)

Bond Angles

Atom	Atom	Atom	Angle/°	Atom	Atom	Atom	Angle/°
C2	S1	C1	95.58(19)	C2	C4	S3	122.5(3)
C3	S2	C2	94.06(19)	C2	C4	S4	123.2(3)
C4	S3	C5	95.56(19)	C6	C5	S3	117.3(3)
C4	S4	C6	95.64(19)	C6	C5	C7	127.5(4)
N	P	C1	107.0(2)	C7	C5	S3	115.2(3)
N	P	C9	101.15(19)	C5	C6	S4	117.1(3)
C9	P	C1	100.58(18)	C5	C6	C8	127.7(4)
C15	N	P	115.5(3)	C8	C6	S4	115.2(3)
C17	N	P	123.9(3)	C10	C9	P	120.7(3)
C17	N	C15	113.9(4)	C14	C9	P	121.1(3)
S1	C1	P	123.6(2)	C14	C9	C10	117.9(4)
C3	C1	S1	115.7(3)	C11	C10	C9	120.6(4)
C3	C1	P	120.3(3)	C12	C11	C10	120.6(5)
S1	C2	S2	114.0(2)	C13	C12	C11	118.8(5)
C4	C2	S1	123.1(3)	C14	C13	C12	121.5(4)
C4	C2	S2	122.9(3)	C13	C14	C9	120.5(4)
C1	C3	S2	119.7(3)	N	C15	C16	113.9(4)

Crystal data and structure refinement for compound 3d



Identification code	GSTR776, SHK-296 // GXraycu_6476f
Crystal Habitus	clear yellow plate
Device Type	Bruker D8 Venture
Empirical formula	$C_{16}H_{27}N_2PS_4$
Moiety formula	$C_{16} H_{27} N_2 P S_4$
Formula weight	406.60
Temperature/K	100.0
Crystal system	triclinic
Space group	P-1
a/Å	7.7693(9)
b/Å	13.0474(15)
c/Å	20.686(2)
$\alpha/^\circ$	101.038(7)
$\beta/^\circ$	90.351(6)
$\gamma/^\circ$	91.520(7)
Volume/Å ³	2057.3(4)
Z	4
$\rho_{\text{calc}}/\text{cm}^3$	1.313
μ/mm^{-1}	4.970
F(000)	864.0
Crystal size/mm ³	0.24 × 0.19 × 0.05
Absorption correction	empirical
Tmin; Tmax	0.2751; 0.7536

Radiation	CuK α ($\lambda = 1.54178$)
2 θ range for data collection/ $^\circ$	4.352 to 135.48 $^\circ$
Completeness to theta	0.993
Index ranges	$-9 \leq h \leq 8, -15 \leq k \leq 15, -24 \leq l \leq 24$
Reflections collected	47595
Independent reflections	7409 [$R_{\text{int}} = 0.1221, R_{\text{sigma}} = 0.0682$]
Data/restraints/parameters	7409/444/427
Goodness-of-fit on F^2	2.838
Final R indexes [$ I \geq 2\sigma(I)$]	$R_1 = 0.2465, wR_2 = 0.5886$
Final R indexes [all data]	$R_1 = 0.2911, wR_2 = 0.6285$
Largest diff. peak/hole / e \AA^{-3}	3.61/-3.09

Bond Lengths

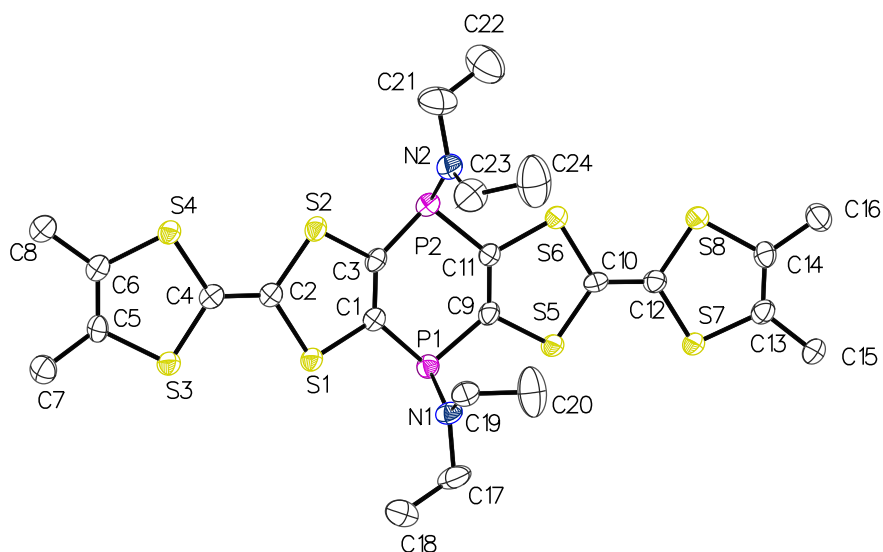
Atom	Atom	Length/ \AA	Atom	Atom	Length/ \AA
S1	C1	1.764(16)	N1	C9	1.469(19)
S1	C2	1.771(16)	N2	C11	1.47(2)
S2	C1	1.787(16)	N2	C13	1.49(2)
S2	C3	1.774(16)	C1	C4	1.29(2)
S3	C4	1.756(14)	C2	C3	1.32(2)
S3	C5	1.768(15)	C5	C6	1.320(19)
S4	C4	1.764(14)	C5	C15	1.47(2)
S4	C6	1.754(15)	C6	C16	1.48(2)
P1	N1	1.671(13)	C7	C8	1.60(3)
P1	N2	1.675(13)	C9	C10	1.485(19)
P1	C2	1.828(17)	C11	C12	1.48(2)
N1	C7	1.39(2)	C13	C14	1.49(2)

Bond Angles

Atom	Atom	Atom	Angle/ $^\circ$	Atom	Atom	Atom	Angle/ $^\circ$
C1	S1	C2	96.7(7)	C3	C2	S1	116.1(13)
C3	S2	C1	94.9(7)	C3	C2	P1	125.0(13)
C4	S3	C5	96.7(7)	C2	C3	S2	118.8(13)
C6	S4	C4	95.8(7)	S3	C4	S4	112.6(8)
N1	P1	N2	115.3(7)	C1	C4	S3	123.7(12)
N1	P1	C2	99.4(7)	C1	C4	S4	123.6(12)
N2	P1	C2	97.7(7)	C6	C5	S3	115.8(11)
C7	N1	P1	126.6(11)	C6	C5	C15	128.4(14)
C7	N1	C9	114.3(13)	C15	C5	S3	115.7(10)
C9	N1	P1	116.5(11)	C5	C6	S4	118.5(12)

C11	N2	P1	123.4(12)	C5	C6	C16	126.6(14)
C11	N2	C13	114.4(14)	C16	C6	S4	114.8(10)
C13	N2	P1	114.4(11)	N1	C7	C8	114.5(15)
S1	C1	S2	112.5(9)	N1	C9	C10	114.8(14)
C4	C1	S1	123.4(12)	N2	C11	C12	116.9(16)
C4	C1	S2	123.8(13)	N2	C13	C14	116.9(15)
S1	C2	P1	118.2(9)				

Crystal data and structure refinement for compound *cis-11d*



Identification code	GSTR689, SHK-150 // GXray6209f
Crystal Habitus	clear orange plate
Device Type	Bruker X8-KappaApexII
Empirical formula	$C_{49}H_{66}Cl_2N_4P_4S_{16}$
Moiety formula	$C\ H_2\ Cl_2, 2(C_{24}\ H_{32}\ N_2\ P_2\ S_8)$
Formula weight	1418.79
Temperature/K	100
Crystal system	monoclinic
Space group	$P2_1/n$
$a/\text{\AA}$	15.909(2)
$b/\text{\AA}$	11.9462(15)
$c/\text{\AA}$	17.630(2)
$\alpha/^\circ$	90
$\beta/^\circ$	107.950(3)
$\gamma/^\circ$	90
Volume/ \AA^3	3187.4(7)
Z	2
$\rho_{\text{calc}}/\text{cm}^3$	1.478
μ/mm^{-1}	0.765
F(000)	1476.0
Crystal size/ mm^3	$0.18 \times 0.1 \times 0.05$
Absorption correction	empirical

Tmin; Tmax	0.5748; 0.7461
Radiation	MoK α (λ = 0.71073)
2 θ range for data collection/ $^{\circ}$	4.554 to 55.996 $^{\circ}$
Completeness to theta	0.997
Index ranges	-19 \leq h \leq 21, -15 \leq k \leq 15, -23 \leq l \leq 14
Reflections collected	33038
Independent reflections	7663 [R _{int} = 0.1087, R _{sigma} = 0.1051]
Data/restraints/parameters	7663/6/360
Goodness-of-fit on F ²	1.060
Final R indexes [$I \geq 2\sigma(I)$]	R ₁ = 0.0826, wR ₂ = 0.1757
Final R indexes [all data]	R ₁ = 0.1361, wR ₂ = 0.2018
Largest diff. peak/hole / e \AA^{-3}	1.00/-0.50

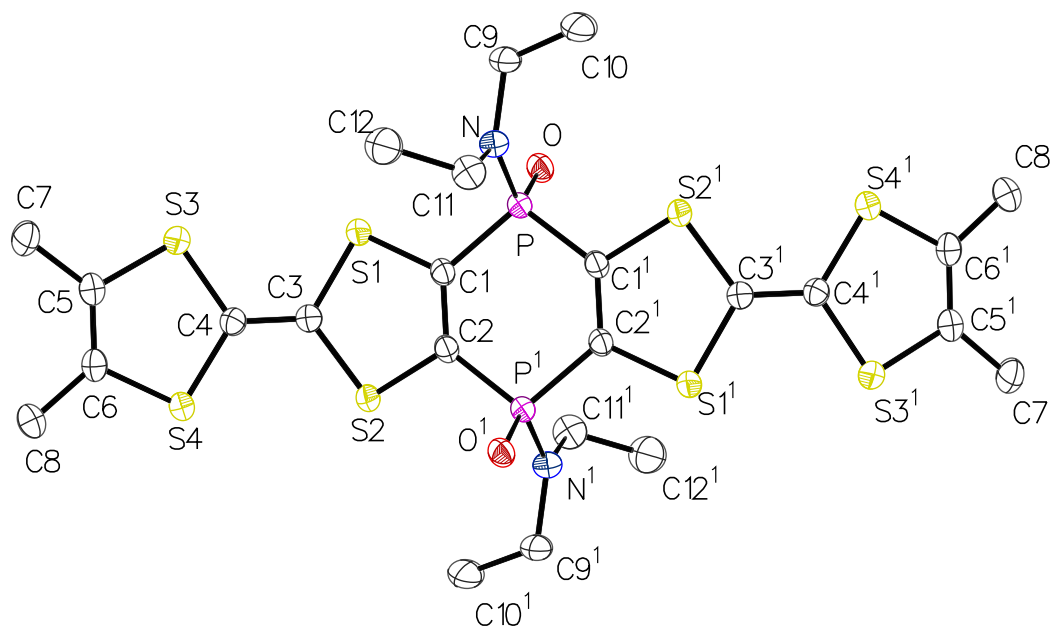
Bond Lengths

Atom	Atom	Length/ \AA	Atom	Atom	Length/ \AA
Cl1	C25	1.726(17)	P2	N2	1.657(5)
Cl2	C25	1.722(18)	P2	C3	1.819(5)
S1	C1	1.762(5)	P2	C11	1.816(5)
S1	C2	1.763(5)	N1	C17	1.466(7)
S2	C2	1.760(5)	N1	C19	1.451(7)
S2	C3	1.769(5)	N2	C21	1.479(8)
S3	C4	1.751(5)	N2	C23	1.465(8)
S3	C5	1.750(5)	C1	C3	1.342(7)
S4	C4	1.751(5)	C2	C4	1.338(8)
S4	C6	1.753(6)	C5	C6	1.353(8)
S5	C9	1.753(5)	C5	C7	1.501(8)
S5	C10	1.750(5)	C6	C8	1.498(7)
S6	C10	1.759(5)	C9	C11	1.343(7)
S6	C11	1.770(5)	C10	C12	1.358(8)
S7	C12	1.749(5)	C13	C14	1.338(8)
S7	C13	1.759(6)	C13	C15	1.503(7)
S8	C12	1.747(5)	C14	C16	1.501(8)
S8	C14	1.758(6)	C17	C18	1.473(10)
P1	N1	1.684(5)	C19	C20	1.474(8)
P1	C1	1.821(5)	C21	C22	1.429(10)
P1	C9	1.827(5)	C23	C24	1.455(10)

Bond Angles

Atom	Atom	Atom	Angle/°	Atom	Atom	Atom	Angle/°
Cl2	C25	Cl1	111.2(8)	C2	C4	S3	122.8(4)
C1	S1	C2	95.3(3)	C2	C4	S4	123.7(4)
C2	S2	C3	95.0(2)	C6	C5	S3	116.5(4)
C5	S3	C4	96.1(3)	C6	C5	C7	126.8(5)
C4	S4	C6	95.8(3)	C7	C5	S3	116.5(4)
C10	S5	C9	95.0(3)	C5	C6	S4	116.9(4)
C10	S6	C11	95.0(2)	C5	C6	C8	126.2(5)
C12	S7	C13	94.7(3)	C8	C6	S4	116.8(4)
C12	S8	C14	95.1(3)	S5	C9	P1	112.3(3)
N1	P1	C1	100.3(2)	C11	C9	S5	118.0(4)
N1	P1	C9	104.0(2)	C11	C9	P1	129.5(4)
C1	P1	C9	98.5(2)	S5	C10	S6	114.4(3)
N2	P2	C3	103.2(2)	C12	C10	S5	123.6(4)
N2	P2	C11	104.2(2)	C12	C10	S6	122.0(4)
C11	P2	C3	97.7(2)	S6	C11	P2	113.5(3)
C17	N1	P1	119.2(4)	C9	C11	S6	116.3(4)
C19	N1	P1	124.1(4)	C9	C11	P2	129.4(4)
C19	N1	C17	116.6(5)	S8	C12	S7	114.5(3)
C21	N2	P2	119.3(5)	C10	C12	S7	122.7(4)
C23	N2	P2	123.8(4)	C10	C12	S8	122.8(4)
C23	N2	C21	115.9(5)	C14	C13	S7	117.5(4)
S1	C1	P1	113.2(3)	C14	C13	C15	126.8(5)
C3	C1	S1	117.1(4)	C15	C13	S7	115.6(4)
C3	C1	P1	129.7(4)	C13	C14	S8	116.7(4)
S2	C2	S1	113.4(3)	C13	C14	C16	127.4(5)
C4	C2	S1	122.8(4)	C16	C14	S8	115.9(4)
C4	C2	S2	123.8(4)	N1	C17	C18	113.8(6)
S2	C3	P2	113.8(3)	N1	C19	C20	114.9(5)
C1	C3	S2	116.8(4)	C22	C21	N2	114.9(7)
C1	C3	P2	129.2(4)	C24	C23	N2	115.6(7)
S3	C4	S4	113.5(3)				

Crystal data and structure refinement for compound *trans*-12a



Identification code	GSTR782, SHK-499 // GXray7037
Crystal Habitus	clear brown plate
Device Type	STOE STADIVARI
Empirical formula	C ₂₅ H ₃₂ Cl ₂ N ₂ O ₂ P ₂ S ₈
Moiety formula	C H2 Cl2, C24 H32 N2 O2 P2 S8
Formula weight	781.84
Temperature/K	100
Crystal system	monoclinic
Space group	C2/c
a/Å	23.9063(4)
b/Å	7.61506(10)
c/Å	19.2661(3)
α/°	90
β/°	102.0920(10)
γ/°	90
Volume/Å ³	3429.53(9)
Z	4
ρ _{calc} /cm ³	1.514
μ/mm ⁻¹	7.374
F(000)	1616.0
Crystal size/mm ³	0.075 × 0.07 × 0.02
Absorption correction	multi-scan

Tmin; Tmax	0.4930; 0.6081
Radiation	CuK α (λ = 1.54186)
2 θ range for data collection/ $^\circ$	7.564 to 135.468 $^\circ$
Completeness to theta	1.000
Index ranges	-26 \leq h \leq 28, -7 \leq k \leq 9, -22 \leq l \leq 22
Reflections collected	87125
Independent reflections	3093 [R_{int} = 0.0524, R_{sigma} = 0.0121]
Data/restraints/parameters	3093/238/231
Goodness-of-fit on F^2	1.038
Final R indexes [$I \geq 2\sigma(I)$]	R_1 = 0.0352, wR_2 = 0.0917
Final R indexes [all data]	R_1 = 0.0400, wR_2 = 0.0954
Largest diff. peak/hole / e \AA^{-3}	0.70/-0.46

Bond Lengths

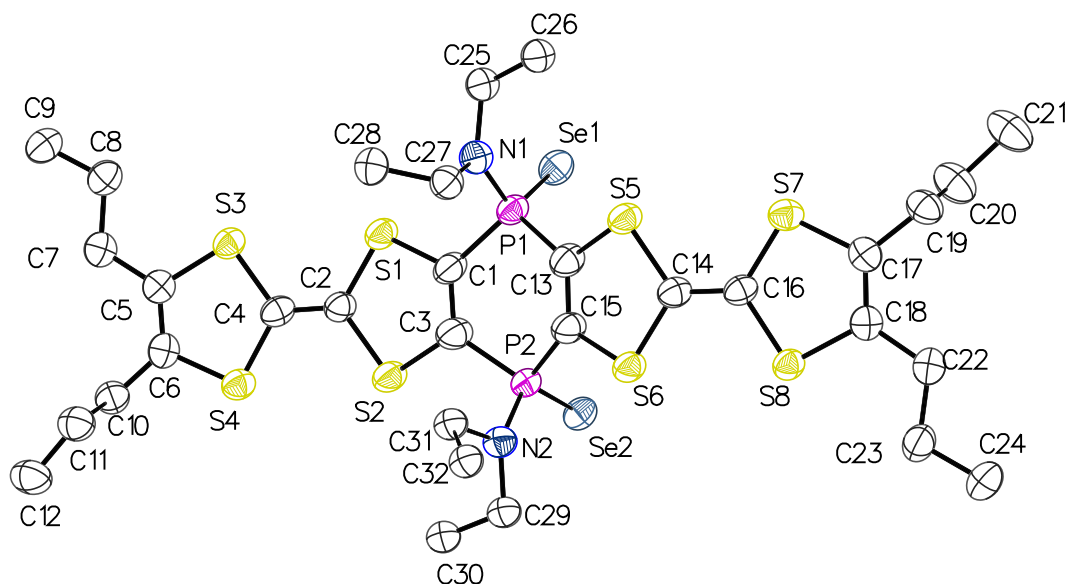
Atom	Atom	Length/ \AA	Atom	Atom	Length/ \AA
Cl1	C13	1.708(8)	P	N	1.629(2)
Cl2	C13	1.728(9)	P	C1	1.800(2)
Cl1S	C13S	1.702(10)	P	C2 ¹	1.802(2)
Cl2S	C13S	1.703(10)	N	C9	1.476(3)
S1	C1	1.761(2)	N	C11	1.481(3)
S1	C3	1.760(2)	C1	C2	1.347(3)
S2	C2	1.770(2)	C3	C4	1.345(3)
S2	C3	1.757(2)	C5	C6	1.332(4)
S3	C4	1.749(2)	C5	C7	1.500(4)
S3	C5	1.767(2)	C6	C8	1.492(3)
S4	C4	1.750(2)	C9	C10	1.502(4)
S4	C6	1.766(2)	C11	C12	1.525(4)
P	O	1.4905(17)			

Bond Angles

Atom	Atom	Atom	Angle/ $^\circ$	Atom	Atom	Atom	Angle/ $^\circ$
Cl1	C13	Cl2	110.4(6)	S2	C2	P ¹	115.06(13)
Cl1S	C13S	Cl2S	98.6(18)	C1	C2	S2	116.59(18)
C3	S1	C1	93.39(11)	C1	C2	P ¹	128.34(18)
C3	S2	C2	93.08(11)	S2	C3	S1	113.39(13)
C4	S3	C5	95.53(12)	C4	C3	S1	122.41(19)
C4	S4	C6	95.39(12)	C4	C3	S2	124.07(19)
O	P	N	113.18(10)	S3	C4	S4	113.89(13)

O	P	C1	111.10(11)	C3	C4	S3	122.43(19)
O	P	C2 ¹	112.67(10)	C3	C4	S4	123.68(19)
N	P	C1	108.28(11)	C6	C5	S3	116.73(19)
N	P	C2 ¹	107.61(11)	C6	C5	C7	128.7(2)
C1	P	C2 ¹	103.45(11)	C7	C5	S3	114.51(19)
C9	N	P	121.18(18)	C5	C6	S4	117.14(19)
C9	N	C11	118.2(2)	C5	C6	C8	128.4(2)
C11	N	P	119.98(17)	C8	C6	S4	114.46(19)
S1	C1	P	115.20(13)	N	C9	C10	114.2(2)
C2	C1	S1	117.00(18)	N	C11	C12	112.5(2)
C2	C1	P	127.13(18)				

Crystal data and structure refinement for compound *cis-14b*



Identification code	GSTR783, SHK-474 // GXray7038
Crystal Habitus	clear dark red block
Device Type	STOE STADIVARI
Empirical formula	$C_{32}H_{48}N_2P_2S_8Se_2$
Moiety formula	$C_{32} H_{48} N_2 P_2 S_8 Se_2$
Formula weight	937.06
Temperature/K	100
Crystal system	monoclinic
Space group	$P2_1/c$
a/Å	25.4912(5)
b/Å	7.70630(10)
c/Å	21.8491(5)
$\alpha/^\circ$	90.00
$\beta/^\circ$	108.0643(16)
$\gamma/^\circ$	90.00
Volume/Å ³	4080.54(14)
Z	4
ρ_{calc}/cm^3	1.525
μ/mm^{-1}	7.03
F(000)	1920.0
Crystal size/mm ³	0.15 × 0.13 × 0.1
Absorption correction	multi-scan
Tmin; Tmax	0.1542; 0.3100

Radiation	CuK α ($\lambda = 1.54186$)
2 θ range for data collection/ $^\circ$	7.296 to 135.474 $^\circ$
Completeness to theta	0.999
Index ranges	-30 \leq h \leq 28, -8 \leq k \leq 9, -26 \leq l \leq 24
Reflections collected	63776
Independent reflections	7388 [$R_{\text{int}} = 0.0543$, $R_{\text{sigma}} = 0.0255$]
Data/restraints/parameters	7388/230/561
Goodness-of-fit on F^2	1.183
Final R indexes [$I \geq 2\sigma(I)$]	$R_1 = 0.0697$, $wR_2 = 0.1759$
Final R indexes [all data]	$R_1 = 0.0748$, $wR_2 = 0.1790$
Largest diff. peak/hole / e \AA^{-3}	1.00/-0.72

Bond Lengths

Atom	Atom	Length/ \AA	Atom	Atom	Length/ \AA
Se1	P1	2.081(2)	N1	C27	1.461(10)
Se1S	P1S	2.07(2)	N1S	C25S	1.482(10)
Se2	P2	2.079(2)	N1S	C27S	1.484(10)
Se2S	P2S	2.084(10)	N2	C29	1.477(7)
S1	C1	1.753(6)	N2	C31	1.487(8)
S1	C2	1.745(6)	N2S	C29S	1.485(10)
S2	C2	1.778(6)	N2S	C31S	1.52(3)
S2	C3	1.759(7)	C1	C3	1.344(9)
S3	C4	1.759(6)	C2	C4	1.334(8)
S3	C5	1.762(6)	C5	C6	1.344(8)
S4	C4	1.748(6)	C5	C7	1.502(8)
S4	C6	1.758(6)	C6	C10	1.504(8)
S5	C13	1.739(7)	C7	C8	1.510(9)
S5	C14	1.780(6)	C8	C9	1.523(9)
S6	C14	1.744(6)	C10	C11	1.530(9)
S6	C15	1.772(6)	C11	C12	1.523(9)
S7	C16	1.740(6)	C13	C15	1.357(9)
S7	C17	1.757(7)	C14	C16	1.338(8)
S8	C16	1.756(6)	C17	C18	1.345(9)
S8	C18	1.753(6)	C17	C19	1.507(8)
P1	N1	1.651(6)	C18	C22	1.507(8)
P1	C1	1.806(7)	C19	C20	1.522(10)
P1	C13	1.813(6)	C20	C21	1.526(10)
P1S	N1S	1.65(5)	C22	C23	1.515(9)
P1S	C1	1.963(17)	C23	C24	1.507(9)

P1S	C13	2.074(18)	C25	C26	1.481(11)
P2	N2	1.652(7)	C25S	C26S	1.63(9)
P2	C3	1.824(7)	C27	C28	1.526(11)
P2	C15	1.793(6)	C27S	C28S	1.495(10)
P2S	N2S	1.60(2)	C29	C30	1.507(12)
P2S	C3	2.019(10)	C29S	C30S	1.45(4)
P2S	C15	2.020(10)	C31	C32	1.516(8)
N1	C25	1.480(9)	C31S	C32S	1.511(10)

Bond Angles

Atom	Atom	Atom	Angle/°	Atom	Atom	Atom	Angle/°
C2	S1	C1	95.3(3)	S2	C3	P2	115.4(4)
C3	S2	C2	93.9(3)	S2	C3	P2S	106.4(4)
C4	S3	C5	95.8(3)	C1	C3	S2	117.9(5)
C4	S4	C6	95.6(3)	C1	C3	P2	126.2(5)
C13	S5	C14	93.6(3)	C1	C3	P2S	125.8(6)
C14	S6	C15	93.0(3)	S4	C4	S3	114.4(3)
C16	S7	C17	95.5(3)	C2	C4	S3	122.5(5)
C18	S8	C16	95.4(3)	C2	C4	S4	123.1(4)
N1	P1	Se1	115.2(2)	C6	C5	S3	116.5(5)
N1	P1	C1	105.0(3)	C6	C5	C7	125.5(5)
N1	P1	C13	105.7(3)	C7	C5	S3	118.0(4)
C1	P1	Se1	112.8(2)	C5	C6	S4	117.7(5)
C1	P1	C13	101.5(3)	C5	C6	C10	127.0(5)
C13	P1	Se1	115.1(2)	C10	C6	S4	115.3(4)
Se1S	P1S	C13	132.6(8)	C5	C7	C8	117.0(5)
N1S	P1S	Se1S	118.9(16)	C7	C8	C9	112.6(5)
N1S	P1S	C1	85.4(17)	C6	C10	C11	113.5(5)
N1S	P1S	C13	83.4(18)	C12	C11	C10	111.0(6)
C1	P1S	Se1S	131.8(9)	S5	C13	P1	117.0(4)
C1	P1S	C13	87.9(7)	S5	C13	P1S	110.9(5)
N2	P2	Se2	115.5(2)	C15	C13	S5	116.6(5)
N2	P2	C3	106.0(4)	C15	C13	P1	126.4(5)
N2	P2	C15	102.0(3)	C15	C13	P1S	115.2(6)
C3	P2	Se2	115.8(3)	S6	C14	S5	113.4(3)
C15	P2	Se2	115.1(3)	C16	C14	S5	122.9(5)

C15	P2	C3	100.5(3)	C16	C14	S6	123.7(5)
N2S	P2S	Se2S	115.6(8)	S6	C15	P2	114.8(3)
N2S	P2S	C3	92.8(8)	S6	C15	P2S	104.9(4)
N2S	P2S	C15	97.3(8)	C13	C15	S6	117.2(5)
C3	P2S	Se2S	131.5(5)	C13	C15	P2	127.4(5)
C3	P2S	C15	87.1(4)	C13	C15	P2S	128.6(5)
C15	P2S	Se2S	123.9(4)	S7	C16	S8	114.8(3)
C25	N1	P1	123.3(5)	C14	C16	S7	123.8(5)
C27	N1	P1	119.0(5)	C14	C16	S8	121.5(5)
C27	N1	C25	116.5(6)	C18	C17	S7	117.3(5)
C25S	N1S	P1S	114(4)	C18	C17	C19	126.9(6)
C25S	N1S	C27S	129(5)	C19	C17	S7	115.8(5)
C27S	N1S	P1S	117(4)	C17	C18	S8	117.0(5)
C29	N2	P2	121.5(5)	C17	C18	C22	125.0(6)
C29	N2	C31	117.2(7)	C22	C18	S8	118.0(5)
C31	N2	P2	117.9(6)	C17	C19	C20	113.7(6)
C29S	N2S	P2S	121.3(18)	C19	C20	C21	112.0(6)
C29S	N2S	C31S	116(2)	C18	C22	C23	116.7(5)
C31S	N2S	P2S	121.6(15)	C24	C23	C22	111.8(6)
S1	C1	P1	114.9(3)	N1	C25	C26	113.0(6)
S1	C1	P1S	109.9(5)	N1S	C25S	C26S	109(5)
C3	C1	S1	116.6(5)	N1	C27	C28	114.0(6)
C3	C1	P1	127.8(5)	N1S	C27S	C28S	119(5)
C3	C1	P1S	120.4(7)	N2	C29	C30	114.0(7)
S1	C2	S2	113.8(3)	C30S	C29S	N2S	111(2)
C4	C2	S1	124.1(5)	N2	C31	C32	111.1(7)
C4	C2	S2	122.0(5)	C32S	C31S	N2S	111(2)

Radiation	MoK α ($\lambda = 0.71073$)
2 θ range for data collection/ $^\circ$	5.686 to 55.996 $^\circ$
Completeness to theta	0.980
Index ranges	-18 \leq h \leq 18, -10 \leq k \leq 9, -13 \leq l \leq 16
Reflections collected	7820
Independent reflections	3409 [$R_{\text{int}} = 0.0653$, $R_{\text{sigma}} = 0.0421$]
Data/restraints/parameters	3409/0/149
Goodness-of-fit on F^2	1.069
Final R indexes [$I \geq 2\sigma(I)$]	$R_1 = 0.0355$, $wR_2 = 0.0963$
Final R indexes [all data]	$R_1 = 0.0426$, $wR_2 = 0.1002$
Largest diff. peak/hole / e \AA^{-3}	0.37/-0.40

Bond Lengths

Atom	Atom	Length/ \AA	Atom	Atom	Length/ \AA
S1	C1	1.7598(17)	N2	C8	1.4743(19)
S1	C2	1.7679(16)	N2	C10	1.472(2)
S2	C1	1.7668(17)	C1	C1 ¹	1.344(3)
S2	C3	1.7501(17)	C2	C3	1.338(2)
P	N1	1.6943(14)	C4	C5	1.501(2)
P	N2	1.6907(14)	C6	C7	1.521(2)
P	C2	1.8283(17)	C8	C9	1.519(2)
N1	C4	1.466(2)	C10	C11	1.519(2)
N1	C6	1.470(2)			

Bond Angles

Atom	Atom	Atom	Angle/ $^\circ$	Atom	Atom	Atom	Angle/ $^\circ$
C1	S1	C2	96.04(8)	S1	C1	S2	113.75(9)
C3	S2	C1	94.92(8)	C1 ¹	C1	S1	123.39(18)
N1	P	C2	98.43(7)	C1 ¹	C1	S2	122.86(17)
N2	P	N1	114.05(7)	S1	C2	P	116.72(9)
N2	P	C2	100.24(7)	C3	C2	S1	115.61(12)
C4	N1	P	116.08(11)	C3	C2	P	126.60(13)
C4	N1	C6	116.07(13)	C2	C3	S2	119.07(13)
C6	N1	P	125.75(11)	N1	C4	C5	113.46(15)
C8	N2	P	113.99(11)	N1	C6	C7	114.85(15)
C10	N2	P	124.42(10)	N2	C8	C9	115.27(14)
C10	N2	C8	115.04(13)	N2	C10	C11	113.37(14)